Regional and global scale modeling of the benthic marine nitrogen cycle

Dissertation

zur Erlangung des Doktorgrades
an der Mathematisch-Naturwissenschaftlichen Fakultät
der Christian-Albrechts-Universität zu Kiel

vorgelegt von
Lisa Bohlen

Kiel, 2011

Referent: . . . . . Prof. Dr. Klaus Wallmann
Koreferent: . . . . . Prof. Dr. Andreas Oschlies
Eingereicht am: 22.12.2011
Tag der mündlichen Prüfung: 27.01.2012
Zum Druck genehmigt: 27.01.2012

Der Dekan

Hiermit erkläre ich, dass ich die vorliegende Doktorarbeit selbständig und ohne Zuhilfenahme unerlaubter Hilfsmittel erstellt habe. Weder diese noch eine ähnliche Arbeit wurde an einer anderen Abteilung oder Hochschule im Rahmen eines Prüfungsverfahrens vorgelegt, veröffentlicht oder zur Veröffentlichung vorgelegt. Ferner versichere ich, dass die Arbeit unter Einhaltung der Regeln guter wissenschaftlicher Praxis der Deutschen Forschungsgemeinschaft entstanden ist.

Lisa Bohlen

Abstract

The benthic nitrogen (N) cycle is highly dynamic and diverse due to the strong redox gradients occurring in marine surface sediments and the variety of oxidation states accessible to nitrogen. Since N is a limiting nutrient for biological productivity, fluxes of nitrogenous species across the sediment-water interface may strongly affect the biogeochemistry of nitrogen, carbon and phosphorus in the oceanic water column. In particular, as a major sink for fixed N in the marine environment, benthic denitrification has a profound impact on the availability of bioavailable N in the oceans. Consequently, an understanding of N cycling in marine sediments is of major importance for constraining the global marine nitrogen budget and quantifying benthic-pelagic feedbacks. The thesis addresses benthic nitrogen turnover on local and global scales with a special focus on oxygen minimum zones (OMZ) where strong lateral redox gradients in the water column as well as in the sediments lead to unique and highly interesting interactions in N cycling.

Following a broad introduction to this topic (Chapter 1), Chapter 2 examines benthic nitrogen cycling in sediments at six stations along a transect traversing the Peruvian OMZ at 11°S. A 1-D reaction-transport model constrained by a comprehensive dataset including benthic fluxes of nitrate (NO_3^-), nitrite (NO_2^-) and ammonium (NH_4^+) as well as porewater concentration profiles is used to quantify rates of nitrification, denitrification, anammox and dissimilatory nitrate reduction to ammonium (DNRA). The relative and absolute magnitude of these rates varies greatly between the sampling stations. On the anoxic shelf and upper slope, where sediments were substantially covered by bacterial mats, DNRA was the main N turnover process and accounted for more than half of the benthic NO_3^- and NO_2^- uptake. Due to intense recycling of dissolved inorganic nitrogen (DIN = NO_3^- + NO_3^- + NH_4^+) by DNRA and relatively low rates of denitrification, these stations did not represent a major sink of fixed N. However, at the deeper slope, nitrogen gas (N_2) production by denitrification was the major N turnover process and sediments constituted a strong DIN sink. While not important on the shelf and upper slope, anammox considerably contributed to N_2 production at the deeper slope with maximum importance at the deepest station at 1000 m water depth. This study mainly illustrates the importance of fixed N recycling by DNRA in sediments underlying oxygen-deficient waters which counteracts the loss of fixed N by benthic denitrification and anammox.

To broaden the scope of these results, fixed N loss by sedimentary denitrification and anammox is investigated on a global scale in Chapter 3. Based on a large data compilation including bottom water chemistry and organic carbon degradation or rain rate, empirical transfer functions were derived to predict sedimentary denitrification from the rain rate of organic carbon plus bottom water O_2 and NO_2^- only. A new variable (O_2* = bottom water O_2 minus NO_3^- concentration) was proposed to

have a major control on the fraction of organic carbon being respired through denitrification. Applied to global datasets of rain rate and O_2* on a $1° \times 1°$ resolution, the transfer functions predict a global benthic denitrification rate of ca. 154 Tg N yr^{-1}, which compares favorably with previous literature estimates using very different approaches. Sediments underlying OMZs were identified as key regions for benthic denitrification and contributed significantly to the globally integrated rate. Additional analysis of estimated total fluxes of nitrogen, carbon (C) and phosphorus (P) across the sediment-water interface reveal that C:N:P ratios of the benthic fluxes strongly deviate from Redfield composition and indicate acute N loss in the flux of inorganic nutrients returned to the water column following mineralization of phytodetritus. Owing to its simplicity, the transfer function can be dynamically coupled to general circulation models, thereby providing an easily applied means to estimate benthic feedbacks on the global N cycle.

In chapter 4 the distribution of organic matter degradation in the upper mixed layer of marine sediments is investigated. Forced with known depth-integrated rates of organic matter remineralization and bottom water chemistry, a simple diagenetic model simulates an exponential-type decrease of organic matter degradation with increasing sediment depth. The parameters describing the decrease are optimized in order to reproduce measured fluxes of nitrate and oxygen across the sediment-water interface. Results indicate that the decrease of the organic matter degradation rate with sediment depth is primarily a function of the organic carbon rain rate rather than bottom water oxygen concentrations. The methodology allows the depth-dependent carbon degradation rate profile to be predicted based on knowledge of the carbon rain rate only. This finding provides an easy way to describe organic matter degradation in benthic reaction-transport models. The shape of the organic matter degradation profile predicted by this approach can also be achieved using a G model. However, values for the first order rate constant k derived from the rate profile varied over several orders of magnitude.

The work presented in this thesis advances our current understanding of benthic N cycling, summarized as follows:

i. The benthic uptake of NO_3^- + NO_2^- in sediments underlying oxygen deficient bottom waters is very likely not representative of the fixed N flux lost via denitrification. DNRA can be equal to or greater in magnitude than denitrification in these environments, thus counteracting the overall DIN loss to N_2 from the system.
ii. A new estimate for global benthic denitrification is presented based on empirical data analysis and an easily-applied transfer function which allows the dynamic implementation of benthic N feedbacks in global biogeochemical models.
iii. The poorly-known distribution of organic matter degradation in surface marine sediments including the bioturbated layer have the potential to be estimated from the rain rate of organic carbon to the seafloor only. This provides a straightforward means to estimate depth-dependent mineralization profiles without *a priori* information of carbon reactivity.

Kurzfassung

Bedingt durch starke Redox-Gradienten in marinen Oberflächensedimenten und die Vielzahl von möglichen Oxidationszuständen ist der benthische Stickstoff (N) Kreislauf sehr vielfältig und dynamisch. Da Stickstoff ein limitierender Nährstoff für die biologische Produktivität ist, können Stickstoffflüsse über die Sediment-Wasser Grenze die Biogeochemie von Stickstoff, Kohlenstoff und Phosphor in der Wassersäule stark beeinflussen. Als bedeutendste ozeanische Senke von Stickstoff hat die benthische Denitrifikation schwerwiegende Auswirkungen auf die Verfügbarkeit von biologisch verwertbarem Stickstoff und nimmt damit einen besonderen Stellenwert ein. Folglich ist das Verständnis des Stickstoffkreislaufs in Meeressedimenten von größter Wichtigkeit für die Aufstellung eines globalen marinen Stickstoff-Budgets und für die Quantifizierung von benthisch-pelagischen Rückkopplungen. Diese Doktorarbeit befasst sich mit dem benthischen Stickstoffumsatz auf lokaler und globaler Ebene, mit speziellem Fokus auf Sauerstoffminimumzonen (OMZs), wo starke Redox-Gradienten in der Wassersäule und im Sediment zu einzigartigen und in höchstem Maße interessanten Wechselwirkungen führen.

Nach einer generellen Einführung in das Thema (Kapitel 1) wird in Kapitel 2 der benthische Stickstoffkreislauf an sechs Stationen entlang eines Transekts durch die Sauerstoffminimumzone vor Peru (11°S) untersucht. Ein 1-D Reaktions-Transport-Modell wird genutzt um die Raten von Nitrifikation, Denitrifikation, Anammox und dissimilatorischer Nitratreduktion zu Ammonium (DNRA) zu quantifizieren. Das Model wird durch einen umfangreichen Datensatz eingegrenzt, der benthische Flüsse von Nitrat (NO_3^-), Nitrit (NO_2^-) und Ammonium (NH_4^+) sowie Porenwasserprofile beinhaltet. Die relativen und absoluten Raten variieren deutlich zwischen den Stationen. Auf dem anoxischen Schelf und oberen Hang waren die Sedimente wesentlich von Bakterienmatten bedeckt und DNRA war der hauptsächliche Stickstoffumsatzprozess, verantwortlich für mehr als 50% der benthischen NO_3^-- und NO_2^--Aufnahme. Aufgrund des intensiven Recyclings von gelöstem anorganischen Stickstoff (DIN = NO_3^- + NO_3^- + NH_4^+) durch die DNRA und relativ geringer Denitrifikationsraten waren diese Stationen keine Senken für Stickstoff. Am tieferen Hang war jedoch N_2-Produktion durch Denitrifikation der dominierende Prozess und die Sedimente stellten eine starke DIN-Senke dar. Anammox war auf dem Schelf und oberen Hang nicht von Bedeutung, machte aber an den tiefen Stationen einen erheblichen Anteil der N_2-Produktion aus. Diese Studie verdeutlicht die Wichtigkeit von DIN-Recycling über DNRA in Sedimenten unterhalb sauerstoffarmen Bodenwassers, die dem Verlust von Stickstoff über Denitrifikation und Anammox entgegenwirkt.

Um den Rahmen dieser Ergebnisse auszuweiten, werden in Kapitel 3 benthische Denitrifikation und Anammox auf globaler Ebene untersucht. Basierend auf einer großen Datenzusammenstellung in-

klusive Bodenwasserchemie und Kohlenstoffabbaurate oder Kohlenstofffluss auf das Sediment wurde eine empirische Transferfunktion entwickelt, die die benthische Denitrifikation nur mittels des organischen Kohlenstoffflusses auf das Sediment und den Bodenwasserkonzentrationen von O_2 (bw_{O2})und NO_3^- (bw_{NO3}) vorhersagt. Eine neue Variable (O_2* = bw_{O2} minus bw_{NO3}) wurde definiert, die einen großen Einfluss auf den Anteil des über Denitrifikation abgebauten Kohlenstoffs zu haben scheint. Die Transferfunktion wurde auf globale Datensätze von O_2* und Kohlenstofffluss auf das Sediment mit einer Auflösung von $1° \times 1°$ angewandt. Die berechnete globale benthische Denitrifikationsrate von ca. 154 Tg N a^{-1} ist vergleichbar mit früheren Literaturangaben basierend auf sehr unterschiedlichen Ansätzen. Sedimente unterhalb von OMZs wurden als Hauptregionen für benthische Denitrifikation identifiziert. Zusätzliche Analysen von berechneten, totalen Flüssen von Stickstoff, Kohlenstoff (C) und Phosphor (P) über die Sediment-Wasser Grenze zeigen, dass die C:N:P Verhältnisse der benthischen Flüsse stark von der Redfield Zusammensetzung abweichen. Stattdessen zeigen die Flüsse der in die Wassersäule freigesetzten anorganischen Nährstoffe einen akuten Stickstoffverlust an. Dank der geringen Komplexität der Transferfunktion kann diese dynamisch an generelle Zirkulationsmodelle gekoppelt werden und bietet damit eine Möglichkeit benthische Rückkopplungen auf den globalen Stickstoffkreislauf abzuschätzen.

Kapitel 4 beschäftigt sich mit der Verteilung des Kohlenstoffabbau in der oberen durchmischten Schicht mariner Sedimente. Angetrieben von bekannten, tiefenintegrierten Abbauraten sowie der Bodenwasserchemie simuliert ein einfaches diagenetisches Modell eine exponentielle Abnahme der Kohlenstoffabbaurate mit zunehmender Sedimenttiefe. Die Parameter, welche die Abnahme beschreiben, wurden optimiert um gemessene Flüsse von Nitrat und Sauerstoff über die Sediment-Wasser Grenze zu reproduzieren. Ergebnisse dieser Studie deuten darauf hin, dass die Abnahme der Kohlenstoffabbaurate mit der Sedimenttiefe in erster Linie vom Kohlenstofffluss auf das Sediment und nicht von der Sauerstoffkonzentration im Bodenwasser abhängt. Eine Methodik wurde entwickelt, die es erlaubt, das tiefenabhängige Profil der Abbaurate ausschließlich basierend auf dem Kohlenstofffluss auf das Sediment vorherzusagen. Die Form des Abbauratenprofils kann auch mithilfe eines G-Modells erzielt werden. Die darüber abgeleiteten Werte der Abbaukonstanten erster Ordnung k variierten über mehrere Größenordnungen.

Die in dieser Doktorarbeit vorgestellten Ergebnisse erweitern das derzeitige Verständnis des benthischen Stickstoffkreislaufs wie folgt:

i. Die benthische Aufnahme von NO_3^- und NO_2^- in Sedimente unterhalb sauerstoffarmen Bodenwassers repräsentiert sehr wahrscheinlich nicht den Verlust von Stickstoff über Denitrifikation. DNRA kann in dieser Umgebung von gleicher oder sogar noch größerer Bedeutung sein und dem Gesamtverlust von Stickstoff als N_2 aus dem System entgegenwirken.
ii. Es wird eine neue Abschätzung für die globale Denitrifikationsrate basierend auf empirischer Datenanalyse und einer einfach anzuwendenden Transferfunktion präsentiert. Diese Funktion ermöglicht die dynamische Umsetzung von benthischen Stickstoffrückkopplungen in globalen

biogeochemischen Modellen.

iii. Die Verteilung des Kohlenstoffaubbaus in marinen Oberflächensedimenten, einschließlich der bioturbierten Schicht, bietet das Potential ausschließlich über den Kohlenstofffluss auf das Sediment abgeschätzt zu werden. Dieses Ergebnis eröffnet eine unkomplizierte Möglichkeit die tiefenabhängigen Kohlenstoffabbauprofile zu berechnen ohne die Reaktivität von Kohlenstoff als bekannt vorauszusetzen.

Contents

1. General introduction

1.1. The marine nitrogen cycle

1.1.1. General characteristics

The nitrogen (N) cycle is one of the most complex biogeochemical cycles in the marine environment. As a key nutrient for biological production nitrogen strongly influences other elemental cycles, especially those of carbon (C) and phosphorus (P). Moreover, nitrogen exists in more oxidation states than other elements and is thus subject to a multitude of biogeochemical transformation reactions. However, dinitrogen (N_2) - the most abundant form of nitrogen on earth - is generally not bioavailable to most marine organisms and must first be fixed as inorganic nitrogen. Hence, the marine nitrogen balance is controlled by reactions converting N_2 to fixed nitrogen, i.e. N_2 fixation, and those carrying out the removal of fixed N to N_2, e.g. denitrification.

The main driver of all marine biogeochemical cycles, and thus also the N cycle, is photosynthesis based primary production in the euphotic zone of the oceans. Next to organic carbon, organic matter contains considerable amounts of organic nitrogen and is thus a major pool of N in the oceans. Most of the produced organic matter is consumed within the upper ocean layer, however, a small proportion is exported to the dark deeper ocean. During remineralization of the exported organic material in the deep ocean, the inorganic components, i.e. primarily nitrate (NO_3^-) and phosphate (PO_4^{3-}), are released to the water column. When transported back into surface waters these recycled nutrients become available for new primary production. This loop, also known as the biological "carbon pump", constitutes a coupling between biological and physical processes that controls the distribution of almost all biogeochemically active species in the ocean (Gruber, 2008). Moreover, the uptake of carbon dioxide (CO_2) from the atmosphere associated with marine primary production is an important factor for climate change.
Despite intense degradation in the water column, about 25 % of the organic matter exported from the surface ocean escapes remineralization and reaches the seafloor (Sarmiento and Gruber, 2006). This flux, often referred to as the rain rate of organic matter to the seafloor, is a main source of N to the sediment and mainly determines biogeochemical cycling in the underlying sediment. Around 10 % of the organic matter raining to the seafloor is buried deep in the sediments, and 90 % undergoes remineralization (Sarmiento and Gruber, 2006). Similar to the water column, the organic N compounds are released during organic matter degradation and subsequently either become available for benthic reactions or are released back into the water column. The benthic-pelagic coupling via organic mat-

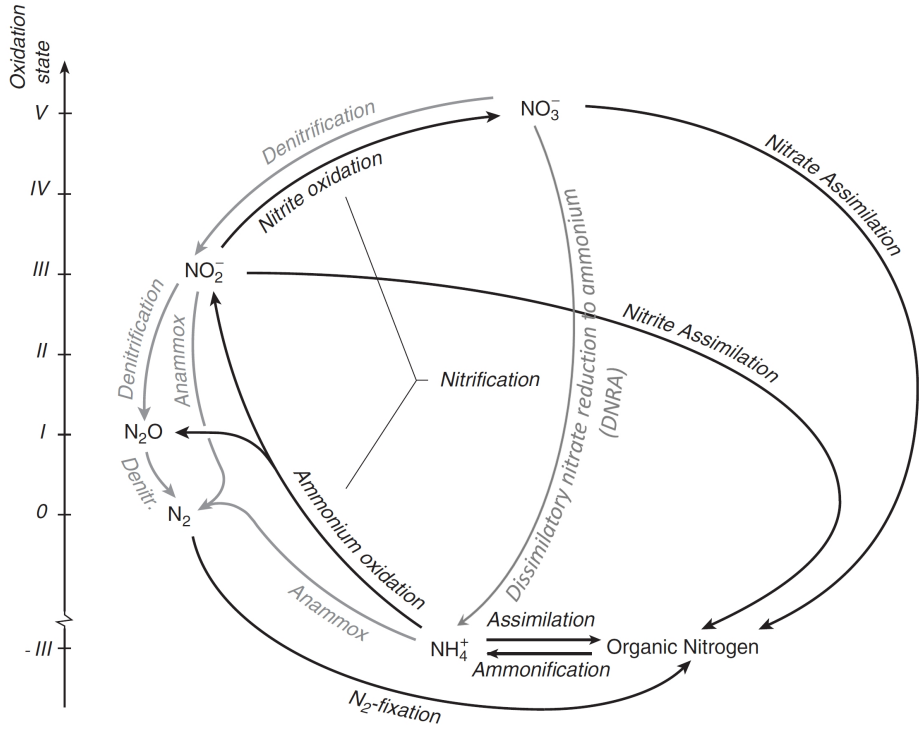

Figure 1.1.: Major chemical forms and reactions of nitrogen in the marine environment. Processes shown in gray occur in anoxic environments only. Modified from Gruber (2008).

ter raining to the seafloor and fluxes across the sediment-water interface is an important feature for biogeochemical cycling, especially in oxygen deficient environments (see section 1.1.4).

1.1.2. Major nitrogen species and reactions

Nitrogen has five stable oxidation states: nitrate (NO_3^-, + V), nitrite (NO_2^-, +III), nitrous oxide (N_2O, +I), dinitrogen gas (N_2, 0), and ammonium (NH_4^+, -III) (Fig. 1.1). The sum of NO_3^- + NO_2^- + NH_4^+ is known as dissolved inorganic nitrogen (DIN). The reason for the stability of so many N forms lies in the fact that N has five valence electrons and is a relatively small atom, such that its electronic orbitals have much flexibility to rearrange (Gruber, 2008). Consequently, the marine N cycle involves a lot of redox reactions shuttling N between its oxidation states (Fig. 1.1). These reactions are usually mediated by biology when organisms perform assimilatory or dissimilatory metabolism.
Marine phytoplankton can take up NH_4^+ and NO_3^- during organic N biomass synthesis or **assimilation** (Table 1.1). Whereas NH_4^+ can easily be incorporated into organic N, NO_3^- has to be reduced to NH_4^+ (assimilatory nitrate reduction) prior to anabolism. Due to the additional energy required to reduce NO_3^- to NH_4^+, the latter is, in general, the preferred N source of phytoplankton (Zehr and Ward, 2002). Since NO_2^- is an intermediate product during the sequential reduction of NO_3^- during assim-

Table 1.1.: Major N turnover reactions in marine sediments. For the assimilation reactions, the stoichiometric ratios of Anderson (1995) were used.

Reaction	Stoichiometry
Ammonium assimilation	$106\ CO_2 + 16\ NH_4^+ + HPO_4^{2-} + 48\ H_2O + 14\ OH^- \rightarrow C_{106}H_{175}O_{42}N_{16}P + 118\ O_2$
Nitrate assimilation	$106\ CO_2 + 16\ NO_3^- + HPO_4^{2-} + 78\ H_2O + 18\ H^+ \rightarrow C_{106}H_{175}O_{42}N_{16}P + 150\ O_2$
Ammonium oxidation	$NH_4^+ + 3/2\ O_2 \rightarrow NO_2^- + 2\ H^+ + H_2O$
Nitrite oxidation	$NO_2^- + 1/2\ O_2 \rightarrow NO_3^-$
Denitrification	$C_{106}H_{175}O_{42}N_{16}P + 104\ NO_3^- \rightarrow\ 106\ CO_2 + 60\ N_2 + H_3PO_4 + 138\ H_2O$
Anammox	$NO_2^- + NH_4^+ \rightarrow 2N_2 + 2\ H_2O$
DNRA (sediments)	$NO_3^- + HS^- + H^+ + H_2O \rightarrow SO_4^{2-} + NH_4^+$
DNRA (water column)	$NO_3^- + C_2H_3O_2^- + H^+ + H_2O \rightarrow NH_4^+ + 2\ HCO_3^-$

ilatory nitrate reduction, phytoplankton that can assimilate NO_3^- can also take up NO_2^-.
During organic matter respiration or remineralization, particulate organic nitrogen (PON) is released as NH_4^+ in a process called **ammonification** (reverse reaction of ammonium assimilation). This process is performed by heterotrophic bacteria which use the oxidation of carbon to yield energy and produce NH_4^+ released from organic N as a waste product. Where oxygen (O_2) is present at high concentrations, the released NH_4^+ may be oxidized to NO_2^- (ammonium oxidation) and then further to NO_3^- (nitrite oxidation) (Table 1.1). Together, these two chemoautotrophic processes are referred to as **nitrification**.

Microbial degradation of organic matter can exploit several electron acceptors (see also section 1.1.3). However, due to its higher energy yield aerobic respiration is the favorite remineralization pathway. Hence, anaerobic degradation of organic matter is usually inhibited as longs as O_2 is available. The next preferred electron acceptor after O_2 during carbon mineralization is typically NO_3^- (Froelich et al., 1979) in a process called **heterotrophic denitrification** (Table 1.1). Since denitrification is generally inhibited by O_2, it is restricted to oxygen-deficient environments such as marine sediments (see section 1.1.3) or oxygen minimum zones (see section 1.1.4). Although the denitrification reaction in Table 1.1 shows the full conversion of NO_3^- to N_2, it should be noted that denitrification is a sequential reduction of NO_3^- to N_2 gas ($NO_3^- \rightarrow NO_2^- \rightarrow N_2O \rightarrow N_2$). All individual steps are associated with different enzyme systems (Devol, 2008) and thus different groups of microorganisms. Denitrification and nitrification mostly do not completely convert NO_3^- to N_2 or NH_4^+ to NO_3^-. Instead, a (small) fraction may be released as the intermediate products NO_2^- or N_2O. While NO_2^- is typically used in some reactions (Fig. 1.1) or accumulates in the surrounding water, gaseous N_2O may escape the ocean to the atmosphere. As a greenhouse-gas, N_2O is >200 times more potent than CO_2 (Ramaswamy et al., 2001) and thus of importance with regards to climate change. Although still debated, the current opinion is that nitrification rather than denitrification is the major source for N_2O in the ocean (e.g. Nevison, 2003).

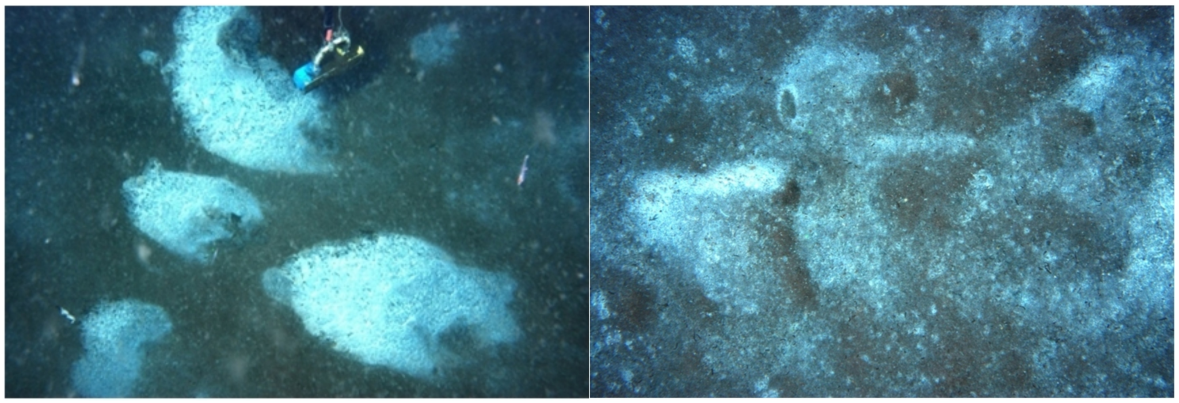

Figure 1.2.: Benthic bacterial mats (white) on a transect at 11°S off Peru (Courtesy of S. Sommer).

For many decades denitrification was believed to be the only reaction transforming bioavailable DIN to N_2 gas, i.e. leading to a loss of fixed N from the marine environment. However, recently another reaction was discovered: the anaerobic ammonium oxidation (**anammox**) (Table 1.1; Strous et al., 1999). In contrast to the heterotrophic process of denitrification, anammox is performed by chemo-autotrophic bacteria which use the simultaneous oxidation and reduction of two N species (NH_4^+ and NO_2^-) as source of energy. First observed in a waste water treatment plant (van de Graaf et al., 1990), anammox is now recognized as an important process in the marine N cycle (Dalsgaard et al., 2005). Since anammox requires NO_2^-, it is mainly found in oxygen deficient waters (Kuypers et al., 2003, Hamersley et al., 2007) or marine sediments (Thamdrup and Dalsgaard, 2002), where NO_2^- oxidation to NO_3^- is limited. Both denitrification and nitrification may supply NO_2^- for anammox, yet since anammox appears to be restricted to low oxygen environments where little O_2 is available for nitrification, partial denitrification is probably the most important supply pathway.

Denitrification and anammox both lead to a loss of fixed DIN. Since these processes occur under suboxic conditions, observed losses of NO_3^- or NO_2^- in low oxygen regimes was generally associated with a loss of DIN. However, the identification of another process, the dissimilatory nitrate reduction to ammonium (**DNRA**) has altered this paradigm. In low oxygen environments, microorganisms which mediate DNRA reduce NO_3^- to NH_4^+ using a variety of electron donors, thus converting one bioavailable N species into the other and preserving the fixed N balance.
In marine sediments DNRA has been recognized for some time as a linkage between the benthic nitrogen and sulfur cycles, especially off the Chilean and Peruvian coast (Gallardo, 1977; Otte et al., 1999). In such sulfide-rich deposits, large vacuolated sulfur bacteria such as filamentous *Beggiatoa* and *Thioploca* can occur at high densities. These bacteria store NO_3^- in their cells for posterior use to oxidize the free sulfide (here HS^-) in the surrounding porewater to sulfate (SO_4^{2-}) (Table 1.1). The filaments can penetrate several centimeters (up to around 10 cm, Schulz et al. (1996)) into the sediment and store NO_3^- in concentrations strongly exceeding the bottom water concentrations (Fossing et al., 1995). *Beggiatoa* and *Thioploca* are motile, and migrate between the oxidized surface

layer and the subsurface redox interface where sulfide is oxidized and potentially stored as elemental sulfur inside the cells. These sulfur inclusions also give the bacteria their bright white appearance (e.g. Preisler et al., 2007; Fig. 1.2). Due to their physiological advantages, large sulfur bacteria can survive long periods of low bottom water NO_3^-. Sediment-dwelling large sulfur bacteria are commonly found in upwelling regions where (i) bottom water NO_3^- is enriched due to upwelling of NO_3^- rich waters while O_2 is depleted due to seasonal anoxia and (ii) high fluxes of organic carbon induce high sulfide production from bacterial sulfate reduction (Jørgensen and Nelson, 2004). Sulfide concentrations in sediments inhabited by large sulfur bacteria may be very low despite high rates of sulfate reduction because sulfide is efficiently removed by DNRA (Schulz, 1996; Thamdrup and Canfield, 1996). In contrast to denitrification, DNRA may lead to a recycling of DIN rather than N_2 gas production. Therefore, it affects the availability of fixed N in the sediment, especially in oxygen minimum zones (e.g. Jørgensen and Gallardo, 1999).
In addition to benthic DNRA which is coupled to the oxidation of free sulfide in the sediment, DNRA has recently also been observed in suboxic water columns (Kartal et al., 2007, Lam et al., 2009). However, "pelagic" DNRA is coupled to the oxidation of organic material rather than sulfide, which usually does not accumulate in the water column (Lam and Kuypers, 2011) (Table 1.1).

The above reactions describe the various redox transformations of N in the marine environment. However, as mentioned above, most organisms are unable to assimilate atmospheric N_2 and the availability of fixed N often limits primary production (Falkowski et al., 1998 and references therein). Biological **N_2 fixation** can alleviate this deficiency. The ability to fix nitrogen is restricted to a few, mainly autotrophic, organisms called diazotrophs. Nitrogen fixation is a major pathway of fixed N supply in DIN-limited regions of the ocean. During recent years much progress has been made in the discovery and identification of marine diazotrophs and the spectrum of N_2 fixing organisms has greatly expanded. Diazotrophs are comprised of free-living species, e.g. the well-studied cyanobacterium *Trichodesmium* (Capone et al., 1997) or uni-cellular bacteria (Zehr et al., 2001), as well as symbionts with dinoflagellates and diatoms hosts (Carpenter and Capone, 2008). The magnitude of marine N_2-fixation has been subject to intense debate in the last years (see section 1.1.5). In addition, the role of benthic N_2-fixation in bioturbated sediments may play an important role in the marine N budget yet the wider significance of this processes is essentially unknown (Bertics et al., 2010).

1.1.3. Benthic nitrogen cycling

In marine sediments, oxygen is usually depleted below the uppermost layer due to high rates of oxygen consumption during the degradation of organic matter. Hence, redox conditions differ from the typically fully oxygenated regime in the water column and induce a sequence of suboxic or anoxic processes. After aerobic respiration, organic matter is degraded by a sequence of alternate electron acceptors according to their decreasing energy yield (Fig. 1.3). Denitrification is the next most

Pore water chemistry	Pathway and stoichiometry of reaction	ΔG_0 (kJ mol^{-1})
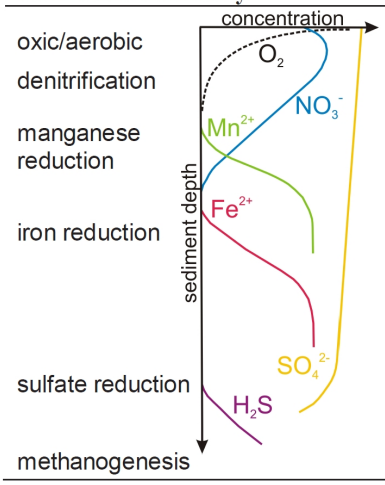	***Oxic respiration:***	
	$[CH_2O] + O_2 \rightarrow CO_2 + H_2O$	-479
	Denitrification:	
	$5[CH_2O] + 4NO_3^- \rightarrow 2N_2 + 4HCO_3^- + CO_2 + 3H_2O$	-453
	Manganese reduction:	
	$[CH_2O] + 3CO_2 + H_2O + 2MnO_2 \rightarrow 2Mn^{2+} + 4HCO_3^-$	-349
	Iron reduction:	
	$[CH_2O] + 7CO_2 + 4Fe(OH)_3 \rightarrow 4Fe^{2+} + 8HCO_3^- + 3H_2O$	-114
	Sulfate reduction:	
	$2[CH_2O] + SO_4^{2-} \rightarrow H_2S + 2HCO_3^-$	-77
	Methanogenesis:	
	$4H_2 + HCO_3^- + H^+ \rightarrow CH_4 + 3H_2O$	-136
	$CH_3COO^- + H^+ \rightarrow CH_4 + CO_2$	-28

Figure 1.3.: Pathways of organic matter degradation and their Gibbs energy yield (ΔG_0) as well as porewater profiles predicted by the successive utilization of electron acceptors. Stoichiometry and energy yield are according to Jørgensen (2006) and schematic porewater profiles were modified from Burdige (2006).

energetically-yielding pathway of organic matter degradation, followed by manganese reduction, iron reduction, sulfate reduction and methanogenesis (Froelich et al, 1979). The result of this cascade of electron acceptors is a vertical zonation of the sediment into oxic (aerobic), suboxic (nitrogenous, manganous and ferruginous) and anoxic (sulfidic and methanic) layers. However, these layers are not strictly separated but show varying degrees of overlap. In deep-sea environments, oxygen is rarely depleted within the sediment and denitrification is of minor importance. However, in coastal sediments where high loads of organic matter reach the seafloor or in sediments underlying oxygen-deficient bottom waters (see section 1.1.4), oxygen penetrates only a few millimeters. Here, denitrification and anaerobic organic matter degradation gain more importance and the suboxic and anoxic pathways N cycling such as anammox and DNRA become more pronounced. Due to the widespread occurrence of denitrification in marine sediments, benthic denitrification is thought to constitute the major avenue of fixed N loss from the oceans (see section 1.1.5).

Due to the close proximity of oxic and suboxic sediment layers, a distinct coupling between aerobic and anaerobic processes is characteristic for N cycling. For example, NO_3^- used in denitrification is either supplied via NO_3^- uptake from the water column or by the aerobic nitrification of NH_4^+ released during ammonification. Moreover, in the transition between oxic and anoxic regimes, several processes compete for a given species. In case of NO_2^-, for example, nitrification, denitrification and anammox are rivaling pathways leading to different end-products (Fig. 1.1). The process(es) that dominate(s) benthic N cycling at a specific site is (are) thus difficult to assess a priori and may require detailed investigation of porewater chemistry, benthic fluxes, rate measurements or application of benthic models (see section 1.2).

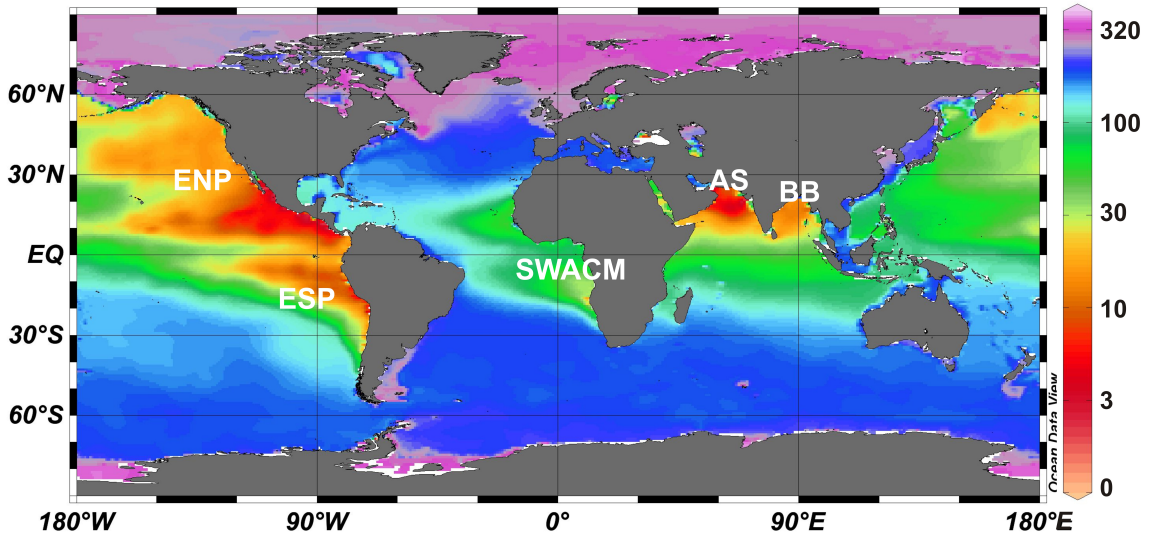

Figure 1.4.: O_2 concentrations (µM) at water depth where O_2 concentration is minimal (according to the World Ocean Atlas 2009, annual objectively analyzed 1°× 1° fields). OMZs are indicated in red.

Naturally, nitrogen cycling in the sediment is influenced by the overlying water column, for example by the flux of organic matter to the sediment or by the concentration of O_2 or NO_3^- in the bottom water. In turn, benthic processes may also affect the overlying waters. A flux of NH_4^+ out of the sediment may be observed where organic matter degradation rates are high or under oxygen-deficient conditions where some of the NH_4^+ produced during ammonification or DNRA may escape oxidation and exit the sediment. Hence, the benthos and its interactions with the water column have to be considered for a complete understanding of the marine N cycle, especially in oxygen minimum zones (see section 1.1.4).

1.1.4. Nitrogen cycling in oxygen minimum zones

In the marine environment, low oxygen concentrations occur within the sediment (see section 1.1.3) and in the O_2-deficient water masses of oxygen minimum zones (OMZs). In the modern ocean, the volume of OMZs (< 20 µM O_2) account for 10.3×10^6 km^3, that is, about 0.7 % of the total ocean volume (Paulmier and Ruiz-Pino, 2009). Subject to many physical and biological factors, low oxygen waters are generally the result of a combination of sluggish ventilation and high rates of oxygen consumption due to the degradation of organic matter (Wyrtki, 1962). Hence, OMZs are mostly tied to the highly productive upwelling regions of eastern boundary current systems (Fig. 1.4). Today's major OMZ are the Eastern North Pacific (ENP), the Eastern South Pacific (ESP), the Arabian Sea (AS), the Bay of Bengal (BB) and, to a lesser degree, the South West African continental

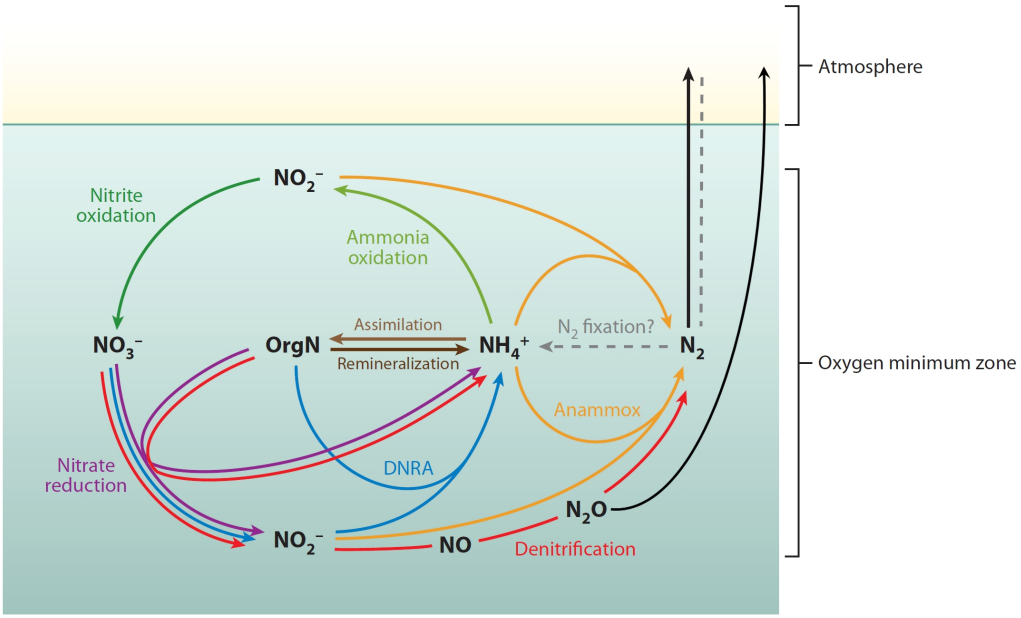

Figure 1.5.: Nitrogen cycling in oxygen minimum zones. Denitrification (red) and nitrification (green) are shown in individual steps. OrgN denotes organic nitrogen. Modified from Lam and Kuypers (2011).

margin (SWACM). However, in contrast to these sites where O_2 levels are as low as < 2 µM, O_2 levels offshore western Africa do not fall below ≈20 µM. Worldwide, permanent suboxic zones impinge on > 1 million km^2 seafloor on the shelf and slope (here defined as < 0.5 ml l^{-1} ≈ 22 µM O_2; Helly and Levin (2004)) thus also affecting biogeochemistry in the underlying sediments. While low oxygen concentrations are usually lethal to or avoided by macroorganisms, many microbes are specialized to such conditions and form unique communities, many of them strongly associated with N cycling.

OMZs are main regions for fixed N loss by denitrification and anammox. Approximately 30 - 50 % of the total N loss from the oceans has been estimated to occur in OMZs (Codispoti et al., 2001; Gruber, 2004, 2008). In the oxygen-rich water column of the open ocean, N cycling is mainly restricted to aerobic pathways and denitrification plays a minor role. However, in OMZs N cycling becomes far more complex (Fig. 1.5). NO_3^- tends to be the preferred electron acceptor and nitrate reduction to nitrite (first step of denitrification) and DNRA are prominent pathways (Lam and Kuypers, 2011). In general, stepwise denitrification, anammox and DNRA, which require oxygen-deficient conditions, are the main reactions in OMZs. Nitrification in or near OMZs leads to the production of NO_3^- or NO_2^- from remineralized NH_4^+ and thereby promotes subsequent N loss by denitrification or anammox (Lam and Kuypers, 2011).

Sediments underlying OMZs are also of importance for the marine N cycle, again with denitrification, DNRA and anammox as the key reactions. In particular, the coupling between N cycling in the wa-

ter column and the underlying sediment is especially pronounced in oxygen minimum zones. Since oxygen concentrations are very low or zero, denitrification is the major process for the degradation of organic matter (Fig. 1.3). Due to the strong demand for NO_3^- as electron acceptor and the proximity of the denitrification zone to the sediment-water interface, high amounts of bottom water nitrate are taken up into the sediment by denitrification thus leading to high rates of benthic N loss. Moreover, only very little of the produced NH_4^+ is oxidized back to NO_3^-, allowing NH_4^+ release from the sediment to the water column. The released NH_4^+ may potentially be transported to the surface ocean and sustain high rates of primary production or anammox. Degradation of sinking phytodetritus contributes to anoxia in the water column and sediments, such that benthic-pelagic coupling may exert a positive feedback on the expansion of OMZs.

1.1.5. Nitrogen budget

Due to the complexities of nitrogen cycling and wide geographical heterogeneity in turnover rates, accurately constraining the global marine N budget is difficult. Nevertheless, some effort has been made to provide numbers for fluxes within, to, and out of the oceans. Quantitatively, the assimilation of NH_4^+ and NO_3^- to organic N in the euphotic zone is the most important process in the global marine N cycles with rates exceeding 7000 Tg N yr^{-1} in the open ocean with an additional $\approx$ 1400 Tg N yr^{-1} on the continental margins (Gruber, 2008). Around 20 % of the primary production is exported from the surface layer to the deeper ocean ($\approx$ 1100 Tg N yr^{-1} and $\approx$ 450 Tg N yr^{-1} for the open ocean and the coastal environments, respectively). In an open ocean regime, almost all the exported organic N is nitrified to NO_3^- resulting in a very low deposition of particulate organic nitrogen (PON) to the seafloor ($\approx$ 50 Tg N yr^{-1}) (Gruber, 2008). In contrast, on the shallow continental margins only little of the PON is nitrified whereas the deposition flux is much higher (350 Tg N yr^{-1}). While the low organic matter flux in the deep sea does not induce anoxic conditions within the upper few cm of sediment, most of the PON reaching the deep sea is nitrified and only $\approx$5 Tg N yr^{-1} is finally denitrified (Gruber, 2008). Contrastingly, denitrification plays an important role for organic matter degradation on the shallow shelves where O_2 is typically exhausted within the uppermost centimeters of the sediment. However, a global value for benthic denitrification is hard to determine accurately, with estimates ranging from 130 to 300 Tg N yr^{-1} (Table 1.2).

Table 1.2 lists the major source and sink N budget in the contemporary ocean, excluding internal N cycling fluxes which do not affect the total amount of oceanic N. Sources of nitrogen to the ocean are N_2 fixation (pelagic and benthic), riverine input and atmospheric deposition. The studies presented in Table 1.2 agree that thereof N_2 fixation is the largest N source (75 - 330 Tg N yr^{-1}). Total source estimates range from 160 to 380 Tg N yr^{-1} (Table 1.2). Sinks of nitrogen from the oceans are denitrification (pelagic and benthic), sediment burial and loss of N_2O to the atmosphere. The major sinks are benthic (180 - 300 Tg N yr^{-1}) and pelagic denitrification (65 - 150 Tg N yr^{-1}), with a total global

Table 1.2.: Global marine nitrogen budgets of Codispoti et al. (2001), Galloway et al. (2004), Gruber (2004) and Brandes and Devol (2002). Modified from Gruber (2008).

Process	Codispoti et al. (2001)	Galloway et al. (2004)	Gruber et al. (2004)	Brandes and Devol (2002)
		Sources (Tg N yr^{-1})		
Pelagic N_2 fixation	117	106	120 ± 50	110 – 330 [a]
Benthic N_2 fixation	15	15	15 ± 10	
River input	76	48	80 ± 20	25
Atmospheric deposition	86	33	50 ± 20	25
Total sources	294	202	265 ± 55	160 - 380
		Sinks (Tg N yr^{-1})		
Benthic denitrification [b]	300	206	180 ± 50	200 - 280
Water column denitrification	150	116	65 ± 20	75
Sediment burial	25	16	25 ± 10	25
N_2O loss to atmosphere	6	4	4 ± 2	
Total sinks	482	342	275 ± 55	300 - 380

(a) Only a combined N_2 fixation rate was given by Brandes and Devol (2002).
(b) In additional studies benthic denitrification was estimated as 230 – 285 Tg N yr^{-1} (Middelburg et al., 1996) and 154 Tg N yr^{-1} (Thullner et al. (2009).

sink of 275 - 482 Tg N yr^{-1}.

The N budget in the studies by Gruber (2004) and Brandes and Devol (2002) are generally balanced, but a N deficit of 200 Tg N yr^{-1} and 140 Tg N yr^{-1} was reported by Codispoti et al. (2001) and Galloway et al. (2004), respectively (Table 1.2). Codispoti et al. (2001) suggest that the alteration of the N cycle by humans could have caused the N deficit, although Galloway et al. (2004) estimated a perturbation by humans on the order of 45 Tg N yr^{-1} only. Note, however, that no uncertainties are given with these latter budget estimates, which complicates any firm conclusions regarding the significance of this apparent deficit. The question whether the global marine N budget shows a net deficit remains a major open question, with much effort placed into better constraining the major sources and sinks in the marine N budget, i.e. N_2 fixation and denitrification.

On timescales of 2 to 3 kyr, i.e. the turnover time of fixed N in the oceans (Codispoti et al., 2001), N_2 fixation and denitrification (including anammox) appear to be in balance since there is little evidence that massive variations have occurred since the last glacial maximum (e.g. Kienast, 2000). Two negative feedback mechanisms have been hypothesized to stabilize the marine N cycle (Gruber, 2008 and references therein). Firstly, supposing that denitrification and/or anammox increase in intensity due to, for example, expanding OMZs as a result of climate change (Stramma et al., 2008; Oschlies et al., 2008), the fixed N pool of the oceans would decrease. As a consequence, biological production in the euphotic zone and export production would decrease and lower O_2 consumption within the water column and the sediment. Thus, the expansion of OMZs and denitrification will be reduced. Secondly, an increase in N_2 fixation, for example, in N limited regions, would continue until the

ecological niche for N_2-fixers diminishes up to the point where denitrification and N_2 fixation are in balance. In addition to these relatively simple feedback processes, many other potential couplings have been proposed (Gruber, 2008). Clearly, the marine N cycle is a highly coupled system and its future direction is difficult to predict in the context of climate change. Hence, a better understanding of the feedbacks and thresholds associated with the marine cycle is required.

1.2. Diagenetic modeling

The mathematical description and quantitative prediction of the rates of coupled biogeochemical processes is an important and growing field in marine sciences. The usefulness of models is several-fold. For example, models can (i) predict the occurrence or rates of process that may not be directly measurable due to analytical or logistical restrictions, (ii) provide an understanding of the interactions between the biogeochemical processes in complex systems, (iii) be used in a heuristic sense to predict responses to future changes or perturbations, (iv) constrain mass budgets and help to verify measured data for errors and inconsistencies, and (v) be applied to develop hypotheses and advancement of ideas.
At least since 1980, when Robert Berner published his book on early diagenesis (Berner, 1980), theoretical modeling approaches became a common tool to examine processes in marine sediments (e.g. Boudreau, 1997; Van Cappellen and Wang, 1996). In the context of marine sciences, the term diagenesis combines all processes leading to a change in sediment after its deposition on the seafloor (Berner, 1980). These processes may be of a physical (e.g. transport due to advection or diffusion), chemical and/or biological nature. While transport due to advection (burial and compaction of the sediment) and diffusion are the major physical transport processes below the upper bioturbated layer, chemical N cycling reactions in marine sediments are usually mediated by organisms. Consequently, chemical and biological aspects should be considered simultaneously with regard to the benthic N cycle. Biologically driven transport processes include bioturbation (the displacement and mixing of sediment due to faunal activity) and bioirrigation (the flushing of burrows by benthic organisms thereby exchanging the burrow water for overlying water). To model diagenesis quantitatively, sediments are divided into the solid phase (sediment grains) and the liquid phase (pore fluid). The porosity (ϕ), that is the fractional volume of total sediment filled with porewater, is required to mass balance the model. The volume fraction filled with sediment grains is then given as 1 - ϕ.

The concept of 1-D early diagenetic models is to calculate changes in mass due to transport and reaction as a function of space and time. Therefore, mass conservation is a fulfillment which must be strictly observed. The standard mass conservation partial differential equation (PDE) (Berner, 1980; Boudreau, 1997) for solutes (C_i) and solids (C_j) due to transport and coupled chemical and biological

reaction can be written as:

$$\phi \frac{\partial C_i}{\partial t} = \underbrace{\frac{\partial \left(\phi \ (D_S + D_B) \frac{\partial C_i}{\partial x}\right)}{\partial x}}_{\text{diffusive mixing}} - \underbrace{\frac{\partial(\phi \ v C_i)}{\partial x}}_{\text{advection}} + \underbrace{\phi \ \alpha_i (C_{i(0)} - C_i)}_{\text{bioirrigation}} + \underbrace{\phi \sum R_i}_{\text{reaction}} \tag{1.1}$$

$$(1-\phi) \frac{\partial C_j}{\partial t} = \underbrace{\frac{\partial \left((1-\phi) \ D_B \frac{\partial C_j}{\partial x}\right)}{\partial x}}_{\text{bioturbation}} - \underbrace{\frac{\partial((1-\phi) \ w C_j)}{\partial x}}_{\text{advection}} + \underbrace{(1-\phi) \sum R_j}_{\text{reaction}} \tag{1.2}$$

where, t is time, x is the depth below the sediment-water interface, v is the burial velocity for solutes, w is the burial velocity for solids, D_S is the molecular diffusion coefficient, D_B is the bioturbation coefficient, α_i is the bioirrigation coefficient, $C_{i(0)}$ is the concentration of solutes at the sediment-water interface and $\sum R$ is the sum concentration change due to chemical and/or biological reactions.

A similar PDE is defined for every solute and solid explicitly included in the model as state variables. The set of the coupled PDEs is commonly solved by applying full or partial differencing techniques. In the "method-of-lines" (e.g. Boudreau, 1996), the PDE is discretized over space to give an time-dependent ordinary differential equation (ODE) at each depth interval which is then solved using commercially or publically-available ODE solvers. The second order PDEs in Eqs. 1.1 and 1.2 require two boundary conditions to obtain the model solution, one at the top and one at the bottom of the modeled sediment column. Boundary conditions can be fixed concentrations (Dirichlet type), for example bottom water concentrations for solutes at the top of the model, fixed fluxes (Robin type), for example carbon rain rates to the seafloor, or constant gradients (Neumann type) in the case of a species undergoing no reaction at and below the bottom of the sediment column and which are transported by burial only.

The multitude of biogeochemical reactions occurring within the sediments is ultimately driven by the deposition and degradation of organic matter, with the associated release of inorganic nitrogen and phosphorous. This is usually achieved in benthic models by using carbon as the model 'currency' and applying stoichiometric factors to define the C:N:P composition of organic matter. The kinetics of organic matter decomposition are fundamental for the accurate description of biogeochemical cycling. Several approaches for these kinetics have been proposed, e.g. G-type kinetics based on single or multiple carbon pools of discrete reactivity (Jørgensen, 1978; Berner, 1980), the power law model by Middelburg (1989) based on the age of organic matter where the reactivity decreases with time and the related continuum model of Boudreau and Ruddick (1991). Whilst these approaches are appropriate ways to simulate organic matter degradation below the depth of biological mixing, the effect of bioturbation on organic matter decomposition in the very surface of the sediment is still not fully understood.

1.3. Thesis outline

In the following three chapters, the scientific results of the work during my time as a PhD student are described. The first two chapters are articles published in or submitted to peer-reviewed journals while the third Chapter summarizes work which is not submitted yet.

Chapter 2 focuses on the benthic N cycle in sediments underlying the Peruvian OMZ along a transect at 11°S. A reaction-transport model is applied to field data, explicitly including the intermediate NO_2^- owing to its increased importance in oxygen-deficient environments. This modeling study is, to my knowledge, the first where in situ flux data and porewater profiles were used to quantify DNRA and anammox under a redox gradient of anoxic to suboxic bottom waters.
The local view of the benthic N cycling in Chapter 2 is brought to a global scale in Chapter 3. Here, benthic denitrification (including anammox) was estimated at sites from all over the world yielding a revised value for global denitrification rates in marine sediments. Simple transfer functions were derived to predict the loss of NO_3^- as N_2 gas via denitrification and/or anammox from bottom water chemistry and carbon rain rates to the seafloor only. This estimate is based on empirical data and provides an additional constraint on the broad range of reported literature values. Owing to its simplicity, the function can easily be dynamically coupled to global circulation models in order to calculate the wider significance of benthic denitrification.
Chapter 4 addresses organic matter degradation during early diagenesis. A compilation of measured benthic NO_3^- and O_2 fluxes, rain rates of organic carbon to seafloor and bottom water chemistry was used to constrain the down-core decrease of organic matter degradation in the well-mixed surface layer of the sediment.
Chapter 5 provides a general summary and synthesis relating the work described in this thesis to the current state of research.

Beyond the work presented in this thesis I was a co-author of the following manuscripts :

Sommer S., **Bohlen L.**, Dale A. W., Wallmann K., Hensen C., Mosch T., Noffke A. and Pfannkuche O. (submitted to *Global Biogeochemical Cycles*) Nitrogen fluxes across Peruvian oxygen minimum zone surface sediments - the potential significance of DNRA.

Dale A. W., Sommer S., **Bohlen L.**, Treude T., Bertics V. J., Bange H. W., Pfannkuche O., Schorp T., Mattsdotter M. and Wallmann K. (2011) Rates and regulation of nitrogen cycling in seasonally hypoxic sediments during winter (Boknis Eck, SW Baltic Sea): Sensitivity to environmental variables. *Estuarine, Coastal and Shelf Science* **95**, 14-28.

Noffke A., Hensen C., Sommer S., Scholz F., **Bohlen L.**, Mosch T. and Wallmann K. (submitted to *Limnology and Oceanography*) Benthic iron and phosphorus fluxes across the Peruvian oxygen minimum zone.

Mosch T., Sommer S., Dengler M., Noffke A., **Bohlen L.**, Pfannkuche O. and Wallmann K. (submitted to *Deep Sea Research I*) Structuring forces on epibenthic communities across the Peruvian oxygen minimum zone.

References

Anderson L. A. (1995) On The Hydrogen And Oxygen-Content Of Marine-Phytoplankton. *Deep-Sea Res. Pt. I* **42**, 1675-1680.

Berner R. A. (1980) *Early Diagenesis - A Theoretial Approach*. Princeton University Press.

Bertics V. J., Sohm J. A., Treude T., Chow C. E. T., Capone D. G., Fuhrman J. A. and Ziebis W. (2010) Burrowing deeper into benthic nitrogen cycling: the impact of bioturbation on nitrogen fixation coupled to sulfate reduction. *Mar. Ecol.-Prog. Ser.* **409**, 1-15.

Brandes J. A. and Devol A. H. (2002) A global marine-fixed nitrogen isotopic budget: Implications for holocene nitrogen cycling. *Global Biogeochem. Cy.* **16(4)**, 1120.

Boudreau B. P. (1996) A method-of-lines code for carbon and nutrient diagenesis in aquatic sediments. *Comput. Geosci.* **22**, 479-496.

Boudreau B. P. (1997) *Diagenetic Models and Their Implementation*. Springer-Verlag.

Boudreau B. P. and Ruddick B. R. (1991) On A Reactive Continuum Representation Of Organic-Matter Diagenesis. *Am. J. Sci.* **291**, 507-538.

Burdige D. (2006) *Geochemistry of Marine Sediments*, Princeton University Press.

Capone D. G., Zehr J. P., Paerl H. W., Bergman B. and Carpenter E. J. (1997) Trichodesmium, a globally significant marine cyanobacterium. *Science* **276**, 1221-1229.

Carpenter E. J. and Capone D. G. (2008) Nitrogen Fixation in the Marine environment. In *Nitrogen in the Marine Environment* (eds. Capone D., Bronk D., Mulholland M. and Carpenter E.) Elsevier Science Inc., pp.141-198.

Codispoti L. A., Brandes J. A., Christensen J. P., Devol A. H., Naqvi S. W. A., Paerl H. W. and Yoshinari T. (2001) The oceanic fixed nitrogen and nitrous oxide budgets: Moving targets as we enter the anthropocene? *Sci. Mar.* **65**, 85-105.

Dalsgaard T., Thamdrup B. and Canfield D. E. (2005) Anaerobic ammonium oxidation (anammox) in the marine environment. *Res. Microbiol.* **156**, 457-464.

Devol A. (2008) Denitrification including anammox. In *Nitrogen in the Marine Environment* (eds. Capone D., Bronk D., Mulholland M. and Carpenter E.) Elsevier Science Inc., pp. 263-301.

Falkowski P. G., Barber R. T. and Smetacek V. (1998) Biogeochemical controls and feedbacks on ocean primary production. *Science* **281**, 200-206.

Fossing H., Gallardo V. A., Jørgensen B. B., Hüttel M., Nielsen L. P., Schulz H., Canfield D. E., Forster S., Glud R. N., Gundersen J. K., Küver J., Ramsing N. B., Teske A., Thamdrup B., and Ulloa O. (1995) Concentration And Transport Of Nitrate By The Mat-Forming Sulfur Bacterium Thioploca. *Nature* **374**, 713-715.

Froelich P. N., Klinkhammer G. P., Bender M. L., Luedtke N. A., Heath G. R., Cullen D., Dauphin P., Hammond D., Hartman B. and Maynard V. (1979) Early Oxidation Of Organic-Matter In Pelagic Sediments Of The Eastern Equatorial Atlantic - Suboxic Diagenesis. *Geochim. Cosmochim. Ac.* **43**, 1075-1090.

Gallardo V. A. (1977) Large benthic microbial communities in sulphide biota under Peru-Chile subsurface countercurrent. *Nature* **268**, 331-332.

Galloway J. N., Dentener F. J., Capone D. G., Boyer E. W., Howarth R. W., Seitzinger S. P., Asner G. P., Cleveland C. C., Green P. A., Holland E. A., Karl D. M., Michaels A. F., Porter J. H., Townsend A. R. and Vorosmarty C. J. (2004) Nitrogen cycles: past, present, and future. *Biogeochemistry* **70**, 153-226.

Gruber N. (2004) The dynamics of the marine nitrogen cycle and its influence on the atmospheric CO_2 variations. In *The Ocean Carbon Cycle and Climate* (eds. Follows M. and Oguz T.). NATO ASI Series. pp. 97-148.

Gruber N. (2008) The marine nitrogen cycle: overview and challenges. In *Nitrogen in the Marine Environment* (eds. Capone D., Bronk D., Mulholland M. and Carpenter E.) Elsevier Science Inc., pp. 1-50.

Hamersley M. R., Lavik G., Woebken D., Rattray J. E., Lam P., Hopmans E. C., Damsté J. S. S., Krüger S., Graco M., Gutiérrez D., and Kuypers M. M. M. (2007) Anaerobic ammonium oxidation in the Peruvian oxygen minimum zone. *Limnol. Oceanogr.* **52**, 923-933.

Helly J. J. and Levin L. A. (2004) Global distribution of naturally occurring marine hypoxia on continental margins. *Deep-Sea Res. Pt. I* **51**, 1159 - 1168.

Jørgensen B. B. (1978) Comparison Of Methods For The Quantification Of Bacterial Sulfate Reduction In Coastal Marine-Sediments. 2. Calculation From Mathematical-Models. *Geomicrobiol. J.* **1**, 29-47.

Jørgensen B.B. (2006). Bacteria and marine biogeochemistry. In *Marine Geochemistry* (eds. Schulz H. D. and Zabel M.), 169-206. Springer Verlag, Berlin.

Jørgensen B. B. and Gallardo V. A. (1999) Thioploca spp: filamentous sulfur bacteria with nitrate vacuoles. *Fems Microbiol. Ecol.* **28**, 301-313.

Jørgensen B. B. and Nelson D. (2004) Sulfide oxidation in marine sediments: Geochemistry meets microbiology. In *Sulfur Biogeochemistry: Past and Present* (eds. Amend J. P., Edwards T. W. and Lyons K. J. E.). *Geological Society of America, Special Paper* **379**. pp. 63-81.

Kartal B., Kuypers M. M. M., Lavik G., Schalk J., den Camp H. J. M. O., Jetten M. S. M. and Strous M. (2007) Anammox bacteria disguised as denitrifiers: nitrate reduction to dinitrogen gas via nitrite and ammonium. *Environ. Microbiol.* **9**, 635-642.

Kienast M. (2000) Unchanged nitrogen isotopic composition of organic matter in the South China Sea during the last climatic cycle: Global implications. *Paleoceanography* **15**, 244-253.

Kuypers M. M. M., Sliekers A. O., Lavik G., Schmid M., Jørgensen B. B., Kuenen J. G., Damsté J. S. S., Strous M. and Jetten M. S. M. (2003) Anaerobic ammonium oxidation by anammox bacteria in the Black Sea. *Nature* **422**, 608-611.

Lam P., Lavik G., Jensen M. M., van de Vossenberg J., Schmid M., Woebken D., Dimitri G., Amann R., Jetten M. S. M. and Kuypers M. M. M. (2009) Revising the nitrogen cycle in the Peruvian oxygen minimum zone. *P. Natl. Acad. Sci. USA* **106**, 4752-4757.

Lam P. and Kuypers M. M. M. (2011) Microbial nitrogen cycling processes in oxygen minimum zones. *Annu. Rev. Mar. Sci.* **3**, 317-345.

Middelburg, J. J. (1989) A Simple Rate Model For Organic-Matter Decomposition In Marine-Sediments. *Geochim. Cosmochim. Ac.* **53**, 1577-1581.

Middelburg J. J., Soetaert K., Herman P. M. J. and Heip C. H. R. (1996) Denitrification in marine sediments: A model study. *Global Biogeochem. Cy.* **10(4)**, 661-673.

Nevison C. D., Butler J. and Elkins J. (2003) Global distribution of N_2O and the dN_2O/AOU yield in the subsurface ocean. *Global Biogeochem. Cy.* **17(4)**, 1119.

Oschlies A., Schulz K. G., Riebesell U. and Schmittner A. (2008) Simulated 21st century's increase in oceanic suboxia by CO_2-enhanced biotic carbon export. *Global Biogeochem. Cy.* **22**, GB4008.

Otte S., Kuenen J. G. , Nielsen L. P., Paerl H. W., Zopfi J., Schulz H. N., Teske A., Strotmann B., Gallardo V.A. and Jørgensen B. B. (1999) Nitrogen, carbon, and sulfur metabolism in natural Thioploca samples. *Appl. Environmental. Microb.* **65**, 3148-3157.

Ramaswamy V., Boucher O., Haigh J., Hauglustaine D., Haywood J., Myhre G., Nakajima T.,Shi G. Y. and Solomon S. (2001). Radiative forcing of climate change. In *Climate Change 2001: The Scientific Basis. Contribution of Working Group I to the Third Assessment Report of the Intergovernmental Panel on Climate Change* (eds. Houghton J. T., Ding Y., Griggs D. J., Noguer M., van der Linden P., Dai X., Maskell K. and Johnson C. A.). Cambridge University Press, Cambridge, Chapter 6. pp. 527-585.

Paulmier A. and Ruiz-Pino D. (2009) Oxygen minimum zones (OMZs) in the modern ocean. *Progr. Oceanogr.* **80**, 113-128.

Preisler A., de Beer D., Lichtschlag A., Lavik G., Boetius A. and Jørgensen B. B. (2007) Biological and chemical sulfide oxidation in a Beggiatoa inhabited marine sediment. *Isme J.* **1**, 341-353.

Sarmiento J. and Gruber, N. (2006) *Ocean Biogeochemical Dynamics*. Princeton University Press, Princeton, New Jersey.

Schulz H. N., Jørgensen B. B., Fossing H. A. and Ramsing N. B. (1996) Community structure of filamentous, sheath-building sulfur bacteria, Thioploca spp, off the coast of Chile. *Appl. Environ. Microbiol.* **62**, 1855-1862.

Stramma L., Johnson G. C., Sprintall J. and Mohrholz V. (2008) Expanding oxygen-minimum zones in the tropical oceans. *Science* **320**, 655-658.

Strous M., Kuenen J. G. and Jetten M. S. M. (1999) Key physiology of anaerobic ammonium oxidation. *Appl. Environ. Microbiol.* **65**, 3248-3250.

Thamdrup B. and Canfield D. E. (1996) Pathways of carbon oxidation in continental margin sediments off central Chile. *Limnol. Oceanogr.* **41**, 1629-1650.

Thamdrup B. and Dalsgaard T. (2002) Production of N_2 through anaerobic ammonium oxidation coupled to nitrate reduction in marine sediments. *Appl. Environ. Microb.* **68**, 1312-1318.

Thullner M., Dale A. W. and Regnier P. (2009) Global-scale quantification of mineralization pathways in marine sediments: A reaction-transport modeling approach. *Geochem. Geophy. Geosy.* **10**, Q10012.

Van Cappellen P. and Wang Y. (1996) Cycling of iron and manganese in surface sediments, a general theory for the coupled transport and reaction of carbon, oxygen, nitrogen, sulfur, iron, and manganese. *Am. J. Sci.* **296**, 197-243.

van de Graaf A. A., Mulder A, Slijkhuis H., Robertson L. A. and Kuenen J. G. (1990) Anoxic ammonium oxidation, In *Proceedings of the Fifth European Congress on Biotechnology*, vol. 1 (eds. Christiansen C., Munck L., Villadsen J.),Munksgaard, Copenhagen, pp. 388-391.

Wyrtki K. (1962) The oxygen minima in relation to ocean circulation. *Deep Sea Research and Oceanographic Abstracts* **9**, 11-23.

Zehr J. P. and Ward B. B. (2002) Nitrogen cycling in the ocean: New perspectives on processes and paradigms. *Appl. Environ. Microbiol.* **68**, 1015-1024.

Zehr J. P., Waterbury J. B., Turner P. J., Montoya J. P., Omoregie E., Steward G. F., Hansen A. and Karl D. M. (2001) Unicellular cyanobacteria fix N-2 in the subtropical North Pacific Ocean. *Nature* **412**, 635-638.

2. Benthic nitrogen cycling in the Peruvian oxygen minimum zone

L. Bohlen*, A. W. Dale, S. Sommer, T. Mosch, C. Hensen, A. Noffke, F. Scholz and K. Wallmann

Leibniz Institute of Marine Sciences (IFM-GEOMAR), Wischhofstr. 1 - 3, 24148 Kiel, Germany
* author for correspondence : lbohlen@ifm-geomar.de

Published in 2011 in *Geochimica et Cosmochimica Acta* 75, pp. 6094-6111

Abstract

Benthic nitrogen (N) cycling was investigated at six stations along a transect traversing the Peruvian oxygen minimum zone (OMZ) at 11 °S. An extensive dataset including porewater concentration profiles and in situ benthic fluxes of nitrate (NO_3^-), nitrite (NO_2^-) and ammonium (NH_4^+) was used to constrain a 1-D reaction-transport model designed to simulate and interpret the measured data at each station. Simulated rates of nitrification, denitrification, anammox and dissimilatory nitrate reduction to ammonium (DNRA) by filamentous large sulfur bacteria (e.g. *Beggiatoa* and *Thioploca*) were highly variable throughout the OMZ yet clear trends were discernible. On the shelf and upper slope (80 - 260 m water depth) where extensive areas of bacterial mats were present, DNRA dominated total N turnover ($\leq$ 2.9 mmol N m^{-2} d^{-1}) and accounted for $\geq$ 65 % of NO_3^- + NO_2^- uptake by the sediments from the bottom water. Nonetheless, these sediments did not represent a major sink for dissolved inorganic nitrogen (DIN = NO_3^- + NO_2^- + NH_4^+) since DNRA reduces NO_3^- and, potentially NO_2^-, to NH_4^+. Consequently, the shelf and upper slope sediments were recycling sites for DIN due to relatively low rates of denitrification and high rates of ammonium release from DNRA and ammonification of organic matter. This finding contrasts with the current opinion that sediments underlying OMZs are a strong sink for DIN. Only at greater water depths (300 - 1000 m) did the sediments become a net sink for DIN. Here, denitrification was the major process ($\leq$ 2 mmol N m^{-2} d^{-1}) and removed 55 - 73 % of NO_3^- and NO_2^- taken up by the sediments, with DNRA and anammox accounting for the remaining fraction. Anammox was of minor importance on the shelf and upper slope yet contributed up to 62 % to total N_2 production at the 1000 m station. The results indicate that the partitioning of oxidized N (NO_3^-, NO_2^-) into DNRA or denitrification is a key factor determining

the role of marine sediments as DIN sinks or recycling sites. Consequently, high measured benthic uptake rates of oxidized N within OMZs do not necessarily indicate a loss of fixed N from the marine environment.

2.1. Introduction

As a limiting nutrient for biological productivity, nitrogen (N) occupies a central role in the biogeochemistry of the marine environment and exerts a significant influence on other elemental cycles, in particular carbon (Falkowski, 1997; Gruber, 2004). Bioavailable, or reactive, N in the ocean includes nitrate (NO_3^-), nitrite (NO_2^-) and ammonium (NH_4^+), whereas dinitrogen gas (N_2) is only accessible for nitrogen fixing bacteria. For the most part, the oceanic inventory of dissolved inorganic nitrogen (DIN = NO_3^- + NO_2^- + NH_4^+) depends on the balance between losses via denitrification (Codispoti et al., 2001; Gruber, 2004) and anammox (Dalsgaard et al., 2003; Kuypers et al., 2003) and gains through N_2 fixation.
Denitrification and anammox occur prominently in the water column in oxygen minimum zones (OMZs) and in anoxic marine sediments and together determine the extent of N deficit in these environments (Gruber and Sarmiento, 1997; Codispoti et al., 2001). An imbalance between sources and sinks of DIN may affect the intensity and potential growth of OMZs. For example, a loss of DIN from the water column due to denitrification or anammox may result in lower primary and export production and diminished oxygen (O_2) consumption rates in deeper water masses. Such a negative feedback could limit the ongoing spreading of OMZs (Oschlies et al., 2008; Stramma et al., 2008). However, benthic release of DIN potentially stimulates primary production and O_2 consumption in the water column, exacerbated by increased phosphorus fluxes from sediments underlying O_2-deficient waters (e.g. Ingall and Jahnke, 1994; Wallmann, 2010). This could drive the expansion of OMZs in a similar way to the biogeochemical feedback mechanisms driving Cretaceous ocean anoxic events (Van Cappellen and Ingall, 1994).
On a global scale marine sediments have been identified as fixed N sinks (e.g. Brandes and Devol, 2002), yet their source-sink function on regional scales is currently unclear (Fulweiler et al., 2007). Sediments underlying the hypoxic waters of upwelling regions are commonly perceived as sinks for DIN (Middelburg et al., 1996; Gruber and Sarmiento, 1997). Rate measurements are scarce, but those which do exist generally support this idea (Berelson et al., 1987; Devol and Christensen, 1993; Hartnett and Devol, 2003; Glud et al., 2009; Schwartz et al., 2009; Woulds et al., 2009). A recent study along 11 °S within the Peruvian OMZ (Sommer et al., submitted) showed the sediments were a sink for DIN on the continental slope at water depths with low dissolved O_2. However, on the shelf and upper slope the opposite was true. Here, mats of large vacuolated sulfur bacteria such as *Thioploca* and *Beggiatoa* (Mosch et al., 2010) were observed. These microorganisms internally store NO_3^- and, potentially NO_2^-, from the overlying seawater at millimolar concentrations (Fossing et al., 1995;

Zopfi et al., 2001). The NO_3^- is used as an electron acceptor for sulfide oxidation in a process termed dissimilatory nitrate reduction to ammonium (DNRA), by which the microorganisms gain metabolic energy (e.g. Otte et al., 1999; Jørgensen and Nelson, 2004; Preisler et al., 2007). Large NH_4^+ effluxes have been measured on the shelf in these areas (Sommer et al., submitted), and a rudimentary N mass balance by these workers indicates that a major proportion of the total NO_3^- + NO_2^- uptake on the Peruvian shelf is channeled into DNRA rather than denitrification and anammox. DNRA by large sulfur bacteria has been identified as an important process in the N cycle and source of NH_4^+ to the porewater in organic matter-rich sediments on the continental shelf (Christensen et al., 2000; Graco et al., 2001; Otte et al., 1999; Dale et al., 2011). Critically, though, DNRA does not result in a net loss of DIN but instead recycles fixed N to the overlying water column in the form of NH_4^+. The significance of this process in the marine N budget is unknown.

The aim of this study is to investigate N cycling in the Peruvian OMZ sediments along 11 °S and identify the major benthic N turnover processes under the changing redox conditions. We used a reaction-transport model constrained by measured in situ N fluxes and porewater geochemical profiles to explain the observed shift of the sediments as recycling sites for DIN on the shelf to DIN sinks down the continental slope. In contrast to previous modeling studies that simulated denitrification as a direct conversion of NO_3^- to N_2 (e.g. Middelburg et al., 1996; Van Cappellen and Wang, 1996), the role of the intermediate species, NO_2^-, is considered here owing to high concentrations in the water column on the shelf. We also focus on the importance of DNRA to N turnover since previous modeling studies suggest that it may dominate benthic sulfur and nitrogen cycling in suboxic upwelling regions as well as organic-rich costal sediments where sulfide accumulates in the porewater (e.g. Dale et al., 2009; 2011). Furthermore, because of the widespread occurrence of bacterial mats off southern Peru and Chile we expect this process to be significant (e.g. Gallardo, 1977; Fossing et al., 1995; Thamdrup and Canfield, 1996). To our knowledge this is the first modeling study to combine in situ flux data and numerical modeling to quantify DNRA and anammox along a redox gradient through fully anoxic to hypoxic bottom waters.

2.2. Study area

The Peruvian upwelling region forms part of the eastern boundary current system of the Eastern Tropical South Pacific. Alongshore winds engender offshore Ekman transport of surface waters which are replaced by O_2-poor, nutrient-rich equatorial subsurface waters of the Peru-Chile undercurrent (Fiedler and Talley, 2006; Silva et al., 2009). Upwelling stimulates high rates of primary productivity (1.8 - 3.6 g C m^{-2} d^{-1}, Reimers and Suess, 1983; Pennington et al., 2006; Fernández et al., 2009) and supports the development of an extensive OMZ (Fiedler and Talley, 2006; Silva et al., 2009). The upwelling intensity is seasonally variable and is most intense in austral winter and

spring with interannual variability imposed by the El Niño Southern Oscillation (Morales et al., 1999; Kessler, 2006). The vertical extension of the OMZ reaches 700 m water depth off Peru (defined as $O_2 < 20$ μmol kg^{-1}; Fuenzalida et al. 2009), with an upper boundary that may be as shallow as 50 m (Morales et al., 1999) and deepen to ca. 200 m (e.g. Levin et al., 2002) during strong El Niño events. The present study area at 11 °S (Fig. 2.1) is located within the most intense coastal upwelling region and falls with the region of maximum primary productivity (Krissek et al., 1980; Pennington et al., 2006). This results in the formation of an upper-slope diatomaceous mud lens rich in organic-carbon and poor in carbonate between 10.5 °S and 13.6 °S (Zuta and Guillén, 1970; Krissek et al., 1980; Reimers and Suess, 1983). Preservation and burial of organic matter within the mud lens is supported by high sediment accumulation rates and diminished bottom current velocities (Suess et al., 1987). Sediment accumulates preferentially at water depths between 100 and 450 m and below 2000 m, whereas lower accumulation rates are found in the middle slope due to fluctuations in bottom current velocities (Reimers and Suess, 1983). At the time of sampling, the OMZ (defined here as < 10 μM O_2) extended from a water depth of ca. 50 - 550 m (Fig. 2.1) and minimum bottom water O_2 concentrations were below the analytical detection limit (2 μM). In these anoxic areas, the surface sediments were characterized by extensive coverage by mats of large vacuolated sulfur bacteria such as *Thioploca* and *Beggiatoa* (Mosch et al., 2010).

2.3. Material and Methods

2.3.1. Sampling and geochemical analysis

Sediment cores were taken at 6 stations during two expeditions on RV Meteor (M77, leg 1 and 2) from October to December 2008 (late austral spring, high upwelling season) using multi-corers (MUC) and benthic lander deployments (BIGO). The latter were used to determine in situ fluxes of NH_4^+, NO_3^-, NO_2^- and, at the 2 deepest stations (5 and 6), total oxygen uptake (TOU). Complete details of the benthic flux measurements are provided by Sommer et al. (submitted). Locations and water depths at the stations are listed in Table 2.1. With the exception of station 2, sediment samples were taken using both MUC and BIGO technologies. The retrieved cores were immediately transferred to a cool room onboard at 4 °C and processed within a few hours. Two parallel cores were taken for all MUC deployments. The first core was sub-sampled for redox sensitive constituents under anoxic conditions using an argon-filled glove bag. Sediment sections for porewater extraction were transferred into tubes pre-flushed with argon gas and subsequently centrifuged at max. 4500 G for 20 minutes. Prior to analysis, the supernatant porewater was filtered with 0.2 μm cellulose acetate Nuclepore® filters within the glove-bag. The centrifugation tubes with the remaining solid phase of the sediment were stored for further analysis onshore. The second core was sub-sampled for porewater (i) without the glove-bag by squeezing 1 - 2 cm thick slices using a low pressure squeezer

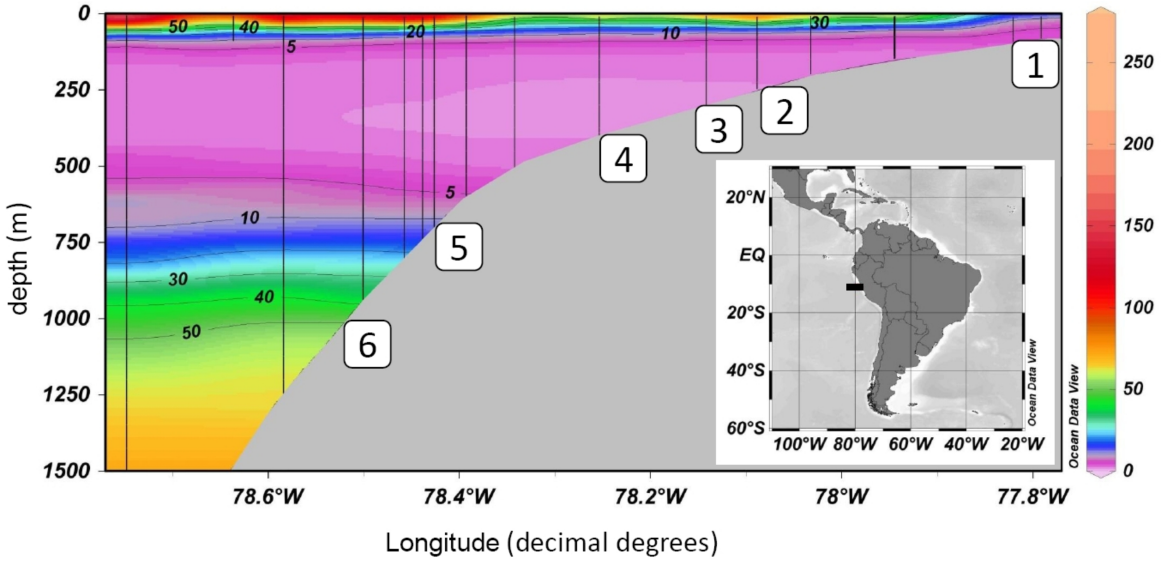

Figure 2.1.: Cross-section of oxygen concentrations (µM) on the shelf and slope of the Peruvian OMZ at 11 °S. The vertical lines denote the CTD casts where O_2 measurements were made on cruise M77 leg 1. Station locations 1 to 6 for benthic studies are indicated. Note concentrations were ca. 45 µM at 10 m depth on the shelf, and that higher concentrations in the surface layers are not visible on this scale.

(argon at 2.5 bar) and filtering (0.2 µm) into recipient vessels, or (ii) anaerobically using rhizons®. For the BIGO deployments containing two chambers one core was taken from each. All BIGO cores were processed anaerobically with the glove bag as described above.
Samples for bottom water analysis were taken from the supernatant water of the sediment cores and from syringes attached to the outside of the benthic lander directly above the seabed.

Ammonium (NH_4^+), nitrite (NO_2^-), dissolved ferrous iron (Fe^{2+}), and total dissolved sulfide ($TH_2S \sim H_2S + HS^-$) were measured onboard using standard photometric techniques (Grasshoff et al., 1999). Aliquots of porewater were diluted with O_2-free artificial seawater prior to analysis where necessary. Porewater samples for Fe^{2+} analysis were treated with ascorbic acid directly after filtering (0.2 µm). Detection limits for NH_4^+, NO_2^- and TH_2S were 1 µM. Total alkalinity (TA) was determined onboard by direct titration of 1 ml porewater with 0.02 M HCl according to Ivanenkov and Lyakhin (1978) with an error of 0.05 meq l^{-1}. The titration method was calibrated using IAPSO seawater standard. Ion chromatography was used to determine nitrate (NO_3^-) and occasionally sulfate (SO_4^{2-}) in the onboard laboratory. Additional SO_4^{2-} analysis was performed onshore in porewater samples stored and transported in plastic vials. NO_3^- and SO_4^{2-} were measured with a detection limit of 1 µM and 10 µM, respectively and a relative error of 5 % and 2 %.
The solid phases were freeze-dried and analyzed for total particulate carbon, particulate organic nitrogen (PON) and total particulate sulfur (TPS) using a Carlo-Erba element analyzer (NA 1500). Particulate organic carbon (POC) content was determined on the residue after acidifying the sample

Table 2.1.: Overview of stations and gear deployments.

Station no.	Core identifier	Date (2008)	Latitude (S)	Longitude (W)	Water depth (m)
1	M77–1 568 BIGO 5	Nov. 15	11°00.02’	77°47.72’	85
	M77–1 543 MUC 52	Nov. 12	10°59.99’	77°47.40’	78
2	M77–2 016 BIGO T6	Nov. 29	10°59.80’	78°05.91’	259
3	M77–1 464 BIGO 1	Nov. 5	11°00.00’	78°09.92’	315
	M77–1 449 MUC 19	Nov. 3	11°00.01’	78°09.97’	319
4	M77–1 626 BIGO 3	Nov. 20	11°00.02’	78°15.27’	397
	M77–1 481 MUC 33	Nov. 6	11°00.00’	78°14.19’	376
5	M77–1 474 BIGO 2	Nov. 5	11°00.01’	78°25.55’	695
	M77–1 459 MUC 25	Nov. 4	11°00.03’	78°25.60’	697
6	M77–2 013 BIGO 6	Nov. 29	10°59.82’	78°31.05’	978
	M77–1 549 MUC 53	Nov. 13	10°59.81’	78°31.27’	1005

with HCl (detection limit < 0.1 wt-% and relative error of 3%). Inorganic carbon was determined by weight difference. Additional sediment samples were embedded in epoxy resin for determination of gamma-ray excess ^{210}Pb activities at 46.5 keV on a low-background coaxial Ge(Li) detector.
Porosity was determined from the weight of the freeze-dried sediment and the water content. The volume fraction of the sediment was calculated using a dry sediment density of 2 g cm^{-3} (Böning et al., 2004). Further analytical details corresponding to the benthic lander deployments are described by Sommer et al. (submitted).

2.3.2. Numerical modeling

Coupling reaction and transport

A 1-D numerical reaction-transport model was developed to simulate the biogeochemical cycles in the surface sediments at the 6 sampling stations along the 11 °S transect. The length of the modeled domain, L, varied between 20 and 50 cm. In total 10 solutes were considered, including O_2, NO_3^-, NO_2^-, NH_4^+, N_2, TH_2S, SO_4^{2-}, Fe^{2+} as well as NO_3^- and NO_2^- stored in large sulfur bacteria ($NO_{3\,bac}^-$, $NO_{2\,bac}^-$). Solid species considered were POC, PON, adsorbed NH_4^+ ($NH_{4\,ads}^+$), reactive iron oxide (FeOOH), sulfide-bound iron (FeII), TPS and excess ^{210}Pb. Solute and solid concentrations were modeled in units of mmol cm^{-3} of porewater and dry weight percent (wt-%), respectively, except for $NH_{4\,ads}^+$ (mmol g^{-1}). The modeled reaction network and rate expressions are described in Table 2.2 and the corresponding parameters are in Tables A.1 and A.2 in Appendix A. Chemical species in the simulated sediment column were transported by advection due to sediment accumulation and compaction, molecular diffusion (for solutes), sediment mixing by fauna (bioturbation), non-local

Table 2.2.: Reaction network used in the model. Model parameters are listed in Tables A.1 and A.2 in Appendix A.

Process	Stoichiometry	Rate expression [a]
R_1	$(CH_2O)(NH_3)_{rNC} + O_2 \rightarrow$ $(1 - r_{NC})CO_2 + (r_{NC})HCO_3^- + r_{NC}\,NH_4^+ + (1 - r_{NC})H_2O$	$R_{POC} \times \frac{[O_2]}{[O_2] + K_1}$
R_2	$(CH_2O)(NH_3)_{rNC} + 2\,NO_3^- \rightarrow$ $2\,NO_2^- + (1 - r_{NC})\,CO_2 + (r_{NC})HCO_3^- + r_{NC}\,NH_4^+ + (1 - r_{NC})H_2O$	$R_{POC} \times \frac{[NO_3^-]}{[NO_3^-] + K_2} \times \frac{K_3}{[NO_2^-] + K_3} \times \frac{K_1}{[O_2] + K_1}$
R_3	$(CH_2O)(NH_3)_{rNC} + 4/3\,NO_2^- + (1/3 + r_{NC})CO_2 \rightarrow$ $2/3\,N_2 + (4/3 + r_{NC})HCO_3^- + r_{NC}\,NH_4^+ + (1/3 - r_{NC})H_2O$	$R_{POC} \times \frac{[NO_2^-]}{[NO_2^-] + K_3} \times \frac{K_1}{[O_2] + K_1}$
R_4	$(CH_2O)(NH_3)_{rNC} + 4\,FeOOH + (7 + r_{NC})CO_2 + (1 + r_{NC})H_2O \rightarrow$ $4\,Fe^{2+} + (8 + r_{NC})HCO_3^- + r_{NC}\,NH_4^+$	$R_{POC} \times \frac{[FeOOH]}{[FeOOH] + K_4} \times \frac{K_2}{[NO_3^-] + K_2} \times \frac{K_3}{[NO_2^-] + K_3} \times \frac{K_1}{[O_2] + K_1}$
R_5	$(CH_2O)(NH_3)_{rNC} + 0.5\,SO_4^{2-} + (r_{NC})CO_2 + (r_{NC})H_2O \rightarrow$ $0.5\,H_2S + (1 + r_{NC})HCO_3^- + r_{NC}\,NH_4^+$	$R_{POC} \times \frac{K_4}{[FeOOH] + K_4} \times \frac{K_2}{[NO_3^-] + K_2} \times \frac{K_3}{[NO_2^-] + K_3} \times \frac{K_1}{[O_2] + K_1}$
R_6	$NH_4^+ + 3/2\,O_2 + 2\,HCO_3^- \rightarrow NO_2^- + 3\,H_2O + 2\,CO_2$	$k_6 \times [O_2] \times [NH_4^+]$
R_7	$NO_2^- + 1/2\,O_2 \rightarrow NO_3^-$	$k_7 \times [O_2] \times [NO_2^-]$
R_8	$NH_4^+ + NO_2^- \rightarrow N_2 + 2\,H_2O$	$k_8 \times [NO_2^-] \times [NH_4^+]$
R_9	$HS^- + NO_3^- + CO_2 + 2\,H_2O \rightarrow SO_4^{2-} + NH_4^+ + HCO_3^-$	$k_9 \times [NO_3^-{}_{bac}] \times [TH_2S]$
R_{10}	$HS^- + 4/3\,NO_2^- + 5/3\,CO_2 + 9/3\,H_2O \rightarrow SO_4^{2-} + 4/3\,NH_4^+ + 5/3\,HCO_3^-$	$k_{10} \times [NO_2^-{}_{bac}] \times [TH_2S]$
R_{11}	$NH_4^+ \leftrightarrow NH_4^+{}_{ads}$	$k_{11} \times (1 - [NH_4^+{}_{ads}]/([NH_4^+] \times K_{NH4}))$ [b]
R_{12}	$Fe^{2+} + 1/4\,O_2 + 2\,HCO_3^- \rightarrow FeOOH + 2\,CO_2 + 1/2\,H_2O$	$k_{12} \times [O_2] \times [Fe^{2+}]$
R_{13}	$HS^- + 2\,O_2 + HCO_3^- \rightarrow SO_4^{2-} + CO_2 + H_2O$	$k_{13} \times [O_2] \times [TH_2S]$
R_{14}	$Fe^{2+} + 1/5\,NO_3^- + 9/5\,HCO_3^- \rightarrow FeOOH + 1/10\,N_2 + 9/5\,CO_2 + 2/5\,H_2O$	$k_{14} \times [NO_3^-] \times [Fe^{2+}]$

(a) The factor $f_i = \varphi/(1-\varphi) \times M_i/(10 \times ds)$ where M_i is the molecular mass of species i (g mol^{-1}), was used to convert between dissolved species in units of mmol cm^{-3} of porewater and solid phase species in dry weight percent (wt–%).
(b) The factor $\varphi/((1-\varphi) \times ds)$ was used to convert between dissolved and adsorbed NH_4^+ (mmol g^{-1}).

transport of solutes by fauna (bioirrigation) and non-local transport of $NO_3^-{}_{bac}$ and $NO_2^-{}_{bac}$ due to chemotaxis of large sulfur bacteria. Low Peclet numbers (« 1) over the length of the modeled sediment column (50 cm) illustrate that diffusion rather than advection is the dominant transport process for solutes below the irrigation layer (Boudreau, 1997). The following mass conservation equations were used to describe the temporal concentration change of solutes (C_i), $NO_3^-{}_{bac}$ and $NO_2^-{}_{bac}$ (C_b), and solids (C_j), due to transport and reaction:

$$\begin{aligned}
\phi\frac{\partial C_i}{\partial t} &= \frac{\partial\left(\phi\ (D_S + D_B)\frac{\partial C_i}{\partial x}\right)}{\partial x} - \frac{\partial(\phi\ vC_i)}{\partial x} + \phi\ \alpha_i(C_{i(0)} - C_i) + \phi\sum R_i \\
\phi\frac{\partial C_b}{\partial t} &= \phi\ \alpha_b(C_{b(0)} - C_b) + \phi\sum R_b \\
(1-\phi)\frac{\partial C_j}{\partial t} &= \frac{\partial\left((1-\phi)\ D_B\frac{\partial C_j}{\partial x}\right)}{\partial x} - \frac{\partial((1-\phi)\ wC_j)}{\partial x} + (1-\phi)\sum R_j
\end{aligned} \tag{2.1}$$

where t (yr) is time, x (cm) is depth below the sediment-water interface, ϕ (dimensionless) is porosity, v (cm yr^{-1}) is the burial velocity for solutes, w (cm yr^{-1}) is the burial velocity for solids, D_S (cm^2 yr^{-1}) is the tortuosity corrected molecular diffusion coefficient, D_B (cm^2 yr^{-1}) is the bioturbation coefficient, α_i (yr^{-1}) is the bioirrigation coefficient, α_b (yr^{-1}) is the coefficient for non-local NO_3^- and NO_2^- transport by bacteria, $C_i(0)$ and $C_b(0)$ are the concentrations of solutes and NO_3^- or NO_2^- in bacteria at the sediment-water interface, respectively, and $\sum R$ is the sum concentration change due to chemical reactions. $NO_3^-{}_{bac}$ and $NO_2^-{}_{bac}$ were assumed to be confined to the vacuoles and thus not transported by diffusion or burial. In these equations ϕ, D_S, D_B, v, w, α_i, α_b are depth-dependent and explained in more detail in Appendix A.

The model was run to steady-state ($\partial C/\partial t = 0$), although we are aware that the shelf is a more transient environment than the deeper slope settings. For example, an increase in POC accumulation rates began around 1820 AD (Gutiérrez et al., 2009) and the shelf bottom waters were renewed and ventilated in 1993 and 1997/98 in response to El Niño events (Gutiérrez et al., 2008). Nonetheless, we argue that (i) the relatively slow change in solid accumulation rates beginning ca. 200 years ago allows the solutes in the upper 50 cm to approach dynamic equilibrium with regard to POM mineralization, and (ii) the 13 year period since the last major oxygenation event on the shelf is sufficiently long for the N fluxes and turnover rates in the surface layers impacted by microbial mats (< 10 cm) also to have reached quasi-steady state conditions. In support of this argument, diffusion time-scales calculated from the modified Einstein-Smoluchowski equation (Jørgensen et al., 2004) for a typical solute are on the order of 10 and 1 yr for the upper 50 and 10 cm of the sediment, respectively.

Reaction network

The biogeochemical reactions considered (Table 2.2) were driven by the degradation of particulate organic matter (POM), defined chemically as $(CH_2O)(NH_3)_{rNC}$ where rNC is the molar ratio of N:C. POM was degraded by aerobic respiration (R_1), denitrification (R_2, R_3), iron oxide reduction (R_4) and sulfate reduction (R_5). Manganese oxide reduction and methanogenesis were neglected because measured dissolved and solid Mn concentrations were low (< 1 μM and < 0.05 wt-%, respectively) and SO_4^{2-} was never exhausted over the modeled sediment layer. The organic nitrogen in POM was liberated as NH_4^+ during mineralization rather than being directly coupled to nitrification (Van Cappellen and Wang, 1996) since these processes are mediated by different groups of microorganisms. The relative rates of each POM degradation pathway were determined using Michaelis-Menten kinetics (e.g. Boudreau, 1996), where the electron acceptors O_2, NO_3^-, NO_2^-, FeOOH and SO_4^{2-} were used sequentially in this order until their concentrations decreased to limiting levels defined by different half saturation constants (K) for each electron acceptor. Bimolecular rate laws were used for all secondary redox reactions (Van Cappellen and Wang, 1996).
TA was not modeled explicitly and was calculated from the major ion concentrations at each depth (x) relative to their concentrations at the sediment-water interface (x = 0) using the explicit conservative expression for TA (Wolf-Gladrow et al., 2007):

$$\begin{aligned} TA(x) = TA(0) &- (NO_3^-(x) - NO_3^-(0)) + (NH_4^+(x) - NH_4^+(0)) - 2 \cdot (SO_4^{2-}(x) \\ &- SO_4^{2-}(0)) - (NO_2^-(x) - NO_2^-(0)) + 2 \cdot (Fe^{2+}(x) - Fe^{2+}(0)) \end{aligned} \tag{2.2}$$

A schematic overview of the modeled N cycle is shown in Fig. 2.2A. Organic nitrogen was released as NH_4^+ during POM mineralization (ammonification, R_{AMF}). Canonical denitrification was modeled as a two-step process (R_2, R_3) with NO_2^- as an intermediate species. The kinetics of this process was formulated such that POM degradation via NO_3^- was inhibited by the accumulation of NO_2^- (Table 2.2), i.e. POM was preferentially degraded by NO_2^-. We took this approach since denitrifying organisms harvest a greater amount of catabolic energy during the reduction of NO_2^- to N_2 compared to NO_3^- reduction to NO_2^- under standard conditions (Thauer et al., 1977; Lam and Kuypers, 2011). Similarly, nitrification, was described as the stepwise oxidation of NH_4^+ to NO_2^- followed by NO_2^- to NO_3^- (R_6, R_7). In our model, therefore, NO_2^- was allowed to accumulate in the porewater, thus permitting competition between denitrification (R_3), nitrification (R_7) and anammox (R_8) for NO_2^-. The latter process produces N_2 gas from NO_2^- and NH_4^+ (Thamdrup and Dalsgaard, 2002; Dalsgaard et al., 2005) and is an important pathway of nitrogen loss in the marine environment (Thamdrup and Dalsgaard, 2002; Daalsgaard et al., 2005; Hamersley et al., 2007; Lam et al., 2009). Denitrification coupled to Fe^{2+} oxidation (Straub et al., 1996) was also considered to compete with canonical denitrification for NO_3^-. However, simulations (not shown) revealed that this process was of minor importance (contributing < 0.1 % to total N_2 production) and will thus not be discussed further. In what follows, the term 'denitrification' applies to canonical denitrification (i.e. R_2 followed by R_3)

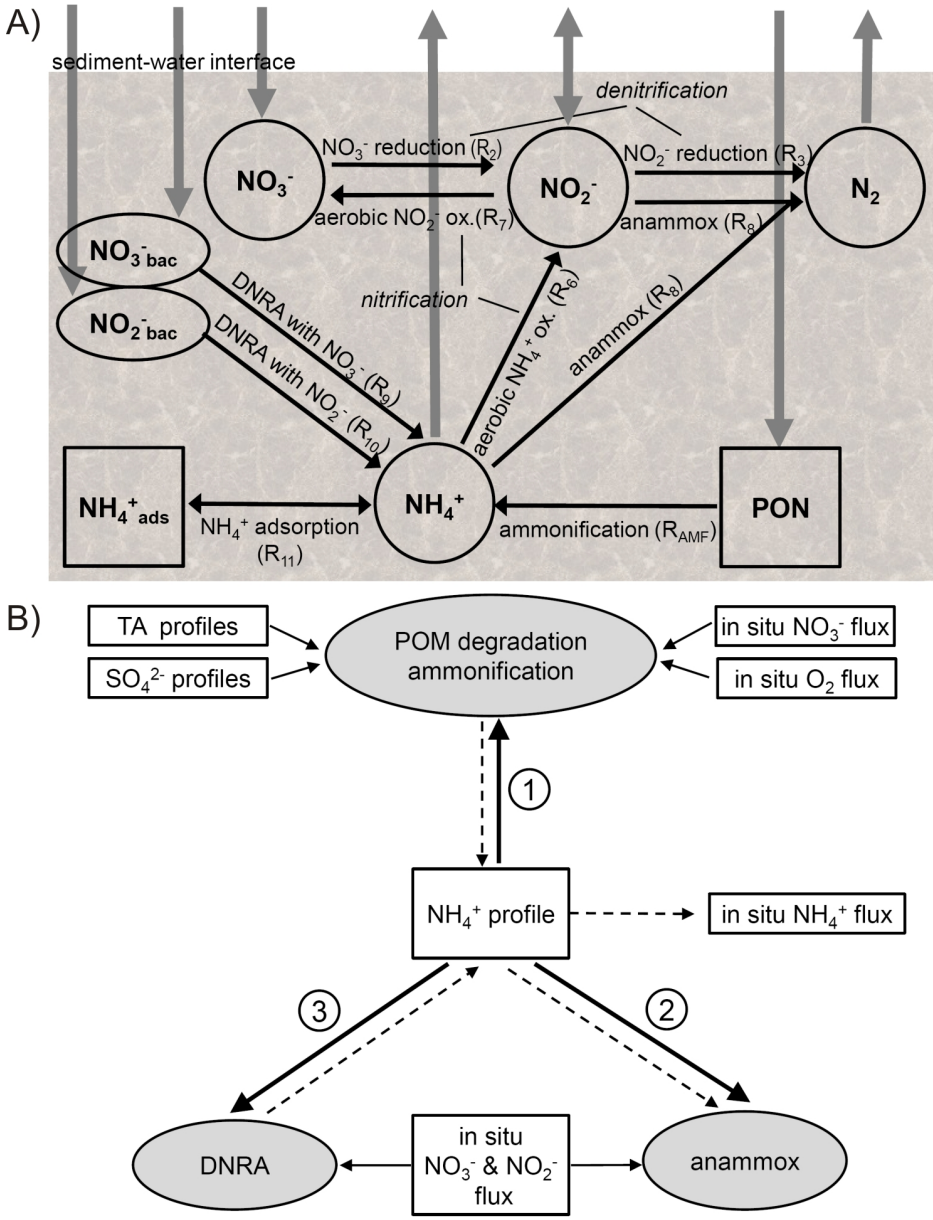

Figure 2.2.: A) The N cycle considered in the model. Circles and squares denote porewater and solid species, respectively, and the ellipses denote filamentous sulfur bacteria. Reactions simulated with the model are shown with black arrows and the fluxes across the sediment-water interface are shown by dashed arrows. The stoichiometry of the reactions is listed in Table 2.2. B) Procedure used to constrain the rates of POM degradation, DNRA and anammox described in the text (steps #1 to 3). Rectangles denote measured data and ellipses denote biogeochemical processes. Black arrows show constraints described in the text and the dashed arrows denote sources and sinks of NH_4^+. The rate constants for NH_4^+ oxidation and adsorption were fixed and these processes are not shown.

Table 2.3.: Model boundary conditions at the sediment-water interface.

	station 1	station 2	station 3	station 4	station 5	station 6
O_2 [µM]	0 [a]	0 [a]	0 [a]	0 [a]	8	40
NO_3^- [µM]	3.1	15	26	33	40	40
NO_2^- [µM]	11.5	2.3	2.85	0.48	0.25	0.27
NH_4^+ [µM]	0.45	1.1	1.14	0.56	0.02	0
SO_4^{2-} [mM]	29	29	29	29	29	29
TH_2S [µM]	0	0	0	0	0	0
Fe^{2+} [µM]	0	0	0	0	0	0
TA [mM]	1.96	2.38	2.23	2.5	2.28	2.35
N_2 [µM] [b]	489	498	501	532	553	574
$NO_{3\,bac}^-$ [µM]	119 [c]	100 [d]	102 [c]	33 [c]	–	–
$NO_{2\,bac}^-$ [µM]	12	–	–	–	–	–
POC (mmol m^{-2} d^{-1}) [e]	14.3	11.8	9.4	6.9	9.1	5.9
PON (mmol m^{-2} d^{-1}) [f]	1.63	1.10	0.99	0.80	0.9	0.53
TPS (mmol m^{-2} d^{-1})	0	0	0	0	0	0
FeOOH (mmol m^{-2} d^{-1})	1.73	0.12	0.11	0.15	0.49	0.46

(a) below analytical detection limit (< 2 µM)
(b) calculated according to Hamme and Emerson (2004) using site-specific temperature (Table A.2) and a salinity of 35
(c) estimated from porewater NO_3^- concentrations after sediment squeezing
(d) estimated from values at stations 1 and 3
(e) determined from the mass balance for upper 10 cm (Sommer et al., submitted)
(f) calculated from the POC flux applying measured N:C values (r_{NC}, Table A.2)

rather than anammox (R_8).

At station 1, where bottom water NO_2^- was elevated and NO_3^- concentrations were low (Table 2.3), DNRA was allowed to proceed using both NO_3^- (R_9) and NO_2^- (R_{10}) as electron acceptors. In support of this assumption, Zopfi et al. (2001) observed positive chemotaxis of *Thioploca* toward NO_2^-, suggesting a direct response of large sulfur bacteria to NO_2^-. At the other stations where seawater NO_2^- concentrations were < 3 µM (Table 2.3), NO_3^- was considered to be the only available electron acceptor for DNRA.

NH_4^+ was allowed to adsorb onto sediment particles (R_{11}). Although this process is more correctly described as a dynamic equilibrium between dissolved and adsorbed NH_4^+ defined by an empirical equilibrium constant, K_{NH4} (Morse and Morin, 2005), it was simulated as a kinetic process whose rate is partially determined by the departure from equilibrium (Table 2.2). The rate constant was set to sufficiently large values to ensure that dynamic equilibrium between dissolved and adsorbed ammonium was always maintained (Wallmann et al., 2008).

Although iron and sulfur cycling were included in the reaction network through their coupling with the nitrogen cycle, only the most relevant reactions were considered. Labile FeOOH can undergo dissimilatory iron reduction (R_4) producing Fe^{2+}. Subsequently, Fe^{2+} may be either oxidized by O_2- (Table 2.2) to FeOOH or be precipitated as sedimentary iron sulfide minerals. Dissolved sulfide may be either oxidized aerobically or anaerobically (i.e. by DNRA) or be precipitated into particulate iron minerals or incorporated in organic matter. The iron and sulfide precipitation reactions are not

described by explicit reactions. Instead, the rates of these processes were estimated from fitting appropriate functions to the Fe^{2+} and TH_2S profiles. This procedure is described in Appendix A.

Constraints on the rates of N cycling

Rates of benthic N turnover processes at each station were not measured directly using, for example, ^{15}N labeling studies but were instead indirectly estimated by applying the numerical model to the measured porewater profiles and benthic fluxes. The procedure is outlined graphically in Fig. 2.2B and described below.

An initial guess for the rate of POM degradation at each station was made from the measured NH_4^+ profiles. At steady state, Eq. (2.1) shows that the net accumulation of NH_4^+ at each depth will be zero due to a balancing of the transport and reaction terms. In this case, the sum of reactions involving NH_4^+, $\sum R_{NH4}(x)$, can be expressed as:

$$\sum R_{NH4}(x) = R_{AMF}(x) - R_6(x) - R_8(x) + R_9(x) + (4/3 \cdot R_{10}(x)) - R_{11}(x) \tag{2.3}$$

where $R_{AMF}(x)$ is the rate of NH_4^+ production during organic matter degradation and the other reactions are listed in Table 2.2. Typically, the NH_4^+ data would be simulated by adjusting the rate constants in the individual reactions expression in the above equation. In our approach, however, a continuous function was fit through the measured NH_4^+ concentrations to obtain a profile of observed NH_4^+ ($NH_4^+{}_{OBS}(x)$). The following fitting function was then used to describe $\sum R_{NH4}(x)$:

$$\sum R_{NH4}(x) = k_{fit} \cdot (NH_4^+{}_{OBS}(x) - NH_4^+(x)) \tag{2.4}$$

where $NH_4^+(x)$ is the modeled NH_4^+ profile and k_{fit} (yr^{-1}) is a kinetic constant. k_{fit} was prescribed a high value to ensure that the modeled concentrations were maintained close to the measured values. With this approach, the observed NH_4^+ concentrations constitute an external forcing to the model which allows $\sum R_{NH4}(x)$ to be quantified without explicitly specifying a kinetic rate expression for ammonium production during organic matter degradation. The rate of ammonification was then determined from Eq. (2.3) and (2.4):

$$\begin{aligned} R_{AMF}(x) = {} & k_{fit} \cdot (NH_4^+{}_{OBS}(x) - NH_4^+(x)) + R_6(x) + R_8(x) - R_9(x) \\ & - (4/3 \cdot R_{10}(x)) + R_{11}(x) \end{aligned} \tag{2.5}$$

Consequently, the rate of POC mineralization (R_{POC}) was estimated from $R_{AMF}(x)$ by the following expression:

$$R_{POC}(x) = R_{AMF}(x)/r_{NC} \tag{2.6}$$

The determination of $R_{AMF}(x)$ thus required knowledge of the rates of nitrification (R_6), anammox (R_8), DNRA (R_9, R_{10}) and NH_4^+ adsorption (R_{11}). The rates of nitrification and NH_4^+ adsorption were parameterized using constants whose values were invariable across the transect (Table A.1 in Appendix A). The rate constants for anammox and DNRA (Table A.2) were variable and adjusted to fit the measured fluxes. To begin with, the rates of anammox and DNRA were initially set to zero which means that ammonification is the only unknown process affecting NH_4^+ concentrations. If this were correct, the modeled NH_4^+, TA and SO_4^{2-} profiles and DIN fluxes would be consistent with the measured data (Fig. 2.2B, step #1). However, this was not the case for any station, which indicates the occurrence of DNRA and/or anammox (Fig. 2.2B, steps #2 and 3). Furthermore, the flux of NO_3^- and/or NO_2^- into the sediment was underestimated at all stations when anammox and DNRA were not considered. This deficit must then be due to one or both of these processes since the rate of denitrification (R_2, R_3) is indirectly imposed by R_{POC} (Eq. 2.6).

Rates of DNRA and anammox at the individual stations were constrained according to three criteria. Firstly, where the initial model simulation underestimated both NO_3^- and/or NO_2^- uptake into the sediment and POM degradation (indicated by too low TA and too high SO_4^{2-} concentrations), anammox was assumed to take place (Fig. 2.2B, step #2). Anammox consumes NO_2^- and NH_4^+, thus leading to higher rates of POM degradation in order to maintain the fit to the observed NH_4^+ data and, consequently, enhanced accumulation of TA and consumption of SO_4^{2-} (Eq. 2.5). If the measured benthic fluxes and concentrations profiles could be simulated by only considering anammox, DNRA was assumed not to occur. Note that for the above criteria, increasing the rate of DNRA instead of anammox would slow down, rather than enhance, the rate of POM degradation since more NH_4^+ would be produced, ultimately leading to a greater misfit with the TA and SO_4^{2-} data.

Secondly, where the initial model simulation underestimated NO_3^- and/or NO_2^- uptake and overestimated POM mineralization (indicated by too high TA and too low SO_4^{2-}concentrations), DNRA was assumed to take place (Fig. 2.2B, step #3). As mentioned, DNRA enhances NO_3^- (and NO_2^-) uptake into the sediment and produces NH_4^+, leading to a decrease of POM degradation and TA concentrations through Eq. 2.5. If the model adequately simulated the measured benthic N fluxes and the porewater profiles with DNRA only, anammox was assumed not to occur.

Finally, if the uptake of NO_3^- and/or NO_2^- into the sediment was underestimated in the model even after DNRA was considered, the remaining NO_3^- and/or NO_2^- uptake was attributed to anammox. This systematic approach, therefore, allows for the occurrence of only DNRA and anammox or, if necessary, both processes together to explain the benthic fluxes.

Boundary conditions and model solution

Boundary conditions for each species at the top and the bottom of the modeled sediment layer were required to solve the differential equations (Eq. 2.1). At the sediment-water interface fixed concen-

trations were imposed for solutes (Dirichlet type) and fixed fluxes for solids (Robin type). Solute concentrations were assigned measured bottom water values where available (Table 2.3). Concentrations of NO_3^- and NO_2^- in large sulfur bacteria were not measured but were estimated from the porewater NO_3^- concentrations in squeezed sediment samples in the uppermost sediment layer which yielded higher NO_3^- concentrations compared to centrifuged samples or rhizon extractions (see section 2.4.1). This assumes that squeezing destroyed the bacterial cells and released the nitrate stored in their vacuoles (Thamdrup and Canfield, 1996). The imposed upper boundary for $NO_3^-{}_{bac}$ and $NO_2^-{}_{bac}$ should be regarded as minimum estimates since repeated freezing and thawing the sediment is required to fully destroy the cells and liberate the intracellular fluid (Dale et al., 2009).
POC fluxes to the sediment-water interface were constrained from a simple mass balance of the sediment at each station developed by Sommer et al. (submitted). The range of the organic carbon flux used in this model (6 - 14 mmol m^{-2} d^{-1}, Table 2.3) compares very well to the TOC flux off Callao at 12 °S (≈ 3 - 14 mmol m^{-2} d^{-1}; Sifeddine et al., 2008) and the organic carbon flux reported by Henrichs and Farrington (1984) at 15 °S (9 - 16 mmol m^{-2} d^{-1}). PON fluxes were calculated using the measured C:N ratio in the top layer of sediment and the POC flux. Reactive FeOOH flux was calculated from the Al deposition rate (derived from the ^{210}Pb measurements) and the Fe/Al ratio of 0.47 in andesitic volcanic rocks (Sarbas and Nohl, 2009) forming the local drainage area. Moreover, we assumed that only 50 % of the total iron reaching the seafloor was reactive in the surface layers (Poulton and Raiswell, 2002). Particulate sulfur fluxes at the top boundary were set to zero. The upper boundary for $NH_4^+{}_{ads}$ was implicitly given by the upper boundary concentration of NH_4^+ and the apparent equilibrium coefficient for adsorption.
Solid species were prescribed zero-gradient (Neumann type) conditions at the lower boundary (x = L) at all stations. A similar condition was also prescribed for solutes at stations 5 and 6 because the concentrations were invariable at the depth of the lower model boundary. At stations 1 to 4 distinct concentrations changes at the bottom boundary were observed, and here a constant gradient condition was imposed:

$$\left.\frac{\partial C_i}{\partial x}\right|_{n=100} = 0.95 \cdot \left.\frac{\partial C_i}{\partial x}\right|_{n=99} \tag{2.7}$$

where n refers to a layer (0 to 100) in the discretized grid space. This gradient resembles the near-linear measured concentration profiles of TA and SO_4^{2-} close to the bottom boundary. For NH_4^+, whose concentration was fit to the observed data, the gradient was set to that of the fitting function at the bottom boundary.

Finite differences and the method of lines were used to solve the set of coupled partial differential equations (Boudreau, 1996). A central differences scheme was applied over an uneven grid for diffusion, bioturbation, and advection in the bioturbated layer whereas upward differences were used for advective transport below the bioturbated zone. Depth intervals increased with sediment depth to a maximum resolution of 1 cm. The set of coupled ordinary differential equations was solved using the

numerical solver NDSolve in MATHEMATICA 7.0. Mass conservation of the model was > 99 % and a typical steady-state simulation was completed within 5 minutes on a personal computer (Intel Core 2 Duo processor).

2.4. Results and Discussion

2.4.1. Sediment geochemistry and POM degradation

Porewater NH_4^+, NO_3^-, TH_2S, SO_4^{2-} and TA profiles for all stations are shown in Fig. 2.3. Maximum TA and NH_4^+ concentrations of 14 meq l^{-1} and 1.2 mM, respectively, were observed at the base of the core at the shallowest site (station 1). Steep NH_4^+ and TA concentration gradients at the sediment-water interface and a strong convex curvature of the profiles indicate high rates of POM mineralization in the surface layers on the shelf. For the Peru upwelling region at 12 °S (183 m water depth), higher concentrations of about 25 meq l^{-1} TA and 2.8 mM NH_4^+ have been reported (Froelich et al., 1988). Further south at 15 °S, NH_4^+ concentrations > 3 mM at 60 cm were measured at a site at 245 m water depth (Rowe and Howarth, 1985). The rates of POM mineralization on the shelf at 11 °S are thus on the low side of previous reports. However, the NH_4^+ concentrations were elevated compared to other high productivity OMZ regions such as offshore central Chile (< 0.8 mM; Thamdrup and Canfield, 1996) and the Pakistan margin (< 0.3 mM; Woulds et al., 2009). The decrease in NH_4^+ and TA concentration gradients from station 1 to station 6 (Fig. 2.3) allude to a decrease in POM degradation rates with increasing water depth. This is confirmed by the SO_4^{2-} concentration data which is progressively less depleted down slope.

These qualitative trends were supported by quantitative modeling of POC degradation rates (Table 2.4). Total mineralization rates decreased from 8.23 mmol C m^{-2} d^{-1} on the shelf to 1.74 mmol C m^{-2} d^{-1} at station 5 on the slope. At stations 1 and 2 sulfate reduction was by far the dominant POC degradation pathway (up to 80 % of total) and became relatively less important with increasing water depth. Empirical data sets predict that sulfate reduction accounts for ca. 70 % of organic carbon mineralization on the shelf (0 - 200 m) whereas aerobic respiration contributes only 10 % (Burdige, 2006). Based on these data, it can be inferred that sulfate reduction consumes the fraction of POM normally respired aerobically. Nonetheless, the modeled sulfate reduction rates (< 6.6 mmol C m^{-2} d^{-1}) were a factor of 7 to 20 lower than measured rates from studies on the shelf off Peru and Chile (Fossing, 1990; Ferdelman et al., 1997), yet our derived total POC degradation rates were too low to support such high sulfate reduction rates except at station 1. Böning et al. (2004) reported sulfate reduction rates for 14 stations on the Peruvian shelf of which only two were > 3.9 mmol S m^{-2} d^{-1} or twice this value for in terms of carbon mineralization. Furthermore, sulfate reduction rates equivalent to ca 2.4 and 1.2 mmol C m^{-2} d^{-1} were reported for 36 °S and 23 °S, respectively (Niggemann et al., 2007). Clearly, there is pronounced spatial heterogeneity in the total organic

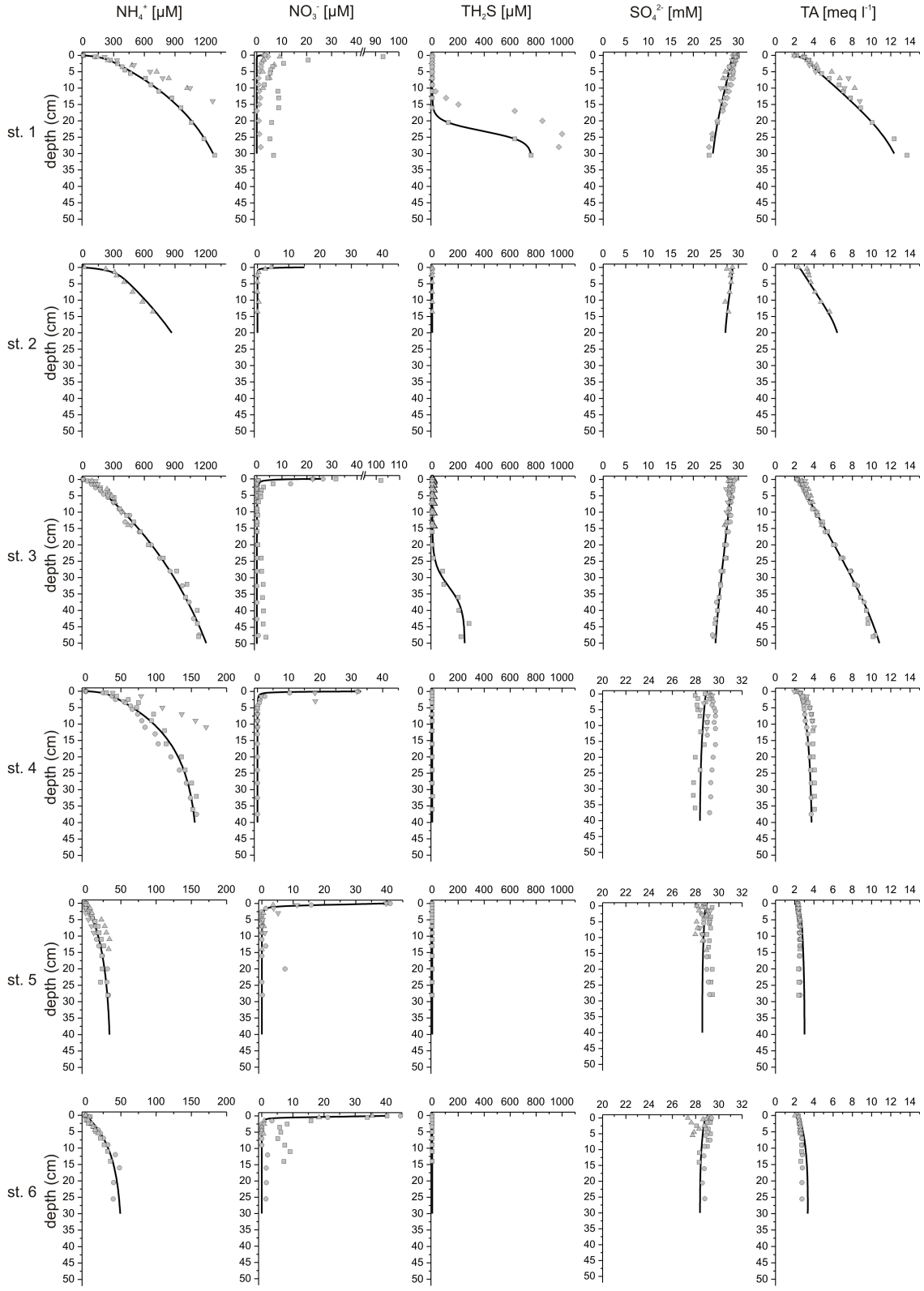

Figure 2.3.: Modeled (lines) and measured (symbols) porewater concentration profiles of NH_4^+, NO_3^-, TH_2S, SO_4^{2-} and TA at stations 1 to 6. Symbols denote the following porewater subsampling methods: circles = MUC, glove-bag; squares = MUC, porewater squeezer; diamonds = MUC, rhizons; triangles = BIGO, glove-bag. NH_4^+ concentrations were fitted using the procedure described in the text. Note the different concentration scales for NH_4^+ and NO_3^- between stations.

Table 2.4.: POC degradation rates (mmol C m^{-2} d^{-1}) across the transect rounded to two decimal places. Percentages of the total POC degradation rate used by each electron acceptor rounded to the nearest integer are given in parenthesis. A 20 % uncertainty is assigned to the rates (see Section 2.4.4).

Process	Station 1	Station 2	Station 3	Station 4	Station 5	Station 6
R_1 (O_2)	0 (0)	0 (0)	0 (0)	0 (0)	0.23 (14)	0.59 (28)
R_2 (NO_3^-)	0.17 (2)	0.65 (8)	0.95 (16)	0.91 (23)	0.28 (16)	0.18 (8)
R_3 (NO_2^-)	1.08 (13)	0.87 (11)	1.51 (26)	1.15 (29)	0.29 (17)	0.15 (7)
R_2 + R_3	1.25 (15)	1.52 (20)	2.46 (42)	2.06 (52)	0.57 (33)	0.33 (16)
R_4 (FeIII)	0.43 (5)	0.03 (<1)	0.03 (<1)	0.04 (<1)	0.12 (7)	0.12 (5)
R_5 (SO_4^{2-})	6.55 (80)	6.19 (80)	3.40 (58)	1.91 (48)	0.82 (47)	1.10 (52)
Total	8.23	7.74	5.89	4.01	1.74	2.14

matter degradation rate in the OMZ off Peru and Chile. The low total mineralization rates at the deep stations 5 and 6 are markedly higher than the measured TOU of ca. 0.5 and 1.5 mmol O_2 m^{-2} d^{-1}, respectively (Fig. 2.4). This indicates that a large fraction of the reduced metabolites (e.g. NH_4^+, TH_2S) escape oxidation and are either buried or transported to the water column. The model underestimates the TOU by up to a factor of 2 and 3 at station 5 and 6, respectively. The reason for this discrepancy is not clear, but may be due to respiration by fauna or oxidation of reduced species in the chamber water rather than the sediments (Sommer et al., 2010). Iron reduction contributed only marginally to the overall POM degradation inside the OMZ (< 1%) but accounted for 7 % at the lower edge. Metal oxide reduction may account for up to 10 - 20 % in highly bioturbated shelf sediments (Burdige, 2006), otherwise only 1 % or less may be expected based on globally averaged studies (Thullner et al., 2009). The relatively high contribution from iron within the OMZ thus indicates that reactive iron fluxes are elevated in the area, perhaps by benthic release of ferrous on the shelf and oxidation to particulate ferric iron at the edges of the OMZ.

Porewater NO_3^- concentrations were depleted below the uppermost centimeter(s) at stations 2 to 5 (Fig. 2.3). Similarly, NO_2^- was generally < 1 μM below the uppermost centimeter(s) (data not shown), yet was elevated at station 1 where measured bottom water concentrations were 11.5 μM (Table 2.3). However, at station 1 and 6, NO_3^- accumulated up to 10 μM below the surface layers. The reason for these anomalies is currently unclear, but may be due to deep bioirrigation at station 6 or experimental artifacts caused by ammonium oxidation as suggested by Woulds et al. (2009) who reported similar observations in the Pakistan margin OMZ. On the shelf there are further potential artifacts from the NO_3^- stored within vacuolated sulfur bacteria. At stations 1 and 3, surface NO_3^- concentrations in samples obtained using the porewater squeezing method exceeded 90 - 100 μM, whereas those using the centrifugation method or rhizons yielded much lower concentrations (< 30 μM). Such elevated porewater NO_3^- concentrations have already been observed in *Thioploca* inhabited sediments off central Chile (Thamdrup and Canfield, 1996). A comparison of the

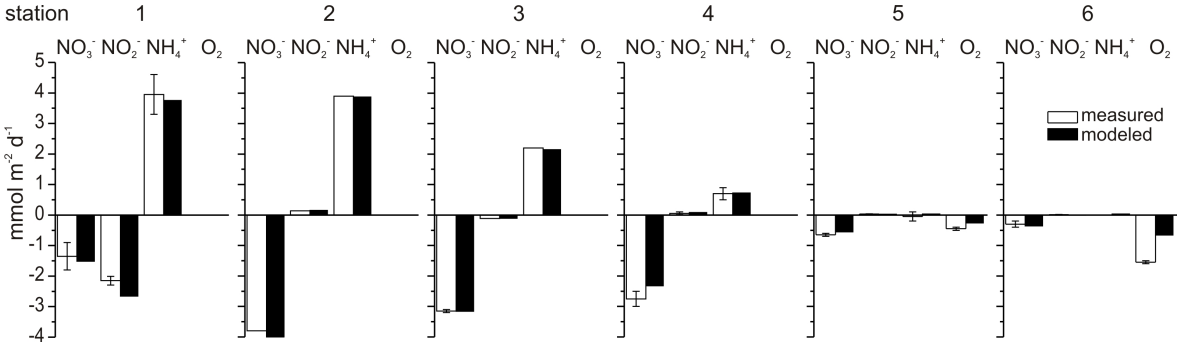

Figure 2.4.: Measured (empty columns) and modeled (filled columns) fluxes of DIN (mmol N m^{-2} d^{-1}) species and O_2 (mmol O_2 m^{-2} d^{-1}) across the sediment-water interface at each station. Error bars correspond to the measured minimum and maximum fluxes (at station 2 only one chamber was deployed). O_2 fluxes at stations 5 and 6 show the measured total oxygen uptake (TOU) in benthic chambers (Sommer et al., submitted). N fluxes are from Sommer et al. (submitted).

different porewater extraction techniques indicates that the porewater squeezing and, to some extent also the centrifugation method, led to elevated NO_3^- concentrations by disrupting cells, whereas the use of rhizons appeared to be free of extraction artifacts (Fig. 2.3). Consequently, the elevated NO_3^- values at depths < 10 cm were attributed to NO_3^- released from large sulfur bacteria and thus not representative of true porewater concentrations. Porewater squeezing was not used at station 2 and the significance of intracellular NO_3^- here is uncertain. In the absence of in situ NO_3^- data obtained from microbiosensors, we are cautious to draw any firm conclusions from our measured NO_3^- concentrations and these are not discussed further.

Nonetheless, the NO_3^- cycling is constrained using the benthic fluxes and we are confident that the modeled rates of denitrification are realistic. At the intermediate water depths (stations 3 and 4), NO_3^- (R_2) and NO_2^- (R_3) reduction accounted for 40 - 50 % of POC degradation (Table 2.4), which is much higher than values of < 10 % predicted for the same water depth in normoxic settings (Thullner et al., 2009). In the absence of an upper oxic layer where aerobic respiration would inhibit denitrification, the denitrification layer would be located at the sediment-water interface. The rate of denitrification would then be much less limited by diffusion of NO_3^- into the sediment since NO_3^- no longer has to traverse the aerobic zone. We hypothesize that this explains why up to half of POM is mineralized through this pathway. Despite anoxic bottom waters on the shelf, denitrification accounts for a lower, yet significant, fraction of carbon degradation (15 - 20 %). We envisage that sediment clogging by microbial mats creates a barrier to NO_3^- diffusion and limits the efficiency of denitrifying bacteria at these depths.

2.4.2. Nitrogen turnover processes along the transect and their regulation

The fluxes of DIN species (NO_3^-, NO_2^-, NH_4^+) measured in the benthic landers were well reproduced by the model (Fig. 2.4). The overall magnitude of the fluxes decreased with increasing water depth which reflects lower organic matter reactivity and degradation rates. Accordingly, NH_4^+ effluxes were highest at the shallowest station 1 and decreased monotonously to almost zero at station 5 and 6. Nitrate fluxes were always directed into the sediment with the maximum uptake rate at station 2, whereas station 1 showed elevated nitrite uptake. This can be attributed to relatively low bottom water NO_3^- concentrations and high NO_2^- concentrations (Table 2.3). With regards to the net flux of DIN, the stations can be distinguished by region, that is, those where DIN was recycled in the sediments (fluxes of $NO_3^- + NO_2^- \approx NH_4^+$, stations 1 and 2) and those where the sediments were a sink for DIN (fluxes of $NO_3^- + NO_2^- > NH_4^+$, station 3 - 6). These trends are discussed in more detail by Sommer et al. (submitted).

The relative contributions of the various N turnover reactions to the measured fluxes along the 11 °S transect are listed in Table 2.5 and an overview of the major pathways along the transect is shown in Fig. 2.5. In agreement with the trend for POM degradation and the benthic NH_4^+ effluxes, ammonification was highest at the shallowest station 1 and decreased with increasing water depth. Rates of POM degradation via nitrate and nitrite (R_2 and R_3, respectively) exhibited a peak at station 3 and 4 (Fig. 2.5) where the relative contribution of these mineralization pathways was also highest (Table 2.4). The relatively lower rates of denitrification at stations 1 and 2, despite higher total POM degradation and the lack of O_2 have been explained as diffusion limitation of NO_3^- and NO_2^- from the bottom water. The predicted range of denitrification rates (R_2, R_3) was 0.2 - 2 mmol N m^{-2} d^{-1} and is consistent with rates measured at other low oxygen environments, for example, Concepción Bay (0.18 - 2.9 mmol N m^{-2} d^{-1}; Graco et al., 2001; Farías et al., 2004) and the Pakistan margin (0.07 - 3.68 mmol N m^{-2} d^{-1}; Schwartz et al., 2009).

In general, nitrification rates were low and could potentially supply < 1.5 % of NO_3^- or NO_2^- requirements for nitrate and nitrite reduction (Table 2.5). The major NO_3^- source for denitrification was thus identified as bottom water NO_3^-. The availability of NO_3^- may limit denitrification at the shallower stations 1 - 4 where bottom water NO_3^- concentrations were lower than those down slope (Table 2.3). In fact, nitrate reduction (R_2) was positively correlated with bottom water NO_3^- concentration at stations 1 - 4, but not at stations 5 and 6 where low rates were associated with high NO_3^- availability (Fig. 2.6). It is likely that aerobic respiration outcompetes denitrification for labile organic carbon here, thus limiting the amount of substrate which can be degraded by denitrification (Dale et al., 2011). The model by Middelburg et al. (1996) predicts similar tendencies for high-nutrient low-oxygen bottom waters.
Total DNRA exhibited highest rates at stations 1 and 2 (ca. 2.8 mmol m^{-2} d^{-1}) where DIN was recycled in the sediments leading to high release rates of NH_4^+ to the overlying water column (Table 2.5).

Table 2.5.: N turnover rates (mmol N m^{-2} d^{-1}) across the transect. A 20 % uncertainty is assigned to the rates (see Section 2.4.4).

Process	Station 1	Station 2	Station 3	Station 4	Station 5	Station 6
R_{AMF} ammonification	0.94	0.74	0.67	0.45	0.17	0.20
R_2 ($NO_3^- \rightarrow NO_2^-$)	0.35	1.31	1.90	1.83	0.55	0.36
R_3 ($NO_2^- \rightarrow N_2$)	1.44	1.16	2.02	1.53	0.39	0.20
R_6 nitrification ($NH_4^+ \rightarrow NO_2^-$)	0	0	0	0	2.2×10^{-4}	2.2×10^{-3}
R_7 nitrification ($NO_2^- \rightarrow NO_3^-$)	0	0	0	0	3.3×10^{-4}	5.6×10^{-4}
R_{11} NH_4^+ adsorption	6.9×10^{-3}	5.8×10^{-4}	8.5×10^{-4}	3.6×10^{-4}	7.2×10^{-5}	1.1×10^{-4}
R_9 DNRA ($NO_3^- \rightarrow NH_4^+$)	1.17	2.93	1.38	0.48	0	0
R_{10} DNRA ($NO_2^- \rightarrow NH_4^+$)	1.55	–	–	–	–	–
ΣDNRA	2.71	2.93	1.38	0.48	0	0
R_8 anammox ($NH_4^+ + NO_2^- \rightarrow N_2$)	0	0	0	0.43	0.28	0.33
% N_2 production by anammox	0	0	0	22	42	62

With increasing water depth, DNRA rates decreased to zero. About 60 % of total DNRA at station 1 occurred with NO_2^- (R_{10}). Simulated DNRA rates are consistent with minimum estimates from a simple mass balance for the upper 10 cm of the sediment column by Sommer et al. (submitted), who calculated rates of 2.1 to 3.2 mmol N m^{-2} d^{-1} for station 1 and 2.9 mmol N m^{-2} d^{-1} for station 2. Within the OMZ, our DNRA rates (0.48 - 2.93 mmol N m^{-2} d^{-1}) were in the same range as found for Concepción Bay in summer (2.7 - 5 mmol N m^{-2} d^{-1}, Graco et al., 2001) and Laguna Madre/Baffin Bay (0.6 - 1.9 mmol N m^{-2} d^{-1}, An and Gardner, 2002) yet far lower than on the highly sulfidic sediments on the Namibian shelf colonized by *Thiomargarita spp.* (17 mmol N m^{-2} d^{-1}; Dale et al., 2009). A porewater sulfide budget (Appendix A) revealed that DNRA removed 50 - 95 % of the available free sulfide at stations 1 - 4 where bacterial mats were observed.

Large sulfur bacteria compete with denitrifying bacteria for oxidized N. However, the sulfur bacteria may have a competitive edge in organic rich sediments where sulfide accumulates in the porewater. The balance between DNRA (favored at high TH_2S concentrations) and denitrification (favored at low TH_2S concentrations) may thus depend on the rate of sulfide sources (sulfate reduction) and sinks (oxidation and mineral sequestration) (An and Gardner, 2002; Dale et al., 2011). A positive linear correlation between the fraction of total NO_3^- consumed by DNRA and the modeled depth-integrated rate of sulfate reduction (Fig. 2.7) supports this idea. Moreover, *Thioploca* and *Beggiatoa* may move through the sediments at a rate of 10 cm per day (Jørgensen and Gallardo, 1999) which makes them more versatile to seek out NO_3^- than non-motile denitrifiers. They can also access bottom water NO_3^- and/or NO_2^- directly with their filaments and hence do not depend on NO_3^- supply by diffusion. Intracellular storage of NO_3^- (and potentially NO_2^-) within their vacuoles further allows them to thrive in areas of lower NO_3^- availability (Schulz and Jørgensen, 2001). Hence, because of these physiological adaptations, it is to be expected that DNRA accounts for the majority of the total NO_3^- uptake at the organic-rich shallower stations where bottom water NO_3^- availability was limited.

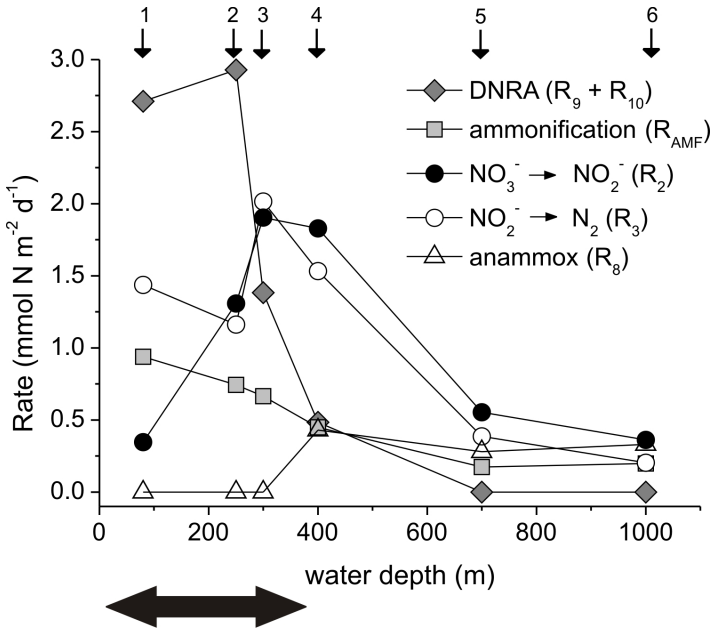

Figure 2.5.: Model-predicted depth-integrated rates of nitrogen turnover along the 11°S transect. Station numbers are indicated by the arrows at the top. The bottom arrow denotes the occurrence of bacterial mats (Mosch et al., 2010).

The data indicate that anammox only occurred at stations 4 - 6, with highest rates at station 4 (Fig. 2.5, Table 2.5). Modeled depth-integrated anammox rates (0 - 0.43 mmol N m^{-2} d^{-1}) were consistent with measurements in sediments of the Skagerrak (0 - 0.6 mmol N m^{-2} d^{-1} from 0 to 1.5 cm; Dalsgaard and Thamdrup, 2002), the Washington margin (0.03 - 0.08 mmol N m^{-2} d^{-1}, Engström et al., 2009) and the North Atlantic ($2.6 \cdot 10^{-3}$ - 0.06 mmol N m^{-2} d^{-1}; Trimmer and Nicholls, 2009). The regulation of anammox is ultimately dependent on the supply of NH_4^+ and NO_2^-. Despite the high rates of ammonification on the shelf, the absence of anammox at stations 1 - 3 likely results from the high demand for NO_2^- by denitrifiers which outcompete ammonium oxidizers for NO_2^- (cf. Dalsgaard et al., 2005; Risgaard-Petersen et al., 2005). At the deeper stations, NO_2^- supply directly from the water column was insufficient to support the simulated anammox rates. Furthermore, due to the low availability of O_2, only a small fraction of total NO_2^- turnover by anammox can be coupled to nitrification. In situ NO_3^- reduction to NO_2^- within the sediment via heterotrophic denitrification thus was the principal NO_2^- supply pathway for anammox. This pattern agrees with the analysis by Dale et al. (2011) who showed that anammox is most likely to be coupled to denitrification in sediments which are poorly ventilated and/or highly reactive and to nitrification in well ventilated sediments with lower fluxes of labile organic material. Other factors not considered here which are also potentially important with regards to anammox are inhibition of anammox by O_2 (Dalsgaard et al., 2005) and reduction of NO_3^- to NO_2^- by *Thioploca* (Prokopenko et al., 2006). Our model is able to explain the benthic fluxes without invoking these additional mechanisms.

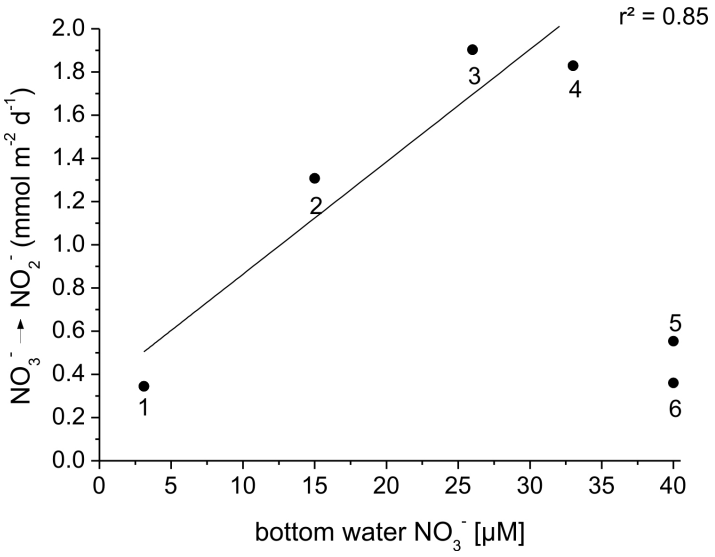

Figure 2.6.: Nitrate reduction (R_2) as a function of bottom water NO_3^- concentration for each station. The linear regression applies to stations 1 - 4 only.

2.4.3. Relative importance of denitrification, DNRA, and anammox in N cycling

Since DNRA retains DIN in the ecosystem while denitrification and anammox remove DIN, the channeling of oxidized N (NO_3^- and NO_2^-) into canonical denitrification and anammox versus DNRA determines the role of sediments as a recycling site or sink for DIN. The main sink for NO_3^- and NO_2^- in the sediments along the 11 °S transect switched from DNRA (≥ 65 % of total uptake at stations 1 and 2) to coupled denitrification-anammox at stations 5 and 6 (Fig. 2.8) where microbial mats and DNRA were absent. Nitrification was negligible throughout (Table 2.5). For comparison, DNRA was responsible for 40 % and 94 % of total NO_3^- reduction in Concepción Bay sediments in spring and summer, respectively (Graco et al., 2001), and 70 % at Boknis Eck (southwestern Baltic; Dale et al., 2011). Percentages in excess of 80 % were observed in estuarine environments that receive high loads of nutrients (Jørgensen and Sørensen, 1985; Gilbert et al., 1997; Kim et al., 1997). Thus, at least at locations where large sulfur bacteria are present, NO_3^- uptake tends to be recycled to NH_4^+ at the expense of denitrifying processes. At stations 1 and 2, where DNRA governed both total N turnover (Fig. 2.5) and NO_3^- + NO_2^- uptake (Fig. 2.8), DIN was recycled and large amounts of NH_4^+ were released by diffusion across the sediment-water interface (Fig. 2.4). The fate of NH_4^+ after being released from the Peruvian sediments is unknown, yet it may reach the euphotic zone and enhance primary production and the spread of the OMZ. This positive effect may be further exacerbated by the simultaneous release of excess phosphate and iron from the sediments that was also measured at the time of sampling (Noffke et al., 2010). At intermediate water depths (stations 3 - 6), where NO_3^- and NO_2^- uptake was mainly attributed to denitrification (Fig. 2.8) the sediments were a net sink for DIN (Fig. 2.4).

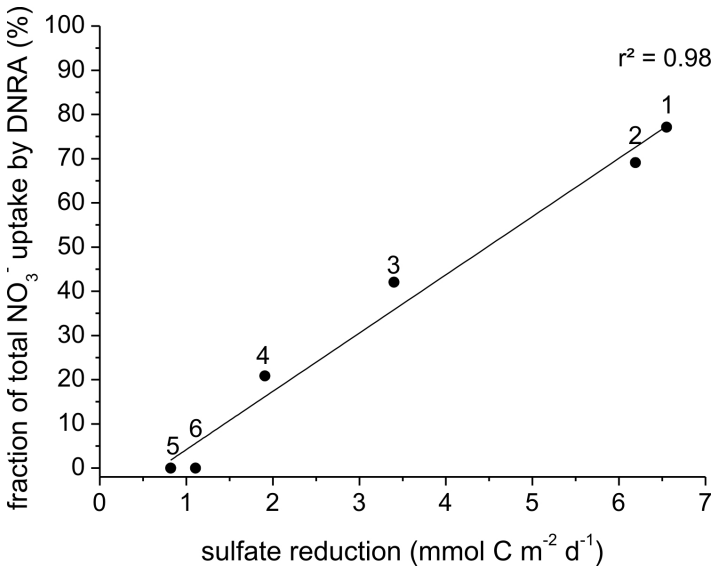

Figure 2.7.: Fraction of total benthic NO_3^- uptake by DNRA (%) as a function of the sulfate reduction rates. The solid denotes the linear fit to the data. Station numbers are indicated.

Anammox accounted for up to 62 % of N_2 production at the deepest station (Table 2.5), which is comparable to coastal sediments with oxic bottom waters in the Skaggerak (4 - 79 %; Thamdrup and Dalsgaard, 2002; Engström et al., 2005) and coastal Greenland (1 - 35 %; Rysgaard et al., 2004). Similar data for sediments underlying oxygen deficient environments are scarce, yet Glud et al. (2009) reported that anammox contributed 37 % to the total N_2 production in the hypoxic Sagami Bay in Japan (55 - 60 μM O_2). In contrast to the absolute anammox rates, the relative importance of anammox in N_2 production increased with water depth from station 4 to 6 (Table 2.5). This negative relationship has been reported for a wide range of marine sediments (Trimmer and Nicholls, 2009; Thamdrup and Dalsgaard, 2002; Dalsgaard et al., 2005) and has been explained as increased coupling between anammox and nitrification because NO_2^- production by denitrification tends to decrease with increase water depth (Dale et al., 2011). In support of this thesis, the relative importance of anammox to total N_2 production was highest at stations 5 and 6 which had the lowest rates of denitrification and highest rates of nitrification (Table 2.5). Possible inhibition of anammox and denitrification on the shelf by sulfide (Dalsgaard et al., 2003; Joye, 2002) was not considered in our model since no free sulfide was observed in the upper sediment layers where anammox and denitrification take place (Fig. 2.3). The dominance of denitrification as the major sink in sediments underlying the OMZ is in contrast to water column studies on the Peru margin which observed that N cycling was dominated by anammox (Hamersley et al., 2007; Lam et al., 2009).

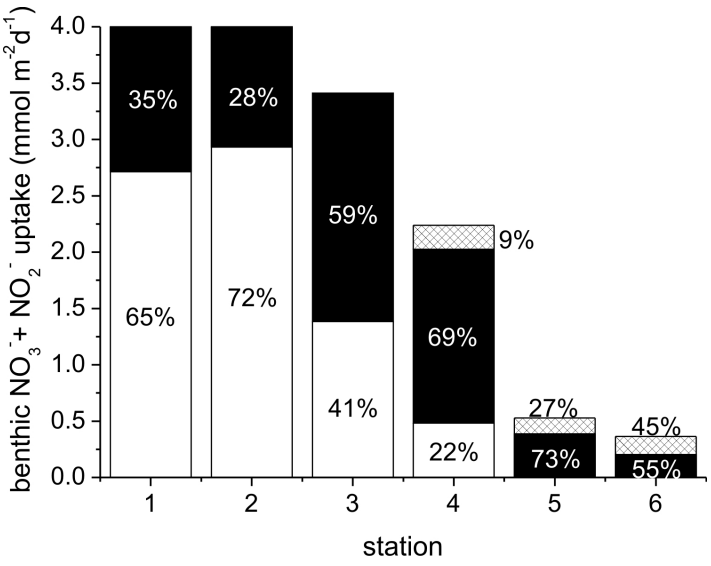

Figure 2.8.: Total model-predicted uptake of NO_3^- + NO_2^- across the sediment-water interface (mmol N m^{-2} d^{-1}). The partitioning of the flux into DNRA (white), denitrification (black), and anammox (hashed) is given as percentage of the total flux.

2.4.4. Potential importance of anammox on the shelf

The data analysis has shown that, under the assumptions imposed by the model, anammox was absent at stations 1 - 3 within the OMZ. However, despite the multiple constraints on the modeled turnover rates, this result remains to be corroborated with experimental evidence. The largest potential uncertainties in the anammox rate are introduced through the rate constant (k_8). The transport and physical parameters are reasonably well known and a realistic variability in their parameterization is likely to have less impact on anammox than the reaction kinetics. Thus, anammox may be occurring to some extent on the shelf, particularly at station 3 on the transition between the sediments dominated by DNRA and denitrification.

To test the potential importance of anammox at this station, we carried out a simple sensitivity analysis which consisted of re-running the baseline model using the lowest ($3 \cdot 10^9$ M^{-1} yr^{-1}) and highest ($1.6 \cdot 10^{10}$ M^{-1} yr^{-1}) values of the anammox rate constant derived from the stations 4 - 6 where anammox was predicted. The lower values resulted in a rate of 1.0 mmol N m^{-2} d^{-1} (Table 2.6) which is about twice as high as simulated for station 4 (Table 2.5). The higher rate constant increases anammox to 2.0 mmol N m^{-2} d^{-1}. However, due to the highly coupled nature of the N cycle, increased anammox also enhances NO_3^- uptake, by 24 and 58 % for the low and high rate constants, respectively. Furthermore, because anammox consumes NH_4^+, the higher rates lead to 2 - 3 fold increase in sulfate reduction (Table 2.6). This is a result of the procedure used to fit the modeled NH_4^+ values with the measured NH_4^+ pore water data (Eq. 2.5, Fig. 2B). Böning et al. (2004) reported a sulfate reduction rate of 1.9 mmol S m^{-2} d^{-1} for a site in close proximity to station 3. Although we

recognize that spatial heterogeneity could account for a 2 - 3 fold increase in depth-integrated sulfate reduction rates, the close similarity of our modeled rate with those measured by Böning et al. (2004) plus the additional constraint of the measured NO_3^- flux indicates that the absence of anammox in the baseline simulation at station 3 is realistic.

Table 2.6.: Sensitivity study for station 3 to estimate the potential impact of anammox on NO_3^-, NO_2^- and N_2 fluxes across the sediment water interface and the depth integrated sulfate reduction rate. The standard run ($k_8 = 0$) is given in the first line of the table.

k_8 (M^{-1} yr^{-1})	Anammox (R_8) (mmol N m^{-2} d^{-1})	% N_2 production by anammox	NO_3^- flux	NO_2^- flux	N_2 flux	Sulfate reduction (R_4) (mmol SO_4^{2-} m^{-2} d^{-1})
			(% change from standard run)			
0	0.0	0	–	–	–	1.7
3×10^9	1.0	29	+ 24	+ 92	+ 68	3.6
1.6×10^{10}	2.0	39	+ 58	+ 224	+ 156	5.3

Finally, it is worth noting that the sensitivity of NO_3^- and NO_2^- fluxes to anammox in Table 2.6 is much larger than the standard deviation of the measured fluxes (Fig. 2.4). Similar results were for the other N cycling reactions. This strongly restricts the leverage with which to vary the biogeochemical rates constant independently of one another. Furthermore, the measured fluxes must be consistent with the porewater profiles of TA, NH_4^+ and SO_4^{2-} which are a robust proxy for POM mineralization. Accordingly, and notwithstanding the usual inconvenience of local heterogeneity issues, the uncertainty in the modeled rates is determined by the uncertainty in the measured data (primarily the fluxes). At station 1 where the highest NH_4^+ release rates were measured, the precision in fluxes is around 20 % (Fig. 2.4). Since NH_4^+ fluxes are the major constraint on the model (Eq. 2.5), this value can be assumed to be reasonable estimate for the uncertainty in the simulated rates.

2.5. Conclusions

The dominant pathways and rates of benthic N cycling change dramatically through the Peruvian oxygen minimum zone (OMZ) at 11 °S. DNRA governed total N turnover on the shelf and the upper slope (80 - 260 m water depth) where organic matter mineralization rates were high and bottom waters were depleted in O_2, NO_3^- and NO_2^-. These sediments represented a DIN recycling site, releasing large amounts of NH_4^+ by diffusion across the sediment-water interface. This may create a positive feedback with primary production and oxygen draw-down within the Peruvian OMZ. At greater water depths (> 300 m), where organic carbon degradation decreased and bottom water NO_3^- concentrations increased, denitrification was the dominant pathway in the benthic N cycle and the sediments here were a net sink for DIN. Anammox was of minor importance on the shelf and upper slope but gained importance at water depths > 400 m where it contributed up to 62 % to total N_2 production at the deepest station.

Sediments underlying the oxygen deficient water of upwelling regions are commonly considered as sinks for DIN associated with high benthic NO_3^- uptake. However, this study shows that high benthic NO_3^- uptake rates in these environments are not always due to high rates of denitrification but may also result from DNRA. Consequently, the role of sediments underlying low oxygen waters as sinks for DIN should be revised and, furthermore, DNRA should be considered when interpreting benthic NO_3^- uptake in such settings. Models predict that OMZs are expanding due to climate change (Oschlies et al., 2008; Shaffer et al., 2009). Due consideration of DNRA versus denitrification with regards to the balance between net removal and recycling of DIN and the potential feedback on primary production is required to accurately predict the rate of spreading of OMZs.

Numerical transport-reaction modeling is an appropriate tool for the identification of pathways and quantification of rates of DIN turnover in marine surface sediments. The strength of the model developed here rests with the multiple constraints on N turnover, which include in situ benthic fluxes in addition to a suite of porewater data which allow the organic matter mineralization rates to be quantified. Both of these different sets of data must be coherent and consistent with one another when coupled to a set of reactions describing the major processes on N cycling on the Peruvian shelf. Our model parameterizations could be further verified using fluxes of stable N isotopes at sites both inside and outside the OMZ.

Acknowledgements

We are grateful for the support of the crew of RV 'Meteor', leg M77-1/2 and B. Domeyer, M. Dibbern, R. Ebbinghaus and C. Ehlert for helping with the biogeochemical analyses. We also thank Jack Middelburg for the editorial handling and four anonymous reviewers for their constructive feedback which improved this manuscript. This work is a contribution of the Sonderforschungsbereich 754 "Climate - Biogeochemistry Interactions in the Tropical Ocean" (www.sfb754.de) which is supported by the Deutsche Forschungsgemeinschaft.

References

An S. M. and Gardner W. S. (2002) Dissimilatory nitrate reduction to ammonium (DNRA) as a nitrogen link, versus denitrification as a sink in a shallow estuary (Laguna Madre/Baffin Bay, Texas). *Mar. Ecol.-Prog. Ser.* **237**, 41-50.

Berelson W. M., Hammond D. E. and Johnson K. S. (1987) Benthic Fluxes And The Cycling Of Biogenic Silica And Carbon In 2 Southern-California Borderland Basins. *Geochim. Cosmochim. Acta* **51**, 1345-1363.

Böning P., Brumsack H.-J., Böttcher M. E., Schnetger B., Kriete C., Kallmeyer J. and Borchers S. L. (2004) Geochemistry of Peruvian near-surface sediments. *Geochim. Cosmochim. Acta* **68**, 4429-4451.

Boudreau B. P. (1996) A method-of-lines code for carbon and nutrient diagenesis in aquatic sediments. *Comput. Geosci.* **22**, 479-496.

Boudreau B. P. (1997) *Diagenetic Models and Their Implementation*. Springer-Verlag.

Brandes, J. A. and Devol, A. H. (2002) A global marine-fixed nitrogen isotopic budget: Implications for holocene nitrogen cycling. *Global Biogeochem. Cy.* **16**, 1120.

Christensen P. B., Rysgaard S., Sloth N. P., Dalsgaard T. and Schwærter S. (2000) Sediment mineralization, nutrient fluxes, denitrification and dissimilatory nitrate reduction to ammonium in an estuarine fjord with sea cage trout farms. *Aquat. Microb. Ecol.* **21**, 73-84.

Codispoti L. A., Brandes J. A., Christensen J. P., Devol A. H., Naqvi S. W. A., Paerl H. W. and Yoshinari T. (2001) The oceanic fixed nitrogen and nitrous oxide budgets: Moving targets as we enter the anthropocene? *Sci. Mar.* **65**, 85-105.

Dale A. W., Brüchert V., Alperin M. and Regnier P. (2009) An integrated sulfur isotope model for Namibian shelf sediments. *Geochim. Cosmochim. Acta* **73**, 1924-1944.

Dale A. W., Sommer S., Bohlen L., Treude T., Bertics V. J., Bange H. W., Pfannkuche O., Schorp T., Mattsdotter M. and Wallmann K. (2011) Rates and regulation of nitrogen cycling in seasonally-hypoxic sediments during winter (Boknis Eck, SW Baltic Sea): sensitivity to environmental variables. *Estuar. Coast. Shelf Sci.* **95**, 14-28.

Dalsgaard T. and Thamdrup B. (2002) Factors controlling anaerobic ammonium oxidation with nitrite in marine sediments. *Appl. Environ. Microb.* **68**, 3802-3808.

Dalsgaard T., Canfield D. E., Petersen J., Thamdrup B. and Acuña-González J. (2003) N_2 production by the anammox reaction in the anoxic water column of Golfo Dulce, Costa Rica. *Nature* **422**, 606-608.

Dalsgaard T., Thamdrup B. and Canfield D. E. (2005) Anaerobic ammonium oxidation (anammox) in the marine environment. *Res. Microbiol.* **156**, 457-464.

Devol A. H. and Christensen J. P. (1993) Benthic Fluxes And Nitrogen Cycling In Sediments Of The Continental-Margin Of The Eastern North Pacific. *J. Mar. Res.* **51**, 345-372.

Engström P., Dalsgaard T., Hulth S. and Aller R. C. (2005) Anaerobic ammonium oxidation by nitrite (anammox): Implications for N_2 production in coastal marine sediments. *Geochim. Cosmochim. Acta* **69**, 2057-2065.

Engström P., Penton C. R. and Devol A. H. (2009) Anaerobic ammonium oxidation in deep-sea sediments off the Washington margin. *Limnol. Oceanogr.* **54**, 1643-1652.

Falkowski P. G. (1997) Evolution of the nitrogen cycle and its influence on the biological sequestration of CO_2 in the ocean. *Nature* **387**, 272-275.

Farías L., Graco M. and Ulloa O. (2004) Temporal variability of nitrogen cycling in continental-shelf sediments of the upwelling ecosystem off central Chile. *Deep-Sea Res. Pt II* **51**, 2491-2505.

Ferdelman T. G., Lee C., Pantoja S., Harder J., Bebout B. M. and Fossing H. (1997) Sulfate reduction and methanogenesis in a Thioploca-dominated sediment off the coast of Chile. *Geochim. Cosmochim. Acta* **61**, 3065-3079.

Fernández C., Farías L. and Alcaman M. E. (2009) Primary production and nitrogen regeneration processes in surface waters of the Peruvian upwelling system. *Prog. Oceanogr.* **83**, 159-168.

Fiedler P. C. and Talley L. D. (2006) Hydrography of the eastern tropical Pacific: A review. *Prog. Oceanogr.* **69**, 143-180.

Fossing H., Gallardo V. A., Jørgensen B. B., Hüttel M., Nielsen L. P., Schulz H., Canfield D. E., Forster S., Glud R. N., Gundersen J. K., Küver J., Ramsing N. B., Teske A., Thamdrup B., and Ulloa O. (1995) Concentration And Transport Of Nitrate By The Mat-Forming Sulfur Bacterium Thioploca. *Nature* **374**, 713-715.

Froelich P., Arthur M., Burnett W., Deakin M., Hensley V., Jahnke R., Kaul L., Kim K.-H., Roe K., Soutar A. and Vathakanon C. (1988) Early diagenesis of organic matter in Peru continental margin sediments: Phosphorite precipitation. *Mar. Geol.* **80**, 309-343.

Fuenzalida R., Schneider W., Garcés-Vargas J., Bravo L. and Lange C. (2009) Vertical and horizontal extension of the oxygen minimum zone in the eastern South Pacific Ocean. *Deep-Sea Res. Pt II* **56**, 1027-1038.

Fulweiler R. W., Nixon S. W., Buckley B. A. and Granger S. L. (2007) Reversal of the net dinitrogen gas flux in coastal marine sediments. *Nature* **448**, 180-182.

Gallardo V. A. (1977) Large benthic microbial communities in sulphide biota under Peru-Chile subsurface countercurrent. *Nature* **268**, 331-332.

Gilbert F., Souchu P., Bianchi M. and Bonin P. (1997) Influence of shellfish farming activities on nitrification, nitrate reduction to ammonium and denitrification at the water-sediment interface of the Thau lagoon, France. *Mar. Ecol.-Prog. Ser.* **151**, 143-153.

Glud R. N., Thamdrup B., Stahl H., Wenzhoefer F., Glud A., Nomaki H., Oguri K., Revsbech N. P. and Kitazatoe H. (2009) Nitrogen cycling in a deep ocean margin sediment (Sagami Bay, Japan). *Limnol. Oceanogr.* **54**, 723-734.

Graco M., Farías L., Molina V., Gutiérrez D. and Nielsen L. P. (2001) Massive developments of microbial mats following phytoplankton blooms in a naturally eutrophic bay: Implications for nitrogen cycling. *Limnol. Oceanogr.* **46**, 821-832.

Grasshoff K., Ehrhardt M. and Kremling K. (1999) *Methods of Seawater Analysis*. Wiley-VCH, Weinheim.

Gruber N. (2004) The dynamics of the marine nitrogen cycle and its influence on the atmospheric CO_2 variations. In *The Ocean Carbon Cycle and Climate* (eds. Follows M. and Oguz T.). NATO ASI Series. pp. 97-148.

Gruber N. and Sarmiento J. L. (1997) Global patterns of marine nitrogen fixation and denitrification. *Global Biogeochem. Cy.* **11**, 235-266.

Gutiérrez D., Enriquez, E., Purca, S., Quipúzcoa, L., Marquina, R., Flores, G., and Graco, M. (2008) Oxygenation episodes on the continental shelf of central Peru: Remote forcing and benthic ecosystem response. *Prog. Oceanogr.* **79**, 177-189.

Gutiérrez D., Sifeddine A., Field D. B., Ortlieb L., Vargas G., Chávez F. P., Velazco F., Ferreira V., Tapia P., Salvatteci R., Boucher H., Morales M. C., Valdés J., Reyss J. L., Campusano A., Boussafir M., Mandeng-Yogo M., García M. and Baumgartner T. (2009) Rapid reorganization in ocean biogeochemistry off Peru towards the end of the Little Ice Age. *Biogeosciences* **6**, 835-848.

Hamersley M. R., Lavik G., Woebken D., Rattray J. E., Lam P., Hopmans E. C., Damsté J. S. S., Krüger S., Graco M., Gutiérrez D., and Kuypers M. M. M. (2007) Anaerobic ammonium oxidation in the Peruvian oxygen minimum zone. *Limnol. Oceanogr.* **52**, 923-933.

Hamme R. C. and Emerson S. R. (2004). The solubility of neon, nitrogen and argon in distilled water and seawater. *Deep-Sea Res. Pt I* **51**, 1517-1528.

Hartnett H. E. and Devol A. H. (2003) Role of a strong oxygen-deficient zone in the preservation and degradation of organic matter: A carbon budget for the continental margins of northwest Mexico and Washington State. *Geochim. Cosmochim. Acta* **67**, 247-264.

Henrichs S. M. and Farrington J. W. (1984). Peru upwelling region sediments near 15 °S. 1. Remineralization and accumulation of organic matter. *Limnol. Oceanogr.* **29**, 1-19.

Ingall E. and Jahnke R. (1994) Evidence For Enhanced Phosphorus Regeneration From Marine-Sediments Overlain By Oxygen Depleted Waters. *Geochim. Cosmochim. Acta* **58**, 2571-2575.

Ivanenkov V. N. and Lyakhin Y. (1978) Determination of total alkalinity in seawater. In *Methods of Hydrochemical Investigations in the Ocean* (eds. Bordovsky O.K. and Ivanenkov V.N.). Nauka Publ. House. pp. 110-114.

Jørgensen, B. B. and Kasten, S. Sulfur cycling and methane oxidation. (2006) In *Marine Geochemistry* 2nd ed., (eds. Schulz, H. D. and Zabel, M.), Springer-Verlag, Berlin, pp. 271-309.

Jørgensen B. B. and Sørensen J. (1985) Seasonal Cycles Of O_2, NO_3^- And SO_4^{2-} Reduction In Estuarine Sediments - The Significance Of An NO_3^--Reduction Maximum In Spring. *Mar. Ecol.-Prog. Ser.* **24**, 65-74.

Jørgensen B. B. and Gallardo V. A. (1999) Thioploca spp: filamentous sulfur bacteria with nitrate vacuoles. *Fems Microbiol. Ecol.* **28**, 301-313.

Jørgensen B. B. and Nelson D. (2004) Sulfide oxidation in marine sediments: Geochemistry meets microbiology. In *Sulfur Biogeochemistry: Past and Present* (eds. Amend J. P., Edwards T. W. and Lyons K. J. E.), Geological Society of America, Special Paper 379. pp. 63-81.

Jørgensen B. B., Böttcher M. E., Luschen H., Neretin L. N. and Volkov I. I. (2004) Anaerobic methane oxidation and a deep H_2S sink generate isotopically heavy sulfides in black sea sediments. *Geochim. Cosmochim. Acta* **68**, 2095-2118.

Joye S. B. (2002) Denitrification in the Marine Environment. In *Encyclopedia of Environmental Microbiology* (ed. G. Collins), Wiley, New York. pp. 1010-1019.

Joye S. B. and Hollibaugh J. T. (1995) Influence Of Sulfide Inhibition Of Nitrification On Nitrogen Regeneration In Sediments. *Science* **270**, 623-625.

Kessler W. S. (2006) The circulation of the eastern tropical Pacific: A review. *Prog. Oceanogr.* **69**, 181-217.

Kim D., Matsuda O., and Yamamoto T. (1997) Nitrification, Denitrification and Nitrate Reduction Rates in the Sediment of Hiroshima Bay, Japan. *J. Oceanogr.* **53**, 317-324.

Krissek L. A., Scheidegger K. F. and Kulm L. D. (1980) Surface Sediments Of The Peru-Chile Continental-Margin And The Nazca Plate. *Geol. Soc. Am. Bull.* **91**, 321-331.

Kuypers M. M. M., Sliekers A. O., Lavik G., Schmid M., Jørgensen B. B., Kuenen J. G., Damsté J. S. S., Strous M. and Jetten M. S. M. (2003) Anaerobic ammonium oxidation by anammox bacteria in the Black Sea. *Nature* **422**, 608-611.

Lam P., Lavik G., Jensen M. M., van de Vossenberg J., Schmid M., Woebken D., Dimitri G., Amann R., Jetten M. S. M. and Kuypers M. M. M. (2009) Revising the nitrogen cycle in the Peruvian oxygen minimum zone. *P. Natl. Acad. Sci. USA* **106**, 4752-4757.

Lam P. and Kuypers M. M. M. (2011) Microbial nitrogen cycling processes in oxygen minimum zones. *Annu. Rev. Mar. Sci.* **3**, 317-345.

Levin L., Gutiérrez D., Rathburn A., Neira C., Sellanes J., Muñoz P., Gallardo V. and Salamanca M. (2002) Benthic processes on the Peru margin: a transect across the oxygen minimum zone during the 1997-98 El Niño. *Prog. Oceanogr.* **53**, 1-27.

Middelburg J. J., Soetaert K., Herman P. M. J. and Heip C. H. R. (1996) Denitrification in marine sediments: A model study. *Global Biogeochem. Cy.* **10**, 661-673.

Morales C. E., Hormazábal S. E. and Blanco J. L. (1999) Interannual variability in the mesoscale distribution of the depth of the upper boundary of the oxygen minimum layer off northern Chile (18-24S): Implications for the pelagic system and biogeochemical cycling. *J. Mar. Res.* **57**, 909-932.

Morse J. W. and Morin J. (2005) Ammonium interaction with coastal marine sediments: influence of redox conditions on K*. *Mar. Chem.* **95**, 107-112.

Mosch T., Sommer S., Pfannkuche O. and Wallmann K. (2010) Habitat Mapping in the Peruvian OMZ. *Eos Trans. AGU* **91(26)**, Ocean Sci. Meet. Suppl., Abstract BO35C-08.

Niggemann J., Ferdelman T. G., Lomstein B. A., Kallmeyer J. and Schubert C. J. (2007) How depositional conditions control input, composition, and degradation of organic matter in sediments from the chilean coastal upwelling region. *Geochim. Cosmochim. Acta* **71**, 1513-1527.

Noffke A., Hensen C., Sommer S., Scholz F. and Wallmann K. (2010) Benthic fluxes of iron, phosphate and silicate across the Peruvian Oxygen Minimum Zone. *Eos Trans. AGU* **91(26)**, Ocean Sci. Meet. Suppl., Abstract BO35C-09.

Otte, S., Kuenen J. G. , Nielsen L. P., Paerl H. W., Zopfi J., Schulz H. N., Teske A., Strotmann B., Gallardo V.A. and Jørgensen B. B. (1999) Nitrogen, carbon, and sulfur metabolism in natural Thioploca samples. *Appl. Environmental. Microb.* **65**, 3148-3157.

Oschlies A., Schulz K. G., Riebesell U. and Schmittner A. (2008) Simulated 21st century's increase in oceanic suboxia by CO2-enhanced biotic carbon export. *Global Biogeochem. Cy.* **22**, GB4008.

Pennington J. T., Mahoney K. L., Kuwahara V. S., Kolber D. D., Calienes R. and Chavez F. P. (2006). Primary production in the eastern tropical Pacific: A review. *Prog. Oceanogr.* **69**, 285-317.

Preisler A., de Beer D., Lichtschlag A., Lavik G., Boetius A. and Jørgensen B. B. (2007) Biological and chemical sulfide oxidation in a Beggiatoa inhabited marine sediment. *Isme J.* **1**, 341-353.

Prokopenko M. G., Hammond D. E., Berelson W. M., Bernhard J. M., Stott L. and Douglas R. (2006) Nitrogen cycling in the sediments of Santa Barbara basin and Eastern Subtropical North Pacific: Nitrogen isotopes, diagenesis and possible chemosymbiosis between two lithotrophs (Thioploca and Anammox) - "riding on a glider". *Earth Planet. Sc. Lett.* **242**, 186-204.

Redfield A. C., Ketchum B. H. and Richards F. A. (1963) The Influence of organisms on the composition of seawater. In *The Sea*, vol. 2 (ed. Hill M. N.), Wiley Interscience. pp. 26-77.

Reimers C. and Suess E. (1983) Spatial and temporal patterns of organic matter accumulation on the Peru continental margin. In *Coastal Upwelling Its Sediment Record, Part B. Sedimentary Records of Ancient Coastal Upwelling* (eds. Thiede J. and Suess E.), Plenum Press, pp. 311-346.

Risgaard-Petersen N., Meyer R. L. and Revsbech N. P. (2005) Denitrification and anaerobic ammonium oxidation in sediments: effects of microphytobenthos and NO_3^-. *Aquat. Microb. Ecol.* **40**, 67-76.

Rowe G. T. and Howarth R. (1985) Early diagenesis of organic matter in sediments off the coast of Peru. *Deep-Sea Res. Pt A.* **32**, 43-55.

Rysgaard S., Glud R. N., Risgaard-Petersen N. and Dalsgaard T. (2004) Denitrification and anammox activity in Arctic marine sediments. *Limnol. Oceanogr.* **49**, 1493-1502.

Poulton S. W. and Raiswell R. (2002) The low-temperature geochemical cycle of iron: From continental fluxes to marine sediment deposition. *Am. J. Sci.* **302**, 774-805.

Sarbas B. and Nohl U. (2009) The GEOROC database - A decade of "online geochemistry". *Geochim. Cosmochim. Acta* **73**, A1158.

Schulz H. N. and Jørgensen B. B. (2001) Big bacteria. *Annu. Rev. Microbiol.* **55**, 105-137.

Schwartz M. C., Woulds C. and Cowie G. L. (2009) Sedimentary denitrification rates across the Arabian Sea oxygen minimum zone. *Deep-Sea Res. Pt II* **56**, 324-332.

Shaffer G., Olsen S. M. and Pedersen J. O. P. (2009) Long-term ocean oxygen depletion in response to carbon dioxide emissions from fossil fuels. *Nat. Geosci.* **2**, 105-109.

Sifeddine A., Gutiérrez D., Ortlieb L., Boucher H., Velazco F., Field D., Vargas G., Boussafir M., Salvatteci R., Ferreira V., Garcia M., Valdés J., Caquineau S., Yogo M. M., Cetin F., Solis J., Soler P. and Baumgartner T. (2008). Laminated sediments from the central Peruvian continental slope: A 500 year record of upwelling system productivity, terrestrial runoff and redox conditions. *Progr. Oceanogr.* **79**, 190-197.

Silva N., Rojas N. and Fedele A. (2009) Water masses in the Humboldt Current System: Properties, distribution, and the nitrate deficit as a chemical water mass tracer for Equatorial Subsurface Water off Chile. *Deep-Sea Res. Pt II* **56**, 992-1008.

Sommer S., Bohlen L., Dale A. W., Wallmann K., Hensen C., Mosch T., Noffke A. and Pfannkuche O. (submitted to Global Biogeochemical Cycles) Nitrogen fluxes across Peruvian oxygen minimum zone surface sediments - the potential significance of DNRA.

Sommer S., Linke P., Pfannkuche O., Niemann H. and Treude T. (2010) Benthic respiration in a seep habitat dominated by dense beds of ampharetid polychaetes at the Hikurangi Margin (New Zealand). *Mar. Geol.* **272**, 223-232.

Sommer S., McGinnis D. F., Linke P., Camilli R., Mosch T. and Pfannkuche O. (2010a) Life at the edge - oscillating lower boundary of the Peruvian oxygen minimum zone. *Eos Trans. AGU* **91(26)**, Ocean Sci. Meet. Suppl., Abstract BO24C-08.

Sørensen J., Tiedje J. M. and Firestone R. B. (1980) Inhibition by sulfide of nitric and nitrous oxide reduction by denitrifying Pseudomonas fluorescens. *Appl. Environ. Microb.* **39**, 105-108.

Stramma L., Johnson G. C., Sprintall J. and Mohrholz V. (2008) Expanding oxygen-minimum zones in the tropical oceans. *Science* **320**, 655-658.

Straub K. L., Benz M., Schink B. and Widdel F. (1996) Anaerobic, nitrate-dependent microbial oxidation of ferrous iron. *Appl. Environ. Microb.* **62**, 1458-1460.

Suess E., Kulm L. D. and Killingley J. S. (1987) Coastal upwelling and a history of organic-rich mudstone deposition off Peru. In *Marine Petroleum Source Rocks* (eds. Brooks J. and Fleet A.J.). Geological Society. pp. 181-197.

Thamdrup B. and Canfield D. E. (1996) Pathways of carbon oxidation in continental margin sediments off central Chile. *Limnol. Oceanogr.* **41**, 1629-1650.

Thamdrup B. and Dalsgaard T. (2002) Production of N_2 through anaerobic ammonium oxidation coupled to nitrate reduction in marine sediments. *Appl. Environ. Microb.* **68**, 1312-1318.

Thauer R. K., Jungermann K. and Decker K. (1977) Energy-Conservation In Chemotrophic Anaerobic Bacteria. *Bacteriol. Rev.* **41**, 100-180.

Thullner, M., Dale, A. W. and Regnier, P. (2009) Global-scale quantification of mineralization pathways in marine sediments: A reaction-transport modeling approach. *Geochem. Geophys. Geosyst.* **10**, Q10012, doi:10.1029/2009GC002484.

Trimmer M. and Nicholls J. C. (2009) Production of nitrogen gas via anammox and denitrification in intact sediment cores along a continental shelf to slope transect in the North Atlantic. *Limnol. Oceanogr.* **54**, 577-589.

Van Cappellen P. and Ingall E. D. (1994) Benthic phosphorus regeneration, net primary production, and ocean anoxia: A model of the coupled marine biogeochemical cycles of carbon and phosphorus. *Paleoceanography* **9**, 677-692.

Van Cappellen P. and Wang Y. (1996) Cycling of iron and manganese in surface sediments; a general theory for the coupled transport and reaction of carbon, oxygen, nitrogen, sulfur, iron, and manganese. *Am. J. Sci.* **296**, 197-243.

Wallmann, K. (2010). Phosphorus imbalance in the global ocean? *Global Biogeochem. Cy.* **24**, GB4030.

Wallmann K., Aloisi G., Haeckel M., Tishchenko P., Pavlova G., Greinert J., Kutterolf S. and Eisenhauer A. (2008) Silicate weathering in anoxic marine sediments. *Geochim. Cosmochim. Acta* **72**, 2895-2918.

Wolf-Gladrow D. A., Zeebe R. E., Klaas C., Körtzinger A. and Dickson A. G. (2007) Total alkalinity: The explicit conservative expression and its application to biogeochemical processes. *Mar. Chem.* **106**, 287-300.

Woulds C., Schwartz M.C., Brand T., Cowie G., Law G. and Mowbray S. (2009). Porewater nutrient concentrations and benthic nutrient fluxes across the Pakistan margin OMZ. *Deep-Sea Research II* **56**, 333-346.

Zopfi J., Kjær T., Nielsen L. P. and Jørgensen B. B. (2001) Ecology of Thioploca spp.: Nitrate and sulfur storage in relation to chemical microgradients and influence of Thioploca spp. on the sedimentary nitrogen cycle. *Appl. Environ. Microb.* **67**, 5530-5537.

Zuta S. and Guillén O. (1970) *Oceanografia de las aguas costeras del Peru*, vol. 2. Instituto del Mar del Peru, Boletin. pp. 161-323.

3. A simple transfer function for calculating benthic fixed nitrogen losses in global biogeochemical models

L. Bohlen*, A. W. Dale and K. Wallmann

Leibniz Institute of Marine Sciences (IFM-GEOMAR), Wischhofstr. 1 - 3, 24148 Kiel, Germany
* author for correspondence : lbohlen@ifm-geomar.de

Submitted to *Global Biogeochemical Cycles*

Abstract

Empirical transfer functions are derived for predicting the total benthic nitrate loss (L_{NO3}) and the net loss of dissolved inorganic nitrogen (L_{DIN}) in marine sediments, equivalent to sedimentary denitrification. The functions are dynamic vertically-integrated sediment models which require the rain rate of particulate organic carbon to the seafloor (RRPOC) and a proposed new variable O_2* (bottom water O_2 - NO_3^-) as the only input parameters. Applied globally to maps of RRPOC and O_2* on a $1^\circ \times 1^\circ$ spatial resolution, the models predict a NO_3^- drawdown of 196 Tg yr^{-1} (L_{NO3}) of which 153 - 155 Tg yr^{-1} is denitrified to N_2 (L_{DIN}). The continental shelf (0 - 200 m) accounts for > 50 % of global L_{NO3} and L_{DIN}, with slope (200 - 2000 m) and deep-sea (>2000 m) sediments contributing ca. 30 % and 20 %, respectively. Denitrification in high-nitrate/low-oxygen regions such as oxygen minimum zones is significant (ca. 15 Tg N yr^{-1}; 10 % of global) despite covering only 1 % of the seafloor. The data are used to estimate the total flux of nitrate (18 Tg N yr^{-1}) and phosphate (27 Tg P yr^{-1}) across the sediment-water interface. The benthic fluxes strongly deviate from Redfield composition, with globally-averaged N:P, N:C and C:P values of 8.3, 0.067 and 122, respectively, indicating severe fixed N losses by denitrification. The transfer functions are designed to be coupled dynamically to general circulation models to better predict the feedback of sediments on pelagic nutrient cycling and dissolved O_2 distributions.

3.1. Introduction

The marine fixed nitrogen (N) budget of the global ocean is poorly constrained since the magnitude of the major input and removal fluxes by nitrogen fixation and denitrification remain poorly constrained. Sediment denitrification is the major sink for fixed nitrogen (Brandes and Devol, 2002; Codispoti et al., 2001; Galloway 2004; Gruber, 2004). Early estimates of global benthic denitrification rates pointed toward fixed N losses on the order of 100 Tg N yr^{-1} or lower (e.g. Codispoti and Christensen, 1985). More recently, however, these estimates have been revised upwards by as much as a factor of 2 - 3 using a variety of different approaches such as global N isotope budgeting (Brandes and Devol, 2002; Deutsch et al., 2004), reaction-transport modeling (Middelburg et al., 1996), and data extrapolation and interpretation (Codispoti et al., 2001). Moreover, although benthic denitrification constitutes the major sink in the modern ocean (Codispoti et al., 2001; Galloway 2004; Gruber, 2004), it is only rarely considered in biogeochemical models of N cycling in the global ocean (e.g. Romaniello and Derry, 2010; Somes et al., 2010).
Shelf and hemipelagic sediments have been identified as important sites for benthic denitrification (Christensen et al., 1987; Devol, 1991). However, the factors that ultimately control the rate of benthic denitrification are difficult to identify. Using a digenetic model forced by parameterizations based on seafloor depth, Middelburg et al. (1996) observed that denitrification was most sensitive to the rain rate of labile particulate organic carbon (POC) to the seafloor. On the other hand, increasing rates of denitrification have also been found to be related to increasing nitrate (NO_3^-) concentrations (e.g. Dale et al., 2011; Fennel et al., 2009). Even though low oxygen (O_2) is a prerequisite for denitrification, the effect of bottom water O_2 is less obvious. For example, higher O_2 concentrations may either lead to an enhancement of denitrification via coupled nitrification-denitrification or may otherwise inhibit denitrification though reduced substrate availability because of higher aerobic respiration rates (Middelburg et al., 1996; Rysgaard et al., 1994). It is the relative concentrations of O_2 and NO_3^- which appear to be important in determining benthic denitrification rates if organic substrate is plentiful (Dale et al., 2011).

The aim of this study is to derive an algorithm, or transfer function, for predicting rates of denitrification in marine sediments based on a small number of globally accessible parameters. The transfer function is equivalent to the 'level 3' dynamic vertically integrated sediment model described by Soetaert et al. (2000) for coupling benthic and pelagic biogeochemical models. First, we developed a function for benthic NO_3^- losses (L_{NO3}) using measured NO_3^- fluxes across the sediment-water interface. Under our assumptions, L_{NO3} is equivalent to the maximum rate of denitrification because it does not account for the loss of fixed N as ammonium (NH_4^+). Thus, in a second step, observed NH_4^+ fluxes were used to calculate the net loss of dissolved inorganic nitrogen (DIN = NO_3^- + NH_4^+), L_{DIN}, which is then used as a proxy for benthic denitrification. Since previous studies have shown the importance of bottom water O_2 and NO_3^- concentrations and the rain rate of POC to the seafloor (RRPOC)

in controlling denitrification rates (Dale et al., 2011; Middelburg et al., 1996), these are used as master variables in the transfer function through a proposed new variable O_2* (O_2 - NO_3^-). Finally, we apply these functions to global fields of bottom water O_2, NO_3^- and RRPOC data to derive global estimates of benthic NO_3^- loss and denitrification that are consistent with previous estimates. These easy-to-apply functions are designed to be coupled to biogeochemical general circulation models (Soetaert et al., 2000) to provide a computationally-efficient means of coupling benthic and pelagic N redox chemistry to evaluate regions of N loss and potential benthic feedbacks on the global inventory of ocean fixed N and dissolved O_2.

3.2. Data aquisition

3.2.1. Site specific data

Literature data of NO_3^- and NH_4^+ fluxes across the sediment-water interface, bottom water O_2 (bw_{O2}) and NO_3^- (bw_{NO3}) concentrations (both in μM), as well as data on benthic carbon oxidation rates (RPOC, mmol C m^{-2} d^{-1}) or particulate organic carbon rain rates to the sediment (RRPOC, mmol C m^{-2} d^{-1}) from sites all over the world were compiled (Table B.1 in Appendix B). Some of the NO_3^- fluxes in Table B.1 were reported as the sum of NO_3^- and nitrite (NO_2^-). Where no such clarifications were made, we assume that NO_2^- fluxes were negligible compared to NO_3^- fluxes. A total of 180 NO_3^- flux measurements are available, compared to 122 NH_4^+ fluxes. In what follows, negative fluxes denote uptake by the sediment.

Since the rate of solute transport across the sediment-water interface by bioirrigation may be up to 3 times higher than the molecular diffusive flux (Devol and Christensen, 1993), only in situ measurements from benthic chamber lander deployments were included in the database. However, for water depths > 3000 m, bioirrigation was assumed to be of minor importance for benthic solute exchange (Glud, 2008) and diffusive fluxes determined from porewater profiles ex situ were used in addition to in situ chamber measurements.

Our database includes sites from anoxic (e.g. oxygen minimum zones, OMZs) to fully oxygenated regions of the ocean from the shallow shelf to the deep sea. Bottom water NO_3^- varied from < 1 μM to 45 μM. At stations where bottom water O_2 and NO_3^- concentrations were not provided in the original references, values were estimated from nearby stations or from the World Ocean Atlas (WOA) 2005 (Garcia et al., 2006a; 2006b). Thus, the database comprises the wide range of redox conditions encountered in the contemporary ocean.

The transfer functions derived below require knowledge of carbon rain rates. However, in almost all cases only RPOC was given. In these cases RRPOC was calculated assuming that the accumulation rate of POC below the bioturbated zone (APOC, mmol C m^{-2} d^{-1}) is equal to the difference between

RRPOC and RPOC at steady state:

$$\text{APOC} = \text{RRPOC} - \text{RPOC} \tag{3.1}$$

This equation introduces another unknown, APOC. Therefore, RRPOC were solved from the above equation and Eq. 3.2 below which relates RRPOC and APOC in shelf/slope ($APOC_{SL}$, < 2000 m) and deep-sea ($APOC_D$, > 2000 m) sediments according to Flögel et al. (2011):

$$\text{APOC} = \begin{cases} 0.14 \cdot \text{RRPOC}^{1.11} & \text{for depths} \leq 2000 \text{ m} \\ 0.014 \cdot \text{RRPOC}^{1.05} & \text{for depths} \geq 2000 \text{ m} \end{cases} \tag{3.2}$$

The equations were solved using the FindRoot function in MATHEMATICA 7.0.

3.2.2. Global datasets

Global data of bw_{O2} and bw_{NO3} concentrations were obtained from annual objectively analyzed mean concentrations from the WOA 2005 (Garcia et al., 2006a; 2006b) with a $1° \times 1°$ horizontal resolution. These data were available for water depths up to 5500 m with a vertical resolution varying from 10 m close to the sea surface to 500 m for water depths > 2000 m. The annual mean data recorded at the deepest water depth for a specific coordinate is assumed to be representative of the bottom water concentration in this study.
Carbon rain rates (Fig. 3.1A) were estimated from primary production and empirical functions as follows. Mean monthly primary production rates were derived from satellite imagery of chlorophyll a (Chl a), photosynthetically available radiation (PAR) and sea-surface temperature (SST) following Behrenfeld and Falkowski (1997). Monthly climatological data (1997 - 2010) for Chl a and PAR were obtained by SeaWIFS (Feldman and McClain, 2010), and monthly objectively analyzed means of SST were derived from the WOA 2005 (Locarni et al., 2006). Based on the spatially-resolved monthly primary production estimates, POC export production at each grid point was then determined using the pe-ratio (Dunne et al., 2005). Particle transport to the sea floor was subsequently calculated using the 'Martin curve' (Martin et al., 1987):

$$F = F_{100} \cdot (z/100)^b \tag{3.3}$$

where F is the POC flux reaching the sea floor (mmol C m^{-2} d^{-1}) and F_{100} is the POC export flux at 100 m (mmol C m^{-2} d^{-1}) which was assumed to be equal to the POC export production. The value of the exponent (b = -0.82) was defined according to Berelson (2001). Finally, monthly RRPOC were integrated over time to annual mean values. The bathymetry of the seafloor was defined according to ETOPO5 (NOAA, 1988).
All data in the figures presented were processed on a $1° \times 1°$ grid. Data available at higher resolution

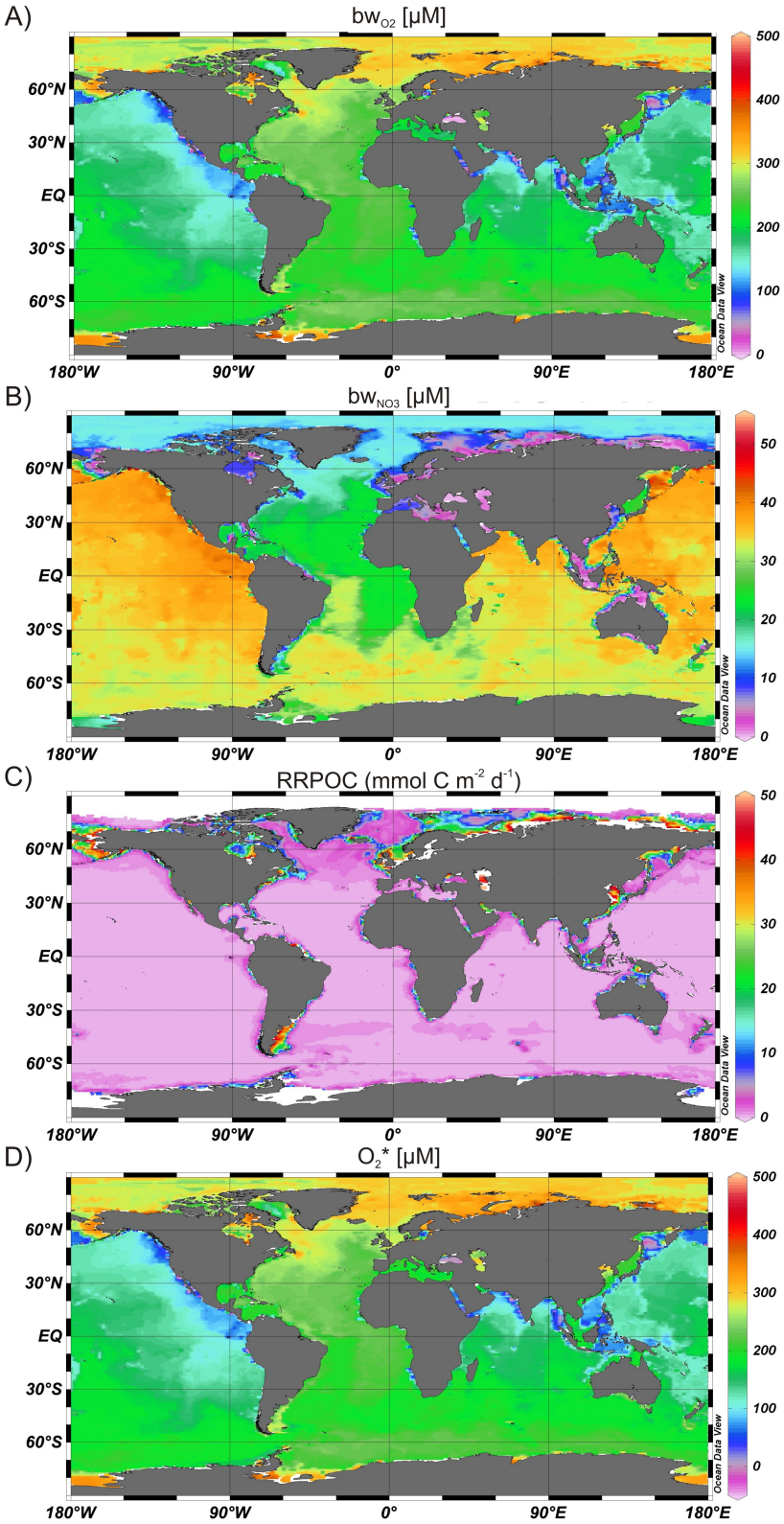

Figure 3.1.: Global datasets on a 1° × 1° horizontal resolution. A) POC rain rates (mmol C m^{-2} d^{-1}). Rain rate data were calculated from primary production estimates (see section 3.2.2). B) O_2* (= bw_{O2} - bw_{NO3}, µM).

(SeaWIFS data at 9 × 9 km, bathymetry at 5' × 5') were averaged within each 1° × 1° grid cell. Upscaling of areal rates to total global fluxes (in Tg yr^{-1}) was achieved using the area of each 1° × 1° grid according to the NASA ISLSCP GDSLAM dataset (Meeson et al., 1995).

3.3. Derivation of the transfer function

3.3.1. Defining benthic NO_3^- and DIN loss

The benthic fluxes of NO_3^- (J_{NO3}) and the POC degradation rates were used to calculate the depth-integrated rate of NO_3^- loss by denitrification (L_{NO3}) within the sediment using the following formula assuming steady state:

$$L_{NO3} = RPON - J_{NO3} = RPOC \cdot 16/106 - J_{NO3} \tag{3.4}$$

where RPON is the degradation of particulate organic nitrogen (PON) determined from RPOC assuming a Redfield C:N ratio of 106:16. The concept behind the foregoing equation relies on the idea that all organic nitrogen released from PON as NH_4^+ is directly coupled to nitrification (Fig. 3.2). Based on the measured fluxes, nitrate is either released to the overlying water column or assumed to be denitrified to N_2 gas and removed from the fixed N pool within the sediment. We consider that nitrite does not accumulate to significant levels in the sediment or water column to warrant inclusion of this reactive intermediate in the conceptual model. Thus, in view of this highly simplified reaction network, our model does not differentiate between fixed N loss to N_2 by canonical denitrification or anammox, but provides the sum of these potential pathways. In what follows, the term denitrification refers to combined denitrification and anammox. Nitrate losses are highest when J_{NO3} is negative (benthic uptake), and vice versa. The error in L_{NO3} incurred by not accounting for solute burial is negligible and ignored in further calculations. Organic-rich sediments or those underlying hypoxic bottom waters may release NH_4^+ directly to the overlying water column. Since L_{NO3} does not consider the flux of NH_4^+ to the water column (J_{NH4}), fixed N loss estimated using the above approach is overestimated and is the maximum potential denitrification rate. Thus, a correction can be made to L_{NO3}, giving an expression for the total loss of DIN (L_{DIN}) which represents our rate estimate of denitrification:

$$L_{DIN} = L_{NO3} - J_{NH4} = RPOC \cdot 16/106 - J_{NO3} - J_{NH4} \tag{3.5}$$

In the above model, dissimilatory nitrate reduction to ammonium (DNRA) by giant sulfur bacteria such as *Beggiatoa* (Otte et al., 1999; Schulz and Jørgensen, 2001) was not considered explicitly as a sink for NO_3^- (Fig. 3.2). However, by considering the fluxes of nitrate and ammonium across the sediment surface, this process is implicitly accounted for in L_{DIN} since the produced NH_4^+ is either

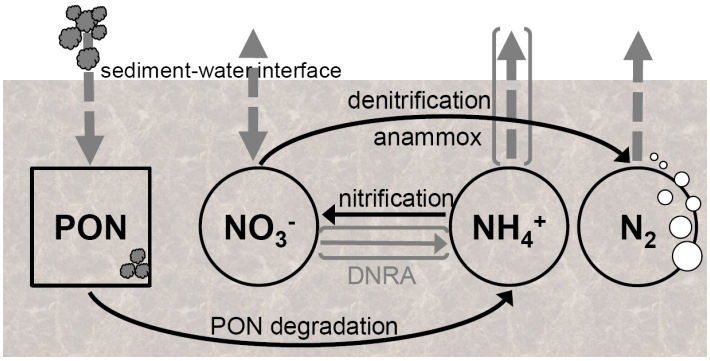

Figure 3.2.: Conceptual model of the reaction network used to derive the transfer function. The arrows in brackets symbolize the potential fluxes of NH_4^+ across the sediment-water interface and NH_4^+ production during dissimilatory nitrate reduction to ammonium (DNRA), which were considered for the loss of DIN (see section 3.3.1). Note that NO_3^- is defined as the sum of NO_3^- + NO_2^-.

nitrified again to NO_3^- or is released from the sediment as NH_4^+.
Table B.1 only includes data from sites where L_{NO3} and L_{DIN} values were positive. Negative values imply that more NO_3^- and/or NH_4^+ are released than produced during PON degradation coupled to nitrification or DNRA. N cycling at these sites (e.g. some stations on the Porcupine Abyssal Plain or in the Equatorial Pacific) may be at non-steady state or, alternatively, particulate organic matter (POM) mineralization may be occurring with C:N ratios lower than Redfield. Whilst there is some evidence to suggest a non-Redfield composition of POM in marine sediments (Sarmiento and Gruber, 2006), a constant C:N is considered here so as to be consistent with the commonly assumed Redfield stoichiometry adopted in general circulation models.

3.3.2. A transfer function for the maximum rate of NO_3^- loss by denitrification

Based on the above dataset, a transfer function for predicting the benthic NO_3^- sink strength was derived using RRPOC, bw_{O2}, and bw_{NO3} as master variables. Previous studies have shown that denitrification and anammox are highly sensitive to these variables (Dale et al., 2011; Dalsgaard et al., 2005; Middelburg et al., 1996) although other workers found less importance of bw_{O2}, and bw_{NO3} (Fennel et al., 2009). Because denitrification rates have been shown to be high in regions with high nitrate and low oxygen levels (HNLO; e.g. Devol and Christensen (1993)), we propose a new variable termed O_2*:

$$O_2* = bw_{O2} - bw_{NO3} \tag{3.6}$$

O_2* allows settings with low bw_{O2} and high bw_{NO3} (i.e. negative O_2* values) which are important sinks for fixed N to be easily distinguished (Middelburg et al., 1996). Using the data from the studies

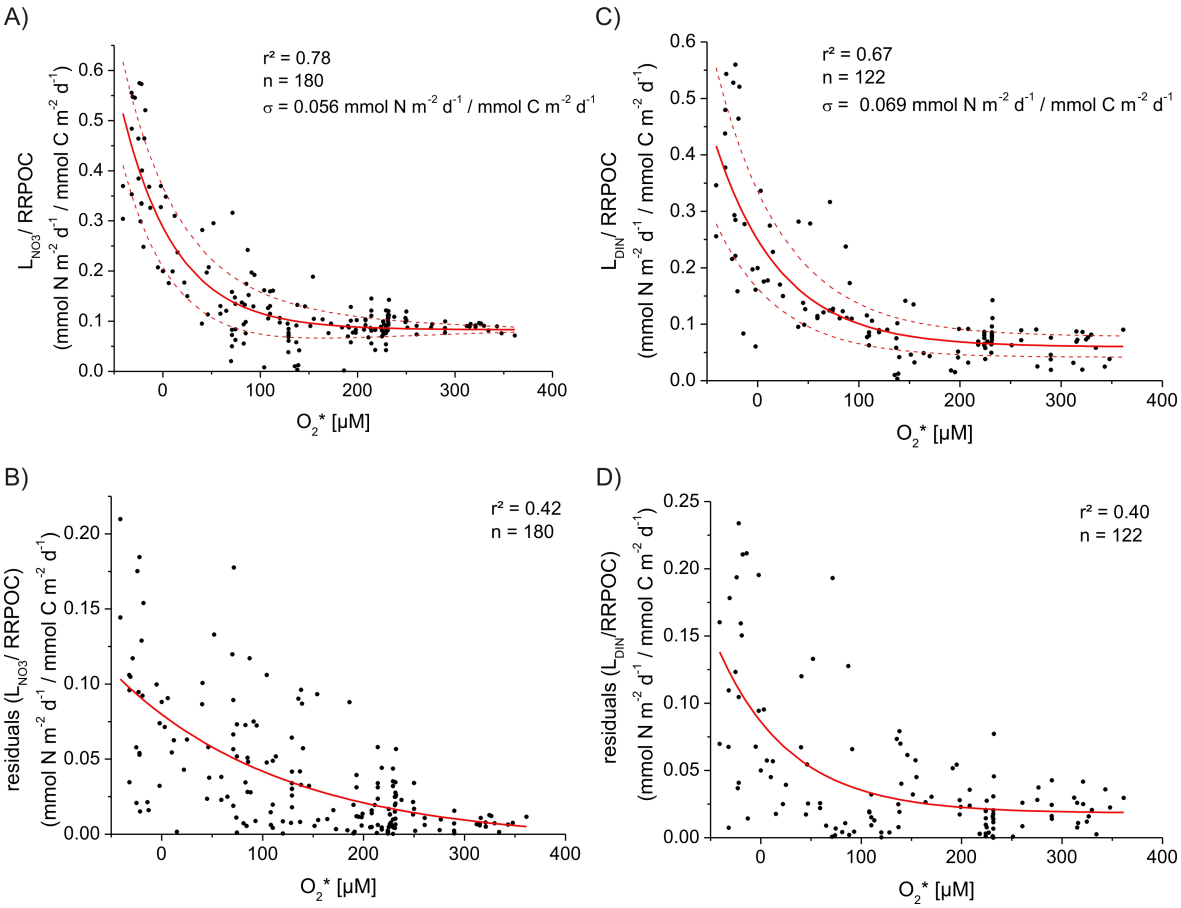

Figure 3.3.: The ratio L_{NO3}/RRPOC (A) and L_{DIN}/RRPOC (B) as a function of O_2*. The solid lines show the non-linear fit through the data (Eq. 3.7, 3.11), the dotted lines denote the error estimated from the residuals given in B) and D). The non-linear fit through the residuals (Eq. 3.9, 3.13) is denoted by the solid line.

listed in Table B.1, we identified a power law relationship between L_{NO3}, RRPOC and O_2*:

$$L_{NO3}/\mathrm{RRPOC} = a + b \cdot c^{\,O_2^*} \tag{3.7}$$

with a = 0.083 ± 0.006, b = 0.21 ± 0.013, c = 0.98 ± 0.002, where RRPOC is in units mmol m^{-2} d^{-1} and O_2* in µM. This function (Fig. 3.3A) shows that L_{NO3}/RRPOC decreases as O_2* increases. The fit shows a high level of significance (r^2 = 0.78, n = 180, $p < 0.001$) with a standard deviation of 0.056 mmol N m^{-2} d^{-1}/mmol C m^{-2} d^{-1}. Rearranging Eq. 3.7 gives the transfer function for NO_3^- loss:

$$L_{NO3} = (0.083 + 0.21 \cdot 0.98^{\,O_2^*}) \cdot \mathrm{RRPOC} \tag{3.8}$$

The error or uncertainty in L_{NO3}/RRPOC, $\Delta(L_{NO3}/\mathrm{RRPOC})$, was determined from the residuals of the fit and the data. As shown in Fig. 3.3B, $\Delta(L_{NO3}/\mathrm{RRPOC})$ is not constant but increases with decreasing

O_2* (Fig. 3.3B) according to the function:

$$\Delta(L_{NO3}/RRPOC) = d + e \cdot f^{\,O_2*} \tag{3.9}$$

with d = - 0.0047 ± 0.015, e = 0.085 ± 0.016, f = 0.99 ± 0.002. Higher errors at low O_2* values are probably due to the limited number of data points at sites with low bottom water oxygen concentrations needed to constrain the NO_3^- loss under such conditions.
Based on error combination rules, ΔL_{NO3} was calculated from $\Delta(L_{NO3}/RRPOC)$ and the mean relative error of the POC rain rate ($\Delta RRPOC/RRPOC$):

$$\Delta L_{NO3} = \sqrt{\left(\frac{\Delta(L_{NO3}/RRPOC)}{L_{NO3}/RRPOC}\right)^2 - \left(\frac{\Delta RRPOC}{RRPOC}\right)^2} \tag{3.10}$$

The relative error in the rain rate was estimated as 20 % based on confidence limits of benthic total oxygen uptake by Andersson et al. (2004).

3.3.3. A transfer function for denitrification

The transfer function for NO_3^- loss (Eq. 3.8) neglects NH_4^+ flux to the water column and provides an estimate of maximum rates of fixed N loss by denitrification. Thus, we took two different approaches to calculate a more realistic rate of fixed N loss, that is, correcting L_{NO3} for the NH_4^+ flux a priori and a posteriori.
In the a priori approach, we identified a correlation between L_{DIN}, RRPOC and O_2* following the procedure for L_{NO3} (Fig. 3.3C):

$$L_{DIN}/RRPOC = a + b \cdot c^{\,O_2*} \tag{3.11}$$

with a = 0.060 ± 0.01, b = 0.19 ± 0.019, c = 0.99 ± 0.003. RRPOC is in units mmol m^{-2} d^{-1} and O_2* in µM. Since fewer NH_4^+ flux data were available than for NO_3^- (n = 122 versus 180), the statistical correlation of this model is understandably lower yet is still highly significant ($r^2 = 0.67$, $p < 0.001$). Rearranging Eq. 3.11 gives the transfer function for L_{DIN}, which thus represents the a priori estimate for benthic denitrification (DEN1):

$$DEN1 = L_{DIN} = (0.060 + 0.19 \cdot 0.99^{\,O_2*}) \cdot RRPOC \tag{3.12}$$

Similarly, the error of the ratio $L_{DIN}/RRPOC$, $\Delta(L_{DIN}/RRPOC)$, was estimated from the residuals (Fig. 3.3D):

$$\Delta DEN1/RRPOC = d + e \cdot f^{\,O_2*} \tag{3.13}$$

with d = 0.018 ± 0.007, e = 0.068 ± 0.011, f = 0.99 ± 0.004. The error for the a priori denitrification estimate, ΔDEN1, was then calculated in the same way as Eq. 3.10.
Because L_{DIN} corrects for the NH_4^+ flux, the term L_{DIN}/RRPOC is akin to the fraction of POC rained to the seafloor which is denitrified. Similarly, L_{NO3}/RRPOC refers to the maximum fraction of RRPOC being denitrified. Considering that 0.8 moles of NO_3^- are required to oxidize 1 mole of carbohydrate organic carbon with a nominal oxidation state of zero (i.e. CH_2O) to CO_2, producing 0.4 mol of N_2 in the process, this model therefore predicts that roughly 10 % of carbon is respired by denitrification in the ocean basins (O_2* > 200 μM, Fig 3 A, C) in agreement with previous studies (Thullner et al., 2009; Middelburg et al., 1996). However, in HNLO regions such as OMZs, denitrification is predicted to account for > 40 % of carbon respired, which is again in agreement with previous results (Bohlen et al., 2011).

In the second approach, the correction for benthic NH_4^+ efflux to L_{NO3} was done a posteriori. Measured NH_4^+ efflux as the percentage of the total NO_3^- loss is shown in Fig. 3.4. Only data with positive NH_4^+ fluxes were considered and the steady-state assumption further requires that percentages exceeding 100 % were disregarded since this would imply that more NH_4^+ was released from the sediment than produced during either organic matter degradation or DNRA, or C:N ratios lower than Redfield. NH_4^+ release was generally minor for water depths > 1000 m and for these sites we assume that the calculated L_{NO3} equals the total loss of fixed N in the sediment. In contrast, NH_4^+ fluxes were equivalent to as much as 80 % of NO_3^- fluxes for water depths < 1000 m. However, the NH_4^+ flux showed no robust single or multiple regression correlation with RRPOC, bw_{O2}, bw_{NO3} or O_2* (data not shown). As a first approximation, therefore, we assumed that for water depths < 1000 m the NH_4^+ flux was equal to the average value, that is, 27 ± 23 % of the NO_3^- flux.
The final function for the a posteriori benthic denitrification estimate (DEN2) is thus calculated by correcting the transfer function for the NO_3^- loss (Eq. 3.8) directly:

$$\mathrm{DEN2} = \begin{cases} L_{NO3} & \text{for depths} \geq 1000 \text{ m} \\ 0.73 \cdot L_{NO3} & \text{for depths} \leq 1000 \text{ m} \end{cases} \tag{3.14}$$

3.3.4. Stoichiometry of benthic nitrogen and phosphorus fluxes

The transfer function for the benthic NO_3^- and DIN losses allow the flux of NO_3^- (J_{NO3}) and DIN (J_{DIN}) across the sediment water interface to be estimated (Eq. 3.4, 3.8 and 3.5, 3.12):

$$J_{NO3} = \mathrm{RPOC} \cdot 16/106 - L_{NO3} \tag{3.15}$$

$$J_{DIN} = \mathrm{RPOC} \cdot 16/106 - L_{DIN} \tag{3.16}$$

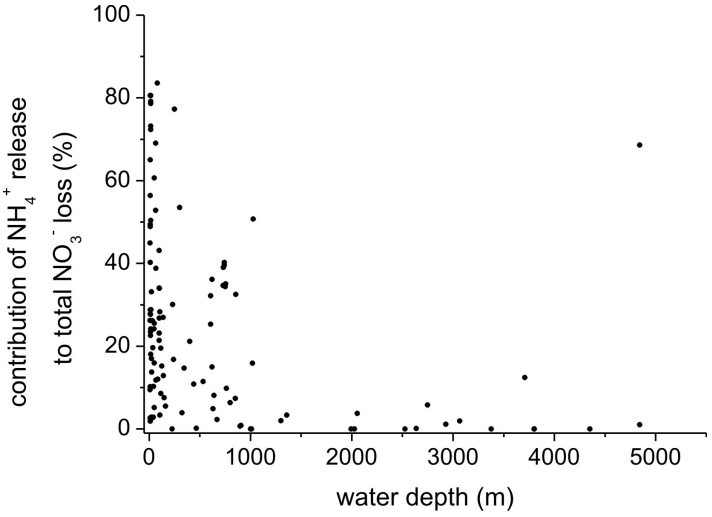

Figure 3.4.: Contribution of NH_4^+ release into the water column to the total fixed nitrogen loss (%) as a function of water depth (n = 116). Only percentages < 100 % were considered.

Note that J_{NO3} includes nitrate uptake by denitrification and DNRA, whereas J_{DIN} corrects for potential NO_3^- consumption by DNRA through the NH_4^+ correction. The derived J_{NO3} (Eq. 3.15) and measured J_{NO3} (Table B.1) are significantly correlated ($r^2 = 0.87$, n = 180, $p < 0.001$) with a standard deviation of 0.34 mmol N m^{-2} d^{-1} (Fig. 3.5). The measured DIN fluxes were also reproduced significantly by Eq. 3.16 (data not shown), yet here the correlation was weaker due to the lower number of data pairs ($r^2 = 0.70$, n = 122, $p < 0.001$). The total error of the NO_3^- and DIN flux estimates (ΔJ_{NO3} and ΔJ_{DIN}) were assumed to be equal to the error of the NO_3^- loss and DIN loss, respectively, i.e. $\Delta J_{NO3} = \Delta L_{NO3}$ and $\Delta J_{DIN} = \Delta L_{DIN}$.

Wallmann (2010) collated worldwide literature data of benthic phosphate (PO_4^{3-}) effluxes (mmol P m^{-2} d^{-1}), bottom water dissolved O_2 concentrations (μM) and, together with RPOC (mmol C m^{-2} d^{-1}), derived a relationship for a C:P regeneration ratio in marine sediments, that is, the number of moles of POC mineralized per mole of PO_4^{3-} released (r_{REG}):

$$r_{REG} = RPOC/\, J_{PO4} = a - b \cdot \exp(-bw_{O2} \cdot c^{-1}) \tag{3.17}$$

where a (123), b (112) and c (32 μM) are empirical constants and J_{PO4} is the benthic PO_4^{3-} flux (Wallmann, 2010). The empirically-based function shows that r_{REG} is higher than the Redfield ratio under oxic conditions, indicating preferential P burial in most sedimentary environments. On the other hand, excess P is strongly released from continental margins when $O_2 < 20$ μM. Transformation of Eq. 3.17 enables the calculation of the PO_4^{3-} flux directly:

$$J_{PO4} = RPOC/(a - b \cdot \exp(-bw_{O2} \cdot c^{-1})) \tag{3.18}$$

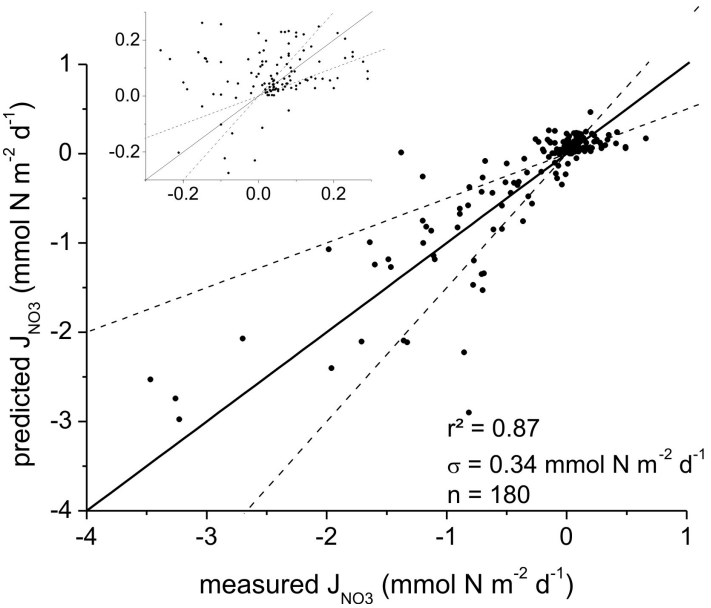

Figure 3.5.: Crossplot of the benthic NO_3^- flux in the database vs. NO_3^- flux calculated using the transfer function (Eq. 3.15). The black line denotes the 1:1 correlation, the dotted lines the 50 % deviation interval. The standard deviation (σ) and the correlation coefficient (r^2) are indicated.

The stoichiometry of N to P flux across the sediment-water interface can thus be calculated as:

$$J_{N:P} = J_{DIN}/J_{PO4} \tag{3.19}$$

We do not define $J_{N:P}$ as J_{NO3}/J_{PO4} since the NH_4^+ released from the sediment will be oxidized in the ocean to nitrate. The molar N:C and C:P ratios of the fluxes (excluding the benthic C flux associated with the dissolution of $CaCO_3$) are:

$$J_{N:C} = J_{DIN}/RPOC \tag{3.20}$$

and

$$J_{C:P} = RPOC/J_{PO4} = r_{REG} \tag{3.21}$$

These metrics are used below to assess the stoichiometry and global distribution of benthic N and P fluxes.

3.4. Global application of the new transfer function

3.4.1. Comprehensiveness of the database

Observed NO_3^- fluxes (J_{NO3}, mmol N m^{-2} d^{-1}) were directed into and out of the sediment, yet higher rates were found for NO_3^- uptake (Fig. 3.6A). Maximum NO_3^- uptake rates occurred on the shelf and slope in conjunction with high NH_4^+ effluxes (Fig. 3.6B) and carbon rain rates (Fig. 3.6C). In these settings, high rates of NO_3^- uptake may be favored by a combination of lower bottom water O_2 concentrations leading to enhanced denitrification, and higher POC fluxes and reactivity to support denitrification. Hence, maximum uptake rates in our database were from the highly productive OMZs off Peru (Sommer et al., submitted), northwest Mexico, and Washington (Devol and Christensen, 1993; Hartnett and Devol, 2003). Release of NO_3^- out of the sediment was often observed at sites with low bottom water NO_3^- concentrations that drive a diffusive flux of NO_3^- out of the sediment and sites with well-oxygenated bottom waters and high benthic carbon degradation rates that favor nitrification of NH_4^+ to NO_3^- (e.g. Hammond et al., 1999). The range of NO_3^- (and NH_4^+) fluxes in the dataset is similar to that reported by Middelburg et al. (1996) in their study on denitrification in marine sediments.

NH_4^+ fluxes (J_{NH4}, mmol N m^{-2} d^{-1}) were directed out of the sediment with maximum rates occurring in shallow water depths (Fig. 3.6B). Very high fluxes ($\geq$ 2 mmol NH_4^+ m^{-2} d^{-1}) were found for sites exhibiting normoxic bottom water conditions and high POC degradation rates of $\geq$ 17 mmol C m^{-2} d^{-1} (e.g. Hammond et al., 1999), probably as a result of high ammonification and concomitant NH_4^+ release by bioirrigation (Dale et al., 2011). However, fluxes in the same range were also reported for the Peruvian OMZ (Sommer et al., submitted) despite lower POC degradation rates ($\approx$ 6 - 8 mmol C m^{-2} d^{-1}). These high NH_4^+ fluxes result from the activity of giant sulfur bacteria performing dissimilatory nitrate reduction to ammonium (DNRA) which cover the seabed in this region (Bohlen et al., 2011). In HNLO environments, DNRA can be an important source of NH_4^+ (e.g. Otte et al., 1999), but may also be significant in more oxygenated settings, especially those where hypoxia occurs on variable time scales (Dale et al., 2011).

Carbon rain rates ranged from 0.3 - 50 mmol C m^{-2} d^{-1} with highest values on the shelf as expected, and decreased exponentially down the continental slope (Fig. 3.6C). A wide range of rain rates occurred on the shelf, which may be related to regional differences in primary production or particle settling velocities (Rullkötter, 2006).

3.4.2. Application of the transfer functions

Global maps of total benthic NO_3^- losses (= maximum denitrification rate) and denitrification (after correcting for NH_4^+ efflux) predict high rates on the continental shelf (Fig. 3.7). Particularly note-

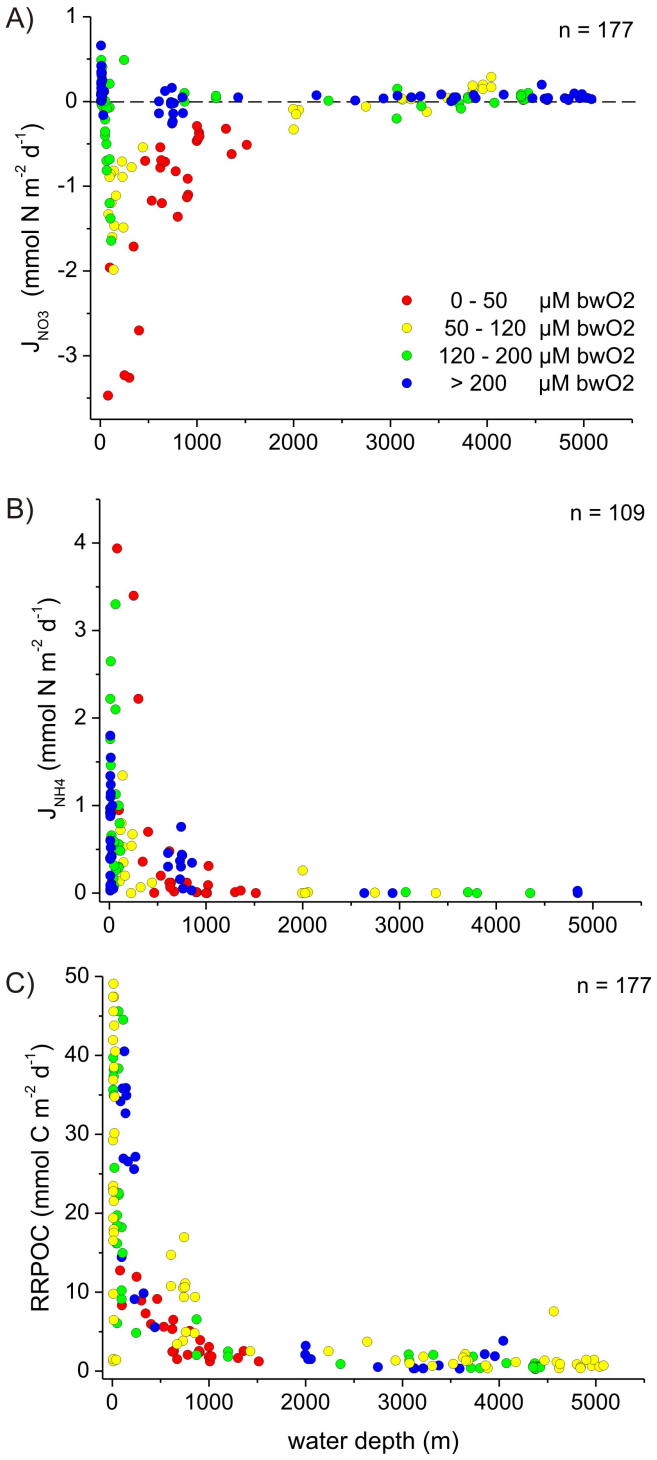

Figure 3.6.: Benthic fluxes (mmol m^{-2} d^{-1}) as a function of water depth (m). A) NO_3^- (incl. NO_2^-); B) NH_4^+; C) Organic carbon rain rates (RRPOC). Negative fluxes denote uptake by the sediment.

worthy are the areas off northern Russia, Alaska and Argentina as well as the North Sea and East China Sea (Fig. 3.7). At greater water depths, especially in the deep ocean basins, sedimentary NO_3^- loss and denitrification rates were low. The distribution of denitrification using the two estimates (DEN1 and DEN2) were very similar (DEN2 distribution not shown). At eight grid points, DEN1 and DEN2 rates of up to 13 and 11 mmol N m^{-2} d^{-1} were predicted, respectively, although for illustrative purposes the scale in Fig. 7B and D was set to an upper limit of 5 mmol N m^{-2} d^{-1}. These sites included the oxygen deficient waters off the Oregon coast (13 mmol N m^{-2} d^{-1} for DEN1), Pakistan (11.7 mmol N m^{-2} d^{-1} for DEN1), Namibia (8.8 mmol N m^{-2} d^{-1} for DEN1), Mexico (7.6 mmol N m^{-2} d^{-1} for DEN1), the Red Sea (6.5 and 6.9 mmol N m^{-2} d^{-1} for DEN1), and Peru (5.5 and 5.9 mmol N m^{-2} d^{-1} for DEN1). For comparison, measured rates for the Washington shelf close to the Oregon coast were < 4.7 mmol N m^{-2} d^{-1} (Devol and Christensen, 1993), which is lower but in the same order of magnitude than predicted values in this study. Furthermore, previous estimates for the Pakistan (< 3.8 mmol N m^{-2} d^{-1}, Schwartz et al. (2009)) and the Peru margin (< 2 mmol N m^{-2} d^{-1}, Bohlen et al. (2011)) were also lower but similar to our findings. In view of spatial and temporal heterogeneity, these studies confirm the dimension of the denitrification rates reported here. Considered collectively, this emphasizes the importance of OMZs as hotspots of benthic denitrification (Fig. 3.7C).

Denitrification rates in shelf, slope, and deep sea sediments are presented in Table 3.1 alongside globally-integrated rates. The model predicts that marine sediments consume 196 ± 33 Tg yr^{-1} of NO_3^- (L_{NO3}), of which more than half occurs on the continental shelf. After correcting for the ammonium release, the globally integrated rate of denitrification amounts to 153 ± 40 Tg N yr^{-1} and 155 ± 67 Tg N yr^{-1} for DEN1 and DEN2, respectively. These similar estimates corroborate our assumption in the a posteriori approach that the NH_4^+ efflux is equal to ca. 27 % of the NO_3^- influx for water depths < 1000 m (section 3.3.3). Again, more than 50 % of denitrification takes place in the shelf despite its relatively small surface area. This contribution is higher than the values predicted by the reaction-transport model approaches of Middelburg et al. (1996) (35 - 44 %) and Thullner et al. (2009) (29 %). However, these authors considered a shelf extending to 150 m water depth while in this study the shelf has been defined down to 200 m. The deep sea contributes roughly 20 % to the total global rate owing to the large expanse of the deep ocean basins, and the continental slope thus accounts for the difference (26 - 27 %).

The global rates for benthic denitrification are well within the range of previously published estimates (Table 3.2). Therefore, coupling of the transfer function (Eq. 3.12, 3.14) to global models should provide a realistic estimate of regional variations in benthic denitrification and associated pelagic feedbacks. The values given by Thullner et al. (2009), Gruber (2004) and Deutsch et al. (2004) are more similar to ours than the estimates by Brandes and Devol (2002), Seitzinger et al. (2006), Middelburg et al. (1996) and Codispoti et al. (2001) which are up to ca. 2 times higher. Moreover, the value obtained by Archer et al. (2002) is an order of magnitude greater than ours (1960 Tg N yr^{-1}), which

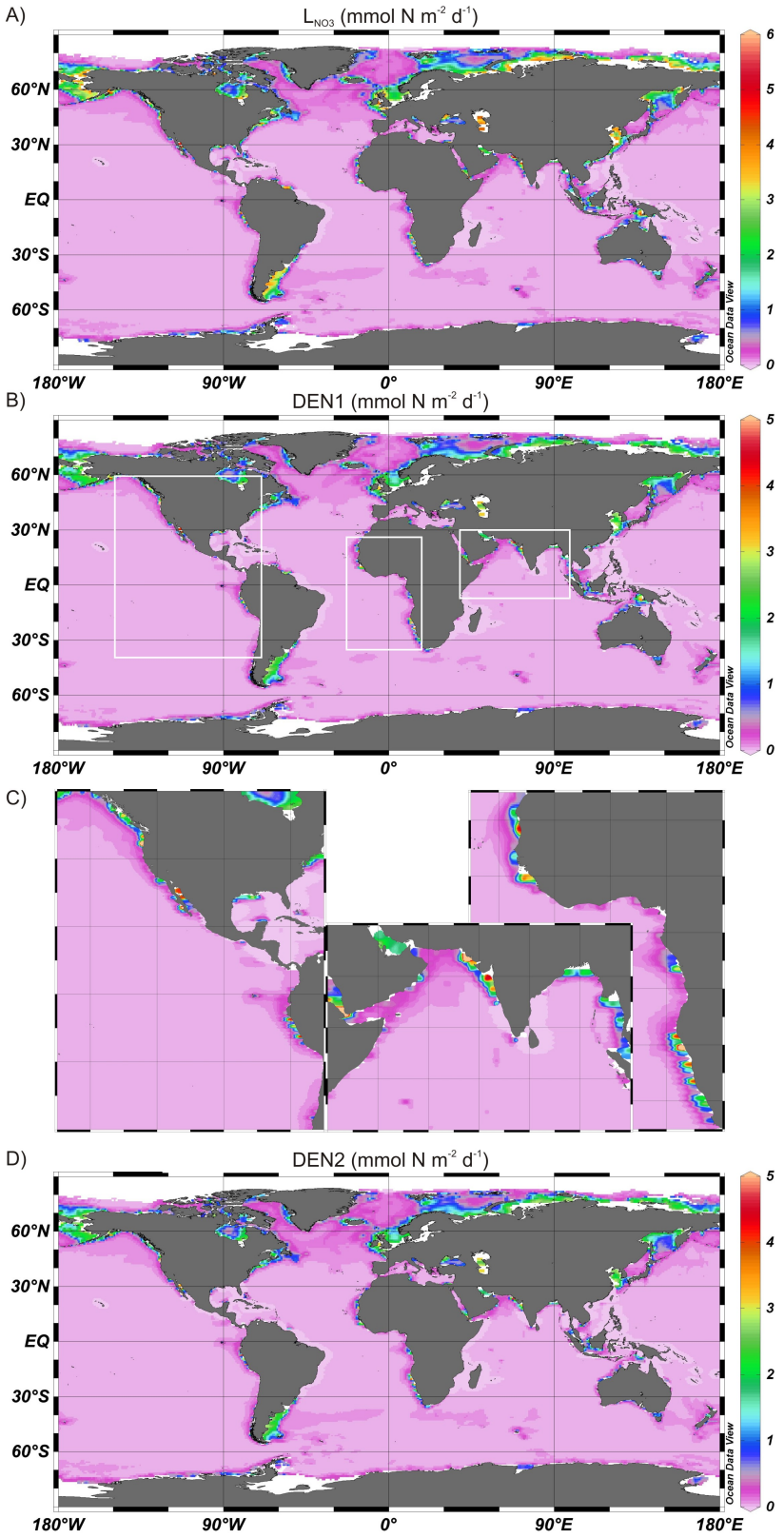

Figure 3.7.: Global maps of the predicted A) NO_3^- loss (L_{NO3}, mmol N m^{-2} d^{-1}); B) a priori benthic denitrification estimate (DEN1, mmol N m^{-2} d^{-1}); C) Enlargements of DEN1 in major OMZ regions. For clarity the scale was set to a limit of 6 and 5 mmol N m^{-2} d^{-1} for L_{NO3} and DEN1, respectively, although higher rates were predicted for a limited number of grid points (see text).

may be due to their extrapolation procedure which is based on bathymetry rather than biogeochemical gradients.

Because most of the studies listed in Table 3.2 use various simplifications and averaging procedures to estimate denitrification rates globally, the spatial distribution of benthic denitrification remains poorly understood. Nevertheless, Seitzinger et al. (2006) provide a global map for denitrification in continental shelf and OMZ regions which highly resembles the distribution in this study. However, their estimate for denitrification in continental shelf sediments is 62 % higher (Table 3.2) and the importance of sediments underlying oxygen-deficient waters is hardly distinguishable since water column estimates are shown for the three major OMZs (Eastern Tropical North and South Pacific, Arabian Sea) rather than benthic rates. Moreover, a recent study by Somes et al. (2010) using a general circulation model reports similar hotspots of benthic denitrification as our findings, yet with distinctively lower maximum rates ($\leq$ 2.7 mmol N m^{-2} d^{-1}) and much lower globally-integrated rates (38.2 Tg N yr^{-1}). These workers calculated benthic denitrification based on the labile organic carbon flux to the seafloor from the parameterization by Middelburg et al. (1996). Since the function developed by these authors yields denitrification rates which are of the same order of magnitude as ours (see section 3.4.5), differences in rain rate are most likely the reason for the discrepancy with the estimate of Somes et al. (2010). In fact, the spatial distribution of denitrification (Fig. 3.7) strongly resembles that of RRPOC (Fig. 3.1A) because denitrification is scaled linearly with the rain rate (Eq. 3.12). On the other hand, a decrease of O_2* from 50 µM to - 50 µM increases DEN1 by a factor of 3.2 while a decrease of O_2* from 250 µM to 150 µM increases denitrification only by factor of 1.2. Consequently, benthic denitrification rates are more sensitive to changes in O_2* at low or negative values of O_2*, that is, in HNLO settings.

The world's oxygen minimum zones are notable HNLO environments yet they impinge on only ca. 1 % of the seafloor (defined as < 0.5 ml l^{-1} O_2, Helly and Levin (2004); defined as < 50 µM O_2*, Table 3.1). Nevertheless, areas with < 50 µM O_2* accounted for around 10 % of the total benthic denitrification rate (Table 3.1). Most of the oceanic bottom waters are characterized by O_2* values of 150 µM or more. Above this level, L_{DIN}/RRPOC changes little with further increase in O_2* (Fig. 3.3C). Hence, globally the geographical distribution of denitrification can mainly be explained by the rain rate of organic carbon throughout much of the ocean despite the local effect of O_2* in HNLO environments. Furthermore, the contributions of shelf, slope, and deep sea sediments to the RRPOC is very similar to their contributions to L_{NO3} and denitrification (Table 3.1). Similar findings have been described by Fennel et al. (2009) who found that sediment oxygen consumption (i.e. POC degradation) and the benthic flux of NO_3^- were the most effective predictors of the denitrification rate while O_2 and NO_3^- concentrations were the least effective predictors. Our results are likely to be biased to some extent since extremely low and localized O_2* values may not be accurately represented by a $1^\circ \times 1^\circ$ resolution of the bottom water O_2 and NO_3^- data, such as on the narrow continental shelf off South America (Fig. 3.1B, 3.7).

Table 3.1.: Mean rates and fluxes estimated in this study (Tg yr^{-1}) as well as molar N:P, N:C and C:P ratio of the fluxes. Negative nitrate fluxes indicate uptake by the sediment. Percentages of global seafloor area, effluxes and rates are given in parentheses.

	L_{NO3}	DEN1	DEN2[a]	J_{NO3}	J_{DIN}	J_{PO4}	RRPOC	$J_{N:P}$[b, c]	$J_{N:C}$[b, c]	$J_{C:P}$[c]
shelf (200 m, 6 %)	110 ± 17 (56 %)	84 ± 21 (55 %)	80 ± 42 (52 %)	4.3 ± 17 (19%)	30.0 ± 21 (50 %)	13.8 (52 %)	1056 (60 %)	5.5	0.044	122.7
slope (200–2000 m, 10 %)	51 ± 10 (26 %)	41 ± 11 (27 %)	40 ± 19 (26 %)	– 4.9 ± 10	5.0 ± 11(8 %)	6.1 (23 %)	393 (22 %)	4.3	0.031	121.7
deep sea (> 2000 m, 84 %)	35 ± 6 (18 %)	28 ± 8 (18 %)	35 ± 6 (22 %)	18.7 ± 6 (81 %)	25.5 ± 8 (42 %)	6.6 (25 %)	312 (18 %)	9.0	0.073	122.6
global	196 ± 33	153 ± 40	155 ± 67	18.1 ± 33	60.5 ± 40	26.5	1761	8.3	0.067	122.4
< 50 µM O_2* (1 %)	18 ± 4 (9 %)	16 ± 5 (11 %)	14 ± 7 (9 %)	– 11 ± 4	– 8.8 ± 5	0.7 (3 %)	61 (4 %)	–10.9	–0.13	93

[a] $\Delta DEN2 = \begin{cases} \Delta L_{NO3} + 0.23 \times L_{NO3} & \text{for water depths} < 1000 \text{ m} \\ \Delta L_{NO3} & \text{for water depths} > 1000 \text{ m} \end{cases}$ (23 % error in *a posteriori* correction of NH_4^+ for < 1000 m)

[b] N = DIN

[c] The stoichiometry of the fluxes is calculated as the average of sum of the values from the individual grid cells.

Table 3.2.: Comparison of published denitrification rates (L_{DIN}) and organic carbon rain rates (Tg yr^{-1}).

Parameter	Value	Reference	Method
denitrification (global)	**153 – 155**	**this study**	
	230 – 285	*Middelburg et al.* (1996)	reaction–transport model
	300	*Codispoti et al.* (2001)	data extrapolation and interpretation
	1960	*Archer et al.* (2002)	reaction–transport model
	200 – 280	*Brandes and Devol* (2002)	N isotope budget
	190	*Deutsch et al.* (2004)	N isotope box model
	180 ± 50	*Gruber* (2004)	data extrapolation and interpretation
	250 [a]	*Seitzinger et al.* (2006)	model based on depth–integrated water column primary production (PP)
	154	*Thullner et al.* (2009)	reaction–transport model
	88[b] – 115[c]	*Romaniello and Derry* (2010)	intermediate–complexity box model
	38.2	*Somes et al.* (2010)	global circulation model
RRPOC (global)	**1761**	**this study**	
	3094 [d]	*Middelburg et al.* (1997)	empirical function based on water depth
	930	*Muller–Karger et al.* (2005)	satellite PP estimate plus empirical settling function
	2300, 2628 [e]	*Burdige* (2007)	global compilation of organic matter remineralization rates
	2290 ± 900	*Dunne et al.* (2007)	satellite PP estimate plus series of conversion functions (see text)
RRPOC shelf and slope	**1449 (82 %)**	**this study**	
(< 2000 m)	620 (67 %)	*Muller–Karger et al.* (2005)	satellite PP estimate plus empirical settling function
	1684, 2013 (73 %, 77 %) [e]	*Burdige* (2007)	global compilation of organic matter remineralization rates
	1980 (86 %)	*Dunne et al.* (2007)	satellite PP estimate plus series of conversion functions (see text)
RRPOC deep sea	**312 (18 %)**	**this study**	
(> 2000 m)	310 (33 %)	*Muller–Karger et al.* (2005)	satellite PP estimate plus empirical settling function
	616 (27 %, 23 %) [e]	*Burdige* (2007)	global compilation of organic matter remineralization rates
	310 (14 %)	*Dunne et al.* (2007)	satellite PP estimate plus series of conversion functions (see text)

[a] continental shelf only
[b] intermediate-complexity box model with 79 boxes
[c] intermediate-complexity box model with 13 boxes
[d] labile organic carbon flux calculated as described by *Middelburg et al.* (1996] with the bathymetric grid used in this study (see section 4.1)
[e] from sediment organic carbon budget with and without accounting for relict sand on the continental shelf, respectively

3.4.3. Dependency of nitrate and DIN losses on POC rain rate

The estimation of the benthic NO_3^- loss and denitrification includes uncertainties within the global datasets of bottom water O_2 and NO_3^- concentrations and POC rain rate. Since the bottom water chemistry is well known for most of the ocean, the rain rate is likely associated with the most uncertainty. Our globally integrated rain rate and its distribution on shelf, slope, and deep sea environments are similar to those previously reported (Table 3.2). However, since the shelf and slope were the main regions for benthic denitrification (82 and 78 % for DEN1 and DEN2, respectively), the variability in RRPOC for water depths < 2000 m is of most significance globally. Accordingly, we tested the sensitivity of RRPOC to different values of the Martin curve exponent, b, which controls the fraction of exported carbon reaching the sediment. Berelson et al. (2001) reported that values for b may vary substantially from the average value of -0.82 used in our study. Consequently, L_{NO3} and denitrification were recalculated applying values ± 1 standard deviation, i.e. b = -0.82 ± 0.16 (Berelson, 2001). Furthermore, we also tested the Martin curve used by Dunne et al. (2007), who estimated the POC rain rate based on the export out of the 75 m depth horizon using an exponent of 0.9, i.e. $F = F_{75} \cdot (z/75)^{0.9}$.

Based on these three additional estimates, new fields for RRPOC were derived for water depths < 2000 m and complemented with RRPOC data from the standard run with b = -0.82 (Fig. 3.8). Globally integrated RRPOC ranged from a minimum of ca. 1564 Tg C yr^{-1} when applying the Martin curve used in Dunne et al. (2007) to ca. 1893 Tg C yr^{-1} for an exponent of -0.66. Using these rain rates in the transfer function changes the estimate for global NO_3^- loss and denitrification rate by ± 23 and ± 17 Tg N yr^{-1}, respectively (Fig. 3.8), from our previous result (196 and 153 - 155 Tg N yr^{-1}, Table 3.1). The maximum deviation of the rain rate from the former value (1761 Tg C yr^{-1}) is 197 Tg C yr^{-1}, which is associated with the Martin-type curve of Dunne et al. (2007). Similarly, the associated deviation in the denitrification estimates is 17 Tg N yr^{-1}. In relative terms, these differences equate to a 11 % change, which demonstrates that the error in the global benthic NO_3^- loss and denitrification estimates scales with the uncertainty in the rain rate (Eq. 3.8 and 3.12). Consequently, our global benthic N losses are accurate to the same order as the rain rate. A decoupling of rain rate and bottom water chemistry due to regional heterogeneities in productivity and rain rate very likely lead to the scatter in the data used to derive the transfer functions (Fig. 3.3).

3.4.4. Enhanced N loss in sandy sediments?

The transfer functions are derived from data from mainly muddy sediments and do not consider permeable, sandy ocean bottoms. Most denitrification and benthic flux estimates have been made for muddy, fine-grained sediments (e.g. Christensen et al., 1987) while coarser-grained shelves are not as well represented, probably due to methodological difficulties when working with coarse grained

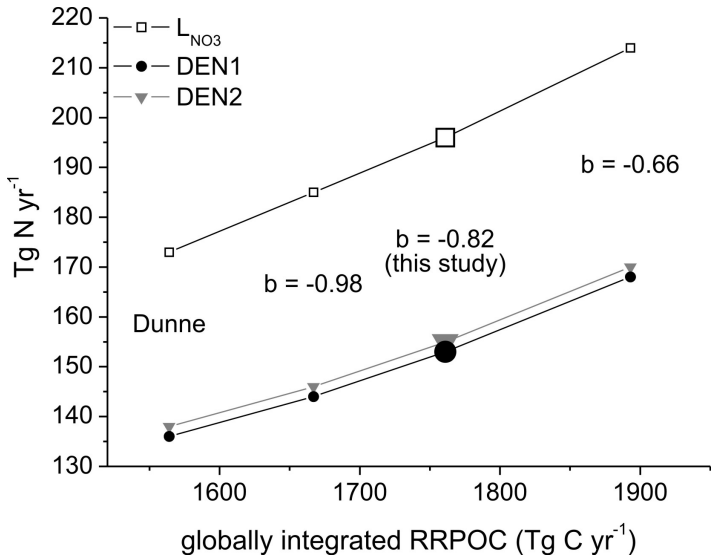

Figure 3.8.: Globally integrated benthic NO_3^- losses and denitrification rates (DEN1 and DEN2) as a function of POC rain rate. RRPOC for < 2000 m water depth have been calculated with different coefficients for the Martin curve (b) and following Dunne et al. (2007) while RRPOC for > 2000 m water depth are all according to the standard run (b = -0.82). The values used in this study are indicated with bigger symbols.

material and complex transport pathways (e.g. Jahnke et al., 2005). Nonetheless, large areas of the shelf, up to 70 % for water depths ≤ 200 m, are covered with non-accumulating relict sands with low organic carbon content (Emery, 1968). Some reports suggest that denitrification rates in such settings could be significant yet lower than those in fine-grained sediments (Vance-Harris and Ingall, 2005), whereas other studies claim that sandy shelves are important sites for organic matter mineralization due to efficient ventilation of surface sands by advective processes (e.g. Huettel and Rusch, 2000; Rao et al., 2007). In global terms, the denitrification estimate by Brandes and Devol (2002) based on an isotopic mass balance, and therefore inclusive of all sediment types, yields rates which are 30 - 80 % higher than those obtained here based on benthic data mainly representative of muddy sediments (Table 3.2). This discrepancy may indeed allude to high rates of denitrification in sandy sediments or, more likely, simply reflect the uncertainty associated with the two very different approaches. Clearly, the range of estimates in Table 3.2 illustrates that there is still much room for refining global benthic denitrification rates, and more data from sandy shelf sediments is required to resolve their importance as sites of fixed N loss.

3.4.5. Comparison with Middelburg's metamodel

The first systematic study estimating global denitrification in sediments was carried out by Middelburg et al. (1996) using a 1-D diagenetic model constrained by measured pore water concentrations

and fluxes from different marine settings. By varying bottom water O_2 and NO_3^- concentrations and rain rates over realistic ranges, these authors derived a semi-empirical transfer function ('meta-model') to predict benthic denitrification as a function of these variables and water depth. Their globally integrated denitrification rates of 230 - 285 Tg N yr^{-1} (Table 3.2) are around 70 % higher than ours. Given the number of parameters and associated uncertainties when extrapolating benthic models globally, there could be many possible explanations for these differences. However, in view of our previous arguments, it is likely that the 76 % higher rain rate used by these workers (1761 c.f. 3094 Tg C yr^{-1}; Table 3.2) can explain most of this discrepancy. Our transfer function employs a new method for calculating rain rates based on published rates of benthic carbon degradation (RPOC) and empirical relationships between RPOC and RRPOC (Flögel et al., 2011).
Applying their meta-model to the global datasets used in this study yields a denitrification rate of 121 Tg N yr^{-1}. This is lower than our estimate of 153 - 155 Tg N yr^{-1}, but still closer to our value than the Middelburg et al. (1996) estimate. Alternatively, applying the rain rates used by Middelburg et al. (1996) with our transfer function results in a benthic denitrification rate of 232 - 241 Tg N yr^{-1}, which agrees closely with the estimate by Middelburg et al. (1996) (Table 3.2). Thus, the modeling based meta-model yields a global benthic denitrification rate that is comparable to our empirical flux-based transfer function when using the same RRPOC, which demonstrates a high degree of coherency between the two very different approaches. This reiterates the importance of accurate rain rates for estimating global rates of benthic denitrification.

3.4.6. Benthic nitrogen and phosphorus fluxes

Applying the NO_3^- and DIN flux transfer function (Eq. 3.15, 3.16) to the global databases yields the geographical distribution of the benthic NO_3^- and DIN fluxes (Fig. 3.9A, B). In the deep-sea areas, the fluxes were close to zero due to low organic matter degradation rates and dominance of aerobic respiration (e.g. Thullner et al., 2009). As expected, maximum NO_3^- and DIN uptake rates into the sediment were associated with the OMZ regions where denitrification rates were highest (Oregon, Pakistan, Namibia, Mexico, Red Sea, Peru), with NO_3^- and net DIN fluxes approaching - 12 and - 9 mmol N m^{-2} d^{-1}, respectively, for the Oregon shelf. NO_3^- and DIN uptake was predicted at all locations with low O_2* (Fig. 3.1 B). High effluxes of NO_3^- ($\leq$ 0.3 mmol m^{-2} d^{-1}) and DIN ($\leq$ 1.4 mmol m^{-2} d^{-1}) were mainly restricted to the continental shelf in colder regions such as the Russian Arctic, Hudson Bay, the North Sea and the Argentine Basin, most likely due to high rates of nitrification of ammonium released from organic nitrogen (e.g. Hensen et al., 1998). Interestingly, for the coastal OMZs offshore Peru and West Africa, sites with net DIN uptake and DIN realease are predicted in close proximity, as exemplified by the enlargement of the Peruvian OMZ in Fig. 3.9B. Regime shifts in benthic N cycling dominated by denitrification (DIN sink) and DNRA (DIN recycling) have been shown to cause such features along a transect of the Peruvian OMZ at

11°S (Bohlen et al., 2011).
For the global ocean, the transfer function yielded a total benthic DIN release of 60.5 ± 40 Tg N yr^{-1} (Table 3.1). The shelf contributed 50 % to this flux, followed by the deep sea with 42 % and the slope with only 8 %. Comparison with the efflux of nitrate, shows that the efflux of DIN was dominated by nitrate in the deep sea. In contrast, NH_4^+ release from organic matter remineralization and potentially DNRA supports most of the DIN efflux on the shelf and also the slope. Globally integrated benthic NO_3^- release was estimated to be 18.1 ± 33 Tg N yr^{-1}, which contrasts with the findings of Thullner et al. (2009) who modeled an overall benthic NO_3^- uptake of 95 Tg N yr^{-1}. However, these authors did not consider the polar-regions (> 60° N, S) which are shown here to be major contributors (47 %) to the overall NO_3^- release to the water column. The model predicted a net uptake of nitrate of - 4.9 Tg N yr^{-1} on the slope, where the HNLO regions impinge on the seafloor (< 50 μM O_2*). Interestingly, the shelf appears to act as a source of nitrate (4.3 Tg N yr^{-1}) due to nitrification as others have noted (Middelburg et al., 1996). This is reflected in the average O_2* for slope sediments (190 μM) which is distinctly lower than the average O_2* for the shelf (270 μM), thus leading to greater NO_3^- losses for a given POC rain rate. The importance of OMZs as global NO_3^- sinks is further demonstrated by their removal of 11 Tg N yr^{-1}, equivalent to 61 % of the total benthic flux NO_3^- input (Table 3.1).

The distribution of benthic phosphorus release fluxes (Fig. 3.9 C) predicted based on the algorithm of Wallmann (2010) was similar to that for nitrate and rain rate (Fig. 3.1A), that is, low fluxes in the deep sea basins and high fluxes on the Arctic shelf, Argentine Basin and OMZs (e.g. Peru, Pakistan/India, Westafrica). The globally integrated PO_4^{3-} flux was estimated to be 26.5 Tg P yr^{-1}, mainly due to release from the shelf sediments (Table 3.1). This complies with the pre-anthropogenic global benthic release of 33 Tg P yr^{-1} derived by Wallmann (2010). Moreover, this author mentioned human activities and a declining oxygen level in response to anthropogenic CO_2 emissions may have increased the flux of TPO_4 from the continental margins, so our slightly higher benthic TPO_4 fluxes are supported by this earlier study.

3.4.7. Regeneration ratios

Based on the global distribution of the nitrate and phosphate fluxes and the organic carbon degradation rate (RPOC), the molar N:P ($J_{N:P}$), N:C ($J_{N:C}$) and C:P ($J_{C:P}$) ratios of the benthic exchange flux between porewater and seawater are shown globally in Fig. 3.10A-C. The values of $J_{N:P}$, $J_{N:C}$ and $J_{C:P}$ expected from Redfield are 16, 0.15 and 106, respectively (Redfield et al., 1963).
On the continental shelf the mean $J_{N:P}$ was very low (5.5) despite the net DIN release while in the deep sea where nitrification was most prevalent the ratio was higher (9.0). For OMZ regions, a negative N:P ratio was calculated as a result of net DIN uptake (Table 3.1), thus illustrating extreme non-Redfield flux stoichiometry in these highly reactive sediments. In general, low $J_{N:P}$ were associated

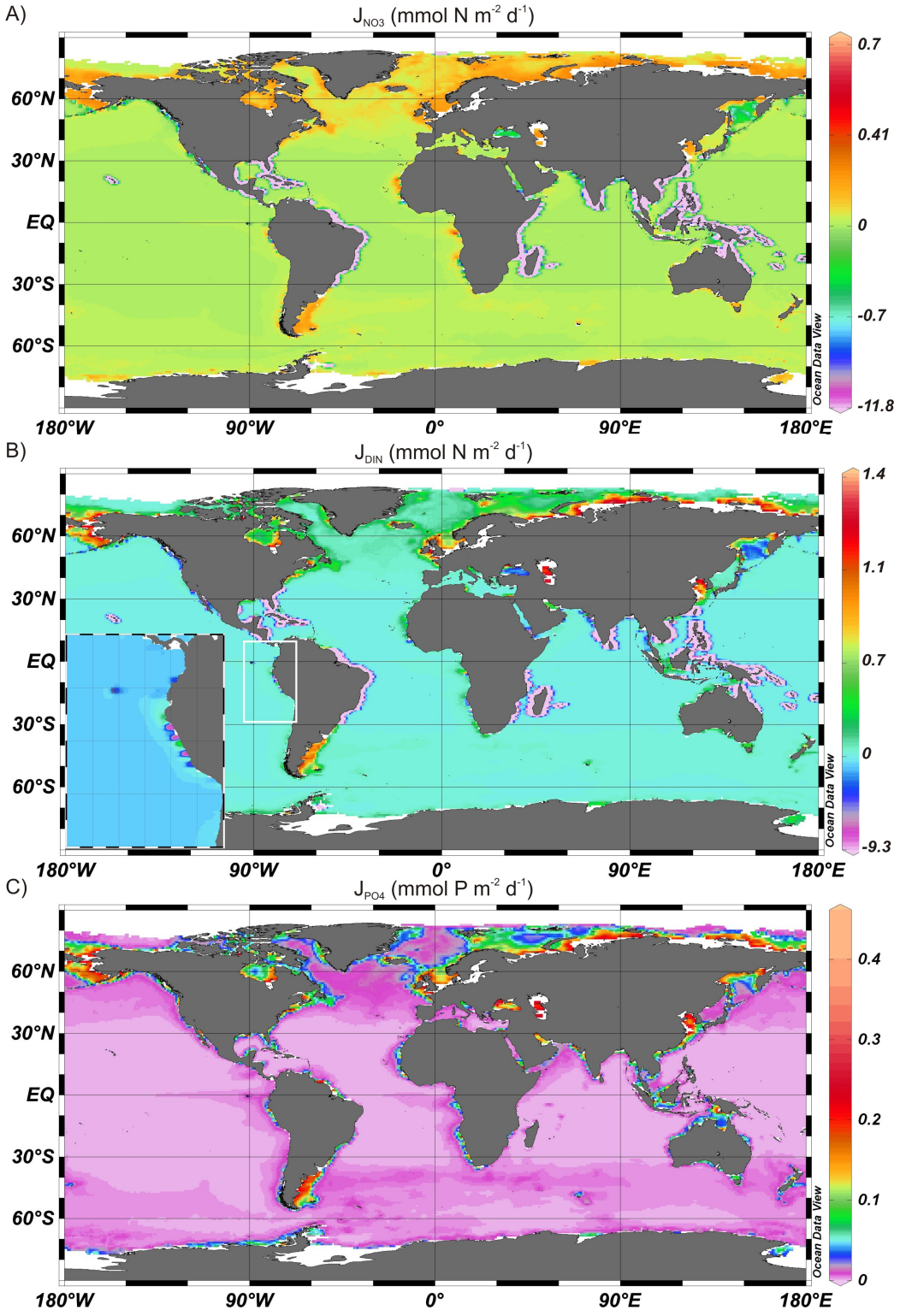

Figure 3.9.: Global map of the predicted A) nitrate (J_{NO3}), B) DIN (J_{DIN}), and C) phosphate (J_{PO4}) fluxes in mmol m^{-2} d^{-1}. The inset in B) shows an enlargement of J_{DIN} for the Peruvian margin. Note the non-linear scaling in A) and B).

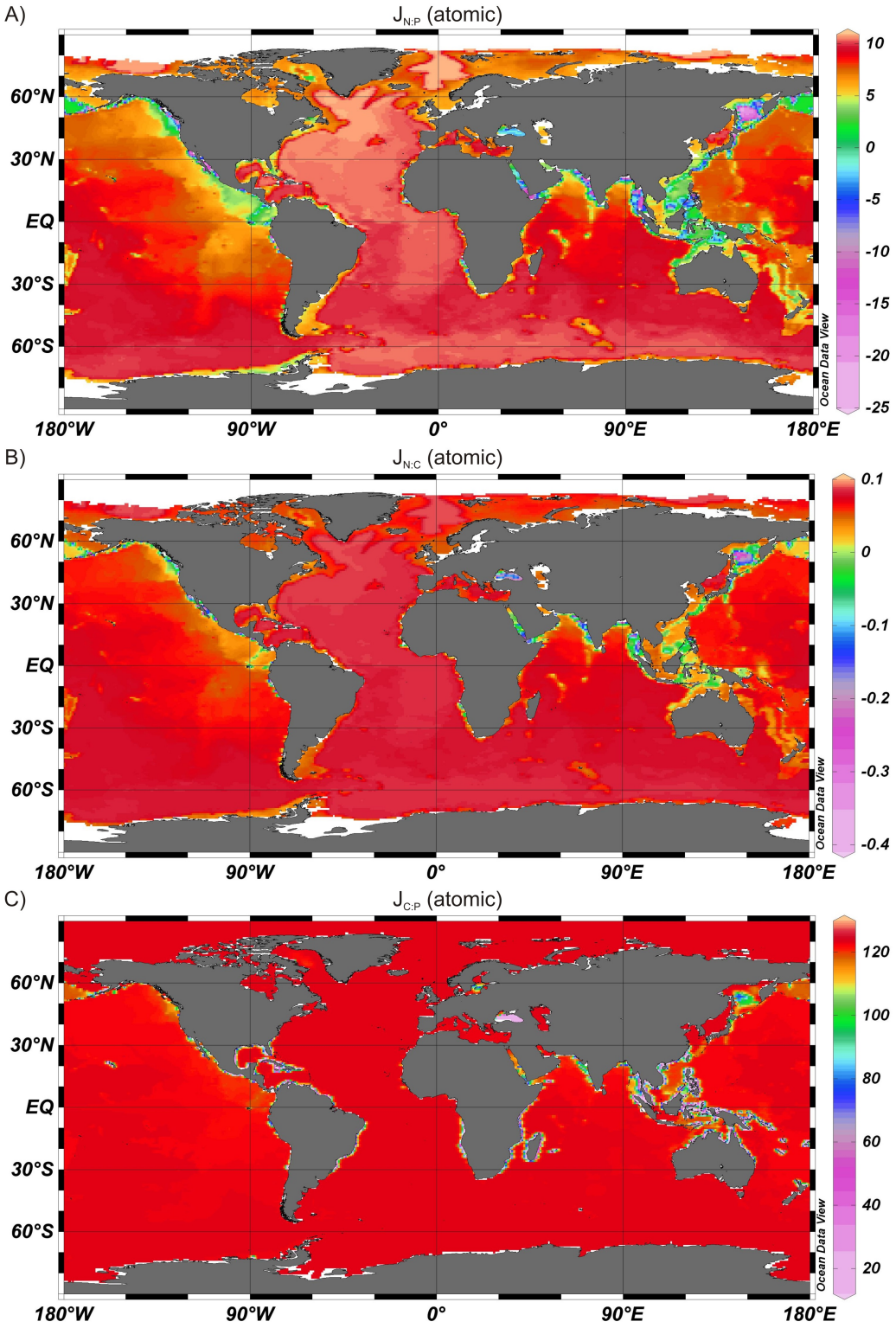

Figure 3.10.: Global maps of the atomic A) N:P ($J_{N:P}$), (B) N:C ($J_{N:C}$) and C) C:P ($J_{C:P}$) ratios of the predicted fluxes. The benthic C flux was assumed to equal RPOC neglecting release of dissolved inorganic carbon associated with the $CaCO_3$ dissolution (see section 3.3.4). $J_{C:P}$ (Eq. 3.21) was calculated as the regeneration ratio during organic matter degradation by applying the function derived by Wallmann (2010). Note the non-linear scaling in B).

with HNLO environments (Fig. 3.11A), a feature that has already been observed previously (Hartnett and Devol, 2003). These workers reported average N:P ratios of 2.9 and 10.6 (considering NH_4^+ fluxes only) for the oxygen deficient margins of northwest Mexico and Washington, respectively. The globally-averaged $J_{N:P}$ of the benthic fluxes was 8.3 (Table 3.1), which takes into account NO_3^- uptake by the sediments. This value, and even the maximum predicted ratio of 10.9 (Fig. 3.10A), is much below the expected Redfield value of 16 (Redfield et al., 1963; Anderson et al., 1995). To illustrate these findings further, $J_{N:P}$ is plotted against O_2* in Fig. 3.11A using data from each grid point. The flux stoichiometry adheres to a clear saturation-type behavior with O_2* and never reaches Redfield proportions. Negative $J_{N:P}$, indicating net benthic fixed N loss, are predicted for regions where O_2* is below ca. 100 μM, which includes the major OMZs in the contemporary ocean (Fig. 3.1B). These findings strikingly demonstrate that the major ocean basins release nutrients to the bottom water in highly non-Redfield composition, implying a consumption of DIN or an excess release of phosphate. Values for $J_{N:C}$ were positive for most of the seafloor due to DIN release (Fig. 3.10 B). Nonetheless, the globally-averaged $J_{N:C}$ of 0.067 is a factor of 2 - 3 lower than Redfield (0.151), and a factor of 2 lower than the revised N:C phytoplankton composition of 0.137 (Anderson and Sarmiento, 1994). As shown in Table 3.1, the shelf, slope and deep sea sediments release nutrients to the water column which are deficient in N relative to C (and P). Therefore, the low $J_{N:P}$ throughout the ocean is due to nitrogen loss rather than excess P release (see also following paragraph). Hartnett and Devol (2003) also measured lower N:C ratios (NH_4^+ fluxes considered only) than Redfield with average values of 0.093 and 0.039 for the oxygen-deficient environments off Mexico and the Washington margin, respectively. By comparison, our OMZ estimate for $J_{N:C}$ is high and negative (-0.13) because it considers both NO_3^- and NH_4^+, and again illustrates the strong sink for DIN in HNLO settings. Plotting the individual data from each grid point against O_2* again shows the switch to negative $J_{N:C}$ in the OMZ regions (Fig. 3.11B).

The global distribution of $J_{C:P}$ (Fig. 3.10 C) shows that, for most regions of the ocean, carbon-to-phosphate fluxes were higher than predicted by Redfield (106). The same was true for the shelf, slope, deep sea and global averages (Table 3.1). The oceans are generally well oxygenated and C:P ratios up to 123:1 are expected for high bottom water O_2 concentrations (Wallmann, 2010), thus indicating preferential burial of phosphorus and P-limiting fluxes with regards to C. However, some individual locations such as the Peruvian and Pakistani OMZs or the Black Sea had considerably lower $J_{C:P}$ with a minimum of 13. Such low C:P regeneration ratios in shelf sediments are believed to result from massive amounts of excess phosphorous release under low-oxygen conditions due to the reductive dissolution of P-adsorbed manganese and iron (hydr)oxides and the preferential degradation of particulate organic phosphorous in anoxic sediments (e.g. Ingall et al., 1994). Consequently, and as expected from Eq. 3.17, the C:P regeneration ratio decreases on eastern boundaries where bottom water O_2 concentrations were diminished (Fig. 3.10C). Interestingly, however, the value of O_2* where $J_{C:P}$ falls below Redfield is predicted to be around 20 μM. At this concentration, sediments become net sources of excess phosphate whilst acting as strong sinks for fixed N.

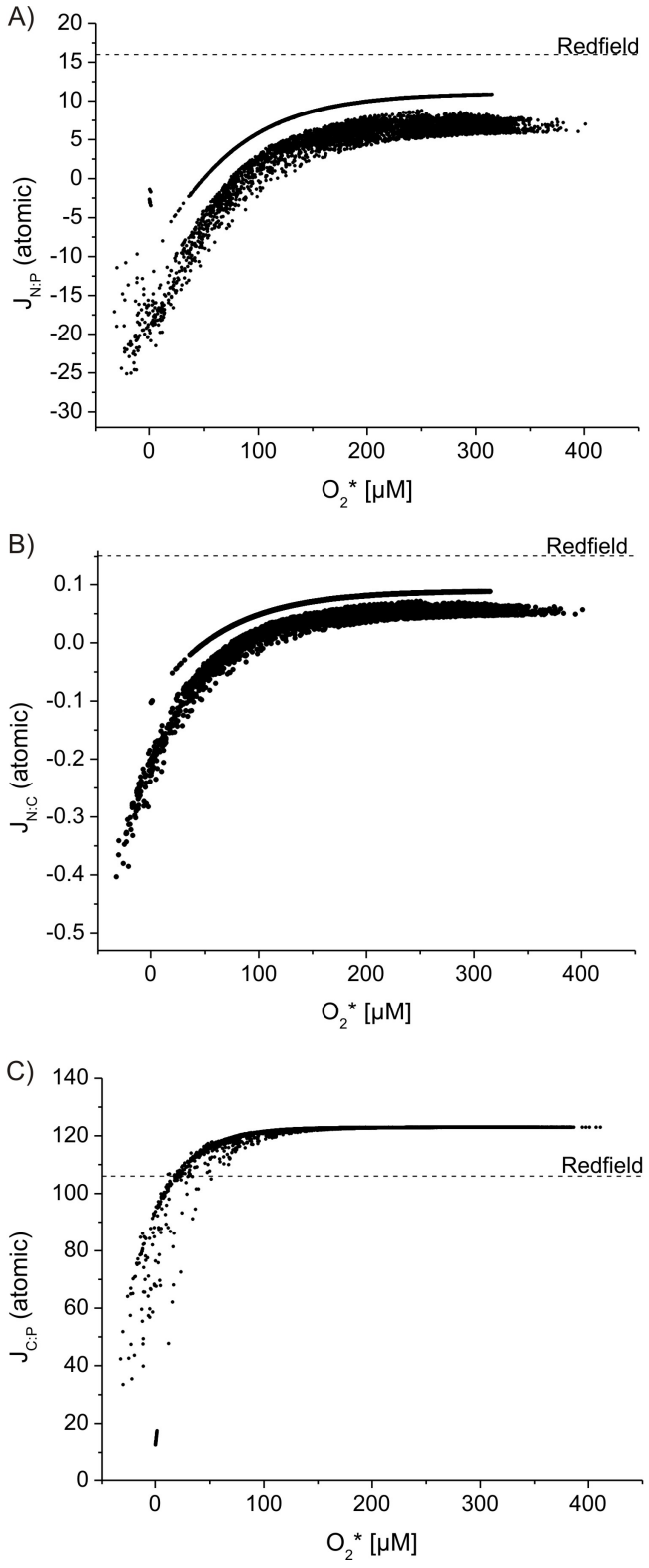

Figure 3.11.: Regeneration ratio of the benthic fluxes for each $1° \times 1°$ grid cell as a function of O_2*. A) $J_{N:P}$, B) $J_{N:C}$, and C) $J_{C:P}$.

To our knowledge, the impact of these highly non-Redfield C:N:P remineralization ratios and benthic fluxes has yet to be evaluated in global circulation models which typically assume Redfield mineralization (c.f. Paulmier et al., 2009). We hypothesize that proper consideration of this behavior in global models will lead to a more accurate spatial description of water column denitrification which typically reply on dissolved N and P distributions (Sarmiento and Gruber, 2006).

3.5. Conclusions

A vertically-integrated sediment model, or dynamic transfer function, is derived to calculate rates of N loss by denitrification. The only input parameters required are the organic carbon rain rate and a newly proposed variable O_2*; equivalent to the bottom water O_2 concentration minus that of NO_3^-. Low or negative O_2* thus indicate high-nitrate low-oxygen regions (HNLO) where denitrification rates are highest. Globally integrated benthic denitrification rates of 153 - 155 Tg N yr^{-1} were estimated by applying the model to global maps of O_2* and rain rate. These are well within the range of previously reported values. Shelf sediments contributed > 50 % to the total N sink, followed by the slope (ca. 30 %) and the deep sea (ca. 20 %). Highest areal rates were found for the oxygen minimum zones off the Oregon coast, Pakistan, Namibia, Mexico, the Red Sea, and Peru, as well as high latitude continental shelf. Despite only covering about 1 % of the seafloor, sediments underlying these settings have been identified as important contributors to global benthic denitrification (ca. 10 %). By applying a similar transfer function for predicting carbon-to-phosphorus regeneration ratios in marine sediments (Wallmann, 2010), a strong deviation from Redfield stoichiometry of the rate of the N:P, N:C, and C:P ratios of the benthic fluxes has been demonstrated for the entire ocean. Although, on average, P is preferentially buried, the loss of fixed N through denitrifying pathways is much more severe and widespread, resulting in nitrate limitation of benthic fluxes with regard to both carbon and phosphorus.

The transfer functions leading to our revised "bottom-up" estimates for global benthic denitrification are based on empirical data analysis. Therefore, they sidestep the need for uncertain global parameterizations required for reaction-transport modeling approaches (e.g. Thullner et al., 2009), yet rely on a sufficiently large supporting database covering a broad range of marine environments. The present function meets these requirements. Furthermore, the function is designed to be coupled easily to biogeochemical general circulation models which routinely employ organic carbon rain rates, bottom water O_2 and NO_3^- concentrations. Given the importance of benthic processes to nitrogen and phosphorus drawdown, we anticipate that global circulation models that account for these sinks will reveal new and exciting information on the importance of preferential nutrient mineralization during export and sinking of new production, the potential spreading of OMZs and the scale of N limitation in the contemporary, past and future ocean.

Acknowledgements

This work is a contribution of the Sonderforschungsbereich 754 "Climate - Biogeochemistry Interactions in the Tropical Ocean" (www.sfb754.de) which is supported by the Deutsche Forschungsgemeinschaft.

References

Anderson L. A. (1995) On the hydrogen and oxygen-content of marine-phytoplankton. *Deep-Sea Res. Pt. I* **42(9)**, 1675-1680.

Anderson L. A. and Sarmiento J. L. (1994) Redfield Ratios Of Remineralization Determined By Nutrient Data-Analysis. *Global Biogeochem. Cy.* **8(1)**, 65-80.

Andersson J. H., Wijsman J. W. M., Herman P. M. J., Middelburg J. J., Soetaert K. and Heip C. (2004) Respiration patterns in the deep ocean. *Geophys. Res. Lett.* **31(3)**, L03304.

Archer D. E., Morford J. L. and Emerson S. R. (2002) A model of suboxic sedimentary diagenesis suitable for automatic tuning and gridded global domains. *Global Biogeochem. Cy.* **16(1)**, 1017.

Behrenfeld M. J. and Falkowski P. G.(1997) Photosynthetic rates derived from satellite-based chlorophyll concentration. *Limnol. Oceanogr.* **42(1)**, 1-20.

Berelson W. M. (2001) The flux of particulate organic carbon into the ocean interior: A comparison of four U.S. JGOFS regional studies. *Oceanography* **14**, 59-67.

Bohlen L., Dale A. W., Sommer S., Mosch T., Hensen C., Noffke A., Scholz F. and Wallmann K. (2011) Benthic nitrogen cycling traversing the Peruvian oxygen minimum zone. *Geochim. Cosmochim. Ac.* **75**, 6094-6111

Brandes J. A. and Devol A. H. (2002) A global marine-fixed nitrogen isotopic budget: Implications for holocene nitrogen cycling. *Global Biogeochem. Cy.* **16(4)**, 1120.

Burdige D. J. (2007) Preservation of organic matter in marine sediments: Controls, mechanisms, and an imbalance in sediment organic carbon budgets? *Chem. Rev.* **107(2)**, 467-485.

Christensen J. P., Murray J. W., Devol A. H. and Codispoti L. A. (1987) Denitrification in continental shelf sediments has major impact on the oceanic nitrogen budget. *Global Biogeochem. Cy.* **1(2)**, 97-116.

Codispoti L. A. and Christensen J. P. (1985) Nitrification, denitrification and nitrous oxide cycling in the eastern Tropical South Pacific Ocean. *Mar. Chem.* **16(4)**, 277-300.

Codispoti L. A., Brandes J. A., Christensen J. P., Devol A. H., Naqvi S. W. A., Paerl H. W. and Yoshinari T. (2001) The oceanic fixed nitrogen and nitrous oxide budgets: Moving targets as we enter the anthropocene? *Sci. Mar.* **65**, 85-105.

Dale A. W., Sommer S., Bohlen L., Treude T., Bertics V. J., Bange H. W., Pfannkuche O., Schorp T., Mattsdotter M. and Wallmann K. (2011) Rates and regulation of nitrogen cycling in seasonally-hypoxic sediments during winter (Boknis Eck, SW Baltic Sea): sensitivity to environmental variables. *Estuar. Coast. Shelf Sci.* **95**, 14-28.

Dalsgaard T. Thamdrup B. and Canfield D. E. (2005) Anaerobic ammonium oxidation (anammox) in the marine environment. *Res. Microbiol.* **156**, 457-464.

Deutsch C., Sigman D. M., Thunell R. C., Meckler A. N. and Haug G. H. (2004) Isotopic constraints on glacial/interglacial changes in the oceanic nitrogen budget. *Global Biogeochem. Cy.* **18(4)**, GB4012.

Devol A. H. (1991) Direct Measurement Of Nitrogen Gas Fluxes From Continental-Shelf Sediments. *Nature* **349(6307)**, 319-321.

Devol A. H. and Christensen J. P. (1993) Benthic Fluxes And Nitrogen Cycling In Sediments Of The Continental-Margin Of The Eastern North Pacific. *J. Mar. Res.* **51(2)**, 345-372.

Dunne J. P., Armstrong R. A., Gnanadesikan A. and Sarmiento J. L. (2005) Empirical and mechanistic models for the particle export ratio. *Global Biogeochem. Cy.* **19(4)**, GB4026.

Dunne J. P., Sarmiento J. L. and Gnanadesikan A. (2007) A synthesis of global particle export from the surface ocean and cycling through the ocean interior and on the seafloor. *Global Biogeochem. Cy.* **21(4)**, GB4006.

Emery K. O. (1968) Relict sediments on continental shelves of world. *AAPG Bull.* **52(3)**, 445-464.

Feldman G. C. and McClain C. R. (2010) Ocean Color Web, SeaWIFS Reprocessing 5, NASA Goddard Space-FlightCenter. Kuring, N.,Bailey, S.W. (Eds.), http://oceancolor.gsfc.nasa.gov/.

Fennel K., Brady D., DiToro D., Fulweiler R. W., Gardner W. S., Giblin A., McCarthy M. J., Rao A., Seitzinger S., Thouvenot-Korppoo M. and Tobias C. (2009) Modeling denitrification in aquatic sediments. *Biogeochemistry* **93**, 159-178.

Flögel S., Wallmann K., Poulsen C., Zhou J., Oschlies A., Voigt S. and Kuhnt W. (2011) Simulating the biogeochemical effects of volcanic CO2 degassing on the oxygen-state of the deep ocean during the cenomanian/turonian anoxic event (OAE2). *Earth Planet. Sc. Lett.* **305(3-4)**, 371-384.

Galloway J. N., Dentener F. J., Capone D. G., Boyer E. W., Howarth R. W., Seitzinger S. P., Asner G. P., Cleveland C. C., Green P. A., Holland E. A., Karl D. M., Michaels A. F., Porter J. H., Townsend A. R. and Vorosmarty C. J. (2004) Nitrogen cycles: past, present, and future. *Biogeochemistry* **70(2)**, 153-226.

Garcia H. E., Locarnini R. A., Boyer T. P. and Antonov J. I. (2006a) World Ocean Atlas 2005, Volume 3: Dissolved Oxygen, Apparent Oxygen Utilization, and Oxygen Saturation, S. Levitus (Ed.), NOAA Atlas NESDIS 63, U.S. Government Printing Office, Washington, D.C., 342 pp. (available online at http://iridl.ldeo.columbia.edu)

Garcia H. E., Locarnini R. A., Boyer T. P. and Antonov J. I. (2006b) World Ocean Atlas 2005, Volume 4: Nutrients (phosphate, nitrate, silicate), S. Levitus (Ed.), NOAA Atlas NESDIS 64, U.S. Government Printing Office, Washington, D.C., 396 pp. (available online at http://iridl.ldeo.columbia.edu)

Glud R. N. (2008) Oxygen dynamics of marine sediments. *Mar. Biol. Res.* **4(4)**, 243-289.

Gruber N. (2004) The dynamics of the marine nitrogen cycle and its influence on the atmospheric CO_2 variations. In *The Ocean Carbon Cycle and Climate*, NATO ASI Series, (eds. Follows, M. and Oguz, T.), pp. 97-148, Kluver Academic Publishers, Dordrecht.

Hammond D. E., Giordani P., Berelson W. M. and Poletti R. (1999) Diagenesis of carbon and nutrients and benthic exchange in sediments of the northern Adriatic Sea. *Mar. Chem.* **66(1-2)**, 53-79.

Hartnett H. E. Devol and A. H. (2003) Role of a strong oxygen-deficient zone in the preservation and degradation of organic matter: A carbon budget for the continental margins of northwest Mexico and Washington State. *Geochim. Cosmochim. Ac.* **67**, 247-264.

Helly J. J. and Levin L. A. (2004) Global distribution of naturally occurring marine hypoxia on continental margins. *Deep-Sea Res. Pt. I* **51**, 1159 - 1168.

Hensen C., Landenberger H., Zabel M. and Schulz H. D. (1998) Quantification of diffusive benthic fluxes of nitrate, phosphate and silicate in the southern Atlantic Ocean. *Global Biogeochem. Cy.* **12(1)**, 193 - 210.

Huettel M. and Rusch A. (2000) Transport and degradation of phytoplankton in permeable sediment. *Limnol. Oceanogr.* **45(3)**, 534-549.

Ingall E. and Jahnke R. (1994) Evidence For Enhanced Phosphorus Regeneration From Marine Sediments Overlain By Oxygen Depleted Waters. *Geochim. Cosmochim. Ac.* **58(11)**, 2571-2575.

Jahnke R., Richards M., Nelson J., Robertson C., Rao A. and Jahnke D. (2005) Organic matter remineralization and porewater exchange rates in permeable South Atlantic Bight continental shelf sediments. *Cont. Shelf Res.* **25(12-13)**, 1433-1452.

Locarnini R. A., Mishonov A. V., Antonov J. I., Boyer T. P. and Garcia H. E. (2006) World Ocean Atlas 2005, Volume 1: Temperature, S. Levitus (Ed.), NOAA Atlas NESDIS 61, U.S. Government Printing Office, Washington, D.C., 182 pp. (available online at http://iridl.ldeo.columbia.edu).

Martin J. H., Knauer G. A., Karl D. M. and Broenkow W. W. (1987) Vertex: carbon cycling in the Northeast Pacific. *Deep-Sea Res.* **34(2)**, 267-285.

Meeson B. W., Coprew F. E., McManus J. M. P., Myers D. M., Closs J.W., Sun K.-J., Sunday D. J. and Sellers P. J. (1995) ISLSCP Initiative I-Global Data Sets for Land-Atmosphere Models, 1987-1988, Vols. 1-5, NASA, CD-ROM. (available online at http://iridl.ldeo.columbia.edu/SOURCES/.NASA/.ISLSCP/.GDSLAM/.Miscellaneous).

Middelburg J. J., Soetaert K., Herman P. M. J. and Heip C. H. R. (1996) Denitrification in marine sediments: A model study. *Global Biogeochem. Cy.* **10(4)**, 661-673.

Middelburg J. J., Soetaert K. and Herman P. M. J. (1997) Empirical relationships for use in global diagenetic models. *Deep-Sea Res. Pt. I* **44(2)**, 327-344.

Muller-Karger F. E., Varela R., Thunell R., Luerssen R., Hu C. M. and Walsh J. J. (2005) The importance of continental margins in the global carbon cycle. *Geophys. Res. Lett.* **32(1)**, L01602.

NOAA, National Geophysical Data Center, Boulder, Colorado (1988) Data Announcement 88-MGG-02, Digital relief of the Surface of the Earth. ETOPO5 5-minute gridded elevation data.(available online at http://iridl.ldeo.columbia.edu/SOURCES/.NOAA/.NGDC/.ETOPO5)

Otte S., Kuenen J. G., Nielsen L. P., Paerl H. W., Zopfi J., Schulz H. N., Teske A., Strotmann B., Gallardo V. A. and Jørgensen B. B. (1999) Nitrogen, carbon, and sulfur metabolism in natural Thioploca samples. *Appl. Environmental. Microb.* **65**, 3148-3157.

Paulmier A., Kriest I. and Oschlies O. (2009) Stoichiometry of remineralisation and denitrification in global biogeochemical models. *Biogeosciences* **6**, 923-935.

Rao A. M. F., McCarthy M. J., Gardner W. S. and Jahnke R. A. (2007) Respiration and denitrification in permeable continental shelf deposits on the south Atlantic Bight: Rates of carbon and nitrogen cycling from sediment column experiments. *Cont. Shelf Res.* **27(13)**, 1801-1819.

Redfield A. C., Ketchum B. H. and Richards F. A. (1963) The Influence of organisms on the composition of seawater. In *The Sea*, vol. 2, pp. 26-77, Wiley Interscience.

Rullkötter J. (2006) Organic Matter: The Driving Force for Early Diagenesis. In *Marine Geochemistry*, 2nd edition, (eds. Schulz H. D. and Zabel M.), pp. 125 - 162, Springer-Verlag, Berlin Heidelberg, Germany.

Rysgaard S., Risgaard-Petersen N., Sloth N. P., Jensen K. and Nielsen L. P. (1994) Oxygen Regulation Of Nitrification And Denitrification In Sediments, *Limnol. Oceanogr.* **39(7)**, 1643-1652.

Romaniello S. J. and Derry L. A. (2010) An intermediate-complexity model for simulating marine biogeochemistry in deep time: Validation against the modern global ocean. *Geochem. Geophy. Geosy.* **11**, Q08001.

Sarmiento J. L. and Gruber N. (2006) Organic Matter Production. In *Ocean biogeochemical dynamics*, pp. 102-172, Princeton University Press.

Schulz H. N. and Jørgensen B. B. (2001) Big bacteria. Annu. Rev. Microbiol. **55**, 105-137.

Schwartz M. C., Woulds C. and Cowie G. L. (2009) Sedimentary denitrification rates across the Arabian Sea oxygen minimum zone. *Deep-Sea Res. Pt II* **56**, 324-332.

Seitzinger S., Harrison J. A., Bohlke J. K., Bouwman A. F., Lowrance R., Peterson B., Tobias C. and Van Drecht G. (2006) Denitrification across landscapes and waterscapes: A synthesis. *Ecol. Appl.* **16**, 2064-2090.

Soetart K., Middelburg J. J., Herman P. M. J. and Buis K. (2000) On the coupling of benthic and pelagic biogeochemical models. *Earth-Sci. Rev.* **51**, 173 - 201.

Somes C. J., Schmittner A., Galbraith E. D., Lehmann M. F., Altabet M. A., Montoya J. P., Letelier R. M., Mix A. C., Bourbonnais A. and Eby M. (2010) Simulating the global distribution of nitrogen isotopes in the ocean. *Global Biogeochem. Cy.* **24**, GB4019.

Sommer S., Bohlen L., Dale A. W., Wallmann K., Hensen C., Mosch T., Noffke A. and Pfannkuche O. (submitted to Global Biogeochemical Cycles) Nitrogen fluxes across Peruvian oxygen minimum zone surface sediments - the potential significance of DNRA.

Thullner M., Dale A. W. and Regnier P. (2009) Global-scale quantification of mineralization pathways in marine sediments: A reaction-transport modeling approach. *Geochem. Geophy. Geosy.* **10**, Q10012.

Vance-Harris C. and Ingall E. (2005) Denitrification pathways and rates in the sandy sediments of the Georgia continental shelf, USA. *Geochem. T.* **6(1)**, 12-18.

Wallmann K. (2010) Phosphorus imbalance in the global ocean? *Global Biogeochem. Cy.* **24(4)**, GB4030.

4. Kinetics of organic matter degradation by aerobic respiration and denitrification in marine surface sediments

Abstract

The depth distribution of organic matter degradation in the upper layer of marine sediments including the bioturbated zone was investigated at 154 stations from sites world-wide using a simple 1-D reaction-transport model. The model simulates transport and biogeochemical transformations of the 5 porewater species oxygen (O_2), nitrate (NO_3^-), nitrite (NO_2^-), ammonium (NH_4^+) and oxygen demand units (ODU); the latter represents the sum of reduced species such as sulfide, ferrous iron and dissolved manganese. Organic matter is degraded by aerobic degradation, denitrification in two steps (using NO_3^- and NO_2^- as electron acceptors), and a generic oxidant which represents the sum of sulfate, iron and manganese. An exponential decrease of mineralization with sediment depth was assumed. The rate of decay, described by the mineralization rate at the sediment surface and the exponential coefficient, was optimized to match the depth-integrated carbon degradation rate as well as the measured fluxes of NO_3^- and O_2 across the sediment-water interface at each site. As a check on the model performance, the model output was compared to measured porewater NO_3^- and O_2 profiles where possible. Results indicate that the initial rate of organic matter degradation at the sediment surface is significantly correlated with the rain rate of organic carbon to the seafloor rather than bottom water concentrations of O_2 and NO_3^-. This confirms the well-established paradigm that the degradation rate of organic matter is mainly first-order in carbon concentrations and that the total availability of oxidants is of minor importance. The results further allow the depth profile of organic matter mineralization in the aerobic and denitrification layers to be predicted based on knowledge of the organic carbon flux to the seafloor only. Using a simple 2-G model, the carbon mineralization rate profiles in surface sediments including the bioturbated layer can only be reproduced with a first-order decay constant varying over several orders of magnitude.

4.1. Introduction

Biogeochemical cycling in marine sediment is mainly driven by the degradation of reactive organic matter raining onto the seafloor. Knowledge of the distribution of the rate of organic matter degradation is fundamental for the overall understanding of benthic processes. Generally, the rate of organic matter degradation can be described by a simple first-order decay process where the amount of organic matter (G) decays according to a rate constant (k) (Berner, 1980). However, owing to strong variations in the reactivity of different organic matter pools, so called 'multi-G' models consider several fractions of organic matter with different reactivities (e.g. Westrich and Berner, 1984). Since the partitioning of organic matter into more labile or refractive compounds is very subjective, other diagenetic models consider the organic matter as a reactivity continuum (Middelburg, 1989; Boudreau and Ruddick, 1991).

Multi-G models allow the interpretation of data when adjusting the individual pools and their reactivity to site-specific conditions. However, since the reactivity is difficult to assess in highly bioturbated sediments where labile and refractory particles are mixed and may be unevenly distributed, these models do not work well in the upper mixed layer. The model by Middelburg (1989) yields a relation of the rate constant k with time and thus provides a more general approach for organic matter degradation in surface sediments. However, due to the dependence on time, the use of continuum models in the upper bioturbated zone of the sediment, where particles of different ages are well mixed, is not easily implemented.

The above approaches have all been used in diagenetic modeling to different degrees. Nevertheless, the description of organic matter degradation especially in the bioturbated zone of the sediment remains difficult. The upper layers of marine sediments are usually inhabited by benthic macrofauna and meiofauna. As a consequence of their burrowing activity, these organisms mix and rework the sediment in a process commonly referred to as bioturbation (e.g. Berner, 1980; Boudreau, 1997). Bioturbation usually results in the formation of an upper mixed layer at the top of the sediment (Burdige, 2006). However, these organisms also affect redox conditions within the sediments (Aller, 1994) due to the flushing of burrows with oxygenated bottom waters into regions where O_2 is generally depleted. Bioturbation activity thus has a profound impact on biogeochemical cycling of redox sensitive elements and the degradation of organic matter (Aller, 1994; Burdige, 2006). For example, by exposing old buried material to oxygen, bioturbation may enhance the integrated rate of organic matter mineralization in marine sediments (Hulthe et al., 1998).

The common method to quantify bioturbation is the modeling of radionuclide distributions in the sediment (e.g. Meysman et al., 2005). However, several studies determined different mixing coefficients at the same sites when based on different tracers such as ^{210}Pb, ^{234}Th, ^{137}Cs (Smith et al., 1993; Legeleux et al., 1994). In particular, shorter lived tracer such as ^{234}Th often yield higher mixing rates compared to the longer lived tracer ^{210}Pb. These differences are most likely caused by the different particle types the tracers are associated with, e.g. ^{210}Pb rather reflecting larger grains and ^{137}Cs small

clay particles (Meysman et al., 2005). Moreover, it appears that deposit feeders favor fresh, food-rich organic matter over older, refractory material and thus mix these fresh particles more efficient than the refractory part (e.g. Smith et al, 1993). In general, the kinetics of organic matter mineralization in the mixed layer are thus poorly understood.

The aim of this study is to predict the distribution of organic matter degradation in the upper sediments within the bioturbated layer based on the measured total rate of organic matter degradation and benthic NO_3^- and, to a lesser extent, O_2 fluxes. A better understanding of the kinetics of organic matter mineralization in the bioturbated surface layer is of prime importance not only for carbon and nitrogen cycling but also for the biogeochemistry of carbonate, phosphorus, manganese and iron (Burdige, 1993; Sarmiento and Gruber, 2006; Hensen et al., 2006). A diagenetic model was developed to reproduce measured NO_3^- fluxes across the sediment-water interface using data from 180 stations covering different organic matter degradation regimes and bottom water conditions. We take this approach since NO_3^- fluxes are known to be very sensitive to the down-core change of the organic matter degradation rate and bottom water chemistry (e.g. Devol and Christensen, 1993; Devol et al., 1997; Hartnett and Devol, 2003). The total rate of organic matter degradation was imposed in the model, and the depth distribution of the rate was adjusted to yield the best fit to the measured fluxes. Since organic matter degradation may, in general, be described by an exponential-like decrease with sediment depth (e.g. Berner, 1980), the distribution of organic matter degradation was described by a simple exponential function with an initial rate at the sediment surface RPOC(0) (mmol cm^{-3} d^{-1}) and an exponential coefficient describing the decrease of mineralization with increasing sediment depth (B, cm^{-1}).

4.2. Numerical model

4.2.1. Reaction-transport model

A 1-D model was used to simulate transport and biogeochemical reactions of five porewater species in the uppermost 50 cm of the sediment including the bioturbated layer at each of the 180 stations in the database. The considered species were oxygen (O_2), nitrate (NO_3^-), nitrite (NO_2^-), ammonium (NH_4^+) and oxygen demand units (ODU, Soetaert et al., 1996), which combine reduced species such as sulfide, dissolved ferrous iron and dissolved manganese. Solid species were not explicitly modeled. Solutes were transported by advection due to sediment accumulation and compaction, molecular diffusion and non-local transport (bioirrigation). Although potentially enhancing diffusive-like transport of solutes, bioturbation was assumed to be of low importance compared to molecular diffusion and was thus neglected for solute transport. Partial differential equations were used to solve the concen-

tration changes of the solutes (C_i) with time:

$$\phi \frac{\partial C_i}{\partial t} = \frac{\partial \left(\phi \, D_S \frac{\partial C_i}{\partial x} \right)}{\partial x} - \frac{\phi \, \partial (v C_i)}{\partial x} + \phi \, \alpha_i (C_{i(0)} - C_i) + \phi \sum R_i \tag{4.1}$$

where t (yr) is time, x (cm) is depth below the sediment-water interface, ϕ (dimensionless) is porosity, v (cm yr^{-1}) is the burial velocity, D_S (cm^2 yr^{-1}) is the tortuosity corrected molecular diffusion coefficient, α_i (yr^{-1}) is the bioirrigation coefficient, and $\sum R$ is the sum of biogeochemical reactions affecting each species.
Sediment porosity was assumed to be constant with depth, and was set to 0.85 for shelf sediments (< 200 m water depth) and to 0.8 for slope and deep sea sediments (Van Cappellen and Wang, 1995). Burial velocity was calculated as a function of water depth (m), wd, according to Middelburg et al. (1997):

$$v = 10^{(a + b \cdot wd)} \cdot c \tag{4.2}$$

with a = -0.8748, b = -0.000435 and c = 3.3.
For each species, D_S was calculated from the molecular diffusion coefficients in seawater (D_{SW}) corrected for salinity and pressure using the Stokes-Einstein equation and tortuosity (Φ^2) (Boudreau, 1997):

$$D_S = \frac{D_{SW}}{\Phi^2} = \frac{D_{SW}}{1 - 2 \ln(\phi)} \tag{4.3}$$

Temperature and salinity were set to measured values where available and otherwise estimated with a salinity of 35 and a temperature as given in the World Ocean Atlas 2009 (Locarni et al., 2010). The diffusion coefficient for ODU was set equal to HS^- (Soetaert et al., 1996).
Bioirrigation appears to be of low significance for benthic solute exchange in low oxygen environments (Middelburg and Levin, 2009; here defined as < 20 µM bottom water O_2) and in sediments at > 3000 m water depth (Glud, 2008). In these environments bioirrigation was thus neglected in the model. Elsewhere, bioirrigation was assumed to decrease with sediment depth according to a Gaussian-type function (Christensen, 1982):

$$\alpha_i = \alpha_{(0)} \exp\left(\frac{-x^2}{2 x_{irr}^{\,2}} \right) \tag{4.4}$$

where $\alpha_{(0)}$ (yr^{-1}) is the irrigation coefficient at the sediment-water interface and x_{irr} (cm) controls the depth where irrigations approaches zero. Following the procedure by Thullner et al. (2009), $\alpha_{(0)}$ was determined from the mean bioirrigation rate in the aerobic layer of the sediment ($\bar{\alpha}$, yr^{-1}) and the

penetration depth of O_2 (x_{O_2}, cm) (Thullner et al., 2009; Meile and Van Cappellen, 2003):

$$\alpha_{(0)} = \frac{\bar{\alpha} \cdot x_{O_2}}{x_{irr} \cdot (1 - \exp(^{x_{O_2}}/_{x_{irr}}))} \tag{4.5}$$

with

$$\bar{\alpha} = \frac{-73.071 + 71.912 \cdot \exp(-0.0013846 \cdot TOU)}{bw_{O_2}/1000} \tag{4.6}$$

$$x_{O_2} = \left(0.5 \frac{2\ \phi\ bw_{O_2}\ Ds_{(O_2)}}{DOU} + 0.5 \frac{2\ \phi\ bw_{O_2}\ Ds_{(O_2)}}{DOU^2}\ TOU/1000\right) \tag{4.7}$$

TOU (μmol cm^{-2} yr^{-1}) and DOU (μmol cm^{-2} yr^{-1}) are the total and diffusive oxygen fluxes, respectively, bw_{O2} (μM) is the bottom water oxygen concentration and the empirical coefficients were taken from Meile and Van Cappellen (2003). Where available, TOU was set to measured values, otherwise the TOU was estimated depending on water depth (Wijsman, 2000; Andersson et al., 2004):

$$TOU = J_0 \left[(1 - p) \cdot \exp(\text{-}b_1 \cdot wd) + p \cdot \exp(\text{-}b_2 \cdot wd)\right] \tag{4.8}$$

where J_0 is the TOU at wd = 0 m (986 μmol cm^{-2} yr^{-1}), p (= 0.14) is a partitioning coefficient of J_0, and b_1 (= 0.017 m^{-1}) and b_2 (= 0.00047 m^{-1}) control the slopes of the two exponential functions (values from Wijsman, 2000). For estimating the DOU based on the TOU, the empirical relation of Meile and Van Cappellen (2003) was used:

$$DOU = \frac{500 \cdot TOU}{646 + TOU} \tag{4.9}$$

The same irrigation coefficient was applied to all solutes. For each station, the model simulation time was sufficiently long (5000 years) so that steady-state was reached ($\partial C/\partial t = 0$).

4.2.2. Reaction network

Although solid species were not explicitly modeled, the biogeochemical reactions (Table 4.1) were driven by the degradation of particulate organic carbon (POC). The following exponential function was imposed in the simulations to describe the depth-dependent rate of POC degradation, RPOC(x) (mmol cm^{-3} yr^{-1}):

$$RPOC(x) = RPOC(0) \cdot \exp(-B \cdot x) \tag{4.10}$$

where RPOC(0) (mmol cm^{-3} yr^{-1}) is the POC degradation rate at the sediment-water interface and the coefficient B (cm^{-1}) defines the exponential decrease with increasing sediment depth. The depth-integrated degradation rate of particulate organic carbon ($\sum$RPOC , mmol C m^{-2} d^{-1}) at each station

Table 4.1.: Reaction network used in the model. Model parameters are listed in Table 4.2.

Process	Stoichiometry	Rate expression
R_1	$(CH_2O)(NH_3)_{rNC} + O_2 \rightarrow$ $(1 - r_{NC})CO_2 + (r_{NC})HCO_3^- + r_{NC}\,NH_4^+ + (1 - r_{NC})H_2O$	$\mathrm{RPOC} \times \frac{[O_2]}{[O_2] + K_1}$
R_2	$(CH_2O)(NH_3)_{rNC} + 2\,NO_3^- \rightarrow$ $2\,NO_2^- + (1 - r_{NC})\,CO_2 + (r_{NC})HCO_3^- + r_{NC}\,NH_4^+ + (1 - r_{NC})H_2O$	$\mathrm{RPOC} \times \frac{[NO_3^-]}{[NO_3^-] + K_2} \times \frac{K_3}{[NO_2^-] + K_3} \times \frac{K_1}{[O_2] + K_1}$
R_3	$(CH_2O)(NH_3)_{rNC} + 4/3\,NO_2^- + (1/3 + r_{NC})CO_2 \rightarrow$ $2/3\,N_2 + (4/3 + r_{NC})HCO_3^- + r_{NC}\,NH_4^+ + (1/3 - r_{NC})H_2O$	$\mathrm{RPOC} \times \frac{[NO_2^-]}{[NO_2^-] + K_3} \times \frac{K_1}{[O_2] + K_1}$
R_4	$(CH_2O)(NH_3)_{rNC}$ + an oxidant + $r_{NC}\,CO_2 + r_{NC}\,H_2O \rightarrow$ $(1 - r_{NC})\,CO_2 + \mathrm{ODU} + r_{NC}\,HCO_3^- + r_{NC}\,NH_4^+ + (1 - r_{NC})H_2O$	$\mathrm{RPOC} \times \frac{K_2}{[NO_3^-] + K_2} \times \frac{K_3}{[NO_2^-] + K_3} \times \frac{K_1}{[O_2] + K_1}$
R_5	$NH_4^+ + 3/2\,O_2 + 2\,HCO_3^- \rightarrow NO_2^- + 3\,H_2O + 2\,CO_2$	$k_5 \times [O_2] \times [NH_4^+]$
R_6	$NO_2^- + ½\,O_2 \rightarrow NO_3^-$	$k_6 \times [O_2] \times [NO_2^-]$
R_7	$NH_4^+ + NO_2^- \rightarrow N_2 + 2\,H_2O$	$k_7 \times [NO_2^-] \times [NH_4^+]$
R_8	$\mathrm{ODU} + O_2 \rightarrow$ an oxidant	$k_8 \times [O_2] \times [\mathrm{ODU}]$
R_9	$\mathrm{ODU} + ½\,NO_3^- \rightarrow$ an oxidant + $½\,NH_4^+$ for water depths ≤ 200 m $\mathrm{ODU} + 4/5\,NO_3^- \rightarrow$ an oxidant + $2/5\,N_2$ for water depths > 200 m	$k_9 \times [NO_3^-] \times [\mathrm{ODU}]$

Table 4.2.: Invariable model parameters (L: based on literature values, M: constrained with the model).

Parameter	Description	Value	Unit	Source
r_{NC}	molar N:C ratio in POM	16/106	mol N (mol C)$^{-1}$	L [a]
K_1	Half-saturation constant for O_2	8	µM	L [b,c]
K_2	Half-saturation constant for NO_3^-	10	µM	L [c,d]
K_3	Half-saturation constant for NO_2^-	1	µM	M, L [e]
k_5	Rate constant for aerobic oxidation of NH_4^+	1.5×10^8	M^{-1} yr^{-1}	M, L [c,f]
k_6	Rate constant for aerobic oxidation of NO_2^-	1.5×10^8	M^{-1} yr^{-1}	M, L [c,f]
k_8	Rate constant for aerobic oxidation of ODU	1.5×10^8	M^{-1} yr^{-1}	L [c]
k_9	Rate constant for anaerobic oxidation of ODU	1.5×10^5	M^{-1} yr^{-1}	L [g]

(a) Redfield et al. (1963)
(b) Boudreau (1996)
(c) Van Cappellen and Wang (1995)
(d) Van Cappellen and Wang (1996)
(e) Bohlen et al. (2011)
(f) Berg et al. (2003)
(g) according to Fe^{2+} oxidation with NO_3^-, Dhakar and Burdige (1996)

is known (see compilation in Chapter 3). In order to simulate the ∑RPOC, RPOC(0) and B must meet the following constraint:

$$\int_{0cm}^{50cm} \mathrm{RPOC}(0) \cdot \exp(-\mathrm{B} \cdot \mathrm{x}) \equiv \sum \mathrm{RPOC} \tag{4.11}$$

Thus, a higher fraction of POC degraded at the surface directly leads to a more rapid decrease of the rate with depth and vice versa.

The mineralization pathways considered (Table 4.1) were aerobic degradation (R_1), denitrification (R_2, R_3) and anaerobic degradation (R_4) which represents the sum of iron, manganese, and sulfate reduction (Soertaert et al., 1996). The electron acceptors O_2, NO_3^- and NO_2^-, and the "other oxidants" are used sequentially in this order according to the decreasing Gibbs energy yield per reaction. Anaerobic degradation of 1 mol carbon is assumed to consume 1 mol of the "other oxidants" and produce 1 mol of ODU (Soertaert et al., 1996). The relative importance of each degradation pathways was determined by using Michaelis-Menten kinetics (e.g. Boudreau, 1996) and appropriate half-saturation constants (K) for each reaction. Half-saturation values for O_2 and NO_3^- were taken from the literature, yet little information for NO_2^- is available (Table 4.2). Hence, owing to its high reactivity, the half-saturation constant for NO_2^- (K_3) was set to a low value of 1 µM. Bimolecular rate laws were used for all secondary redox-reactions.

Particulate organic matter (POM) is chemically defined as $(CH_2O)(NH_3)r_{NC}$ with r_{NC} as the Redfield molar ratio of N:C (Table 4.2). During mineralization, the particulate organic nitrogen (PON) in POM is released as NH_4^+ rather than being directly oxidized to NO_3^-. NH_4^+ is then allowed to be oxidized by nitrifying bacteria. This approach considers that different microbial communities are involved in the release and oxidation of NH_4^+. Following the concept by Bohlen et al. (2011) NO_2^- was modeled

as an individual species and canonical denitrification was simulated as two individual steps, i.e. NO_3^- reduction to NO_2^- (R_2) and NO_2^- reduction to N_2 (R_3). Since the reduction of NO_2^- to N_2 supplies more catabolic energy compared to NO_3^- reduction to NO_2^- (Thauer et al., 1977; Lam and Kuypers, 2011) the kinetics of the two denitrification steps were defined such that POM mineralization via NO_3^- was inhibited by the accumulation of NO_2^-. For similar reasons, nitrification was implemented as stepwise oxidation of NH_4^+ to NO_2^- (R_5) and NO_2^- to NO_3^- (R_6) (Bohlen et al., 2011). The same kinetic constants for R_5 and R_6 were assumed and increased by one order of magnitude higher over those reported in previous studies (see Table 4.2) in order to simulate the observed subsurface NO_3^- peaks at some stations.

Introducing NO_2^- as a separate species permits its accumulation in the porewater and, furthermore, allows alternative reactions such as NO_2^- reduction (R_3), NO_2^- oxidation (R_6) or anaerobic ammonium oxidation (anammox, R_7) to utilize and compete for the available nitrite. Anammox, a microbial process where NO_2^- and NH_4^+ react to produce dinitrogen gas, has recently been discovered as an important process for marine nitrogen loss in hypoxic waters and the sediments (Thamdrup and Dalsgaard, 2002; Daalsgaard et al., 2005; Hamersley et al., 2007; Lam et al., 2009). In addition to these redox-reactions, ODU may also be reoxidized by O_2 (R_8) and NO_3^- (R_9). Oxidation of 1 mol ODU requires 4 electrons, i.e. either 1 mol O_2 or 0.8 mol NO_3^- when assuming denitrification to N_2, or 0.5 mol NO_3^- when assuming the reduction to NH_4^+. We assume that ODU mainly consists of sulfide in shelf sediments ($\leq$ 200 m water depths), implying that NO_3^- is converted to NH_4^+ (e.g. during dissimilatory nitrate reduction to ammonium, DNRA) (Otte et al., 1999). On the slope and in deep sea sediments, in contrast, ODU consists mainly of dissolved iron and manganese which are usually oxidized during the denitrification of NO_3^- yielding N_2 gas (e.g. Dhakar and Burdige, 1996; Hulth et al., 2005).

4.2.3. Boundary conditions and model solution

For the numerical solution of the second-order differential equations two boundary species are required for each species. At the top of the sediment (x = 0 cm), measured bottom water concentrations were used as fixed concentrations (Dirichlet-type boundary) while at the bottom of the modeled sediment column (x = 50 cm) boundaries were fixed to a zero gradient (Neumann-type). Where no NO_2^- bottom water concentrations were available, its boundary condition was set to 0 µM since NO_2^- does not accumulate in oxic seawater. Similarly, an upper boundary of 0 µM was assumed for ODU.

The set of coupled ordinary differential equations was solved using the NDSolve algorithm in MATHEMATICA using finite differences (Boudreau, 1996) over an uneven grid with a total of 100 depth intervals. Close to the sediment-water interface where reaction rates are highest a sub mm-scale grid resolution was used while at depth the resolution reached a maximum of 1 cm. The model is > 99% mass conservative and takes ca. 30 seconds for a typical steady-state run on a personal

computer.

4.2.4. Optimization of RPOC(0) and B

The aim of the modeling approach is to better constrain POC degradation in surface sediments based on the reconstruction of measured fluxes of NO_3^- and O_2 across the sediment-water. Hence, the main output of this exercise is to obtain appropriate values for B and RPOC(0). However, the kinetic constants for anammox (k_7) and the depth of irrigation (x_{irr}) are also difficult to constrain from literature estimates. Consequently, B, RPOC(0), k_7 and x_{irr} were varied to fit the measured benthic flux of NO_3^- (J_{NO3}) and, if available, measured NO_3^- porewater profiles. Data were taken from the compilation by Bohlen et al. (submitted) (Table B.1 in Appendix B), covering a broad range of organic carbon rain rates (RRPOC) as well as different bottom water O_2 and NO_3^- regimes from fully oxygenated waters to high-nutrient-low-oxygen (HNLO) regions. Porewater NO_3^- profiles were available at 92 of the 180 stations (Table C.1 in Appendix C).

Since O_2 uptake into the sediment strongly influences the intensity of benthic redox cycling, only reproducing the NO_3^- flux but not considering the O_2 flux (and O_2 porewater profiles) could result in spurious parameter values. Thus, TOU was (if available) used as an additional and independent control on the varied parameter values derived using the NO_3^- fluxes. For all stations, the parameters were adjusted to the measured benthic NO_3^- flux. The additional constraint using the O_2 flux was only applied for the stations with the highest TOU where aerobic respiration rates were expected to be comparable to or higher than denitrification.

A simple automated procedure was used to derive B, RPOC(0), k_7 and x_{irr} to avoid tedious and subjective variation of the parameters. This consists of running the model ca. 1000 times with randomly chosen values of the parameters within a pre-defined range. The combination of parameters giving the best fit to the measured fluxes, that is, the smallest residual of the measured and modeled fluxes was then defined as the best fit parameter combination. We term this approach 'optimization'. Values for B were varied between 0.03 and 16 cm^{-1}, k_7 between 0 and 10^{12} M^{-1} yr^{-1}, and x_{irr} between 0 and 3.5 cm which is equivalent to a bioirrigation depth of up ca. 10 cm. Note that only B needs to be varied to define the mineralization profile, since B and and RPOC(0) are related by Eq. 4.11. Thus, for each individual station and simulation run, B was varied and RPOC(0) subsequently calculated from Eq. 4.11 using the function 'Solve' in MATHEMATICA 7.0. The randomly chosen parameters, the benthic NO_3^- and O_2 fluxes, and the simulated porewater concentration profiles were exported for each run. The optimized parameter values for each station together with the measured and modeled benthic fluxes of NO_3^- and O_2 are listed in Table C.1 in Appendix C.

The optimization procedure is best illustrated using two examples. Figure 1 shows the residuals of the measured and modeled NO_3^- fluxes for each simulated B (Fig. 4.1a) and RPOC(0) (Fig. 4.1b) using data from station BIGO 3 in Sommer et al. (submitted). A clear minimum in the residuals

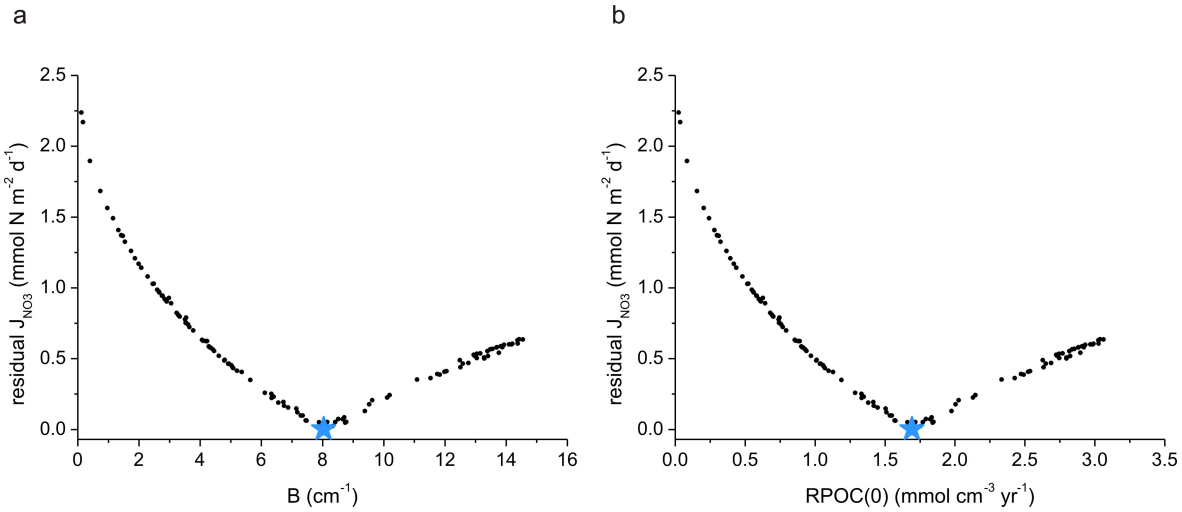

Figure 4.1.: Example of the results for the optimization of (a) B and (b) RPOC(0) using the benthic NO_3^- flux as a constraint (measured data from station BIGO 3 in Sommer et al. (submitted)). Residuals denote the deviation of the modeled and measured benthic NO_3^- flux. Stars denote the optimized model run.

indicates the best-fit of RPOC(0) and B to the measured data (shown by the star). When both the NO_3^- flux and the O_2 flux were used as constraints, different optimal values of RPOC(0) and B were usually obtained (Fig. 4.2a-d). In these cases, the optimized values were determined by weighing the residual O_2 and NO_3^- fluxes by the respective relative errors of the measured fluxes. This procedure mainly yields values reflecting the O_2 flux rather than the NO_3^- flux since the relative error in the O_2 flux measurements was usually lower. In this example, the optimized residual fluxes correspond to the simulation run indicated by the blue star, which lies within the area spanned by the errors of measured NO_3^- and O_2 fluxes (dashed box, Fig. 4.2e).

Out of a total of 180 stations in the database, 154 stations were successfully optimized with the above procedure. For the remaining 26 stations no clear or single minimum in the residuals could be identified and these have been omitted from further analysis.

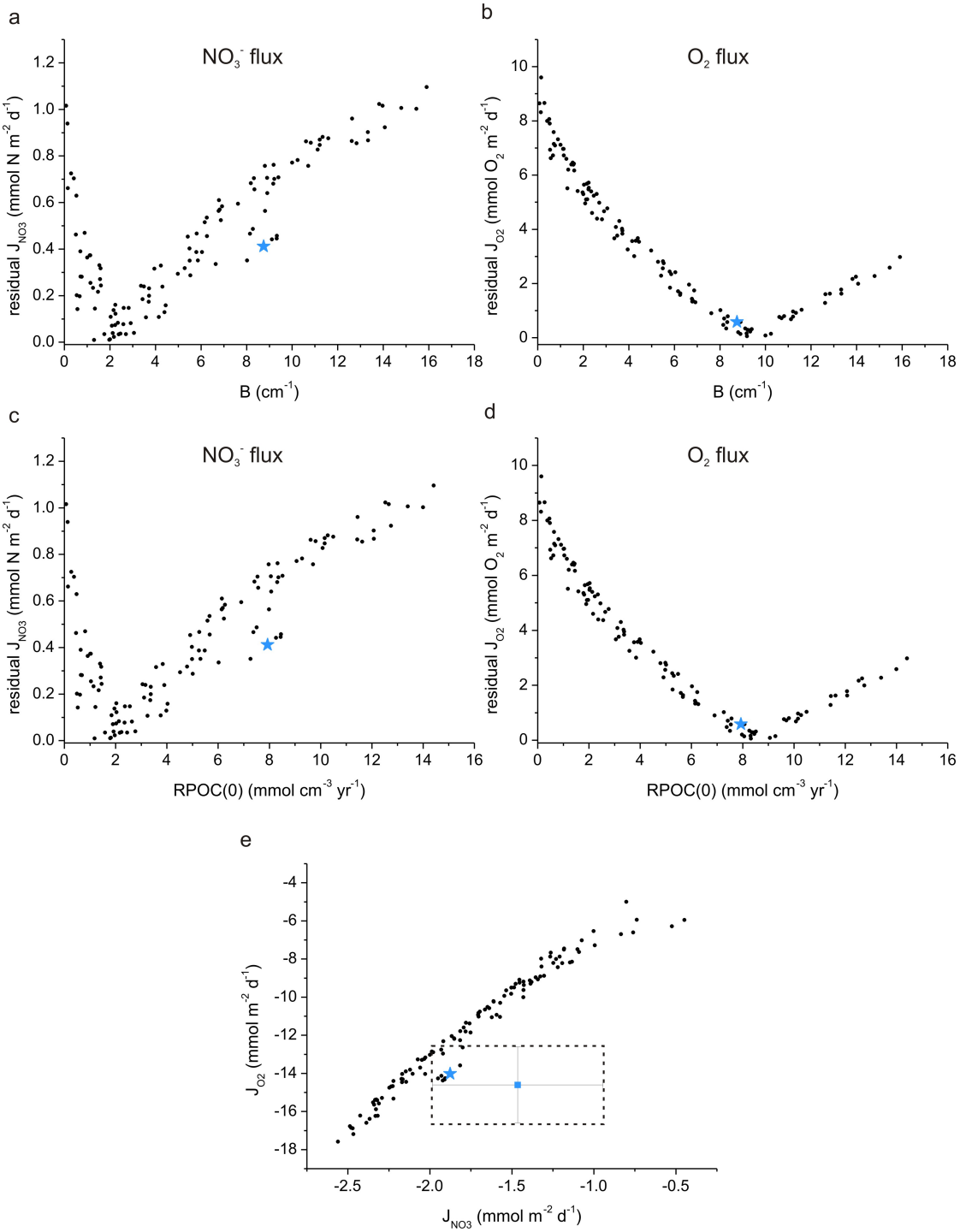

Figure 4.2.: Example of the optimization results using both the benthic NO_3^- and O_2 fluxes as constraints (measured data from the Washington margin, station NH18 in Devol and Christensen (1993)). (a) and (b) show the residuals of the measured NO_3^- and O_2 fluxes as a function of B, respectively, and (c) and (d) show the residuals of the measured NO_3^- and O_2 fluxes as a function of RPOC(0), respectively. (e) Modeled O_2 versus NO_3^- fluxes and the measured values with error bars (blue square), where the dashed box indicates the area spanned by the bars. Stars denote the optimized model run.

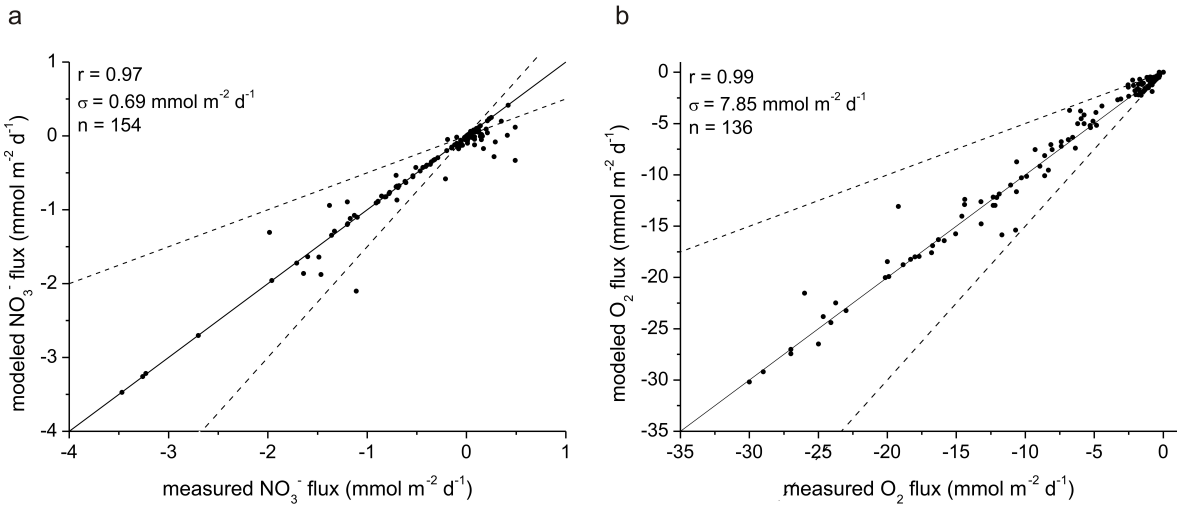

Figure 4.3.: Measured versus modeled benthic fluxes of (a) NO_3^- and (b) O_2 using the optimized parameters. The solid line is the 1:1 line (measured = modeled) and the dotted lines indicate ±50 % deviation. Negative fluxes indicate uptake into the sediment, positive values release from the sediment.

4.3. Results and Discussion

4.3.1. Comparison with data

In what follows, the results of the parameter optimization are described particularly focusing on values for B and RPOC(0), the parameters which describe the depth-distribution of organic matter degradation in the sediment. No trend for the anammox constant (k_7) and the parameter determining the depth of bioirrigation (x_{irr}) were obtained from the optimization routine and these are not discussed further. In future work, k_7 and x_{irr} may thus probably be fixed at all stations using the average values obtained from the routine.

In general, the simulations were able to simultaneously reproduce the measured NO_3^- and O_2 fluxes at a statistically significant level (Fig. 4.3), although the high rates of NO_3^- uptake into the sediment are better captured by the model than low rates of NO_3^- release (Fig. 4.3a). The model was also able to reproduce the measure porewater data. Examples of the porewater data O_2 and NO_3^- for 4 stations characteristic of different marine environments are shown in Figure 4. Stations with strong benthic NO_3^- uptake and denitrification rates exhibit the expected decrease in NO_3^- concentration with depth (station A). These sediment types are generally located on the continental shelf and slope and, especially, in sediments underlying HNLO bottom waters (e.g. Devol and Christensen, 1993; Hartnett and Devol, 2003). In this example, denitrification accounts for 27 % of the total rate of organic matter degradation, although this may rise to 50 % in other HNLO environments (Hartnett and Devol, 2003; Bohlen et al., 2011). Moreover, anaerobic degradation usually contributes substantially to the total

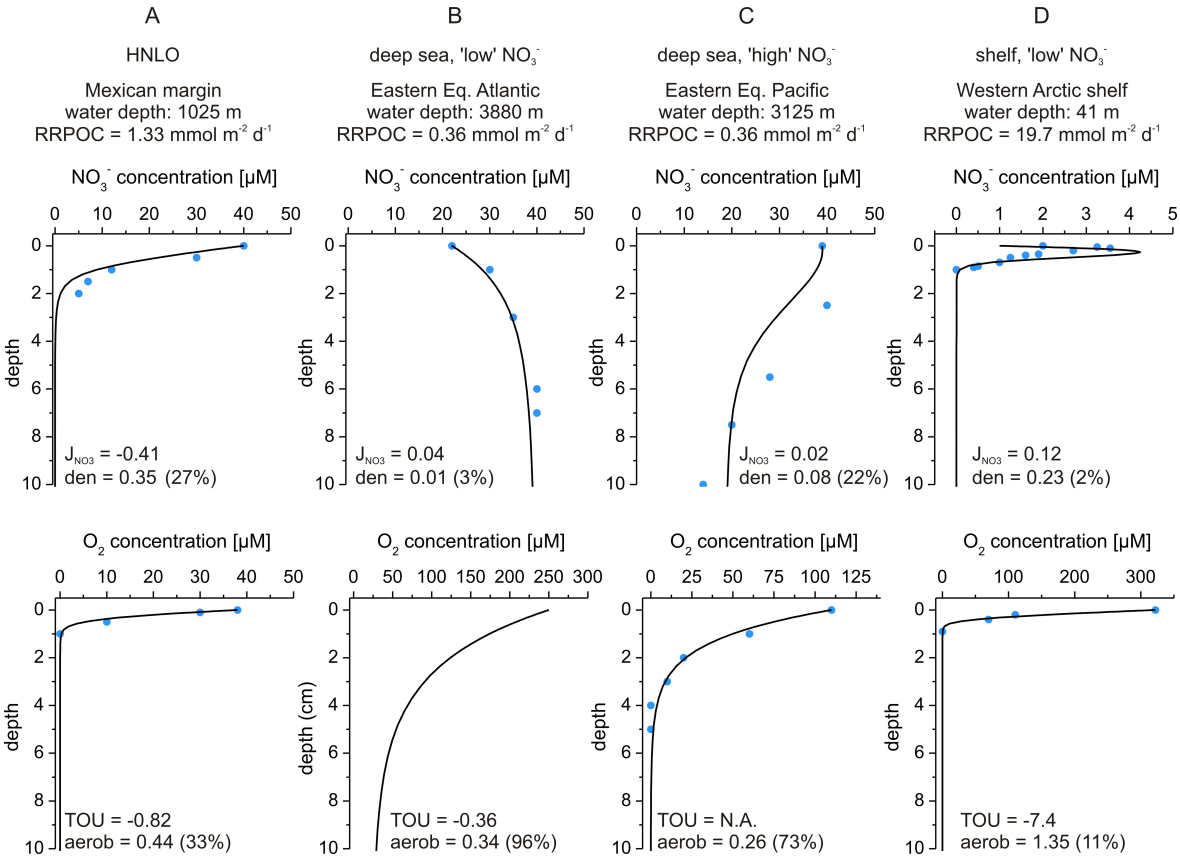

Figure 4.4.: Porewater profiles for NO_3^- and O_2 at four stations with contrasting bottom water chemistry and POC rain rates: A) HNLO slope (station WE206 in Hartnett and Devol (2003)); B) deep sea low bottom water NO_3^- (station 12GC2 in Goloway and Bender (1982), no measured O_2 concentrations available); C) deep sea high bottom water NO_3^- (station 7BC20 in Goloway and Bender (1982)), and D) continental shelf (station H in Devol (1997)). The curves show simulated concentrations and symbols denote measured concentrations. Measured fluxes of nitrate (J_{NO3}, mmol N m^{-2} d^{-1}) and O_2 (TOU, mmol O_2 m^{-2} d^{-1}) across the sediment water interface are indicated. Organic carbon degradation rates by denitrification (den) and aerobic reparation (aerob) are in mmol C m^{-2} d^{-1}.

rate of organic matter degradation while the importance of aerobic mineralization is moderate (in this case 33%).

In deep sea sediments where organic matter fluxes are low, the nitrate profile may display steadily increasing (station B) or decreasing concentrations (station C), eventually reaching an asymptote in the upper decimeters due to a lack of labile carbon at these depths. In both cases, deep penetration of O_2 into the sediment oxidizes NH_4^+ released from POM (e.g. Goloway and Bender, 1982; Supplement to Smetacek et al., 1997) and accounts for the increase in NO_3^- at station B. Furthermore, aerobic respiration accounts for the bulk of POC degradation (> 90 %, Sarmiento and Gruber, 2006). The main difference in the shape of these profiles is due to the bottom water NO_3^- concentration which is twice as high at station C as at station B. Since bottom water NO_3^- concentration is a major control on

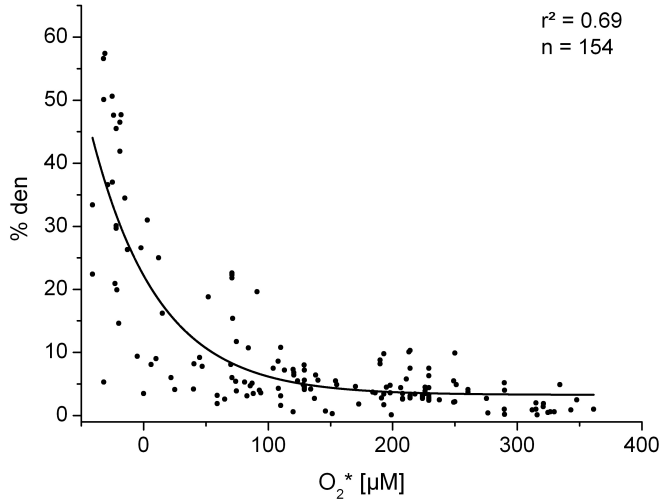

Figure 4.5.: Fraction organic matter degraded by denitrification (%den) predicted by the model as a function of measured O_2* (= bw_{O2} - bw_{NO3}). The fit to the data (Eq. 4.12) is also shown.

denitrification rate (Dale et al., 2011), this pathway accounts for 22 % of POC respiration at station C, compared to only 3 % at station B. Nonetheless, diffusive NO_3^- fluxes across the sediment-water interface are very low (Goloway and Bender, 1982; Grandel et al., 2000).
Sharp subsurface NO_3^- peaks (Fig. 4.4 station D) are mainly observed in reactive shelf sediments with well oxygenated bottom waters depleted in NO_3^-, such as the western Arctic shelf (Devol et al., 1997). Since bottom water NO_3^- is low, the main source of the accumulating and released NO_3^- is nitrification of NH_4^+. Below this peak, NO_3^- is strongly consumed by denitrification. In such shallow environments with high POC rain rates denitrification rates may be relatively high due to coupling with nitrification. Overall, denitrification is a minor pathway of carbon degradation despite high rates, and anaerobic mineralization dominates.

The importance of denitrification predicted by the model is shown in Fig. 4.5 using all simulated data points. The fraction of organic matter degraded via denitrification (% den) is significantly correlated (r^2 = 0.69, n = 154, $p < 0.001$) with the availability of oxygen and nitrate in the bottom water expressed by the O_2* parameter introduced in Chapter 3 (O_2 - NO_3^-):

$$\%\text{den} = a + b \cdot c^{\,O_2*} \tag{4.12}$$

with a = 3.28 ± 0.88 (%), b = 18.92 ± 1.79 (%) and c = 0.98 ± 0.003. Bohlen et al. (submitted) recently showed a very similar trend based on the measured data, which lends to support the parameterization of POC degradation using the present model-based approach.

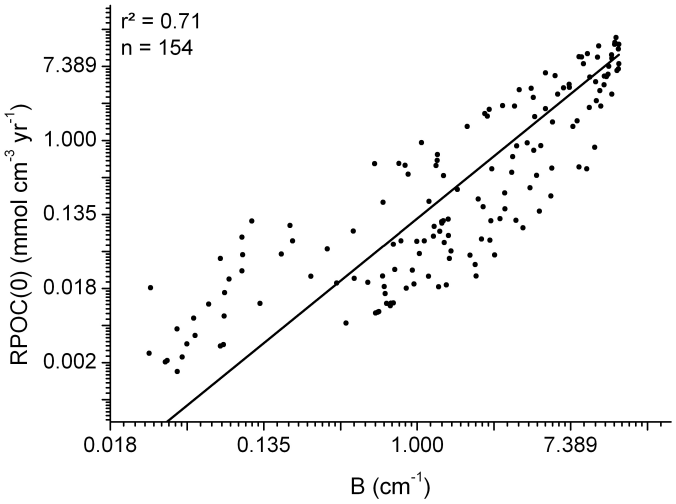

Figure 4.6.: Overview of all optimized values for B and RPOC(0). Note the logarithmic scale. The line indicates an exponential function fitted to the data (correlation coefficient indicated).

4.3.2. Depth distribution of organic matter degradation

The optimized values for B ranged from 0.03 to 13.87 cm^{-1} with RPOC(0) ranging from $1.94 \cdot 10^{-3}$ to 16.05 mmol cm^{-3} yr^{-1} (Fig. 4.6). As mentioned earlier, higher values for B are related with higher values for RPOC(0) and vice versa to yield the given $\sum$RPOC. Due to the use of a simple exponential function in this approach (Eq. 4.10), B and RPOC(0) are also related according to an exponential function of this type (Fig. 4.6). From a practical perspective, a correlation between RPOC(0) or B with a widely-used metric used in pelagic and benthic modeling studies is desirable, that is, the rain rate of organic matter to the seafloor (RRPOC) or bottom water chemistry. Assuming steady-state, RRPOC can be calculated from the total depth-integrated organic matter degradation rate and water depth using the relationship between burial and rain rate of organic carbon by Flögel et al. (2011) (Eq. 3.1 and 3.2 in Chapter 3). RPOC(0) (mmol cm^{-3} yr^{-1}) was found to be significantly correlated with RRPOC (mmol m^{-2} d^{-1}) (Fig. 4.7a) via the power law ($r^2 = 0.62$, n = 154, $p < 0.001$):

$$RPOC(0) = a \cdot RRPOC^{\,b} \tag{4.13}$$

where $a = 0.034 \pm 0.02$ cm^{-1} and $b = 1.49 \pm 0.17$. This trend can be explained as an increase in labile organic carbon flux to the seafloor as the total flux of organic matter increases. Since both, $\sum$RPOC and RRPOC are known, combining Eq. 4.11 and Eq. 4.13 enables B to be derived. Hence, the depth-dependent POC mineralization profile in the aerobic and denitrifying layers can be predicted based on the rain rate only.

There was no trend relating $\sum$RPOC, RPOC(0) or B with O_2 and NO_3^- concentrations individually

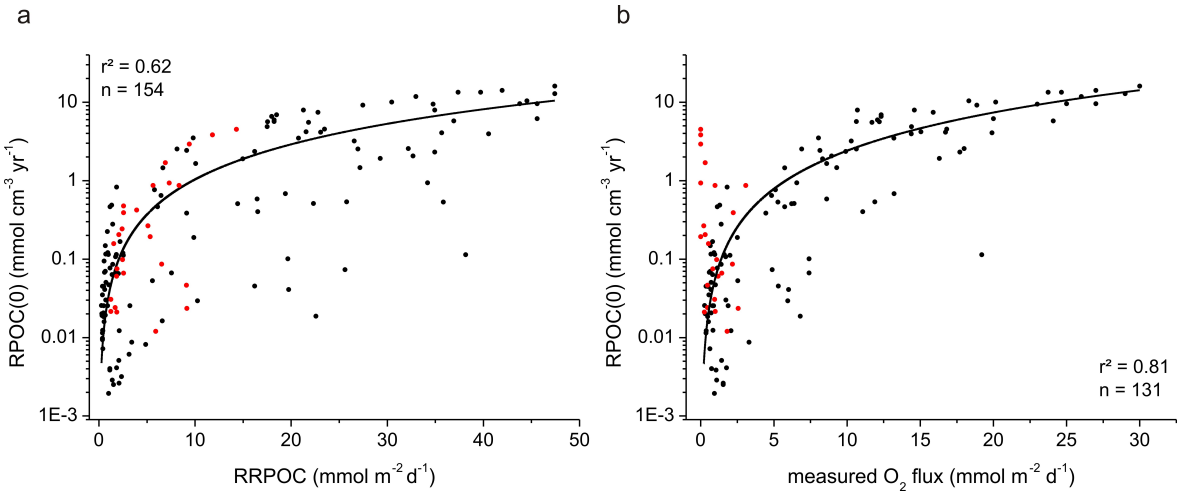

Figure 4.7.: The POC degradation rate at the sediment-water interface (RPOC(0), mmol cm^{-3}, yr^{-1}) as a function of the flux of organic carbon flux to the seafloor (RRPOC, mmol m^{-2} d^{-1}) (left) and the measured O_2 flux (mmol m^{-2} d^{-1}) (right). Stations with < 50 µM bottom water O_2 are indicated in red.

or combined as O_2*. This may seem surprising since O_2 availability has long been discussed to affect organic matter degradation and preservation (e.g. Hedges and Keil, 1995; Burdige, 2007). Freshly, labile organic matter has been found to be effectively degraded under both, anoxic and oxic conditions (e.g. Cowie and Hedges, 1992; Kristensen and Holmer, 2001). In contrast, degradation of aged, refractory organic matter appears to be more effective under oxic compared to anoxic conditions (e.g. Kristensen et al., 1995; Hulthe et al., 1998). This has been partly explained by the finding that the initial depolymerization of more refractory organic matter, i.e. breaking high-molecular-weight particles into lower molecular weight, appears to be associated with processes where O_2 is involved (Burdige, 2007). Hence, at sites with high and labile organic matter flux to the seafloor, anoxic or suboxic conditions appear to have a minor influence on the rate of degradation; however, at sites with lower rain rate of organic carbon which consists of more refractory material, lower degradation rates have been associated with lower O_2 concentrations (Canfield, 1994).

Our finding that the POC degradation rate at the sediment-water interface is a function of the rain rate of organic carbon rather than the bottom water chemistry supports the idea that bottom water oxygen concentrations are not the major factor controlling organic matter degradation. Stations with low bottom water O_2 concentration do not generally show a lower RPOC(0) compared to stations underlying oxygenated bottom waters (Fig. 4.7a). Nonetheless, this does not necessarily mean oxygen has no effect on POC mineralization. The effect of bottom water O_2 concentrations on the POC degradation rate at the surface of the sediment is a function of two opposing processes. On one hand, higher O_2 levels may enhance mineralization, at least at sites characterized by low sedimentation rates and a large fraction of more refractory material. On the other hand, however, oxygenated regimes favor faunal mixing activity while anoxic conditions generally lead to the absence or reduction of bioturbation

and bioirrigation processes (Middelburg and Levin, 2009). As a result, POC degradation may concentrate at the sediment-water interface at suboxic or anoxic settings but may spread over a broader mixed layer at well oxygenated settings. Due to the absence of faunal mixing in low oxygen environments, the initial degradation rate at the very surface of the sediment may be as high as in oxygenated environments although high bottom water O_2 concentrations probably enhance mineralization. However, since bioturbation has been shown to mix organic matter pools differently according to their reactivity (e.g. Smith et al., 1993), the overall effect of faunal mixing on the mineralization of organic matter has not been resolved yet.
In summary, O_2 levels may or may not affect organic matter degradation rates. In any case, bottom water O_2 concentration may not be the appropriate measure to investigate this effect. The concept of oxygen exposure time, i.e. the duration of exposure of organic matter to O_2 before being permanently buried (e.g. Hedges and Keil, 1995), could potentially be more useful. For continental margin sediments, oxygen exposure times have been found to have a direct effect on the preservation/degradation of organic matter (Hartnett et al., 1998). However, at this stage O_2 exposure time cannot be extracted from our model and can thus not be used to further investigate the control of O_2 on organic matter degradation. Broadly speaking, the observation that RPOC(0) is mainly correlated with rain rate confirms the well-established paradigm that the degradation rate of organic matter is mainly first-order in carbon concentrations. The availability of a particular oxidant is thus only of importance when considering the corresponding individual pathway of carbon degradation.

A similar correlation was also obtained for RPOC(0) and TOU (Fig. 4.7b), described using the following expression ($r^2 = 0.81$, n = 131, $p < 0.001$):

$$\mathrm{RPOC}(0) = a \cdot \mathrm{TOU}^{\,b} \tag{4.14}$$

where $a = 0.058 \pm 0.02$ cm^{-1} mol C (mol O_2)$^{-1}$ and $b = 1.62 \pm 0.11$. TOU data were not available for all stations and the fitting procedure did not include stations with zero O_2 flux. Nevertheless, this trend is robust. There may be several reasons for this trend. As mentioned above, a higher oxygen flux could enhance initial organic matter mineralization simply by a higher availability of O_2. However, higher O_2 fluxes could also indicate elevated bioturbation activity, especially in shallow shelf and slope sediments where the fauna mediated O_2 flux may contribute as much as 50 % to the TOU (Glud, 2008). Bioturbation may enhance overall POC degradation by exposing previously buried material to oxygen (Hulthe et al., 1998). However, bioturbation should not generally enhance the degradation rate at the surface, but rather at depth due to mixing of material downward.
It may also be possible that TOU represents a proxy for total organic matter degradation (Canfield, 1993). Since the total rate of organic matter degradation has been used to derive estimates for RRPOC (Eq. 3.1, 3.2), TOU may also be viewed as a proxy for RRPOC. The trend observed for RPOC(0) and TOU might thus only be a different way of representing the relation between RRPOC and RPOC(0). However, this theory does not explain why the correlation with TOU is better compared to correlation

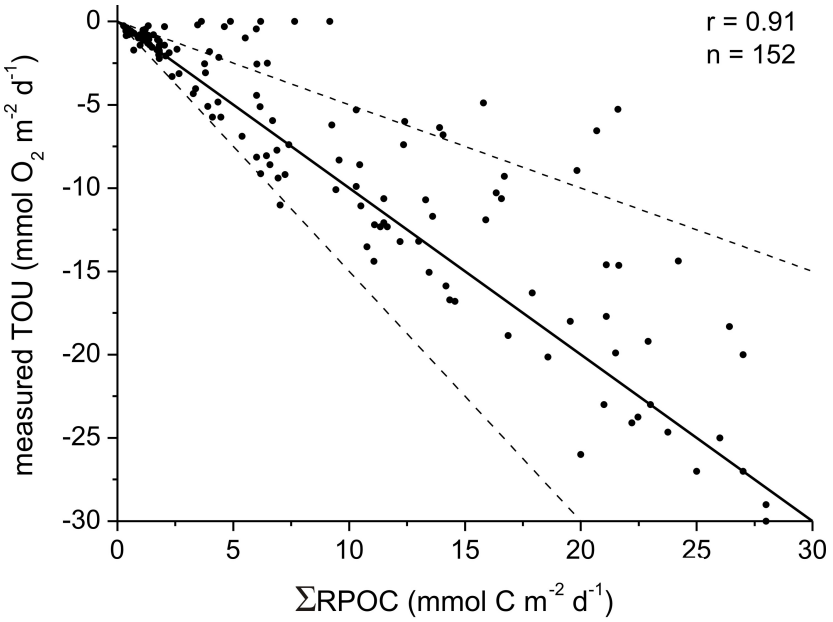

Figure 4.8.: Measured total oxygen fluxes across the sediment-water interface (TOU) as a function of depth-integrated organic matter degradation rates as given in the data compilation by Bohlen et al. (submitted). The solid line indicates the 1:1 line, dashed lines denote ±50 % deviation.

with RRPOC. One possible source of uncertainties in the RRPOC data could be the simplification made when transforming ∑RPOC into RRPOC (see Chapter 3). Nevertheless, in this case ∑RPOC and RPOC(0) would show a more robust trend compared to RRPOC and RPOC(0), which was not the case (r^2 = 0.61, n = 154, data not shown). The other possible reason is that TOU does not strictly track ∑RPOC exactly. In our database, TOU significantly correlates with the total rate of organic matter degradation (Fig. 4.8, r = 0.91, n = 152) and thus can be seen as valid proxy for the total depth-integrated organic matter degradation rate. However, at several stations the values for TOU and ∑RPOC also differ distinctly. The inconsistencies between TOU and ∑RPOC are probably due to the ∑RPOC estimates which are based on electron balances or flux summations and thus involve cumulative errors.

Hence, TOU may be, at least in this case, the better estimate for total organic matter degradation and thus yield a more robust fit with RPOC(0). Yet, since the POC rain rate is a standard metric parameter in sediment and global ocean models, the correlation between RPOC(0) and RRPOC is more appropriate for upscaling globally even though the statistical significance of this fit is weaker than for TOU.

Table 4.3.: Parameters used for the 2-G analytical model approach, values of the rate constats *k* derived in this study, and literature values for the rate constant of the reactive POC fraction. The rain rate of labile organic carbon ($RRPOC_{lab}$) is assumed to equal ∑RPOC, and the rain rate of refractory organic carbon ($RRPOC_{ref}$) is estimated as RRPOC - RPOC (see text for details).

station		wd (m)	w (cm yr^{-1})	D_B [a] (cm^2 yr^{-1})	RRPOC (mmol m^{-2} d^{-1})	$RRPOC_{lab}$ (= ΣRPOC) (mmol m^{-2} d^{-1})	$RRPOC_{ref}$ (mmol m^{-2} d^{-1})	*k* (yr^{-1})	k_1 [b] (yr^{-1})	k_1 [c] (yr^{-1})	k_1 [d] (yr^{-1})
A	Mexican shelf [e]	100	0.135[f]	1[g]	8.33	5.51	2.82	15.94	3.61	0.12	0.86
B	Peru slope [h]	1000	0.052	0.3	5.9	3.98	1.92	3.35	1.75	0.07	0.47
C	deep equatorial Pacific [i]	3591	0.75×10^{-3} [j]	1.2 [k]	0.32	0.316	0.004	0.34	0.004	0.01	0.03

(a) bioturbation coefficient represent values at the sediment surface, $D_B(0)$;
(b) k_1 for POC degradation in the top 10-20 cm of the sediment based on organic carbon rain rate, Boudreau (1997): $k_1 = 2.2\cdot10^{-5} \cdot RRPOC\ [\mu mol\ cm^{-2}\ yr^{-1}]^{2.1}$;
(c) k_1 for POC degradation in the top 10-20 cm based on burial velocity, Boudreau (1997): $k_1 = 0.38\ w^{0.59}$;
(d) k_1 for oxic POC degradation in the top 10-20 cm based on burial velocity, Tromp et al. (1995): $k_1 = 2.97\ w^{0.62}$;
(e) station NH003 in Hartnett and Devol (2003);
(f) estimated, similar range for this region reported in Hartnett et al. (1998);
(g) estimated to be low at this low-oxygen environment, fitted to POC profile;
(h) station 6 in Bohlen et al. (2011);
(i) station 9BC, MANOP H in Goloway and Bender (1982);
(j) estimated, similar range for this region reported in Lyle (1988);
(k) according to Middelburg et al. (1997);

4.3.3. Comparison with a G-type model

In this section we show how our predictor for the depth distribution of POC degradation based on RRPOC can be used in conjunction with an analytical solution for carbon degradation in bioturbated sediments to provide information on the reactivity of the organic carbon pool being degraded. The objective is to reproduce the derived depth-dependent rate of carbon degradation with the analytical solution by tuning the rate constant k assuming first-order decay of POC. Data from 3 sites with different bioturbation rates are used (Table 4.3). These stations cover the different sedimentation regimes on the shelf, slope and deep sea as well as different bottom water oxygen concentrations. In order to keep the model conceptually simple, a 2-G model approach was used, that is, with particulate organic carbon (POC) being split into a labile ($POC_{(l)}$) and refractory fraction ($POC_{(r)}$). Only $POC_{(l)}$ undergoes mineralization whereas $POC_{(r)}$ is unreactive. Assuming constant porosity, the following mass conservation equations were used to calculate the concentration of $POC_{(l)}$ (wt-%) and $POC_{(r)}$ (wt-%) with depth in the sediment:

$$\frac{\partial \mathrm{POC_{(l)}}}{\partial \mathrm{t}} = \frac{\partial\left(\mathrm{D_B}\frac{\partial \mathrm{POC_{(l)}}}{\partial \mathrm{x}}\right)}{\partial \mathrm{x}} - \frac{\mathrm{w}\,\partial(\mathrm{POC_{(l)}})}{\partial \mathrm{x}} - \mathrm{RPOC(x)} \tag{4.15}$$

$$\frac{\partial \mathrm{POC_{(r)}}}{\partial \mathrm{t}} = \frac{\partial\left(\mathrm{D_B}\frac{\partial \mathrm{POC_{(r)}}}{\partial \mathrm{x}}\right)}{\partial \mathrm{x}} - \frac{\mathrm{w}\,\partial(\mathrm{POC_{(r)}})}{\partial \mathrm{x}} \tag{4.16}$$

where w (cm yr^{-1}) is the burial velocity for solids and RPOC(x) is the POC degradation rate at each depth, x, in the sediments. Values for w and D_B were measured at each site or estimated according to empirical logistic relations based on water depth (Middelburg et al., 1997) (Table 4.3).

RPOC(x) in Eq. (4.15), derived from the rain rate, can be formulated as a first-order rate expression:

$$\mathrm{RPOC(x)} = k \cdot \mathrm{POC_{(l)}(x)} \tag{4.17}$$

where k (yr^{-1}) is the decay constant for $POC_{(l)}$ (wt-%). For this 2-G model approach we assume that all reactive carbon raining onto the seafloor is degraded. Hence, the rain rate of labile POC ($RRPOC_{lab}$) equals the total rate of organic matter degradation, given by $\sum$RPOC (Table 4.3). The rain rate of refractory POC ($RRPOC_{ref}$) was then determined by subtracting $RRPOC_{lab}$ from the total RRPOC.

If bioturbation is assumed to be constant with depth over the simulated aerobic and denitrifying sediment layers, a steady state general analytical solution of Eq. 4.15 can be derived (not shown). Two boundary conditions are necessary to fully specify the particular of this solution. For the upper boundary condition (x = 0 cm) the flux of labile organic carbon ($RRPOC_{lab}$) is used and for infinite depth the concentration of POC_l is assumed to be zero:

$$\mathrm{RRPOC_{lab}} = -\mathrm{D_B}\frac{\partial \mathrm{POC_l}}{\partial \mathrm{x}}\bigg|_{\mathrm{x=0\ cm}} + \mathrm{w\ POC_{lab}(0\ cm)} \tag{4.18}$$

$$\mathrm{POC_l(x = \infty)} = 0 \tag{4.19}$$

Hence, the particular solution is given with:

$$\mathrm{POC_{(l)}(x)} = \mathrm{POC_{(l)}(0)} \cdot \exp\left(\frac{\left(\mathrm{w} - \sqrt{4\ \mathrm{D_B}\ k + \mathrm{w}^2}\right) \cdot \mathrm{x}}{2\mathrm{D_B}}\right) \tag{4.20}$$

with

$$\mathrm{POC_{(l)}(0)} = \frac{2\ \mathrm{RRPOC_{lab}}}{\mathrm{w} + \sqrt{4\ \mathrm{D_B}\ k + \mathrm{w}^2}} \frac{\mathrm{M_C}}{\mathrm{ds} \cdot 10} \tag{4.21}$$

where $\mathrm{M_C}$ (g $\mathrm{mol^{-1}}$) is the molecular weight of carbon and ds is the density of dry sediment (2.5 g $\mathrm{cm^{-3}}$). Note that the last term in the latter equation is a unit conversion for $\mathrm{POC_{(l)}}$ from mmol $\mathrm{cm^{-3}}$ to wt-%. The imposed degradation rate (RPOC(x), mmol $\mathrm{cm^{-3}\ yr^{-1}}$) in the sediments would then be:

$$\mathrm{RPOC(x)} = k \cdot \frac{2\ \mathrm{RRPOC_{lab}}}{\mathrm{w} + \sqrt{4\ \mathrm{D_B}\ k + \mathrm{w}^2}} \cdot \exp\left(\frac{\left(\mathrm{w} - \sqrt{4\ \mathrm{D_B}\ k + \mathrm{w}^2}\right) \cdot \mathrm{x}}{2\mathrm{D_B}}\right) \tag{4.22}$$

The unit conversion (second term in Eq. 4.21) is redundant for the calculation of the rate RPOC(x) (mmol $\mathrm{cm^{-3}\ yr^{-1}}$). In order to reproduce the mineralization profile based on the parameter optimization, we use the RPOC(0) as given by Eq. 4.13:

$$\mathrm{RPOC(0)} = k \cdot \frac{2\ \mathrm{RRPOC_{lab}}}{\mathrm{w} + \sqrt{4\ \mathrm{D_B}\ k + \mathrm{w}^2}} = 0.034 \cdot \mathrm{RRPOC}^{1.49} \tag{4.23}$$

This equation is solved for k at each station to calculate the depth profile of labile organic carbon from Eq. 4.20. However, the simulation of the total organic carbon concentrations requires the inclusion of the refractory fraction. $\mathrm{POC_{(r)}}$ was calculated using an analgous solution as Eq. 4.20 wit k set to zero. Combining $\mathrm{POC_{(l)}}$ and $\mathrm{POC_{(r)}}$ then yields the POC distribution shown in Fig. 4.9.

In general, the decrease of RPOC(x) with sediment depth could always be expressed with a single labile POC pool (Fig. 4.9, left panel). Since both approaches assume a simple exponential decay of reactivity with depth, RPOC(x) fitted with a G model were identical to the original parameter optimization results at all 3 stations. The derived rate constant, k, was highest for the shelf sediment (16 $\mathrm{yr^{-1}}$), as expected (Table 4.3). The magnitude of k decreased by two orders-of-magnitude with increasing water depth to 3 $\mathrm{yr^{-1}}$ at the slope station and 0.3 $\mathrm{yr^{-1}}$ for the deep-sea site. Although only

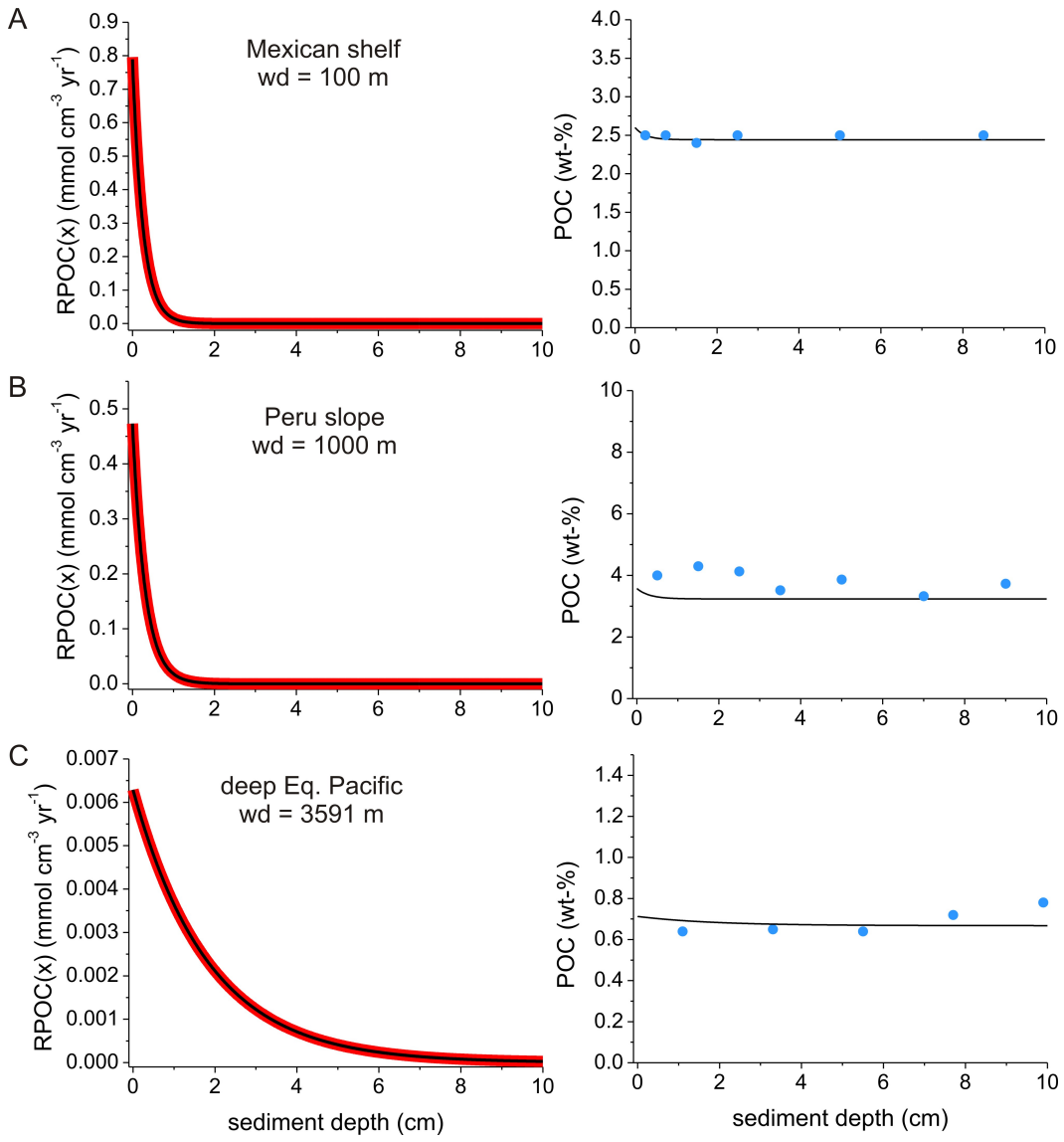

Figure 4.9.: Organic matter degradation rate as a function sediment depth (left panels) and associated organic carbon (right panels). The black curves in the left panels indicate RPOC(x) as calculated according to Eq. 4.11 and 4.13, the red curves indicate results using the 2-G analytical approach (see text). The blue dots in the right panels denote measured carbon concentrations, and the carbon profile calculated from the analytical solution of the 2-G model is indicated by the black curves. For station details see Table 4.3.

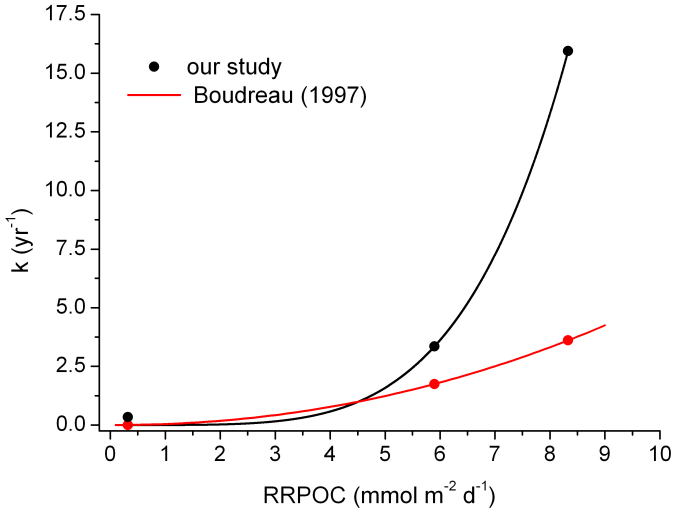

Figure 4.10.: Rate constant for POC degradation, k, as a function of the organic carbon rain rate to the seafloor. Results of this study are shown in black, the relation reported by Boudreau (1997) is indicated in red ($k_1 = 2.2 \cdot 10^{-5} \cdot$ RRPOC [µmol cm^{-2} yr^{-1}] $^{2.1}$). The power law function fitted to the data (black line) is given with $k = a \cdot$ RRPOC [mmol m^{-2} d^{-1}] ^{b} with a = $8.90 \cdot 10^{-4} \pm 5.12 \cdot 10^{-4}$, b = 4.62 ± 0.27.

based on three points, one could infer that k shows a similar dependency with RRPOC as RPOC(0), i.e. an increase of k with increasing RRPOC according to a power law (Fig. 4.10). Such a relation of k with the rain rate of organic carbon has already been hypothesized earlier (Boudreau, 1997), however, yielding lower values for k when applied to the three station in Table 4.3 (Fig. 4.10). Moreover, several other studies reported a correlation of the decay constant for reactive organic carbon, k_1, with the burial velocity, w (e.g. Boudreau, 1997; Tromp et al., 1995). The values for k_1 are thought to represent the decay in the top 10 - 20 cm of the sediment (Boudreau, 1997). However, there is also a highly reactive fraction which decomposes largely close to the sediment-water interface and is not predicted by k_1 (Boudreau, 1997). Currently, there are no predictive correlations for k considering this extremely reactive fraction. Nevertheless, in order to evaluate the magnitude of our derived k, the values estimated in this study were compared with the k_1 predicted by two relationships in Boudreau (1997) and another in Tromp et al. (1994) (Table 4.3). It is obvious that our values for k are generally higher, ocassionally by two orders of magnitude. However, as mentioned above, the reported k_1 values are associated with decay up to 20 cm sediment depth. In contrast, our k values reflect the degradation up to only 10 cm depth. At the shelf and slope station where POC degradation does only occur at the very surface of the sediment (Fig. 4.9), k reflects the decay in the upper < 2 cm only. At the deep sea station C, however, POC degradatation continues down to ca. 10 cm depth and k reflects the mineralization in the upper ca. 10 cm. Moreover, the estimate by Tromp et al. (1995) considers oxic organic matter degradation only while the k in this study covers both, aerobic mineralization

and denitrification. Consequently, our values for k are probably higher because they reflect organic matter decay at the very surface of the sediment while the literature values reflect lower decay down to 20 cm depth.

As a further application of the latter results, the burial velocity, w, and the bioturbation coefficient, D_B, in Eq. 4.23 can also be predicted from more commonly known parameters such as the rain rate of organic carbon or water depth. Using the relationship between RRPOC and D_B by Archer et al. (2002) (their Eq. 13) as well as the function predicting the burial velocity from water depth as given by Burwicz et al. (2011) (their Eq. 1), Eq. 4.23 can be reformulated as:

$$\mathrm{RPOC}(0) = \mathrm{k} \cdot \frac{2\ \mathrm{RRPOC_{lab}}}{\mathrm{w} + \sqrt{4\ D_B\ \mathrm{k} + \mathrm{w}^2}} = 0.034 \cdot \mathrm{RRPOC}^{1.49} \tag{4.24}$$

with

$$\mathrm{w} = \frac{w_1}{1 + \left(\frac{\mathrm{wd}}{z_1}\right)^{c_1}} + \frac{w_2}{1 + \left(\frac{\mathrm{wd}}{z_2}\right)^{c_2}} \tag{4.25}$$

$$D_B = 0.0232 \cdot \mathrm{RRPOC}^{\,0.85} \tag{4.26}$$

where $w_1 = 0.117$ cm yr^{-1}, $w_2 = 0.006$ cm yr^{-1}, $z_1 = 200$ m, $z_2 = 4000$ m, $c_1 = 3$, $c_2 = 10$, wd (m) is water depth and RRPOC is in units μmol cm^{-2} yr^{-1}. By solving this equation for k, a first estimate for the decay constant associated with the highly reactive fraction decomposing at the very surface of the sediment is calculated only from the two general parameters rain rate of organic carbon to the seafloor and water depth. This function may help to determine values for k on global scale, e.g. by applying to the $1° \times 1°$ grids of RRPOC and water depth presented in Chapter 3.
For the examples in Table 4.3, k values were predicted with 47, 24, and 0.06 for station A-C, respectively. These values show the same trend as described above, however, the absolute values differed. One source of uncertainty is obviously the estimate of w from water depth. However, the main reason why the two approaches yield such different values has been found to be the estimate of the bioturbation coefficient (not shown). In any case, the bioturbation coefficient is difficult to determine in the upper layer of the sediment. Hence, a simple sensitivity analysis of the derived values for k on variations in the bioturbation coefficient was investigated using station A ($k = 16$ yr^{-1}) as an example. Therefore, D_B was increased and decreased by a factor of 10 and all other parameters were kept as described in Table 4.3. An increase of D_B by a factor of 10 resulted in a k value of 155; in contrast, a decrease of D_B by a factor of 10 lead to a k of 2.07. Hence, k almost scales linearly with variations in the bioturbation coefficient. This finding indicates that the estimate for the bioturbation coefficient may have caused the discrepancies with the values described in the literature. Moreover, this emphasizes the difficulty to find the correct values for k in well-mixed surface sediments.

4.4. Conclusions

A diagenetic reaction-transport model was used to reproduce measured benthic fluxes of oxygen and nitrate across the sediment-water interface. In the model, the total rate of organic matter degradation ($\sum$RPOC) was imposed while the depth distribution was optimized to give the best fit to the measured NO_3^- and O_2 fluxes. The results indicate that the initial degradation rate at the surface of the sediment (RPOC(0)) is controlled by the rain rate of organic carbon (RRPOC) rather than the availability of electron acceptors - such as O_2 or NO_3^- - in the bottom water. A statistically significant fit then allows the determination of RPOC(0) and the parameter describing the decrease of the degradation rate with sediment depth (B) from RRPOC only. Hence, this approach predicts the profile of organic matter degradation in aerobic and nitrogenous sediments, which is of clear value for coupling benthic models to pelagic biogeochemical models at the global scale. In particular, RRPOC is commonly used as a boundary condition in benthic models and is also a universal metric in global biogeochemical models. The reproduction of the mineralization profile determined with this new approach with a simple 2-G model indicated that first order decay constant k commonly used in such G models may vary over several orders-of-magnitude. This results has yet to be fully interpreted, yet emphasizes the difficulties in correctly parameterizing k in the upper well mixed layer of marine sediments based on the carbon concentration only. Nonetheless, our optimization approach to calculate the depth profile of organic matter degradation in the aerobic and denitrifying layer implicitly includes carbon concentration, bioturbation rates and organic matter reactivity.

References

Aller R. C (1994) Bioturbation and remineralization of sedimentary organic matter: effects of redox oscillation. *Chemical Geology* **114**, 331-345.

Andersson J. H., Wijsman J. W. M., Herman P. M. J. , Middelburg J. J., Soetaert K. and Heip C. (2004) Respiration patterns in the deep ocean. *Geophys. Res. Lett.* **31(3)**, L03304.

Archer D. E., Morford J. L. and Emerson S. R. (2002) A model of suboxic sedimentary diagenesis suitable for automatic tuning and gridded global domains. *Global Biogeochem. Cy.* **16**.

Berg P., Rysgaard S. and Thamdrup B. (2003) Dynamic modeling of early diagenesis and nutrient cycling. A case study in an Arctic marine sediment. *Am. J. Sci.* **303**, 905-955.

Berner R. A. (1980) *Early Diagenesis - A Theoretial Approach*. Princeton University Press, Princeton, New Jersey.

Bohlen L., Dale A. W., Sommer S., Mosch T., Hensen C., Noffke A., Scholz F. and Wallmann K. (2011) Benthic nitrogen cycling traversing the Peruvian oxygen minimum zone. *Geochim. Cosmochim. Ac.* **75**, 6094-6111.

Bohlen L., Dale A. W. and Wallmann K. (submitted to *Global Biogeochem. Cy.*) A simple transfer function for calculating benthic fixed nitrogen losses in global biogeochemical models.

Boudreau B. P. (1996) A method-of-lines code for carbon and nutrient diagenesis in aquatic sediments. *Comput. Geosci.* **22**, 479-496.

Boudreau B. P. (1997) *Diagenetic Models and Their Implementation*. Springer-Verlag, Berlin, Heidelberg, New York.

Boudreau B. P. and Ruddick, B. R. (1991) On A Reactive Continuum Representation Of Organic-Matter Diagenesis. *Am. J. Sci.* **291**, 507-538.

Burdige D. J. (1993) The Biogeochemistry Of Manganese And Iron Reduction In Marine-Sediments. *Earth-Sci. Rev.* **35**, 249-284.

Burdige D. J. (2006) *Geochemistry of Marine Sediments*. Princeton University Press, Princeton, New Jersey.

Burdige D. J. (2007) Preservation of organic matter in marine sediments: Controls, mechanisms, and an imbalance in sediment organic carbon budgets? *Chem. Rev.* **107**, 467-485.

Burwicz E. B., Rupke L. H. and Wallmann K. (2011) Estimation of the global amount of submarine gas hydrates formed via microbial methane formation based on numerical reaction-transport modeling and a novel parameterization of Holocene sedimentation. *Geochim. Cosmochimi. Ac.* **75**, 4562-4576.

Canfield D. (1993) Organic matter oxidation in marine sediments. In *Interactions of C, N, P, and S Biogeochemical Cycles* (eds. Wollast R., Mackenzie F. and Chou L.). NATO ASI Series 14, pp. 333-363, Springer-Verlag, Berlin.

Canfield D. E. (1994) Factors Influencing Organic-Carbon Preservation In Marine-Sediments. *Chem. Geol.* **114**, 315-329.

Christensen E. R. (1982) A Model For Radionuclides In Sediments Influenced By Mixing And Compaction. *J. Geophys. Res.-Oc. Atm.* **87**, 566-572.

Cowie G. L. and Hedges J. I. (1992) The Role Of Anoxia In Organic-Matter Preservation In Coastal Sediments - Relative Stabilities Of The Major Biochemicals Under Oxic And Anoxic Depositional Conditions. *Org. Geochem.* **19**, 229-234.

Dale A.W., Sommer S., Bohlen L., Treude T., Bertics V. J., Bange H.W., Pfannkuche O., Schorp T., Mattsdotter M. and Wallmann K. (2011) Rates and regulation of nitrogen cycling in seasonally-hypoxic sediments during winter (Boknis Eck, SW Baltic Sea): sensitivity to environmental variables. *Estuar. Coast. Shelf Sci.* **95**, 14-28.

Dalsgaard T., Thamdrup B. and Canfield D. E. (2005) Anaerobic ammonium oxidation (anammox) in the marine environment. *Res. Microbiol.* **156**, 457-464.

Devol A. H. and Christensen J. P. (1993) Benthic Fluxes And Nitrogen Cycling In Sediments Of The Continental-Margin Of The Eastern North Pacific. *J. Mar. Res.* **51**, 345-372.

Devol A. H., Codispoti L. A. and Christensen J. P. (1997) Summer and winter denitrification rates in western arctic shelf sediments. *Cont. Shelf Res.* **17(9)**, 1029-1050.

Dhakar S. P. and Burdige D. J. (1996) Coupled, non-linear, steady state model for early diagenetic processes in pelagic sediments. *Am. J. Sci.* **296**, 296-330.

Flögel S., Wallmann K., Poulsen C., Zhou J., Oschlies A., Voigt S. and Kuhnt W. (2011) Simulating the biogeochemical effects of volcanic CO_2 degassing on the oxygen-state of the deep ocean during the cenomanian/turonian anoxic event (OAE2). *Earth Planet. Sc. Lett.* **305(3-4)**, 371-384.

Glud R. N. (2008), Oxygen dynamics of marine sediments, *Mar. Biol. Res.* **4(4)**, 243-289.

Goloway F. and Bender M. (1982) Diagenetic models of interstitial nitrate profiles in deep sea suboxic sediments. *Limnol. Oceanogr.* **27(4)**, 624-638.

Grandel S., Rickert D., Schlüter M. and Wallmann K. (2000) Pore-water distribution and quantification of diffusive benthic fluxes of silicic acid, nitrate and phosphate in surface sediments of the deep Arabian Sea. *Deep-Sea Res. Pt. II* **47(14)**, 2707-2734.

Hamersley M. R., Lavik G., Woebken D., Rattray J. E., Lam P., Hopmans E. C., Damsté J. S. S., Krüger S., Graco M., Gutiérrez D., and Kuypers M. M. M. (2007) Anaerobic ammonium oxidation in the Peruvian oxygen minimum zone. *Limnol. Oceanogr.* **52**, 923-933.

Hartnett H. E. and Devol A. H. (2003) Role of a strong oxygen-deficient zone in the preservation and degradation of organic matter: A carbon budget for the continental margins of northwest Mexico and Washington State. *Geochim. Cosmochim. Ac.* **67**, 247-264.

Hartnett H. E., Keil R. G., Hedges J. I. and Devol A. H. (1998) Influence of oxygen exposure time on organic carbon preservation in continental margin sediments. *Nature* **391**, 572-574.

Hedges J. I. and Keil R. G. (1995) Sedimentary Organic-Matter Preservation - An Assessment And Speculative Synthesis. *Mar. Chem.* **49**, 81-115.

Hensen C., Zabel M and Schulz H. D (2006) Benthic cycling of Oxygen, Nitrogen and Phosphorus. In *Marine Geochemistry*, 2nd edition (eds. Schulz H D. and Zabel M.). Springer Verlag, Berlin, Heidelberg, New York.

Hulth S., Aller R. C., Canfield D. E., Dalsgaard T., Engstrom P., Gilbert F., Sundback K. and Thamdrup B. (2005) Nitrogen removal in marine environments: recent findings and future research challenges. *Marine Chemistry* **94**, 125-145.

Hulthe G., Hulth S. and Hall P. O. J. (1998) Effect of oxygen on degradation rate of refractory and labile organic matter in continental margin sediments. *Geochim. Cosmochim. Ac.* **62**, 1319-1328.

Kristensen E. and Holmer M. (2001) Decomposition of plant materials in marine sediment exposed to different electron accepters (O_2, NO_3^-, and SO_4^{2-}), with emphasis on substrate origin, degradation kinetics, and the role of bioturbation. *Geochim. Cosmochim. Ac.* **65**, 419-433.

Kristensen E., Ahmed S. I. and Devol A. H. (1995) Aerobic and anaerobic decomposition of organic matter in marine sediment: Which is fastest? *Limnol. Oceanogr.* **40**, 1430-1437.

Lam P. and Kuypers M. M. M. (2011) Microbial nitrogen cycling processes in oxygen minimum zones. *Annu. Rev. Mar. Sci.* **3**, 317-345.

Lam P., Lavik G., Jensen M. M., van de Vossenberg J., Schmid M., Woebken D., Dimitri G., Amann R., Jetten M. S. M. and Kuypers M. M. M. (2009) Revising the nitrogen cycle in the Peruvian oxygen minimum zone. *P. Natl. Acad. Sci. USA* **106**, 4752-4757.

Legeleux F., Reyss J. L. and Schmidt S. (1994) Particle Mixing Rates In Sediments Of The Northeast Tropical Atlantic - Evidence From Pb-210_{XS}, Cs-137, Th-228_{XS} And Th-234_{XS} Downcore Distributions. *Earth Planet. Sc. Lett.* **128**, 545-562.

Locarnini R. A., Mishonov A. V., Antonov J. I., Boyer T. P., Garcia H. E., Baranova O. K., Zweng M. M. and Johnson D. R. (2010). *World Ocean Atlas 2009*, Volume 1: Temperature. S. Levitus, Ed. NOAA Atlas NESDIS 68, U.S. Government Printing Office, Washington, D.C., 184 pp.

Lyle M. W. et al. (1988) Sedimentation rate and geochemistry of core VULCAN-1-49GC from eastern tropical Pacific. doi:10.1594/PANGAEA.754648.

Meile C. and Van Cappellen P. (2003). Global estimates of enhanced solute transport in marine sediments. *Limnol. Oceanogr.* **48(2)**, 777-786.

Meysman F. J. R., Boudreau B. P. and Middelburg J. J. (2005) Modeling reactive transport in sediments subject to bioturbation and compaction. *Geochim. Cosmochim. Ac.* **69**, 3601-3617.

Middelburg J. J. (1989). A simple rate model for organic-matter decomposition in marine sediments. *Geochim. Cosmochim. Ac.* **53**, 1577-1581.

Middelburg J. J. and Levin L. A. (2009) Coastal hypoxia and sediment biogeochemistry. *Biogeosciences* **6**, 1273-1293.

Middelburg J. J., Vlug T. and Vandernat F. J. W. A. (1993) Organic-Matter Mineralization In Marine Systems. *Global And Planetary Change* **8**, 47-58.

Middelburg J. J., Soetaert K. and Herman P. M. J. (1997) Empirical relationships for use in global diagenetic models. *Deep-Sea Res. Pt. I*, **44(2)**, 327-344.

Otte S., Kuenen J. G., Nielsen L. P., Paerl H. W., Zopfi J., Schulz H. N., Teske A., Strotmann B., Gallardo V.A. and Jørgensen B. B. (1999) Nitrogen, carbon, and sulfur metabolism in natural Thioploca samples. *Appl. Environmental. Microb.* **65**, 3148-3157.

Redfield A. C., Ketchum B. H. and Richards F. A. (1963) The Influence of organisms on the composition of seawater. In *The Sea*, vol. 2, pp. 26-77, Wiley Interscience.

Sarmiento J. and Gruber, N. (2006) *Ocean Biogeochemical Dynamics*. Princeton University Press, Princeton, New Jersey.

Smetacek V., De Baar H. J. W., Bathmann U. V., Lochte K. and Rutgers Van Der Loef M. M. (1997) Ecology and biogeochemistry of the Antarctic circumpolar current during austral spring: a summary of southern ocean JGOFS cruise ANT X/6 of R.V. Polarstern. *Deep-Sea Res. Pt. II* **44(1-2)**, 1-21.

Smith C. R., Pope R. H., DeMaster D. J. and Magaard L. (1993) Age-Dependent Mixing Of Deep-Sea Sediments. *Geochim. Cosmochim. Ac.* **57**, 1473-1488.

Soetaert K., Herman P. M. J. and Middelburg J. J. (1996) A model of early diagenetic processes from the shelf to abyssal depths. *Geochim. Cosmochim. Ac.* **60(6)**, 1019-1040.

Sommer S., Bohlen L., Dale A. W., Wallmann K., Hensen C., Mosch T., Noffke A. and Pfannkuche O. (submitted to *Global Biogeochem. Cy.*) Nitrogen fluxes across Peruvian oxygen minimum zone surface sediments - the potential significance of DNRA.

Thamdrup B. and Dalsgaard T. (2002) Production of N_2 through anaerobic ammonium oxidation coupled to nitrate reduction in marine sediments. *Appl. Environ. Microb.* **68**, 1312-1318.

Thauer R. K., Jungermann K. and Decker K. (1977) Energy-Conservation In Chemotrophic Anaerobic Bacteria. *Bacteriol. Rev.* **41**, 100-180.

Thullner M., Dale A. W. and Regnier P. (2009) Global-scale quantification of mineralization pathways in marine sediments: A reaction-transport modeling approach. *Geochem. Geophys. Geosyst.* **10**, Q10012.

Tromp T. K., Van Cappellen P. and Key R. M. (1995) A globa model for the early diagenesis of organic carbon and organic phosphorus in marine sediments. *Geochim.Cosmochim. Ac.* **59**, 1259-1284.

Van Cappellen P. and Wang Y. (1995) Metal cycling in surface sediments: Modeling the interplay of transport and reaction. In *Metal contaminated aquatic sediments* (ed. Allen, H.E.). Ann Arbor Press. pp. 21-64.

Van Cappellen P. and Wang Y. (1996) Cycling of iron and manganese in surface sediments; a general theory for the coupled transport and reaction of carbon, oxygen, nitrogen, sulfur, iron, and manganese. *Am. J. Sci.* **296**, 197-243.

Westrich J. T. and Berner R. A. (1984) The Role Of Sedimentary Organic-Matter In Bacterial Sulfate Reduction - The G Model Tested. *Limnol. Oceanogr.* **29**, 236-249.

Wijsman J. W. M. (2000) Early diagenetic processes in north-western Black Sea sediments, Ph.D. thesis, Groningen Univ., Groningen, Netherlands.

5. Synthesis

All three studies presented in this thesis constitute different approaches investigating benthic nitrogen cycling in marine sediments. In Chapter 2, a 1-D reaction transport model including a detailed nitrogen reaction network is applied to better understand N turnover processes in sediments along a transect traversing the Peruvian oxygen minimum zone (OMZ). This transect covers the transition from fully anoxic to suboxic bottom waters and thus is an ideal region for studying the triggers of different N turnover processes under altering redox conditions. A more global approach was adopted in Chapter 3, where benthic nitrogen loss via combined denitrification and anammox was investigated. A database of nitrate fluxes across the sediment-water interface, the degradation or rain rate of organic carbon and bottom water O_2 and NO_3^- concentrations for sites all over the world was compiled. A transfer function was then developed for estimating benthic N loss from the rain rate of organic carbon and bottom water chemistry only. In Chapter 4 the redox sensitivity of the sedimentary N cycle was used to gain insight on the distribution of organic matter degradation in marine surface sediments, including the bioturbated layer, at > 150 sites worldwide. A diagenetic model was forced with the total depth-integrated degradation rate and bottom water chemistry yielding an exponential-type decrease of organic matter remineralization with sediment depth. The distribution of the organic matter degradation rate was constrained by simulating measured benthic fluxes of NO_3^- and O_2 at each site.

A major finding of the modeling study in Chapter 2 is that dissimilatory nitrate reduction to ammonium (DNRA) may be an important process in reactive sediments underlying oxygen-deficient bottom waters. This process leads to the recycling of fixed N and thus counteracts the loss of fixed N by sedimentary denitrification and anammox. In the past, high NO_3^- uptake rates into the sediment observed in OMZs were assumed to fuel denitrification and thus N loss (e.g. Devol and Christensen, 1993). However, this work shows that DNRA may account for ≥ 65 % of the benthic NO_3^- uptake (Bohlen et al., 2011) and, consequently, has to be considered in order to accurately estimate the amount of fixed N loss in OMZ sediments. Moreover, the model indicates that anammox is of minor importance in sediments underlying the permanent anoxic layer (ca. 80 - 400 m water depth). This is in stark contrast to observations in the water column, where anammox was found to dominate N cycling (Hamersley et al., 2007; Lam et al., 2009). However, this finding supports the idea that high organic matter fluxes to the seafloor augment denitrification much more than anammox, the latter process being of minor importance in shallow organic matter-rich sediments (Daalsgaard et al., 2005).
In this study, OMZs have been identified as regions with a pronounced benthic-pelagic feedback. Where O_2 concentrations are low, a high production of ammonium during DNRA and ammonification was found to drive a large flux of ammonium out of the sediment (Bohlen et al., 2011). Subsequently, the ammonium may potentially fuel primary production or anammox in the water column.

Moreover, the availability of fixed N in the oceans is affected by the high rates of benthic N loss via denitrification and anammox in such low-oxygen regions. Consequently, this work encourages the need to investigate biogeochemical cycling in OMZs and emphasizes their importance for the future development of the world's ocean and climate.

The new estimates for global benthic N loss via denitrification given in the third Chapter (154 ± 40 and 155 ± 67 Tg N yr^{-1}) helps to narrow the broad range of 130 - 300 Tg N yr^{-1} circulating for sedimentary denitrification on a global scale (e.g. Middelburg et al., 1996; Gruber, 2004). In contrast to previous studies which used modeling approaches or data extrapolation and interpretation (e.g. Middelburg et al., 1996; Codispoti et al., 2001), the estimate given here is based on empirical data analysis only. Hence, this approach has the advantage to be less dependent on parameterizations and far-reaching assumptions. Despite only covering a very limited area of the oceans, sediments underlying OMZs have been found to contribute significantly to the total fixed N loss by denitrification. As a major sink for fixed N in the oceans, an accurate estimate for benthic denitrification is of vital importance for the set-up of a marine N budget. This study's denitrification estimate falls within the lower range of previously reported values and, if compared to reported sources and sinks of N in the oceans (e.g. Codispoti et al., 2001; Gruber, 2004), indicates a rather more balanced budget for the global marine N cycle than currently assumed. This work thus contributes to the discussion whether the marine N cycle is out of balance or stabilized by internal feedbacks.
The transfer function used to derive the global benthic denitrification estimate requires the organic carbon rain rate and bottom water chemistry only and can thus be dynamically coupled to global model approaches. Accordingly, the transfer function can provide a site-specific benthic feedback and improve the understanding of the benthic-pelagic coupling of biogeochemical cycles in the global ocean. Furthermore, benthic fluxes of total carbon, nitrogen and phosphorus have been observed to strongly deviate from Redfield composition but rather indicate acute N loss. This finding thus emphasizes the need to better describe C:N:P ratios in global biogeochemical models (Paulmier et al., 2009). Although Middelburg et al. (1996) already proposed a similar dependency of sedimentary denitrification and bottom water chemistry derived from a global model approach ('meta-model'), the empirically-based transfer function presented here should yield more robust results since it doesn't rely on water depth as an input parameter. Nevertheless, the meta-model by Middelburg et al. (1996) and the approach developed in his study yield very similar numbers when based on the same datasets, even though their estimate was derived using a sophisticated diagenetic model. This re-affirms the notion that benthic N loss is strongly dependent on the organic carbon rain rate and bottom water oxygen and nitrate concentrations.

The results described in Chapter 4 may help to improve knowledge on organic matter remineralization in the surface layer of marine sediments. Where organisms induce intense benthic reworking and mixing of the sediment, the common approaches to modeling organic matter remineralization based on organic matter reactivity and age are limited (e.g. Westrich and Berner, 1984; Middelburg, 1989).

Consequently, the depth distribution of organic matter degradation in such sediments is, to date, basically unknown. In contrast, the approach evolved here constrains the distribution of organic matter degradation rate using measured oxygen and nitrate fluxes only and is thus independent of the reactivity of organic carbon and bioturbation rates. Since the remineralization profile is controlled by the rain rate of organic carbon to the seafloor rather than bottom water redox conditions, this work enables the depth distribution of organic matter degradation to be estimated from organic carbon flux to the seafloor only. The results can be extrapolated to any other sedimentary regime where the organic carbon flux to the seafloor is known. In terms of diagenetic modeling, this finding provides an easy way to describe organic matter degradation in benthic reaction-transport models when key data are missing.

The reproduction of the mineralization profile suggested by the latter approach can also be expressed by a simple G model. However, the first-order rate constant k derived by this approach varied over several orders of magnitude. This finding emphasizes the difficulty of defining the correct values for k in G models from carbon concentration profiles only.

References

Bohlen L., Dale A. W., Sommer S., Mosch T., Hensen C., Noffke A., Scholz F. and Wallmann K. (2011) Benthic nitrogen cycling traversing the Peruvian oxygen minimum zone. *Geochim. Cosmochim. Ac.* **75**, 6094-6111.

Codispoti L. A., Brandes J. A., Christensen J. P., Devol A. H., Naqvi S. W. A., Paerl H. W. and Yoshinari T. (2001) The oceanic fixed nitrogen and nitrous oxide budgets: Moving targets as we enter the anthropocene? *Sci. Mar.* **65**, 85-105.

Dalsgaard T., Thamdrup B. and Canfield D. E. (2005) Anaerobic ammonium oxidation (anammox) in the marine environment. *Res. Microbiol.* **156**, 457-464.

Devol A. H. and Christensen J. P. (1993) Benthic Fluxes And Nitrogen Cycling In Sediments Of The Continental-Margin Of The Eastern North Pacific. *J. Mar. Res.* **51**, 345-372.

Gruber N. (2004) The dynamics of the marine nitrogen cycle and its influence on the atmospheric CO_2 variations. In *The Ocean Carbon Cycle and Climate* (eds. Follows M. and Oguz T.). NATO ASI Series. pp. 97-148.

Hamersley M. R., Lavik G., Woebken D., Rattray J. E., Lam P., Hopmans E. C., Damsté J. S. S., Krüger S., Graco M., Gutiérrez D., and Kuypers M. M. M. (2007) Anaerobic ammonium oxidation in the Peruvian oxygen minimum zone. *Limnol. Oceanogr.* **52**, 923-933.

Lam P. and Kuypers M. M. M. (2011) Microbial nitrogen cycling processes in oxygen minimum zones. *Annu. Rev. Mar. Sci.* **3**, 317-345.

Middelburg, J. J. (1989). A simple rate model for organic-matter decomposition in marine sediments. *Geochim. Cosmochim. Ac.* **53**, 1577-1581.

Middelburg J. J., Soetaert K., Herman P. M. J. and Heip C. H. R. (1996) Denitrification in marine sediments: A model study. *Global Biogeochem. Cy.* **10(4)**, 661-673.

Paulmier A., Kriest I and Oschlies A. (2009) Stoichiometries of remineralisation and denitrification in global

biogeochemical ocean models. *Biogeosciences* **6**, 923-935.

Westrich J. T. and Berner R. A. (1984) The Role Of Sedimentary Organic-Matter In Bacterial Sulfate Reduction - The G Model Tested. *Limnol. Oceanogr.* 29, 236-249.

Appendix A.

Supplementary Material to Chapter 2

A.1. Description of depth-dependent model parameters

Porosity was described using an exponential function assuming steady-state compaction:

$$\phi = \phi_L + (\phi_{(0)} - \phi_L) \exp(-\frac{x}{p_x}) \tag{A.1}$$

where $\phi_{(0)}$ is the porosity at the sediment-water interface, ϕ_L is the porosity below the depth of compaction and p_x (cm) is the porosity depth attenuation coefficient. These parameters were determined from the measured data at each station. The burial velocities of solids and solutes were described as:

$$w = \frac{u_f\,(1 - \phi_L)}{1 - \phi} \tag{A.2}$$

$$v = \frac{u_f\,\phi_L}{\phi} \tag{A.3}$$

where u_f corresponds to the sediment burial velocity at the depth of compaction. u_f was calculated by modeling measured excess ^{210}Pb profiles at stations 1, 3, 5 and 6, an example of which is shown in Fig. A.1 for stations 5 and 6. Burial velocities for stations 2 and 4 were estimated from adjacent stations since no excess ^{210}Pb data were available (Table A.2). Solute-specific diffusion coefficients in sediments were calculated from the temperature-dependent molecular diffusion coefficients in seawater (D_{SW}) (Boudreau, 1997) corrected for salinity and pressure using the Stokes-Einstein equation and tortuosity (Φ^2) (Boudreau, 1997):

$$D_S = \frac{D_{SW}}{\Phi^2} = \frac{D_{SW}}{1 - 2\ln(\phi)} \tag{A.4}$$

D_{SW} values for the dissolved gases O_2 and N_2 were calculated according to Hayduk and Laudie (1974). The decrease in bioturbation intensity with depth was described with a Gaussian-type function (Christensen, 1982):

$$D_B = D_{B(0)} \exp \frac{-x^2}{2x_s^2} \tag{A.5}$$

where $D_{B\,(0)}$ ($cm^2\ yr^{-1}$) is the bioturbation coefficient at the sediment-water interface and x_s (cm) is an effective mixing depth. For stations 1 to 4 within the OMZ, $D_{B(0)}$ was set to low values (0.05 $cm^2\ yr^{-1}$, Table A.2) since bioturbation here is probably of minor importance (Levin, 2003; Middelburg and Levin, 2009). At stations 5 and 6 with measurable bottom water O_2 concentrations, $D_{B(0)}$ and x_s were estimated by modeling of the measured ^{210}Pb profiles (Fig. A.1) applying Eq. 2.1 and appropriate boundary conditions (Meysman et al., 2005). Bioirrigation was neglected within the OMZ due to its low significance in anoxic environments (Middelburg and Levin, 2009). At stations 5 and 6, bioirrigation was indicated by observed fauna and burrows. Here bioirrigation was included in the model and defined in a similar way to Eq. (A.5):

$$\alpha_i = \alpha_{i\,(0)} \exp \frac{-x^2}{2x_i^2} \tag{A.6}$$

where $\alpha_{i\,(0)}$ (yr^{-1}) is the irrigation coefficient at the sediment-water interface and x_i (cm) controls the depth where irrigations approaches zero. The same irrigation coefficient and depth were applied to all solutes. Since no measurements of bioirrigation were available, $\alpha_{i\,(0)}$ was set to 100 yr^{-1} to be of the same order of magnitude as reported in previous studies (Burdige, 2006). The parameter x_i was maintained at low values since the porewater data do not indicate intense irrigation of surface layers. Since *Thioploca* and *Beggiatoa* filaments can penetrate several centimeters into the sediment down to the sulfidic layers (Jørgensen and Gallardo, 1999), the transport of $NO_3^-{}_{bac}$ and $NO_2^-{}_{bac}$ was described using a pseudo-irrigation formulation (Dale et al., 2009; 2011). The depth-dependency of the non-local transport coefficient α_b was described as:

$$\alpha_b = \alpha_{b\,0} \exp \frac{-x^2}{2x_b^2} \tag{A.7}$$

where $\alpha_{b\,(0)}$ (yr^{-1}) is the non-local transport coefficient at the sediment-water interface and x_b (cm) is

an adjustable parameter that controls the depth to which the process occurs. Values for $\alpha_{b\,(0)}$ and x_b were adjusted to fit the TA and SO_4^{2-} profiles and the DIN fluxes.

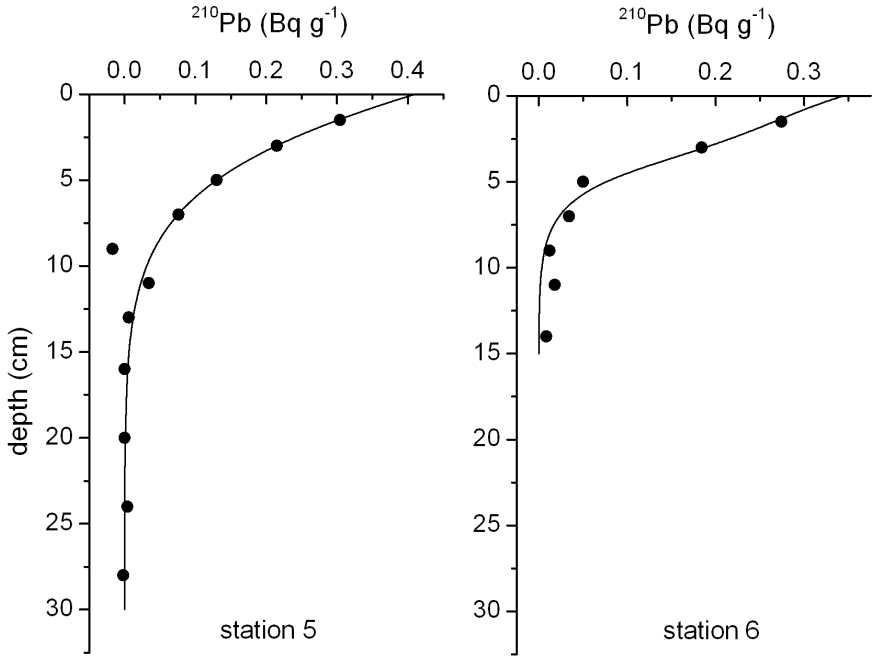

Figure A.1.: Excess ^{210}Pb concentration profiles in sediments at station 5 and 6. Lines denote best model fits to the data.

Table A.1.: Model parameters which are invariable across the transect (L: based on literature values, M: constrained with the model).

Parameter	Description	Value	Unit	Source
ds	Density of dry solids	2.0	g cm^{-3}	L [a]
x_s	Effective mixing depth for bioturbation	2	cm	M
K_1	Half–saturation constant for O_2	1	µM	L [b]
K_4	Half–saturation constant for FeOOH	0.028	wt–%	L [b]
k_6	Rate constant for aerobic oxidation of NH_4^+	1.5×10^7	M^{-1} yr^{-1}	L [b,c]
k_7	Rate constant for aerobic oxidation of NO_2^-	1.5×10^7	M^{-1} yr^{-1}	L [b,c]
k_{11}	Rate constant for NH_4^+ adsorption	0.1	M^{-1} yr^{-1}	M
k_{12}	Rate constant for aerobic oxidation of Fe^{2+}	2×10^9	M^{-1} yr^{-1}	L [b,c]
k_{13}	Rate constant for aerobic oxidation of TH_2S	6×10^8	M^{-1} yr^{-1}	L [b,c]
k_{14}	Rate constant for anaerobic oxidation of Fe^{2+}	1.5×10^5	M^{-1} yr^{-1}	L [d]
k_{fit}	Kinetic constant for ammonification	10^9	yr^{-1}	M
K_{NH4}	Equilibrium constant for NH_4^+ adsorption	1.6	cm^3_{pw} g^{-1}	L [e,f]

(a) Böning et al. (2004)
(b) Van Cappellen and Wang (1995)
(c) Boudreau (1996)
(d) Dhakar and Burdige (1996)
(e) Mackin and Aller (1984)
(f) Berg et al. (2003)

Table A.2.: Model parameters which vary across the transect (L: based on literature values, M: constrained with the model, I: independently determined from site specific data).

Parameter	Description	station 1	station 2	station 3	station 4	station 5	station 6	unit	source
T	Bottom water temperature	12.7	11.7	11.4	8.3	6.4	4.7	°C	I
u_f	Burial velocity of compacted sediment [a]	0.3	0.06	0.05	0.05	0.08	0.052	cm yr^{-1}	I
φ_0	Porosity at x = 0	0.93	0.955	0.95	0.95	0.84	0.78	1	I
φ_L	Porosity at x = L	0.8	0.89	0.85	0.63	0.71	0.67	1	I
p_x	Porosity depth attenuation coefficient	12.5	6.7	16.7	33.3	10	4	cm	I
$D_{B(0)}$	Bioturbation coefficient at x = 0 [b]	0.05	0.05	0.05	0.05	0.05	0.3	cm^2 yr^{-1}	I
$\alpha_{i(0)}$	Bioirrigation coefficient at x = 0	0	0	0	0	100	100	yr^{-1}	M
x_i	Bioirrigation exchange parameter	–	–	–	–	0.6	0.95	cm	M
$\alpha_{b(0)}$	Coefficient for bacterial NO_3^- (NO_2^-) transport at x=0	400 (12000)	1300	1700	1000	–	–	yr^{-1}	M
x_b	NO_3^- (NO_2^-) exchange parameter	0.58 (0.33)	0.69	0.23	0.44	–	–	cm	M
K_2	Half–saturation constant for NO_3^-	15	30	30	15	20	20	µM	M, L[c,d]
K_3	Half–saturation constant for NO_2^-	10	8	4	1	2	1	µM	M, L[c,d]
k_8	Rate constant for anammox	0	0	0	3×10^9	4×10^9	1.6×10^{10}	M^{-1} yr^{-1}	M
k_9	Rate constant for DNRA with NO_3^-	1.2×10^{14}	1×10^{15}	1.1×10^{13}	8.9×10^{13}	0	0	M^{-1} yr^{-1}	M
k_{10}	Rate constant for DNRA with NO_2^-	7×10^{15}	–	–	–	–	–	M^{-1} yr^{-1}	M
r_{NC}	molar N:C ratio in POM [e]	0.11	0.096	0.11	0.11	0.1	0.092	mol N (mol C)$^{-1}$	I

(a) Calculated from excess ^{210}Pb profiles. At stations 2 and 4 values have been estimated since no excess ^{210}Pb data were available.
(b) Set to low values (0.05 cm^2 yr^{-1}) for stations 1 to 4 and calculated from excess ^{210}Pb profiles for stations 5 and 6. At station 5 no indication of bioturbation was observed and the value was set to a similar value as station 1 to 4.
(c) Van Cappellen and Wang (1995)
(d) Rabouille and Gaillard (1991)
(e) Calculated from measured POC and PON concentrations in the upper sediment layer

A.2. Fe^{2+} and TH_2S precipitation and sulfide budget

Solid phase iron and sulfur precipitation rates were determined using an inverse modeling procedure. Firstly, Fe and TH_2S concentrations were simulated in a similar to NH_4^+ (Eq. 2.3, 2.4) by approximating the measured profiles with a fitting function. The sum of reactions involving Fe and TH_2S, $\sum$RFe(x) and $\sum$RTH_2S(x), respectively, are then given by:

$$\sum \mathrm{RFe(x)} = +4 \times \mathrm{R_4(x)} - \mathrm{R_{12}(x)} - \mathrm{R_{14}(x)} - \mathrm{R_{Feprec\ (x)}} \tag{A.8}$$

and

$$\sum \mathrm{RTH_2S(x)} = +0.5 \times \mathrm{R_5(x)} \text{ - } \mathrm{R_{13}(x)} \text{ - } \mathrm{R_9(x)}\ (-\mathrm{R_{10}(x)}) \text{ - } \mathrm{R_{TH2Sprec}(x)} \tag{A.9}$$

where $R_{Feprec}(x)$ denotes combined FeS and FeS_2 precipitation and $R_{TH2Sprec}$ represents TH_2S precipitation into iron and/or organic minerals. The fitting procedure is then expressed by:

$$\sum \mathrm{RFe(x)} = \mathrm{k_{Fefit}} \times (\mathrm{Fe_{OBS}(x)} \text{ - } \mathrm{Fe(x)}) \tag{A.10}$$

and

$$\sum \mathrm{RTH_2S(x)} = \mathrm{k_{TH2Sfit}} \times (\mathrm{TH_2S_{OBS}(x)} \text{ - } \mathrm{TH_2S(x)}) \tag{A.11}$$

where $TH_2S_{OBS}(x)$ and $Fe_{OBS}(x)$ are the respective measured concentrations at a specific depth x (cm) and Fe(x) and $TH_2S(x)$ are the modeled concentrations, respectively. k_{Fefit} and $k_{TH2Sfit}$ (yr^{-1}) are kinetic constants with a high value to ensure that the modeled concentrations were maintained close to the measured values. This procedure was used to calculate a sulfide budget (Table A.3) which shows that DNRA is the main consumer of TH_2S on the shelf and upper slope while at the deeper station all TH_2S was precipitated.

Table A.3.: Sulfide budget in surface sediments of the Peruvian OMZ (mmol S m^{-2} d^{-1}). Numbers in parenthesis denote percentage of total TH_2S consumption. Diffusion from sulfidic deeper layers and TH_2S burial were negligible.

Process	Station 1	Station 2	Station 3	Station 4	Station 5	Station 6
TH_2S production (R_5)	3.27	3.09	1.69	0.95	0.41	0.55
TH_2S oxidation (by DNRA)	2.32 (70.7%)	2.93 (94.8%)	1.38 (81.7%)	0.48 (50.5%)	0 (0%)	0 (0%)
TH_2S precipitation	0.96 (29.3%)	0.16 (5.2%)	0.31 (18.3%)	0.47 (49.5%)	0.41 (100%)	0.55 (100%)

References

Berg P., Rysgaard S. and Thamdrup B. (2003) Dynamic modeling of early diagenesis and nutrient cycling. A case study in an Arctic marine sediment. *Am. J. Sci.* **303**, 905-955.

Boudreau B. P. (1996) A method-of-lines code for carbon and nutrient diagenesis in aquatic sediments. *Comput. Geosci.* **22**, 479-496.

Boudreau B. P. (1997) Diagenetic Models and Their Implementation. Springer-Verlag.

Böning P., Brumsack H.-J., Böttcher M. E., Schnetger B., Kriete C., Kallmeyer J. and Borchers S. L. (2004) Geochemistry of Peruvian near-surface sediments. *Geochim. Cosmochim. Acta* **68**, 4429-4451.

Burdige, D. (2006). Geochemistry of Marine Sediments. Princeton University Press, Princeton, New Jersey.

Christensen E. R. (1982) A Model For Radionuclides In Sediments Influenced By Mixing And Compaction. *J. Geophys. Res.-Oc. Atm.* **87**, 566-572.

Dale A. W., Brüchert V., Alperin M. and Regnier P. (2009) An integrated sulfur isotope model for Namibian shelf sediments. *Geochim. Cosmochim. Acta* **73**, 1924-1944.

Dale A. W., Sommer S., Bohlen L., Treude T., Bertics V. J., Bange H. W., Pfannkuche O., Schorp T., Mattsdotter M. and Wallmann K. (2011) Rates and regulation of nitrogen cycling in seasonally-hypoxic sediments during winter (Boknis Eck, SW Baltic Sea): sensitivity to environmental variables. *Estuar. Coast. Shelf Sci.* **95**, 14-28.

Dhakar S. P. and Burdige D. J. (1996) Coupled, non-linear, steady state model for early diagenetic processes in pelagic sediments. *Am. J. Sci.* **296**, 296-330.

Hayduk W. and Laudie H. (1974) Prediction Of Diffusion-Coefficients For Nonelectrolytes In Dilute Aqueous-Solutions. *Aiche J.* **20**, 611-615.

Jørgensen B. B. and Gallardo V. A. (1999) Thioploca spp: filamentous sulfur bacteria with nitrate vacuoles. *Fems Microbiol. Ecol.* **28**, 301-313.

Levin L. (2003) Oxygen minimum zone benthos: Adaptation and community response to hypoxia. *Oceanogr. Mar. Biol.* **41**, 1-45.

Mackin J. E. and Aller R. C. (1984) Ammonium Adsorption In Marine-Sediments. *Limnol. Oceanogr.* **29**, 250-257.

Meysman, F. J. R., Boudreau, B. P., and Middelburg, J. J. (2005) Modeling reactive transport in sediments subject to bioturbation and compaction. *Geochim. Cosmochim. Acta* **69**, 3601-3617.

Middelburg J. J. and Levin L. A. (2009) Coastal hypoxia and sediment biogeochemistry. *Biogeosciences* **6**, 1273-1293.

Rabouille C. and Gaillard J. F. (1991) Towards The Edge - Early Diagenetic Global Explanation - A Model Depicting The Early Diagenesis Of Organic-Matter, O_2, NO_3, Mn, And PO_4. *Geochim. Cosmochim. Acta* **55**, 2511-2525.

Van Cappellen P. and Wang Y. (1995) Metal cycling in surface sediments: Modeling the interplay of transport and reaction. In *Metal contaminated aquatic sediments* (ed. Allen, H.E.). Ann Arbor Press. pp. 21-64.

Appendix B.

Supplementary Material to Chapter 3

Table B.1.: Database used for the derivation of the transfer function (see text for details) including water depth, method used to calculate the benthic fluxes, number of stations (n) where fluxes (J) were determined and details on POC fluxes.

Location	Water depth (m)	Method	J_{NO3}	J_{NH4}	Carbon flux [a]	Reference
Galveston Bay	2.5	lander	n = 1	n = 0	RPOC	*Warnken et al.* (2008)
Port Philip Bay	7–24	lander	n = 6	n = 6	RPOC	*Berelson et al.* (1998)
Gulf of Cádiz	8–34	lander	n = 5	n = 5	RPOC	*Ferrón et al.* (2009)
Adriatic sea	10–42	lander	n = 5	n = 5	RPOC	*Hammond et al.* (1999)
Mid–Atlantic Bight	11–15	lander	n = 17	n = 15	RPOC	*Laursen and Seitzinger* (2002)
Western Arctic shelf	11–48	lander	n = 10	n = 10	RPOC	*Devol et al.* (1997)
Santa Monica Bay	50–65	lander	n = 6	n = 6	RPOC	*Lehmann et al.* (2004)
Goban Spur	50–4468	lander	n = 5	n = 0	RPOC	*Lohse et al.* (1998)
San Pedro shelf	63–64	lander	n = 2	n = 2	RPOC	*Berelson et al.* (2002)
Washington continental margin	85–630	lander	n = 14	n = 14	RPOC	*Devol and Christensen* (1993)
Peruvian shelf/slope	85–1000	lander	n = 6	n = 6	RPOC	*Sommer et al.* (submitted to *Global Biogeochem. Cy.*)
Monterey Bay	95–100	lander	n = 5	n = 5	RPOC	*Berelson et al.* (2003)
Northwest Mexico & Washington margin	100–3065	lander	n = 14	n = 14	RPOC	*Hartnett and Devol* (2003)
Central and south California	231–3707	lander	n = 14	n = 14	RPOC	*Berelson et al.* (1996)
Adriatic and Northern Ionian Sea	246–2360	lander	n = 6	n = 0	RPOC	*Giordani et al.* (2002)
North Carolina slope	607–2927	lander	n = 13	n = 13	RPOC	*Jahnke and Jahnke* (2000)
Central California	781–4076	lander	n = 5	n = 0	RPOC	*Reimers et al.* (1992)
Santa Monica Basin	908	lander	n = 1	n = 0	RPOC	*Jahnke* (1990)
Eastern Indonesia	3072	profiles	n = 1	n = 0	RPOC	*Helder* (1989)
Southern Ocean	3073–5078	profiles	n = 7 [b]	n = 0	RPOC[c]	Supplement to *Smetacek et al.* (1997) [d]
Deep sea suboxic sediments	3116–4980	profiles	n = 20	n = 0	RPOC [c], RRPOC [e]	*Goloway and Bender* (1982), *Emerson et al.* (1985)
Arabian Sea	3188–4041	profiles	n = 7	n = 0	RPOC [c]	*Grandel et al.* (2000), *Witte and Pfannkuche* (2000)
Equatorial Pacific	3300–4500	lander	n = 5	n = 5	RPOC	*Hammond et al.* (1996)
Eastern Tropical Atlantic	3860–5036	profiles	n = 2 [b]	n = 0	RPOC [c]	Supplement to *Jahnke et al.* (1989) [e]
Porcupine Abyssal Plain	4802–4842	lander	n = 3	n = 2	RPOC	*Brunnegård et al.* (2004), *Ståhl et al*. (2004)
Total			n = 180	n = 122		

[a] RPOC = RPOC available, RRPOC calculated using Eq. (1) and (2), RRPOC = RRPOC from literature data. RPOC calculated using Eq. (1) and (2).
[b] Diffusive flux calculated in this study from the published data using temperature– and tortuosity–corrected diffusion coefficients
[c] Estimated as total oxygen uptake
[d] Data available in PANGAEA: doi:10.1594/PANGAEA.728865
[e] Data available in PANGAEA: doi:10.1594/PANGAEA.140267

References

Berelson W. M., McManus J., Coale K. H., Johnson K. S., Kilgore T., Burdige D. and Pilskaln C. (1996) Biogenic matter diagenesis on the sea floor: A comparison between two continental margin transects. *J. Mar. Res.* **54(4)**, 731-762.

Berelson W. M., Heggie D., Longmore A., Kilgore T., Nicholson G. and Skyring G. (1998) Benthic nutrient recycling in Port Phillip Bay, Australia. *Estuar. Coast. Shelf S.* **46(6)**, 917-934.

Berelson W. M., Johnson K., Coale K. and Li H. C. (2002) Organic matter diagenesis in the sediments of the San Pedro Shelf along a transect affected by sewage effluent. *Cont. Shelf Res.* **22(6-7)**, 1101-1115.

Berelson W. M., McManus J., Coale K., Johnson K., Burdige D., Kilgore T., Colodner D., Chavez F., Kudela R. and Boucher J. (2003) A time series of benthic flux measurements from Monterey Bay, CA. *Cont. Shelf Res.* **23(5)**, 457-481.

Brunnegård J., Grandel S., Stahl H., Tengberg A. and Hall P. O. J.(2004) Nitrogen cycling in deep-sea sediments of the Porcupine Abyssal Plain, NE Atlantic. *Prog. Oceanogr.* **63(4)**, 159-181.

Devol A. H. and Christensen J. P. (1993) Benthic Fluxes And Nitrogen Cycling In Sediments Of The Continental-Margin Of The Eastern North Pacific. *J. Mar. Res.* **51(2)**, 345-372.

Devol A. H., Codispoti L. A. and Christensen J. P. (1997) Summer and winter denitrification rates in western arctic shelf sediments. *Cont. Shelf Res.* **17(9)**, 1029-1050.

Emerson S., Fischer K., Reimers C. and Heggie D. (1985) Organic carbon dynamics and preservation in deep-sea sediments. *Deep-Sea Res.* **32(1)**, 1-21.

Ferrón S., Alonso-Pérez F., Anfuso E., Murillo F. J., Ortega T., Castro C. G. and Forja J. M. (2009) Benthic nutrient recycling on the northeastern shelf of the Gulf of Cadiz (SW Iberian Peninsula). *Mar. Ecol.-Prog. Ser.* **390**, 79-95.

Giordani P., Helder W., Koning E., Miserocchi S., Danovaro R. and Malaguti A. (2002) Gradients of benthic-pelagic coupling and carbon budgets in the Adriatic and Northern Ionian Sea. *J. Mar. Syst.* **33**, 365-387.

Goloway F. and Bender M. (1982) Diagenetic models of interstitial nitrate profiles in deep sea suboxic sediments. *Limnol. Oceanogr.* **27(4)**, 624-638.

Grandel S., Rickert D., Schlüter M. and Wallmann K. (2000) Pore-water distribution and quantification of diffusive benthic fluxes of silicic acid, nitrate and phosphate in surface sediments of the deep Arabian Sea. *Deep-Sea Res. Pt. II* **47(14)**, 2707-2734.

Hammond D. E., McManus J., Berelson W. M., Kilgore T. E. and Pope R. H. (1996) Early diagenesis of organic material in equatorial pacific sediments: Stoichiometry and kinetics. *Deep-Sea Res. Pt. II* **43(4-6)**, 1365-1412.

Hammond D. E., Giordani P., Berelson W. M. and Poletti R. (1999) Diagenesis of carbon and nutrients and benthic exchange in sediments of the northern Adriatic Sea. *Mar. Chem.* **66(1-2)**, 53-79.

Hartnett H. E. and Devol A. H. (2003) Role of a strong oxygen-deficient zone in the preservation and degradation of organic matter: A carbon budget for the continental margins of northwest Mexico and Washington State. *Geochim. Cosmochim. Ac.* **67**, 247-264.

Helder W. (1989) Early diagenesis and sediment-water exchange in the Savu Basin (eastern Indonesia). *Neth. J. Sea Res.* **24(4)**, 555-572.

Jahnke R. A. (1990) Early diagenesis and recycling of biogenic debris at the sea-floor, Santa-Monica basin, California. *J. Mar. Res.* **48(2)**, 413-436.

Jahnke R. A. and Jahnke D. B. (2000) Rates of C, N, P and Si recycling and denitrification at the US mid-atlantic continental slope depocenter. *Deep-Sea Res. Pt. I* **47(8)**, 1405-1428.

Jahnke R. A., Emerson S., Reimers C., Schuffert J., Ruttenberg K. and Archer D. (1989) Benthic recycling of biogenic debris in the eastern tropical Atlantic ocean. *Geochim. Cosmochim. Ac.* **53(11)**, 2947-2960.

Laursen A. E. and Seitzinger S. P. (2002) The role of denitrification in nitrogen removal and carbon mineralization in mid-atlantic bight sediments. *Cont. Shelf Res.* **22(9)**, 1397-1416.

Lehmann M. F., Sigman D. M. and Berelson W. M. (2004) Coupling the N-15/N-14 and O-18/O-16 of nitrate as a constraint on benthic nitrogen cycling. *Mar. Chem.* **88(1-2)**, 1-20.

Lohse L., Helder W., Epping E. H. G. and Balzer W. (1998) Recycling of organic matter along a shelf-slope transect across the NW european continental margin (Goban Spur). *Progr. Oceanogr.* **42(1-4)**, 77-110.

Reimers C. E., Jahnke R. A. and McCorkle D. C. (1992) Carbon fluxes and burial rates over the continental slope and rise off central California with implications for the global carbon cycle. *Global Biogeochem. Cy.* **6(2)**, 199-224.

Smetacek V., De Baar H. J. W., Bathmann U. V., Lochte K. and Rutgers Van Der Loeff M. M. (1997) Ecology and biogeochemistry of the Antarctic circumpolar current during austral spring: a summary of southern ocean JGOFS cruise ANT X/6 of R.V. Polarstern. *Deep-Sea Res. Pt. II* **44(1-2)**, 1-21.

Ståhl H., Tengberg A., Brunnegård J. and Hall P. O. J. (2004) Recycling and burial of organic carbon in sediments of the Porcupine Abyssal Plain, NE Atlantic. *Deep-Sea Res. Pt. I* **51(6)**, 777-791.

Warnken K. W., Santschi P. H., Roberts K. A. and Gill G. A. (2008) The cycling and oxidation pathways of organic carbon in a shallow estuary along the Texas gulf coast. *Estuar. Coast. Shelf S.* **76(1)**, 69-84.

Witte U. and Pfannkuche O. (2000) High rates of benthic carbon remineralisation in the abyssal Arabian Sea. *Deep-Sea Res. Pt. II* **47(14)**, 2785-28.

Appendix C.

Supplementary Material to Chapter 4

Table C.1.: Overview of all stations optimized for the depth-distribution of organic matter remineralization. Empty cells denote stations have been omitted from further analysis (see Chapter 4). Stars indicate stations where porewater profile are available. For references see Appendix B.

identifier	depth (m)	bw_{O2} (µM)	bw_{NO3} (µM)	measured J_{NO3} (mmol m^{-2} d^{-1})	measured J_{O2} (mmol m^{-2} d^{-1})	RPOC (mmol m^{-2} d^{-1})	RRPOC (mmol m^{-2} d^{-1})	RPOC(0) mmol cm^{-3} yr^{-1}	B (cm^{-1})	k_8 (10^9 M^{-1} yr^{-1})	x_{irr} (cm)	modeled J_{NO3} (mmol m^{-2} d^{-1})	modeled J_{O2} (mmol m^{-2} d^{-1})
Berelson et al. (1996)-Cat	1300	19	42	-0.32 (±0.05)	-0.46 (±0.12)	1.20	1.67	0.024	0.44	20.0	off	-0.32	-0.38
Berelson et al. (1996)-CCI-5	532	48	36	-1.17 (±0.31)	-3.08 (±0.46)	3.80	5.62	0.870	5.02	723.2	0.8	-1.12	-2.59
Berelson et al. (1996)-CCI-6	231	77	32	-0.89 (±0.19)	-4.44 (±1.56)	6.00	9.11	0.387	1.41	438.6	1.2	-0.89	-3.30
Berelson et al. (1996)-CCI-7	638	16	40	-1.20 (±0.08)	-2.22 (±0.32)	1.80	2.56	0.390	4.74	831.5	1.5	-0.89	-0.77
Berelson et al. (1996)-CCII-2	670	18	40	-0.71 (±0.05)	-0.57 (±0.08)	1.10	1.53	0.158	3.15	466.4	0.9	-0.53	-0.53
Berelson et al. (1996)-CCII-3	1010	24	43	-0.44 (±0.02)	-0.94 (±0.13)	0.90	1.24	0.031	0.75	646.4	1.8	-0.43	-0.45
Berelson et al. (1996)-CCII-4	2025	80	40	-0.15 (±0.02)	-1.05 (±0.13)	1.10	1.12	0.004	0.08	72.0	2.2	-0.15	-0.71
Berelson et al. (1996)-CCII-5	3375	113	42	-0.12 (±0.02)	-1.71 (±0.25)	0.70	0.71	0.030	0.94	411.7	off	-0.12	-0.68
Berelson et al. (1996)-CCII-6	1358	47	44	-0.62 (±0.04)	-1.43 (±0.29)	1.80	2.56	0.066	0.81	652.3	2.4	-0.62	-1.05
Berelson et al. (1996)-PE	3707	131	40	-0.02 (±0.02)	-0.63 (±0.25)	0.40	0.41	0.007	0.40	3.4	2.0	-0.02	-0.45
Berelson et al. (1996)-SCI	2053	58	43	-0.10 (±0.02)	-0.73 (±0.26)	1.10	1.12	0.004	0.08	0.2	1.8	-0.13	-0.70
Berelson et al. (1996)-SM	905	5	37	-0.91 (±0.09)	N/A	1.70	2.41	0.243	3.13	503.0	off	-0.91	-0.25
Berelson et al. (1996)-SP	896	8	39	-1.13 (±0.16)	N/A	1.80	2.56	0.475	5.78	543.8	off	-1.08	-0.49
Berelson et al. (1996)-TB	1514	25	43	-0.51 (±0.05)	-0.99 (±0.21)	0.90	1.24	0.022	0.53	627.6	2.5	-0.43	-0.48
Berelson et al. (1998)-11	17	225	0	0.02 (±0.01)	-29 (±5)	28.00	47.42	12.829	10.67	0.0	3.5	-0.03	-29.20
Berelson et al. (1998)-13	20	225	0	0.06 (±0.02)	-25 (±4)	26.00	43.77	9.535	8.54	0.1	3.4	-0.02	-26.48
Berelson et al. (1998)-19	12	225	0	0.11 (±0.02)	-27 (±4)	27.00	45.59	9.574	8.26	0.1	3.2	0.09	-27.00
Berelson et al. (1998)-3	7	225	0	0.01 (±0.01)	-30 (±5)	28.00	47.42	16.048	13.35	0.8	2.9	-0.07	-30.19
Berelson et al. (1998)-37	24	225	0	0.12 (±0.04)	-23 (±4.5)	21.00	34.76	9.460	10.49	0.6	2.6	0.05	-23.23
Berelson et al. (1998)-8	8	225	0	0.08 (±0.08)	-27 (±4)	25.00	41.95	14.109	13.14	1.0	3.3	-0.05	-27.43
Berelson et al. (2002)-2	63	166	11	-0.70 (±0.2)	-20 (±2)	27.00	45.59	6.177	5.33	0.5	0.2	-0.87	-18.46
Berelson et al. (2002)-3	64	175	11	-0.50 (±0.1)	-23 (±2)	23.00	38.34						
Berelson et al. (2003)-CC3*	95-100	153	15	-0.68 (±0.05)	-12.1 (±1.5)	11.50	18.22	5.954	12.06	15.2	1.4	-0.67	-12.22
Berelson et al. (2003)-TS1 *	95-100	101	30	-0.89 (±0.16)	-6.21 (±0.74)	9.25	14.44	0.508	1.28	86.0	0.5	-0.89	-5.01
Berelson et al. (2003)-TS2 *	95-100	135	22	-1.20 (±0.27)	-10.6 (±0.88)	11.50	18.22	5.664	11.47	270.7	1.6	-1.20	-11.64
Berelson et al. (2003)-TS3 *	95-100	185	15	0.21 (±0.09)	-8.14 (±1.47)	6.00	9.11	2.434	9.45	0.1	3.0	0.04	-7.05
Berelson et al. (2003)-TS4 *	95-100	133	25	-0.07 (±0.22)	-5.95 (±0.78)	6.70	10.25	0.029	0.10	0.3	0.3	-0.14	-4.53
Brunnegård et al. (2004)-12926#2/B	4802	230	22	0.04 (±0.01)	N/A	0.86	0.88	0.224	5.71	23.0	1.2	0.04	-1.08
Brunnegård et al. (2004)-54901#10/D	4842	230	22	0.03 (±0.01)	N/A	0.52	0.53	0.094	3.98	51.0	3.4	0.03	-0.66
Brunnegård et al. (2004)-54901#3/D	4841	230	22	0.02 (±0.01)	N/A	0.38	0.39	0.012	0.71	517.0	0.8	0.02	-0.48
Devol and Christensen(1993)-NH01	115	100	19	-1.20 (±0.07)	-10.6 (±0.8)	16.57	26.93	2.533	3.56	85.0	0.3	-1.19	-8.72
Devol and Christensen(1993)-NH02	161	113	39	-1.11 (±0.08)	-10.3 (±1.1)	16.35	26.56	3.195	4.55	30.1	0.9	-2.10	-10.28
Devol and Christensen(1993)-NH03	85	86	27	-1.33 (±0.21)	-6.57 (±0.6)	20.68	34.19	0.941	1.06	635.0	0.6	-1.29	-6.34
Devol and Christensen(1993)-NH07	225	104	39	-0.71 (±0.15)	-4.88 (±0.13)	15.80	25.60	0.074	0.10	19.0	1.8	-0.69	-3.92
Devol and Christensen(1993)-NH10	465	47	41	-0.70 (±0.10)	-2.55 (±0.65)	6.02	9.14	0.024	0.09	121.0	2.7	-0.68	-1.22
Devol and Christensen(1993)-NH12	630	38	43	-0.69 (±0.07)	-2.16 (±0.09)	4.37	6.51	0.087	0.43	278.4	0.7	-0.70	-1.29
Devol and Christensen(1993)-NH14A *	114	127	19	-1.64	-18.3	26.42	44.53	10.433	9.20	0.7	0.6	-1.86	-18.24
Devol and Christensen(1993)-NH17	124	112	19	-1.60 (±0.38)	-14.4(±0.91)	24.21	40.53	3.940	3.79	421.0	1.3	-1.63	-12.40
Devol and Christensen(1993)-NH18 *	146	106	22	-1.46 (±0.52)	-14.6 (±1.99)	21.10	34.94	7.928	8.75	0.7	0.2	-1.88	-14.02
Devol and Christensen(1993)-WE101A	106	78	19	-0.86	-5.27	21.60	35.83	0.533	0.57	557.0	0.6	-0.82	-5.38
Devol and Christensen(1993)-WE103	140	68	22	-0.82 (±0.02)	-14.6 (±1.34)	21.63	35.89						
Devol and Christensen(1993)-WE104	137	109	21	-1.12 (±082)	-8.94 (±0.39)	19.83	32.67	2.060	2.42	712.8	0.9	-1.31	-9.15
Devol and Christensen(1993)-WE105	323	58	36	-0.77 (±0.06)	-2.51	6.47	9.87	0.189	0.64	947.0	0.3	-0.76	-2.33
Devol and Christensen(1993)-WE107	239	108	34	-1.49 (±0.06)	-9.29 (±0.30)	16.70	27.16	1.463	1.92	687.0	1.4	-1.64	-7.53

Table C.1.: Continued.

identifier	depth (m)	bw_{O2} (µM)	bw_{NO3} (µM)	measured J_{NO3} (mmol m^{-2} d^{-1})	measured J_{O2} (mmol m^{-2} d^{-1})	RPOC (mmol m^{-2} d^{-1})	RRPOC (mmol m^{-2} d^{-1})	RPOC(0) mmol cm^{-3} yr^{-1}	B (cm^{-1})	k_8 (10^9 M^{-1} yr^{-1})	x_{irr} (cm)	modeled J_{NO3} (mmol m^{-2} d^{-1})	modeled J_{O2} (mmol m^{-2} d^{-1})
Devol et al. (1997)-1	11	270	10	0.25 (±0.35)	-8.6 (±1.32)	6.58	10.05	1.649	5.84	0.2	3.0	0.25	-8.12
Devol et al. (1997)-2	11	270	10	0.08 (±0.01)	-14.4 (±0.55)	11.07	17.49	4.871	10.25	4.0	1.8	-0.01	-12.89
Devol et al. (1997)-3	14	285	10	0.09 (±0.09)	-5.1 (±0.55)	3.90	5.78	0.765	4.57	24.0	1.8	0.09	-4.76
Devol et al. (1997)-A *	35	329	3	-0.09 (±0.02)	-16.3 (±3.75)	17.90	29.27	1.922	2.50	187.0	1.4	-0.10	-16.30
Devol et al. (1997)-B *	48	327	3	-0.15	-18	19.55	32.18	2.562	3.05	953.1	1.8	-0.16	-17.99
Devol et al. (1997)-C *	12	317	0	0.00 (±0)	-13.2 (±2)	13.00	20.77	3.483	6.24	956.0	0.2	0.00	-14.78
Devol et al. (1997)-D *	11	316	0	0.10 (±0.05)	-10.7 (±0.15)	13.30	21.28	7.921	13.87	38.0	3.0	0.08	-15.39
Devol et al. (1997)-F	14	316	0	0.07 (±0.07)	-11.7 (±2.35)	13.60	21.80	5.539	9.48	359.3	0.2	0.08	-15.85
Devol et al. (1997)-H *	41	322	1	0.12 (±0.01)	-7.4 (±0.9)	12.35	19.66	0.101	0.19	1.4	3.4	0.11	-7.21
Devol et al. (1997)-I *	11	252	0	0.14 (±0.05)	-8 (±0.5)	10.45	16.44	0.583	1.30	0.0	0.1	0.14	-10.09
Ferrón et al. (2009)-BC1	8	230	5	0.55 (±0.14)	N/A	17.90	29.27						
Ferrón et al. (2009)-BC2	18	230	5	0.38 (±0.07)	N/A	23.10	38.52						
Ferrón et al. (2009)-BC3	22	220	2	0.25 (±0.05)	N/A	18.40	30.15						
Ferrón et al. (2009)-BC4	32	230	3	-0.13 (±0.09)	N/A	24.20	40.50						
Ferrón et al. (2009)-BC5	13	220	2	0.29 (±0.19)	N/A	28.90	49.08						
Giordani et al. (2002)-A1Aug *	1196	196	6	0.04 (±0.02)	N/A	1.75	2.49	0.120	1.50	1.1	0.3	0.06	-2.17
Giordani et al. (2002)-A1Mar *	1196	196	6	0.07	N/A	1.32	1.85	0.066	1.10	0.8	0.1	0.06	-1.66
Giordani et al. (2002)-I1Mar *	2360	198-201	6	0.01 (±0.02)	N/A	0.65	0.66	0.019	0.65	307.8	0.4	0.01	-0.80
Giordani et al. (2002)-O2Aug *	870	195-205	7	0.00 (±0.00)	N/A	4.41	6.58	0.016	0.08	2.6	2.6	0.00	-3.26
Giordani et al. (2002)-O2Mar *	870	195-206	7	0.10 (±0.02)	N/A	1.44	2.03	0.066	1.00	0.2	1.0	0.06	-1.79
Giordani et al. (2002)-P1*	246	169-215	6	0.49 (±0.32)	N/A	3.31	4.86	0.008	0.05	0.1	1.4	0.12	-3.15
Goloway and Bender (1982)-10GC1 *	4956	250	21	0.04	-0.66	0.66	0.67	0.148	4.93	33.0	off	0.04	-0.84
Goloway and Bender (1982)-11TW1 *	4980	250	21	0.09	-1.4	1.40	1.42	0.086	1.35	7.5	off	0.06	-1.76
Goloway and Bender (1982)-12GC2 *	3880	250	21	0.04	-0.36	0.36	0.36	0.011	0.70	105.0	off	0.04	-0.48
Goloway and Bender (1982)-14GC1 *	4170	250	21	0.08	-1.12	1.12	1.14	0.077	1.50	20.9	off	0.08	-1.45
Goloway and Bender (1982)-16GC1 *	3310	250	21	0.06	-0.66	0.66	0.67	0.070	2.32	19.0	off	0.06	-0.87
Goloway and Bender (1982)-23GC1 *	4901	250	21	0.10	-1.4	1.40	1.42	0.278	4.36	5.8	off	0.09	-1.80
Goloway and Bender (1982)-5GC1 *	4563	250	21	0.20	-7.4	7.40	7.55	0.067	0.20	0.0	off	0.09	-6.76
Goloway and Bender (1982)-7BC15 *	3116	110	39	0.04	N/A	0.36	0.36	0.010	0.61	0.1	off	0.00	-0.42
Goloway and Bender (1982)-7BC18 *	3214	110	39	0.03	N/A	0.36	0.36	0.009	0.58	0.1	off	0.00	-0.42
Goloway and Bender (1982)-7BC20 *	3125	110	39	0.02	N/A	0.36	0.36	0.010	0.59	0.1	off	0.00	-0.42
Goloway and Bender (1982)-9BC33 *	3591	110	40	0.04	N/A	0.32	0.32	0.019	1.32	3.0	off	0.03	-0.41
Goloway and Bender (1982)-CBC13 *	4368	167	38	0.07	-0.96	0.96	0.98	0.115	2.62	2.0	off	0.06	-1.23
Goloway and Bender (1982)-CBC21 *	4371	167	38	0.02	-0.26	0.26	0.26	0.026	2.16	49.8	off	0.02	-0.34
Goloway and Bender (1982)-CBC44 *	4391	167	38	0.05	-0.58	0.58	0.59	0.068	2.58	2.8	off	0.05	-0.75
Goloway and Bender (1982)-CBC6-3C *	4394	167	38	0.03	-0.47	0.47	0.47	0.018	0.87	34.6	off	0.03	-0.60
Goloway and Bender (1982)-CBC6-4S *	4394	167	38	0.04	-0.49	0.49	0.50	0.045	2.00	4.7	off	0.04	-0.65
Goloway and Bender (1982)-CGC3 *	4379	167	38	0.02	-0.3	0.30	0.31	0.020	1.46	56.3	off	0.02	-0.39
Goloway and Bender (1982)-LGC02 *	4595	268	18	0.03	-1.12	1.12	1.14	0.466	9.12	37.2	off	0.03	-1.37
Goloway and Bender (1982)-LGC05 *	4621	268	19	0.02	-0.36	0.36	0.36	0.045	2.75	328.5	off	0.02	-0.46
Goloway and Bender (1982)-TC05 *	4629	268	18	0.04	-0.88	0.88	0.89	0.026	0.64	1.9	off	0.04	-1.10
Grandel et al. (2000)-CAST-autumn *	3955	113	38	0.15	N/A	2.30	2.35	0.003	0.03	0.1	off	-0.05	-1.98
Grandel et al. (2000)-CAST-spring *	3955	113	38	0.20 (±0.03)	N/A	2.30	2.35						
Grandel et al. (2000)-EAST-autumn *	3850	120	35	0.13	N/A	2.58	2.63						

Table C.1.: Continued.

identifier	depth (m)	bw_{O2} (µM)	bw_{NO3} (µM)	measured J_{NO3} (mmol m^{-2} d^{-1})	measured J_{O2} (mmol m^{-2} d^{-1})	RPOC (mmol m^{-2} d^{-1})	RRPOC (mmol m^{-2} d^{-1})	RPOC(0) mmol cm^{-3} yr^{-1}	B (cm^{-1})	k_8 (10^9 M^{-1} yr^{-1})	x_{irr} (cm)	modeled J_{NO3} (mmol m^{-2} d^{-1})	modeled J_{O2} (mmol m^{-2} d^{-1})
Grandel et al. (2000)-EAST-spring *	3850	120	35	0.19 (±0.03)	N/A	2.58	2.63						
Grandel et al. (2000)-SAST-autumn *	4424	141	37	0.10	N/A	0.70	0.71						
Grandel et al. (2000)-WAST-autumn *	4041	120	37	0.17	N/A	3.08	3.14	0.006	0.04	5.3	off	-0.17	-2.38
Grandel et al. (2000)-WAST-spring *	4041	120	37	0.29 (±0.34)	N/A	3.08	3.14						
Hammond et al. (1996)-JGOFS 2N *	4200-4500	171	48	0.09 (±0.02)	-0.7 (±0.06)	0.59	0.60	0.041	1.52	2.6	off	0.06	-0.78
Hammond et al. (1996)-JGOFS 2S *	4200-4500	173	33	0.05 (±0.02)	-0.8 (±0.07)	0.48	0.49	0.025	1.16	2.0	off	0.05	-0.65
Hammond et al. (1996)-JGOFS EQ *	4200-4500	172	51	0.07 (±0.01)	-0.71 (±0.05)	0.47	0.48	0.021	0.96	2.0	off	0.05	-0.63
Hammond et al. (1996)-PACFLUX II X *	3300-4300	168	48	0.05 (±0.01)	-0.84 (±0.10)	0.37	0.38	0.012	0.73	1.8	off	0.04	-0.50
Hammond et al. (1996)-PACFLUX II Y *	3300-4300	170	36	0.03 (±0.02)	-0.56 (±0.07)	0.36	0.37	0.035	2.13	5.0	off	0.03	-0.48
Hammond et al. (1999)-1	10	200	5	0.49 (±0.50)	-19.9 (±4.5)	21.50	35.65	4.079	4.42	0.6	2.4	-0.33	-19.92
Hammond et al. (1999)-2	15	200	2	0.29 (±0.06)	-17.7 (±5.4)	21.10	34.94	2.320	2.56	0.7	3.8	-0.08	-17.95
Hammond et al. (1999)-4	42	200	1	-0.10 (±0.07)	-5.3 (±0.4)	10.30	16.19	0.045	0.10	953.7	3.4	-0.02	-5.20
Hammond et al. (1999)-6	15	200	9	0.11 (±0.12)	-19.2 (±9.6)	22.90	38.16	0.114	0.12	0.0	0.1	0.08	-13.08
Hammond et al. (1999)-7	22	200	2	0.41 (±0.22)	-11.9 (±1.6)	15.90	25.77	0.538	0.79	0.0	3.5	0.01	-11.87
Hartnett and Devol (2003)-NH003 *	100	6	28	-1.96	-0.98	5.51	8.33	0.866	3.66	704.0	off	-1.96	-0.73
Hartnett and Devol (2003)-NH006 *	620	0	20	-0.78	0	3.62	5.34	0.193	1.17	234.0	off	-0.78	0.00
Hartnett and Devol (2003)-NH104/208*	1020	4	45	-0.37	-0.25	1.33	1.86	0.021	0.35	37.0	off	-0.38	-0.10
Hartnett and Devol (2003)-NH107 *	345	0	22	-1.71	0	4.88	7.32	0.935	4.20	431.0	off	-1.72	0.00
Hartnett and Devol (2003)-NH206 *	2000	92	45	-0.33	-1.87	2.23	3.21	0.025	0.25	620.0	0.8	-0.33	-1.60
Hartnett and Devol (2003)-NH209 *	800	1	42	-1.36	-0.21	3.46	5.09	0.266	1.69	551.0	off	-1.34	-0.07
Hartnett and Devol (2003)-NH304*	3065	125	38	-0.20	-2.06	2.08	2.12	0.012	0.13	70.0	0.8	-0.20	-1.78
Hartnett and Devol (2003)-WE201 *	2746	90	38	-0.06	-0.37	0.40	0.41	0.012	0.67	98.0	1.6	-0.06	-0.40
Hartnett and Devol (2003)-WE202 *	440	50	40	-0.54	-2.53	3.76	5.56	0.053	0.31	90.0	1.0	-0.55	-1.45
Hartnett and Devol (2003)-WE203 *	1994	65	40	-0.09	-1.54	1.49	2.10	0.003	0.04	586.0	0.4	-0.14	-1.03
Hartnett and Devol (2003)-WE204 *	105	179	25	-1.38	-8.32	9.56	14.96	1.899	4.63	972.6	1.1	-0.94	-9.53
Hartnett and Devol (2003)-WE206 *	1025	38	40	-0.41	-0.82	1.33	1.87	0.075	1.24	541.0	0.7	-0.41	-0.78
Hartnett and Devol (2003)-WE213 *	620	27	40	-0.54	-1.09	1.73	2.46	0.098	1.25	277.0	0.4	-0.54	-0.74
Hartnett and Devol (2003)-WE219 *	2525	82	42	0.08	-1.54	1.49	1.52	0.003	0.04	4.7	0.1	-0.12	-1.19
Helder (1989)-3 *	3072	165	36	0.15	1.08	1.35	1.38	0.003	0.05	0.0	off	0.02	-1.51
Jahnke (1990)	908	5	30	-1.10 (±0.31)	N/A	2.70	3.92	0.423	3.44	81.5	3.2	-1.10	-0.34
Jahnke and Jahnke (2000)-A	850	250	19	0.05 (±0.01)	-4.33 (±0.91)	3.27	4.80						
Jahnke and Jahnke (2000)-B	740	250	19	0.16 (±0.01)	-5.11 (±0.40)	6.16	9.37						
Jahnke and Jahnke (2000)-C	2927	250	18	0.04 (±0.01)	-1.41 (±0.17)	0.97	0.99						
Jahnke and Jahnke (2000)-D	761	250	19	-0.02 (±0.01)	-4.04 (±0.32)	3.37	4.95						
Jahnke and Jahnke (2000)-E	755	250	19	-0.14 (±0.03)	-9.18 (±0.64)	7.23	11.11						
Jahnke and Jahnke (2000)-F	855	250	19	-0.14 (±0.02)	-9.13 (±1.02)	6.18	9.40						
Jahnke and Jahnke (2000)-G	2635	250	18	0.01 (±0.01)	-1.67 (±0.10)	2.58	2.63						
Jahnke and Jahnke (2000)-H	731	250	19	-0.01 (±0.03)	-3.12 (±0.26)	2.66	3.86						
Jahnke and Jahnke (2000)-I	730	250	19	-0.03 (±0.01)	-7.73 (±0.53)	6.89	10.55						
Jahnke and Jahnke (2000)-J	607	250	19	-0.14 (±0.04)	-11 (±1.1)	7.02	10.77						
Jahnke and Jahnke (2000)-K	607	250	19	0.00 (±0.01)	-10.1 (±1.75)	9.43	14.73						
Jahnke and Jahnke (2000)-L	742	250	19	-0.26 (±0.06)	-13.5 (±0.57)	10.77	16.98						
Jahnke and Jahnke (2000)-M	750	250	19	-0.24 (±0.03)	-9.41 (±1.36)	6.94	10.63						
Jahnke et al (1989)-10 *	5036	250	24	0.04	-0.53	0.53	0.54	0.016	0.66	194.6	off	0.03	-0.68

Table C.1.: Continued.

identifier	depth (m)	bw_{O2} (µM)	bw_{NO3} (µM)	measured J_{NO3} (mmol m^{-2} d^{-1})	measured J_{O2} (mmol m^{-2} d^{-1})	RPOC (mmol m^{-2} d^{-1})	RRPOC (mmol m^{-2} d^{-1})	RPOC(0) mmol cm^{-3} yr^{-1}	B (cm^{-1})	k_8 (10^9 M^{-1} yr^{-1})	x_{irr} (cm)	modeled J_{NO3} (mmol m^{-2} d^{-1})	modeled J_{O2} (mmol m^{-2} d^{-1})
Jahnke et al (1989)-12 *	3860	240	22	0.08	-0.71	0.71	0.73	0.050	1.56	7.8	off	0.08	-0.95
Laursen and Seitzinger (2002)-32-Aug96	15	186	2	0.14 (±0.05)	-18.9 (±1.46)	16.86	27.44	9.151	12.64	0.1	3.1	-0.01	-18.76
Laursen and Seitzinger (2002)-32-Aug99	15	138	1	-0.04 (±0.03)	-23.7 (±4.94)	22.46	37.37	13.377	13.87	0.1	3.0	-0.13	-22.49
Laursen and Seitzinger (2002)-32-Jul97	15	276	0	0.02 (±0.05)	-12.3 (±5.12)	11.35	17.96	6.589	13.52	207.5	1.1	0.02	-12.98
Laursen and Seitzinger (2002)-32-Jun98	15	290	0	0.01 (±0.03)	-4.84 (±0.93)	4.34	6.47	0.647	3.47	968.2	1.5	0.01	-5.16
Laursen and Seitzinger (2002)-32-May99	15	321	0	0.06 (±0.03)	-15.1 (±4.22)	13.45	21.54	4.199	7.27	34.4	1.1	0.06	-15.74
Laursen and Seitzinger (2002)-32-Nov98	15	343	0	0.10 (±0.08)	-12.2 (±6.56)	11.10	17.54	5.619	11.79	52.2	0.4	0.10	-12.98
Laursen and Seitzinger (2002)-9-Aug99	11	147	1	-0.19 (±0.08)	-5.74 (±1.51)	4.46	6.66	1.460	7.62	990.1	1.0	-0.05	-5.01
Laursen and Seitzinger (2002)-9-Jul97	11	290	0	0.21 (±0.06)	-16.7 (±1.28)	14.34	23.07	4.147	6.74	0.6	1.3	0.21	-16.90
Laursen and Seitzinger (2002)-9-Jun98	11	334	0	0.23 (±0.01)	-11.1 (±6.11)	10.50	16.53	0.401	0.89	0.5	1.5	0.23	-10.99
Laursen and Seitzinger (2002)-9-May99	11	330	0	0.08 (±0.02)	-8.05 (±1.17)	6.43	9.81	3.496	12.66	86.9	0.6	0.08	-7.54
Laursen and Seitzinger (2002)-9-Nov98	11	348	0	0.42 (±0.15)	-16.8 (±3.73)	14.57	23.47	4.536	7.25	2.2	3.0	0.42	-17.59
Laursen and Seitzinger (2002)-9-Sep98	11	152	0	-0.01 (±0.06)	-24.7 (±3.59)	23.76	39.71	13.396	13.13	511.9	2.7	-0.05	-23.81
Laursen and Seitzinger (2002)-C-Aug96	11	174	1	-0.10 (±0.13)	-20.2 (±13.08)	18.58	30.47	10.055	12.60	18.8	1.5	-0.13	-20.01
Laursen and Seitzinger (2002)-C-Jul97	11	290	0	0.16 (±0.16)	-24.1 (±0.87)	22.20	36.90	5.758	6.04	54.1	3.0	0.00	-24.41
Laursen and Seitzinger (2002)-C-Jun98	11	290	0	0.35 (±0.05)	-13.2 (±10.08)	12.20	19.40	0.683	1.30	0.0	0.5	0.20	-12.62
Laursen and Seitzinger (2002)-C-May99	11	312	0	0.08 (±0.06)	-15.9 (±0.17)	14.18	22.79	7.412	12.17	50.7	3.0	0.08	-16.41
Laursen and Seitzinger (2002)-C-Nov98	11	361	0	0.23 (±0.15)	-6.89 (±0.31)	5.38	8.12	2.531	10.96	6.9	0.7	0.23	-6.57
Lehmann et al. (2004)-Hyperion-August	65	130	10	-0.08 (±0.14)	-6.8 (±1.4)	14.05	22.57	0.019	0.03	205.8	2.6	-0.17	-3.71
Lehmann et al. (2004)-Hyperion-Mar	65	130	20	-0.81 (±0.15)	-6.38 (±1.45)	13.90	22.31	0.510	0.86	582.0	2.7	-0.82	-7.39
Lehmann et al. (2004)-Malibu	<50	130	10	-0.21 (±0.12)	-12.3 (±2.55)	11.65	18.47	6.894	13.78	0.7	0.1	-0.58	-12.17
Lehmann et al. (2004)-Marina del Rey 4-B	<50	130	20	-0.40 (±0.13)	-6 (±1.2)	12.40	19.74	0.041	0.08	809.0	2.9	-0.39	-3.78
Lehmann et al. (2004)-Marina del Rey 8-B	<50	130	2	0.01 (±0.1)	-9.9 (±2.3)	10.30	16.19	2.360	5.34	0.0	2.5	-0.10	-10.15
Lehmann et al. (2004)-Topanga	50	130	20	-0.35 (±0.08)	-5.73 (±1.2)	4.10	6.09	0.466	2.65	5.3	0.4	-0.35	-4.17
Lohse et al. (1998)-Omex E (94) *	4468	250	24	0.04	-0.8	0.98	1.36	0.064	1.42	89.8	off	0.04	-1.23
Lohse et al. (1998)-Omex F (94) *	2235	269	20	0.08	-1.6	1.78	1.82	0.114	1.41	17.6	2.7	0.07	-2.24
Lohse et al. (1998)-Omex I (94) *	670	226	15	0.13	-3.3	2.36	3.40	0.009	0.08	0.1	0.5	0.07	-2.67
Lohse et al. (1998)-Omex II (94) *	1425	231	18	0.05	-2	1.78	2.53	0.112	1.38	1.2	0.5	0.04	-2.17
Lohse et al. (1998)-Omex III (94) *	3649	249	23	0.02	-0.8	1.55	2.19	0.167	2.37	138.0	off	0.00	-1.87
Reimers et al. (1992)-G *	3319	121	35	-0.05 (±0.16)	-1.09 (±0.08)	2.03	2.07	0.005	0.06	0.6	off	-0.08	-1.85
Reimers et al. (1992)-J *	781	12	41	-0.82 (±0.03)	-0.3 (±0.06)	2.03	2.07	0.206	2.22	223.1	off	-0.82	-0.50
Reimers et al. (1992)-K *	998	20	41	-0.47 (±0.03)	-1.18 (±0.11)	1.81	1.84	0.061	0.73	368.5	off	-0.47	-0.50
Reimers et al. (1992)-M *	3728	129	35	-0.08 (±0.03)	-1.75 (±0.08)	1.81	1.84	0.004	0.05	7.1	off	-0.11	-1.70
Reimers et al. (1992)-N *	4076	144	40	-0.01 (±0.03)	-0.93 (±0.15)	0.99	1.01	0.002	0.04	0.2	off	-0.05	-1.01
Smetacek et al. (1997)-PS2357-1 *	3627	246	32	0.00	-1.7	1.70	1.73	0.107	1.38	5.2	off	0.00	-2.03
Smetacek et al. (1997)-PS2361-1 *	3073	246	32	0.07	-1	1.00	1.02	0.047	1.03	12.0	off	0.06	-1.28
Smetacek et al. (1997)-PS2365-2 *	3215	246	32	0.05	-1.8	1.80	1.84	0.830	10.11	7.7	off	0.05	-2.20
Smetacek et al. (1997)-PS2367-1 *	3525	246	32	0.08	-0.9	0.90	0.92	0.121	2.95	4.0	off	0.08	-1.19
Smetacek et al. (1997)-PS2370-4 *	5078	270	32	0.03	-0.7	0.70	0.71	0.116	3.62	139.2	off	0.03	-0.88
Smetacek et al. (1997)-PS2371-1 *	3680	246	32	0.05	-1.3	1.30	1.33						
Smetacek et al. (1997)-PS2376-1 *	3657	246	32	0.05	-1.3	1.30	1.33	0.488	8.24	10.0	off	0.05	-1.61
Sommer(subm)-BIGO1 *	300	1	26	-3.26 (±0.05)	0	6.18	9.40	2.917	10.35	264.0	off	-3.26	0.00
Sommer(subm)-BIGO2 *	700	8	40	-0.61 (±0.05)	-0.45 (±0.05)	5.99	9.10	0.046	0.17	362.0	off	-0.63	-0.33
Sommer(subm)-BIGO3 *	400	1	33	-2.70 (±0.25)	0	4.61	6.90	1.692	8.04	209.0	off	-2.70	0.00

Table C.1.: Continued.

identifier	depth (m)	bw_{O2} (µM)	bw_{NO3} (µM)	measured J_{NO3} (mmol m^{-2} d^{-1})	measured J_{O2} (mmol m^{-2} d^{-1})	RPOC (mmol m^{-2} d^{-1})	RRPOC (mmol m^{-2} d^{-1})	RPOC(0) mmol cm^{-3} yr^{-1}	B (cm^{-1})	k_8 (10^9 M^{-1} yr^{-1})	x_{irr} (cm)	modeled J_{NO3} (mmol m^{-2} d^{-1})	modeled J_{O2} (mmol m^{-2} d^{-1})
Sommer(subm)-BIGO5 *	80	1	16	-3.47 (±0.45)	0	9.17	14.30	4.503	11.44	573.0	off	-3.47	0.00
Sommer(subm)-BIGO6 *	1000	40	40	-0.29 (±0.1)	-1.6	3.98	5.90	0.012	0.07	769.0	0.2	-0.29	-1.17
Sommer(subm)-BIGOT6 *	250	1	20	-3.23	0	7.65	11.80	3.824	10.83	68.0	off	-3.22	0.00
Warnken et al. (2008) *	2.5	210	4	0.28 (±0.16)	-26 (±3.8)	20.00	32.98	11.820	13.76	0.1	0.8	-0.28	-21.53

List of Abbreviations

α	bioirrigation coefficient
anammox	anaerobic ammonium oxidation
APOC	accumulation rate of particulate organic carbon below the bioturbated zone
AS	Arabian Sea
B	exponential coefficient describing the decrease of mineralization with increasing sediment depth
BB	Bay of Bengal
BIGO	Biogeochemical Observatories(benthic landers)
bw_{NO3}	bottom water nitrate concentration
bw_{O2}	bottom water oxygen concentration
Chl a	Cholorophyll a
Δ	total error, uncertainty
DEN1	*a priori* estimate for benthic denitrification
DEN2	*a posteriori* estimate for benthic denitrification
D_B	bioturbation coefficient
D_S	molecular diffusion coefficient in sediments
DIN	dissolved inorganic nitrogen (NO_3^- + NO_2^- + NH_4^+)
DOU	diffusive oxygen uptake
ds	dry sediment density
DNRA	dissimilatory nitrate reduction to ammonium
ENP	Eastern North Pacific
ESP	Eastern South Pacific
HNLO	high nitrate low oxygen
J_{DIN}	flux of dissolved inorganic nitrogen across the sediment-water interface
J_{NO3}	flux of nitrate across the sediment-water interface
$J_{C:P}$	molar C:P ratio of the benthic flux
$J_{N:P}$	molar N:P ratio of the benthic flux
$J_{N:C}$	molar N:C ratio of the benthic flux
J_{NH4}	flux of ammonium across the sediment-water interface
J_{PO4}	flux of phospahte across the sediment-water interface
k	decay constant for organic carbon
L_{DIN}	net loss of dissolved inorganic nitrogen in marine sediments
L_{NO3}	loss of nitrate in marine sediments
M	mol l^{-1}

MUC	multiple corer
O_2*	bottom water O_2 - NO_3^-
ODE	ordinary differential equation
ODU	oxygen demand units
OMZ	oxygen minimum zone
ϕ	porosity
PAR	photosynthetically available radiation
PDE	partial differential equation
POC	particulate organic carbon
POM	particulate organic matter
PON	particulate organic nitrogen
rNC	molar ratio of N:C in particulate organic matter
$\sum$RPOC	total depth-integrated degradation rate of particulate organic carbon
RPOC	degradation rate of particulate organic carbon
RPOC(0)	degradation rate of particulate organic carbon at the sediment-water interface
RPON	degradation rate of particulate organic nitrogen
RRPOC	rain rate of particulate organic carbon to the seafloor
SST	sea-surface temperature
SWACM	South West African continental margin
TA	total alkalinity
Tg	terragramm (10^{12} g)
TOU	total oxygen uptake
TPS	total particulate sulfur
u	burial velocity for solutes
w	burial velocity for solids
wd	water depth
WOA	World Ocean Atlas
x	sediment depth

Acknowledgements/Danksagung

Diese Arbeit hat von der Mithilfe vieler Menschen profitiert, die ich während der Zeit als Doktorandin kennenlernen durfte. An erster Stelle gilt mein Dank meinem Betreuer Andy Dale und meinem Doktorvater Klaus Wallmann, der Vertrauen in mich gesetzt und mich als Doktorandin an das Institut geholt hat. Durch ihre Anleitung, die anregenden Diskussionen und ihre Ideen hat meine Arbeit sehr gewonnen. Der exzellenten Betreuung vor allem von Andy Dale ist es zu verdanken, dass ich die Tücken der mathematischen Modellierung und der englischen Sprache überwinden konnte. Dabei habe ich besonders genossen, dass es immer ein offenes Ohr gab und die Atmosphäre trotz der konzentrierten Arbeit immer entspannt und freundlich blieb.

Weiterhin möchte ich mich bei Stefan Sommer für den Einstieg in den marinen Stickstoffkreislauf bedanken. Unsere Gespräche haben mir geholfen die komplexe Materie zu verstehen und die entscheidenden Elemente zu erkennen. Mein Dank gilt außerdem Andreas Oschlies, der mir einen Einblick in die globale Ozeanmodellierung gegeben und sich als Koreferent zur Verfügung gestellt hat.

Bei zwei Aufenthalten auf Forschungsschiffen durfte ich neben der mathematischen Modellierung auch die analytische Seite kennenlernen. Um so mehr schätze ich die Hilfe der Besatzungen der FS Meteor und FS Maria Merian sowie der technischen Angestellten, besonders Bettina Domeyer, Anke Bleyer und Meike Dibbern.

Meinen Kollegen danke ich für das nette Umfeld, die gemeinsamen Mittagessen und den wissenschaftlichen wie nicht wissenschaftlichen Austausch. Vor allem Tebke Böschen ist dabei weit mehr als nur eine Kollegin geworden.

Unendlich dankbar bin ich für die guten Wünsche und die mentale Unterstützung meiner Freunde und meiner Familie. Besonders meine Eltern haben stets zu mir gehalten, mich gefördert und gestärkt. Zuletzt möchte ich noch die Person würdigen, die mir während der letzten Monate Kraft, Rückhalt und auch mal eine Schulter zum Anlehnen gegeben hat. Danke Matthias!

LISA BOHLEN

Diplom Umweltwissenschaftlerin
Marine Environmental Scientist

Adress:	Harmsstrasse 131
	24114 Kiel
Phone:	+49 (0)431-3853783
Mobile:	+49 (0)160-4449264
E-mail:	lbohlen@ifm-geomar.de
Date of birth:	09.01.1984
Place of birth:	Aurich, Germany
Nationality:	German

Curriculum Vitae

Since 11/2008	Research Associate at the Leibniz Institute of Marine Sciences at Kiel University, IFM-GEOMAR, in the SFB 754: "Climate - Biogeochemistry Interactions in the Tropical Oceans" (TP B1)
08/2006 - 01/2007	Studies of Marine Environmental Sciences at University of Kalmar, Sweden
10/2003 - 09/2008	Studies of Marine Environmental Sciences at the University of Oldenburg, Institute for Chemistry and Biology of the Marine Environment (ICBM)